



Orbital Transfer Rocket Engine Technology Program

Final Report Oxygen Materials Compatibility Testing
Contract/Task Order NAS3-23772-B.5
NASACR-182195

January 1989

Prepared For:
National Aeronautics and Space Administration
Lewis Research Center
Cleveland, Ohio 44135

(NASA-CR-182195) ORBIT TRANSFER ROCKET
ENGINE TECHNOLOGY PROGRAM: OXYGEN MATERIALS
COMPATIBILITY TESTING Final Report (Aerojet
TechSystems Co.) 224 p CSDL 21H

N89-14256

Unclas
G3/20 0185488

Aerojet
TechSystems
Company

ORBIT TRANSFER ROCKET ENGINE TECHNOLOGY PROGRAM

CONTRACT NAS 3-23772 TASK ORDER B.5

FINAL REPORT OXYGEN MATERIALS COMPATIBILITY TESTING

Prepared by:

Leonard Schoenman

For:

NASA - Lewis Research Center
Cleveland, Ohio 44135

January 1989

RPT/CC0134

1. Report No. NASA CR 182195		2. Government Accession No.		3. Recipient's Catalog No.	
4. Title and Subtitle Orbit Transfer Rocket Technology Program Oxygen Compatible Materials Testing Task Order B.5				5. Report Date June 1988	
				6. Performing Organization Code	
7. Author(s) L. Schoenman				8. Performing Organization Report No.	
				10. Work Unit No.	
9. Performing Organization Name and Address Aerojet TechSystems Company Sacramento, California				11. Contract or Grant No. NAS 3-23772	
				13. Type of Report and Period Covered Final Report 1983 to 1987	
12. Sponsoring Agency Name and Address National Aeronautics and Space Administration Washington, D.C. 20546				14. Sponsoring Agency Code	
15. Supplementary Notes Project Manager, John Kazaroff, NASA Lewis Research Center, Cleveland, Ohio					
16. Abstract Particle impact and frictional heating tests of metals in high pressure oxygen, are conducted in support of the design of an advanced rocket engine oxygen turbopump. Materials having a wide range of thermodynamic properties including heat of combustion and thermal diffusivity were compared in their resistance to ignition and sustained burning. Copper, nickel and their alloys were found superior to iron based and stainless steel alloys. Some materials became more difficult to ignite as the oxygen pressure was increased from 7 to 21 MPa (1000 to 3000 psia).					
17. Key Words (Suggested by Author(s)) Metal ignition Oxygen turbopump Particle impact Friction heating None				18. Distribution Statement Unclassified - Unlimited	
19. Security Classif. (of this report) Unclassified		20. Security Classif. (of this page) Unclassified		21. No. of pages 259	
22. Price*					

Acronyms/Nomenclature

FRT	Friction Rubbing Test
GH ₂	Gaseous Hydrogen
GOX	Gaseous Oxygen
ID	Inside Diameter
L	Load or Length
lbM/Sec, Kg/Sec	Mass Flow Rate
LH ₂	Liquid Hydrogen
LOX	Liquid Oxygen
OD	Outside Diameter
OTV	Orbit Transfer Vehicle
PIT	Particle Impact Test
RPM	Rotational Speed Revolutions per Minute
S, Sec	Time Seconds
T	Temperature °F, °K
TPA	Turbopump Assembly

FOREWORD

This Task Order was performed in support of the design, fabrication and testing of an advanced oxygen turbopump required for the Space Based Orbit Transfer Vehicle Propulsion System employing the Aerojet dual propellant expander cycle. The experimental results reported herein are applicable to a wide range of components and applications in which high pressure oxygen flows at high velocities or is in contact with high speed moving metallic surfaces, and where safety and reliability are of primary importance.

This Final Report combines a series of progress reports by Schoenman et al (Ref. 1-6) covering the period from 1983 through 1987 in which five categories of testing were conducted as follows:

1983-1984	Particle Impact Testing Like Material Friction Induced Ignition
1984-1985	Oxygen Pressure Sensitivity in Friction Heating
1985-1986	Unlike Material Friction Induced Ignition
1986-1987	The Effect of Surface Modifications on Monel K-500 Wear and Friction Heating

Three organizations were involved in the execution of this program. NASA LeRC provided funding under the direction of contract monitors; L. Cooper, J.P. Wanhainen, and D Scheer. The NASA Lewis Research Center Task Manager was John Kazaroff. The planning, analysis and documentation were provided by Len Schoenman of the Aerojet TechSystems Company. The testing and data processing were conducted at the NASA-JSC White Sands Test Facility under the direction of Frank Benz, Joel Stoltzfus and Mohan Gungi.

TABLE OF CONTENTS

	<u>Page</u>
I. Introduction	1
II. Program Task Objectives	12
III. Data Base	13
IV. Turbopump and Test Material Selection	18
V. Test Methods	24
A. Selection	24
B. Test System Description	24
1. Particle Impact Test (PIT)	24
2. Frictional Heating Test Apparatus (FRT)	31
VI. Test Results	43
A. Particle Impact Results	43
1. Test with Impact Plates	43
2. Test with Rupture Disks	50
B. Friction Heating Test Results	55
1. Like Materials	56
2. Friction Heating of Unlike Materials	62
3. Gas Composition and Pressure Effects in Friction Rubbing	78
4. Temperature Oscillations	87
5. Burn Factor Correlation	90
VII. Friction Heating and Wear Rates of Monel K-500 in Oxygen	98
A. Objectives and Background Data	98
1. Objectives	98
2. Background	98
B. Test Method	99
1. Apparatus	99
2. Measurements	100
3. Test Procedures	105
C. Surface Modifications	105
1. Test Specimen and Surface Modification Selections	108

TABLE OF CONTENTS (cont.)

	<u>Page</u>
D. Test Summary	111
1. Variable Loading Friction Tests	111
2. Constant Loading Friction Tests	111
E. Results and Discussions	115
1. Friction Heating	115
2. Comparison of Overall Wear	124
F. Effect of Surface Modifications and Oxygen Pressure on Monel K-500 Wear Rates	134
G. Friction Coefficient	148
1. Friction Coefficients Variable Load Testing	148
2. Constant Load Testing	152
H. Analysis of Individual Surface Modifications	152
1. Ion Implanted Oxygen	152
2. Ion Implanted Chromium	153
3. Ion Implanted Silver	154
4. Ion Implanted Lead	155
5. Electrodeposited Chromium	155
6. Composite Plating of NiSiC	156
7. Electrodeposited Silver	157
8. Electroplated Gold	157
I. Photographic and Metallurgical Analyses	157
1. Pre Test Condition	158
2. Post Test Condition	164
VIII. Conclusions and Recommendations	184
References	187
Appendices	
A. Particle Impact Data Summary	A-1
B. White Sands Report on Composition of Surface Modifications	B-1

LIST OF TABLES

<u>Table No.</u>		<u>Page</u>
I	Materials Selection Matrix	19
II	Heat of Combustion of Metals and Alloys	21
III	Burn Factor Ranking of Typical Materials	23
IV	Candidate Materials Tested	23
V	Test Data Compilation for Friction Rubbing (Ramped Load)	58
VI	Summary of Data for Dissimilar Materials	59
VII	Test with Fixed Load Variable O ₂ Pressure	60
VIII	Average Heat Rate per Unit Area (PV Product) Required for Ignition by Frictional Heating of Pairs of Like Materials	61
IX	Baseline Data Comparison for Monel K-500	69
X	Rubbing of Low and High Burn Factor Metals (Copper and Stainless Steel)	71
XI	Rubbing of Low and Moderate Burn Factor Metals (Nickel and Monel K-500)	72
XII	Rubbing of Moderate Burn Factor and High Burn Factor Metals (Monel K-500 vs 316 Stainless Steel)	73
XIII	Rubbing of Moderate Burn Factor Metal and Ceramic (Monel K-500 and Silicon Carbide)	74
XIV	Rubbing of Moderate Burn Factor Ceramic and High Burn Factor Metal (Silicon Carbide and Invar 36)	75
XV	Comparison of Friction Heating Ignition of Copper 150 and Brass 360 in. 6.9 MPa (1000 psia) Oxidizer at 17,000 RPM	95
XVI	Monel K-500 Surface Modifications	107
XVII	Summary of Weight and Length Data for the Variable Load Test	112
XVIII	Constant (50 psi) Load Friction Tests in 6.9 MPa (1000 psi) O ₂	114
XIX	Comparison of Peak Temperatures in the Time Interval 0-40 s for Step Load and Constant Load	125
XX	Comparison of Wear Data for Test Conducted with Step Load Applied to the Samples at Ambient Oxygen and 6.9 MPa (1000 psi) Oxygen Environment Pressure	126

LIST OF TABLES (cont.)

<u>Table No.</u>		<u>Page</u>
XXI	Comparison of Wear Data for Tests Conducted at Constant 50 psi Load in 1000 psi Oxygen	127
XXII	Comparison of Wear Rates for Monel K-500 with Surface Coating with Step Load	135
XXIII	Comparison of Wear Rates for Monel K-500 with Surface Coating and Constant Load with 16-9 MPA (1000 psi) Oxygen Environment Pressure	136

LIST OF FIGURES

<u>Figure No.</u>		<u>Page</u>
1	Standard Design Approach for LOX Turbopumps	2
2	Schematic of Space Shuttle Main Engine High Pressure Oxygen Turbopump Bearings and Seals	4
3	Flow Schematic and Advantages of the Dual Propellant Expander Cycle Engine	6
4	Schematic Design Approach to Gaseous Oxygen-Driven Liquid Oxygen Pump for Dual-Propellant Expander Cycle Engine	7
5	Advanced Turbopump Flow Paths and Seal Locations	8
6	Oxidizer Turbopump Components Fabricated from Monel K-500 and Monel 400	9
7	Advanced Rocket Engine Oxygen Turbopump Design Parameters	10
8	Comparison of Ignition Temperatures of 304 Stainless Steel in Heated Oxygen Gas at High Pressure as Determined by Resistance Heating with and without Rupture	14
9	Range of Ignitability for Non-metallics	16
10	Range of Ignitability for Metals	17
11	Structural and Thermal Properties of Materials for Use in Oxygen	20
12	Test Methods for Material Ignition in Oxygen	25
13	Schematic of Particle Impact Test Apparatus	26
14	Particle Impact Test Assembly for Rupture Disk Evaluation	27
15	Particle Impact Test Assembly for Plate Impact Studies	28
16	Frictional Heating Test Apparatus	32
17	Frictional Rubbing Test Chamber	33
18	Torque Load Measurement as Mode (A) in Original Frictional Heating Apparatus and (B) in Test Apparatus as Modified for the Pressure Study and all Subsequent Tests	35
19	Friction Rubbing Test Specimen Configurations	37

LIST OF FIGURES

<u>Figure No.</u>		<u>Page</u>
20	Selected Material Test Combinations and Their Calculated Burn Factors	38
21	Typical Data from O ₂ Ramped Load Friction Rubbing Test	40
22	5000 rpm - Monel K-500 Friction Rubbing Test Data from GO ₂ Incrementally Stepped Pressure Test; 100, 1000 and 3000 psi	42
23	Impact Plates Showing 9a) No Burning, (b) Slight Evidence of Burning, (c) Partial Burning	44
24	End View of a Test Chamber as it Appeared (a) Before Test and (b) After the Complete Burn of an Impact Plate	46
25	Results of Particle Impact Tests on Impact Plates	47
26	Ignitions Experienced in Particle Impact Testing at 4500 psi	48
27	Examples of the Results of Particle Impact Tests Using 316 Stainless Steel Rupture Disks	51
28	Comparison of Particle Impact Tests on CRES 316 Rupture Disks of Different Thickness and Plate Impact	53
29	Particle Impact Test Results for Ni 200 Plate and Rupture Disks	54
30	Test Specimen Design and Typical Results 9,000 RPM, 1000 psi O ₂	57
31	Total Load vs Time Dissimilar Materials (Cu/Steel) Friction Heating Ignition Tests	63
32	Copper - Stainless Steel Friction Heating Test O ₂ Pressure vs Time	64
33	Copper - Stainless Steel Friction Heating Ignition Test Displacement vs Time	65
34	Copper - Stainless Steel Friction Heating Ignition Test Temperature vs Time	66
35	Copper - Stainless Steel Friction Coefficient	67
36	PV Products Required to Ignite Pairs of Different Materials	68
37	Effect of O ₂ Pressure on Heating Rates of Monel 400	79

LIST OF FIGURES (cont.)

<u>Figure No.</u>		<u>Page</u>
38	Time to Ignition vs Oxygen Pressure	79
39	Load at Ignition vs Oxygen Pressure	80
40	Heat Rate per Unit Area Required for Ignition vs O ₂ Pressure (from Benz and Stoltzfus)	80
41	Effect of O ₂ Pressure on Ignition Temperature	82
42	Effect of Surface Temperature and Oxygen Pressure on Friction Coefficient	84
43	Friction Heating of 1015 Carbon Steel, O ₂ and N ₂	85
44	Effect of Gas Pressure on Friction Heating Rates of 1015 Steel Under Ramped Loading at 5000 RPM	86
45	Phase Comparison of Optical and Thermocouple Temperature Measurements	86
46	Effect of Oxygen Pressure on Thermal Cycle Time in Ramped Loading Tests	88
47	Hypothesis of Events Leading to Ignition in Friction Rubbing Tests	89
48	Burn Factor vs Ignition Temperature in 6.9 MPa (1000 psi) O ₂	91
49	Burn Factor vs Load at Ignition in 6.9 MPa O ₂ at 17,000 RPM	92
50	Thermal Diffusivity Based Burn Factor Correlation vs Experimental Ignition PXV Data	93
51	Comparison of Friction Heating Rate and Ignition of Brass 360 and Copper 150	94
52	Correlation of Heat of Combustion with PV Product for Metal Ignition	96
53	Typical Baseline Monel K-500 Power, Load and Temperature vs Time Data 14.7 psia O ₂ 17,000 RPM	101
54	Representative Data Set Unmodified Surface	103
55	Friction Coefficient Computed from Drive Power for 5 Load Steps (Untreated Monel K-500, 1000 psia O ₂ , 17,000 RPM)	104
56	Test Specimen Design	106
57	Cross-Section of NYE-Carb ®Composite	110
58	Superposition of Friction Heating Data of Monel K-500, 2 Tests at 1000 psia, 2 Tests at 14.7 psia	116

LIST OF FIGURES (cont.)

<u>Figure No.</u>		<u>Page</u>
59	Comparison of Friction Heating of Monel K-500 in 1000 psia O ₂ with Selected Surface Treatments	118
60	Comparison of Maximum Surface Temperatures for Monel K-500 in Low and High Pressure Oxygen with Surface Modifications and a Step Load	119
61	Friction Heating of Monel K-500 in 1000 psia O ₂ at 17,000 RPM Contact Pressure 50 psi for 40 sec	120
62	Maximum Temperature Observed in 6.9 MPa O ₂ , Constant Load Testing	122
63	Maximum Temperature Observed in 6.9 MPa O ₂ , Constant Load Testing	123
64	Sample Wear Rates vs Time, Load, and Oxygen Pressure at 17,000 RPM	129
65	Displacement (Wear) Measurements for Untreated Monel K-500 in 1000 psia Oxygen	130
66	Wear Data at Constant 50 psi Load for 300 sec O ₂ = 1000 psia	131
67	Wear Data for Stepped Loading Cycle (O ₂ = 1000 psia)	132
68	Wear Data for Stepped Loading Cycle (O ₂ = 12.7 psia)	133
69	Wear Rate of Untreated Monel K-500 in 14.7 and 1000 psi Oxygen at a Contact Pressure of 50 psi	138
70	Correlation of Material Loss Rate by the Arrhenius Relation	139
71	Wear Rates vs Time Monel K-500 O ₂ = 1000 psia	140
72	Post Test Hardness Profile Untreated Monel K-500 6.9 MPa (1000 psia) O ₂ Step Loading	142
73	Post Test Hardness Profile Untreated Monel K-500 6.9 MPa (1000 psia) O ₂ , Constant Loading	143
74	Comparison of Displacement Measurements for Ion Implanted Cr from Tests 175 and 181 1000 psi O ₂ , 50 psi Contact Load	145
75	Effect of Surface Modification on Wear Rate and in O ₂ at 6.9 MPa (1000 psi)	146
76	Effect of Surface Modification on Wear Rate as a Function of Contact Pressure in 6.9 MPa (1000 psia) O ₂	147
77	Comparison of Wear Rates in Low (14.7 psia) and High (1000 psia) Oxygen	149

LIST OF FIGURES (cont.)

<u>Figure No.</u>		<u>Page</u>
78	Summary of Friction Coefficients at 14.7 and 1000 psia O ₂ 17,000 RPM	150
79	Comparison of Friction Coefficients in 1000 psi Oxygen	151
80	Pretest Photos of Surface Modified Test Specimen	159
81	Pretest Surface Comparisons of Electrolyzed Cr, Ion Implanted Surfaces and NYE Carb (Ni + SiC)	160
81a	Pretest Surface Comparisons (continued)	161
82	Surface Composition O ₂ Ion Implanted Monel K-500	162
83	Composition Profile O ₂ Ion Implanted Monel K-500	163
84	Surface Modified Monel K-500 After Step Load Testing in Oxygen at Ambient Pressure	165
85	Surface Modified Monel K-500 After Testing 6.9 MPa (1000 psia) Oxygen	166
86	Electroplated Silver Post Test 108, O ₂ = 6.9 MPa (1000 psi)	167
87	Friction Rubbing of Electroplated Gold in Oxygen Testing	168
88	Monel K-500 Without Surface Modifications, Following Test 75 in O ₂ at 1 ATM and Test 86 at 6.9 MPa (1000 psia)	169
89	Ion Implanted Oxygen Post Test 81 and 79 Low and High Oxygen Pressure	170
90	Ion Implanted Chromium Post Test 87 and 80 Low and High Oxygen Pressure	171
91	Monel K-500 with Composite Ni + 30% SiC, Post Test No. 85, 6.9 MPa, 1000 psia	172
92	Photomicrograph FRT Specimen No. 1Pb6, 14.7 psia O ₂ 400 X	173
93	Ion Implanted Lead Specimen Post Test No. 91 O ₂ = 1 ATM	174
94	Blistered Zone Ion Implanted Lead Post Test No. 91 O ₂ 1 ATM	175
95	Spalled Zone Ion Implanted Lead Test Post Test No. 91	176
96	Ion Implanted Lead Post Test No. 82 O ₂ 6.9 MPa (1000 psia)	177

LIST OF FIGURES (cont.)

<u>Figure No.</u>		<u>Page</u>
97	Spalled and Cracked Region Ion Implanted Lead Post Test No. 82 O ₂ 6.9 MPa (1000 psia)	178
98	Ion Implanted Silver Post Test 90 Specimen IAG-4 O ₂ = 1 ATM	179
99	Ion Implanted Silver Post Test No. 81 Specimen IAG-2, O ₂ = 6.9 MPa	180

I. INTRODUCTION

TASK SIGNIFICANCE IN RELATION TO THE ORBIT TRANSFER VEHICLE PROPULSION

The Reusable Orbit Transfer Vehicle represents a national goal which complements a permanent presence of man in Space, starting with the Space Station in the 1990's.

In a continuing effort to develop a more economical Space Transportation System, the NASA (Cooper (Ref. 7) has defined a series of propulsion goals for a new generation of space-based Orbit Transfer Vehicles (OTV). The propulsion system for these vehicles would utilize hydrogen and oxygen as propellants and deliver a specific impulse approaching 500 lbF-sec/lbM. The OTVs would be transported to the space station in the STS Orbiter starting in the mid-1990's. Operating out of a fueling station located near the space station, each of these OTVs will make up to 100 round-trip flights, transporting numerous types of manned and unmanned payloads to and from higher orbits, including geosynchronous and also perform translunar and planetary missions.

The desired performance goals can be approached only by utilizing engines which combine much higher operating pressures with higher expansion ratio nozzles. The need for longer life and a minimum maintenance in conjunction with the higher operating pressures is the real technical challenge.

The use of a fuel rich gas to power a turbine which drives a LOX pump creates a problem in seal maintenance and safety.

The industry standard design approach utilizing fuel or fuel-rich combustion gas to drive a LOX pump is shown schematically in Figure 1. The fuel rich turbine drive gas is selected for bipropellant rocket applications as a means of lowering the combustion temperature to a level compatible with engineering materials. The alternative oxidizer rich drive gas which can also provide acceptable temperatures is not common to the industry because most prior demonstration attempts have resulted metal ignition and burning.

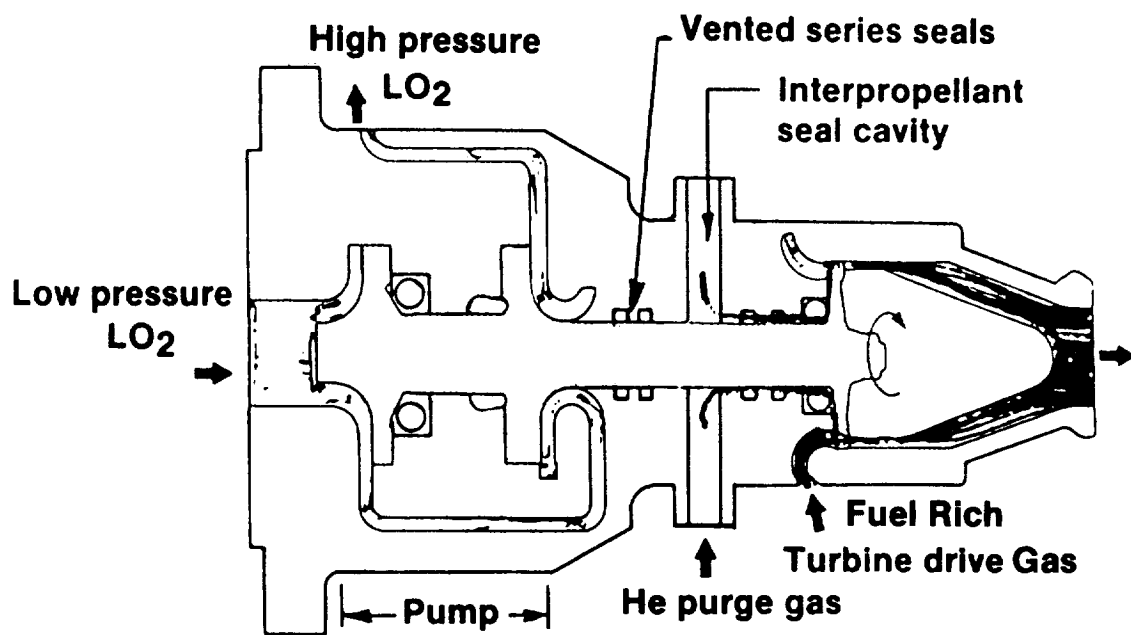


Figure 1. Standard Design Approach for LOX Turbopumps

I, Introduction (cont.)

A detailed review of pump-fed bipropellant engine designs has identified three critical areas of engine maintenance common to all designs, i.e., (1) the high-speed (50,000 to 100,000 rpm) dynamic interpropellant shaft seal which separates the fuel-driven turbine (direct drive or fuel-cooled gearbox) from the oxygen pump, (2) excessive wear rates on propellant-cooled rolling contact bearings, and (3) turbine blade wear and cracking resulting from rapid engine transient heating and high operating temperature.

The hazards and life limitations of interpropellant seals are as follows:

- High rubbing speeds, combined with even a minor level of vibration and repeated thermal cycling, result in seal wear and eventual leakage. The potential of hydrogen and oxygen leakage into a common cavity provides an unacceptable fire or explosion hazard.

Existing engine designs, such as the Titan, avoid the interpropellant seal problem by utilizing an oil lubricated gear system. This, however, results in other maintenance and cooling needs. The RL-10 utilizes H_2 propellant cooled gears to synchronize the hydrogen and oxygen pumps and has similar interpropellant seal limitations.

The SSME utilizes redundant seals and a helium purge, as shown in Figure 2. This solution is acceptable, except for the additional weight of the helium purge system. Since ground checks, maintenance and helium replacement are possible following each flight (one engine start per flight), seals with excessive wear and leakage can be replaced. Such is not the case for space-based OTV where three or more engine restarts may be required for a single mission and between-flight maintenance is even more costly and difficult and helium must be transported from earth.

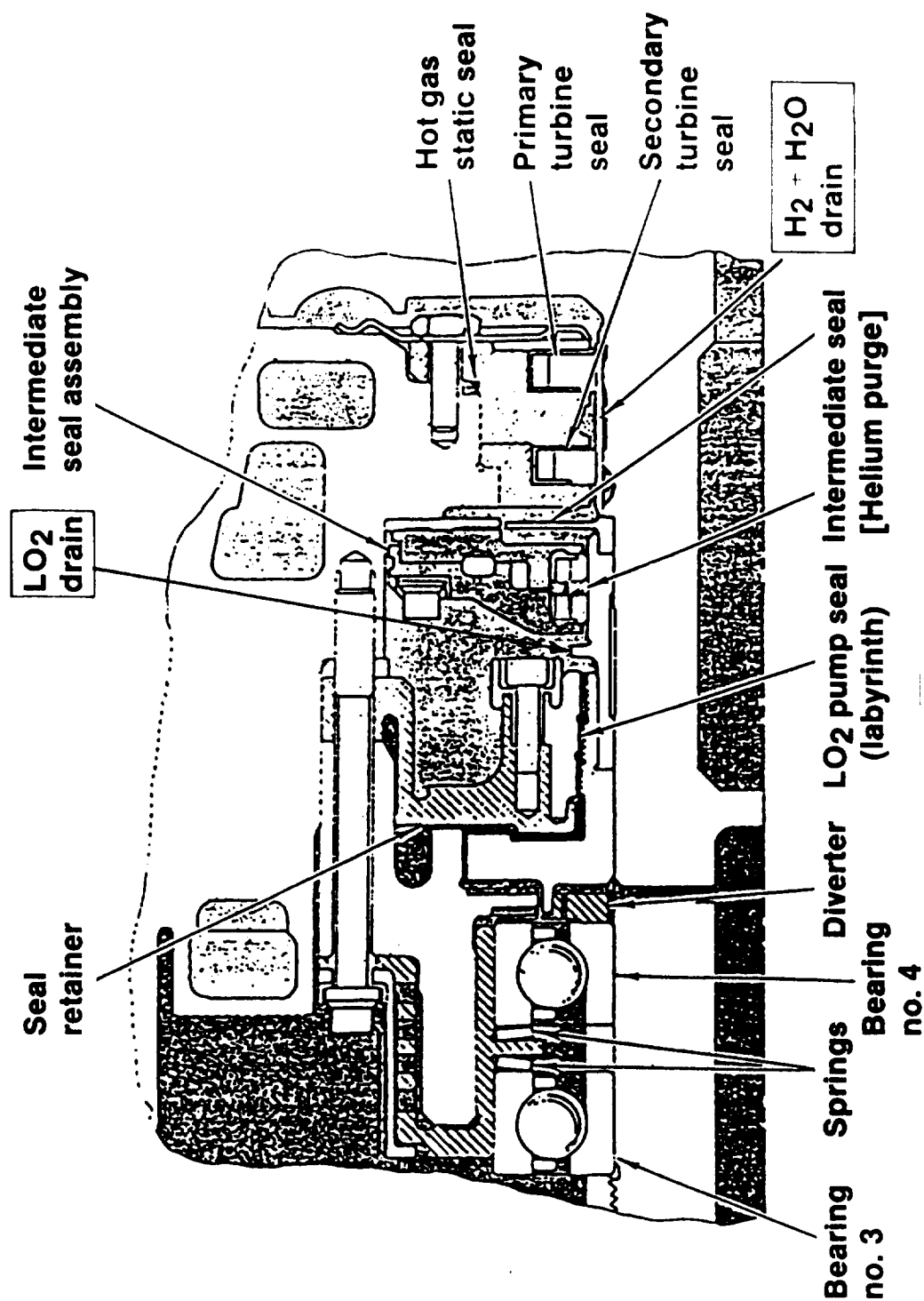


Figure 2. Schematic of Space Shuttle Main Engine High Pressure Oxygen Turbopump Bearings and Seals

I, Introduction (cont.)

The technology being developed for the new Aerojet OTV engine under NASA Contract NAS 3-23772 employs a design concept which eliminates the need for purging and leak-free, high-speed seals. The new engine cycle and pump design schematically shown in Figures 3 and 4 uses GO_2 to drive the LOX pump and GH_2 to drive the LH_2 pump, thus allowing the drive and pumped fluid to commingle without hazard or loss in performance. Leakage past noncontacting labyrinth seals is recycled internal to the respective pumps which can be all-welded assemblies.

The new pump design shown in Figures 5 and 6 eliminates rolling contact bearings which can become a hazard as the bearings age. These are replaced with oxygen pressurized hydrostatic bearings which will provide unlimited wear life capability. The unique material aspects of this design are that it is free of nonmetallic seals which often provide a point of low temperature ignition under adiabatic compression, and it is nearly free of iron and chrome containing alloys. The reason for this unusual design approach will become apparent in the subsequent chapters of this report.

The engine cycle which makes the GO_2 available to drive the turbine does not require high turbine inlet temperatures [478K (400°F)] at maximum power and therefore eliminates the usual turbine hot section life problems.

This new approach, however, is not without concerns relative to the use of high-pressure, high-velocity oxygen as noted by the operating speeds, pumping power and severe weight and size limitations defined in Figure 7.

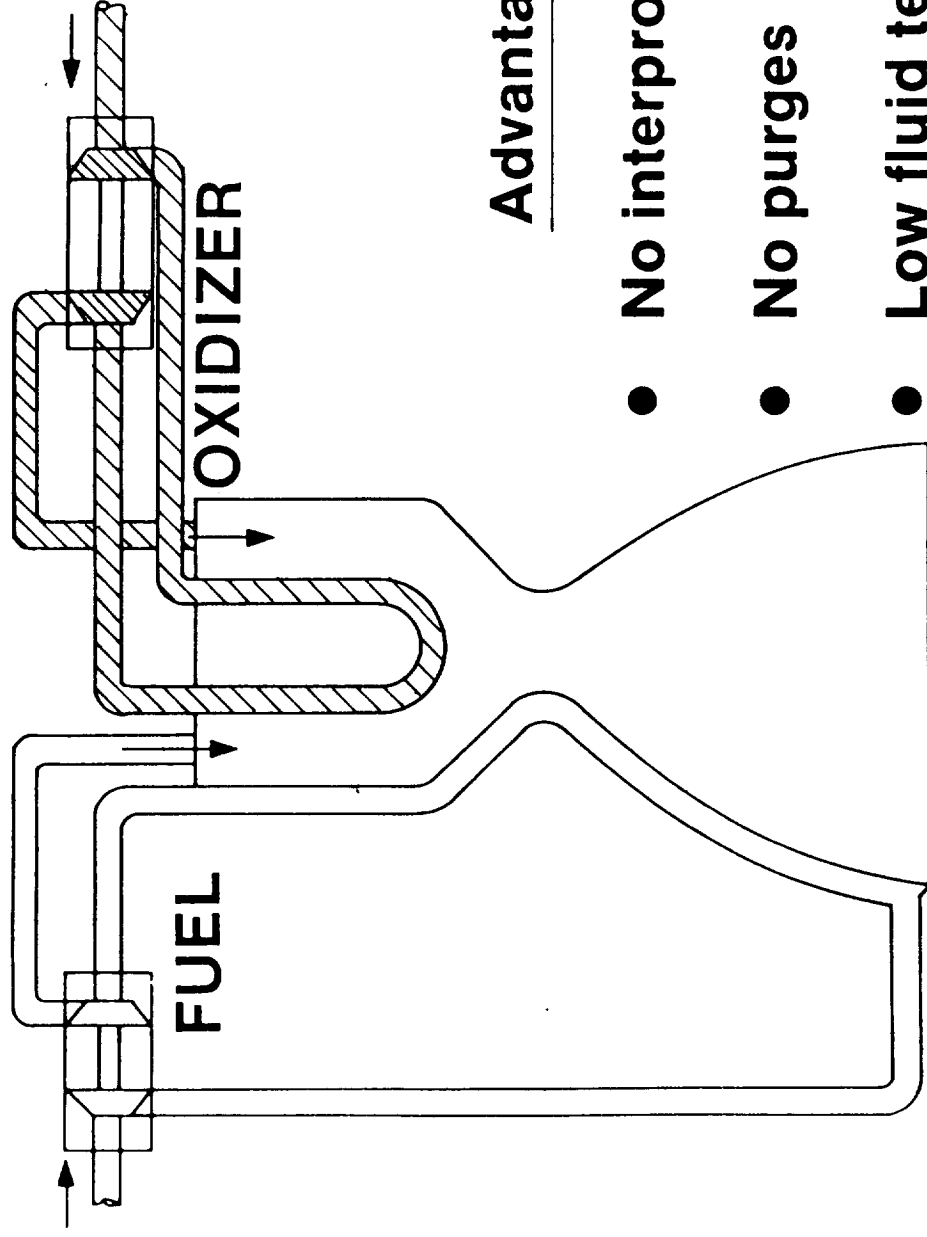


Figure 3. Flow Schematic and Advantages of the Dual Propellant Expander Cycle Engine

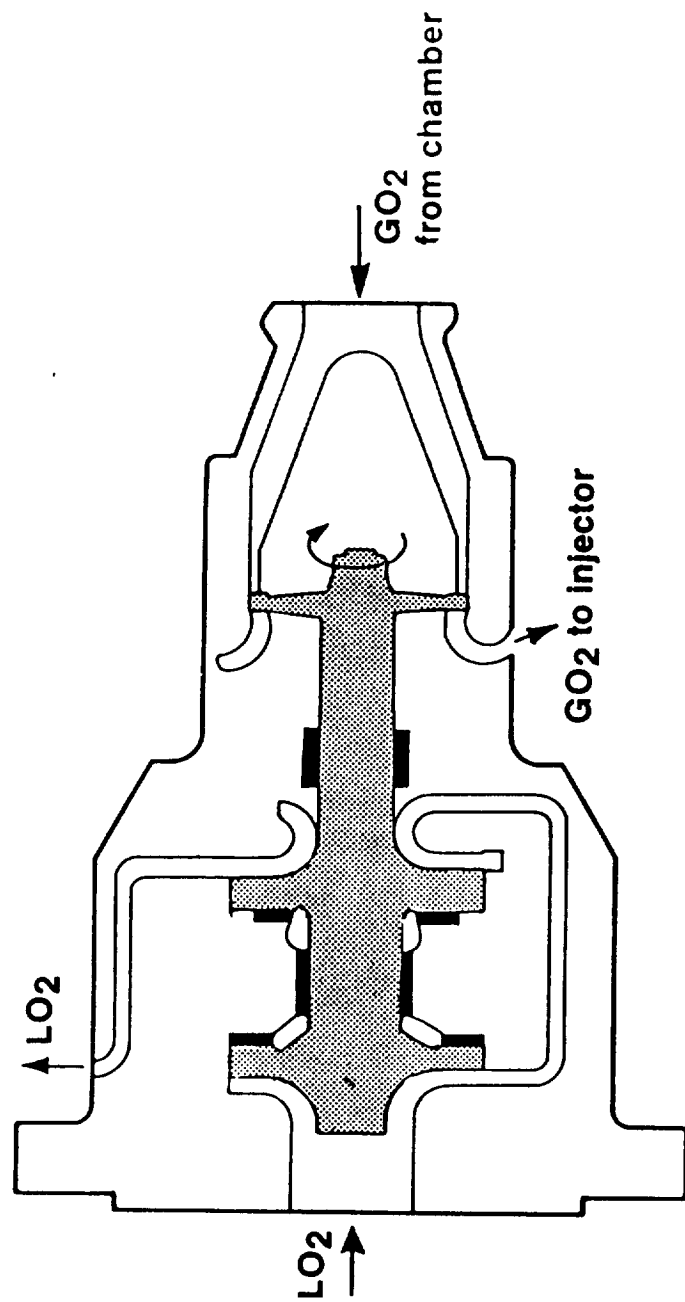


Figure 4. Schematic Design Approach to Gaseous Oxygen-Driven Liquid Oxygen Pump for Dual-Propellant Expander Cycle Engine

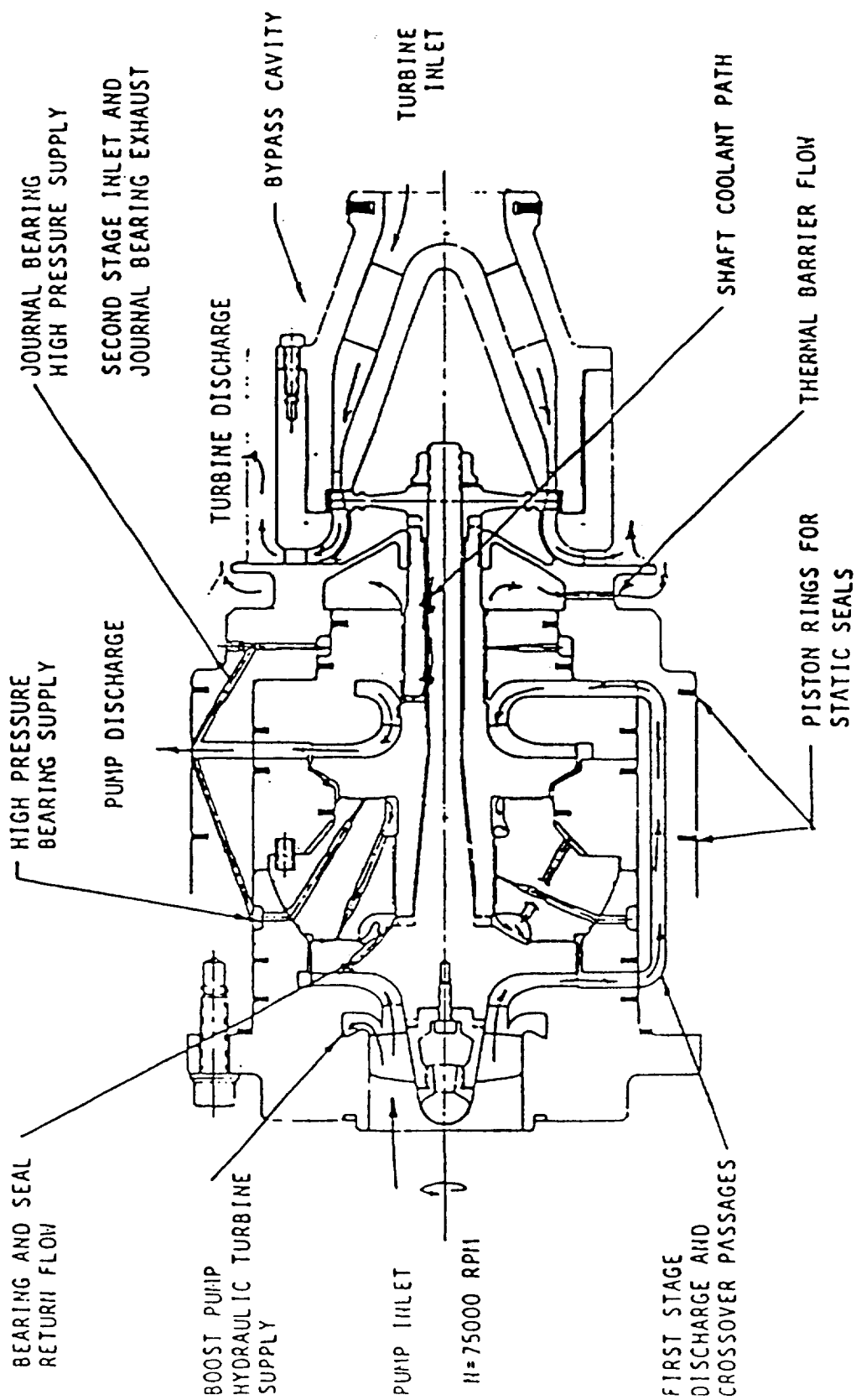


Figure 5. Advanced Turbopump Flow Paths and Seal Locations

ORIGINAL PAGE IS
OF POOR QUALITY

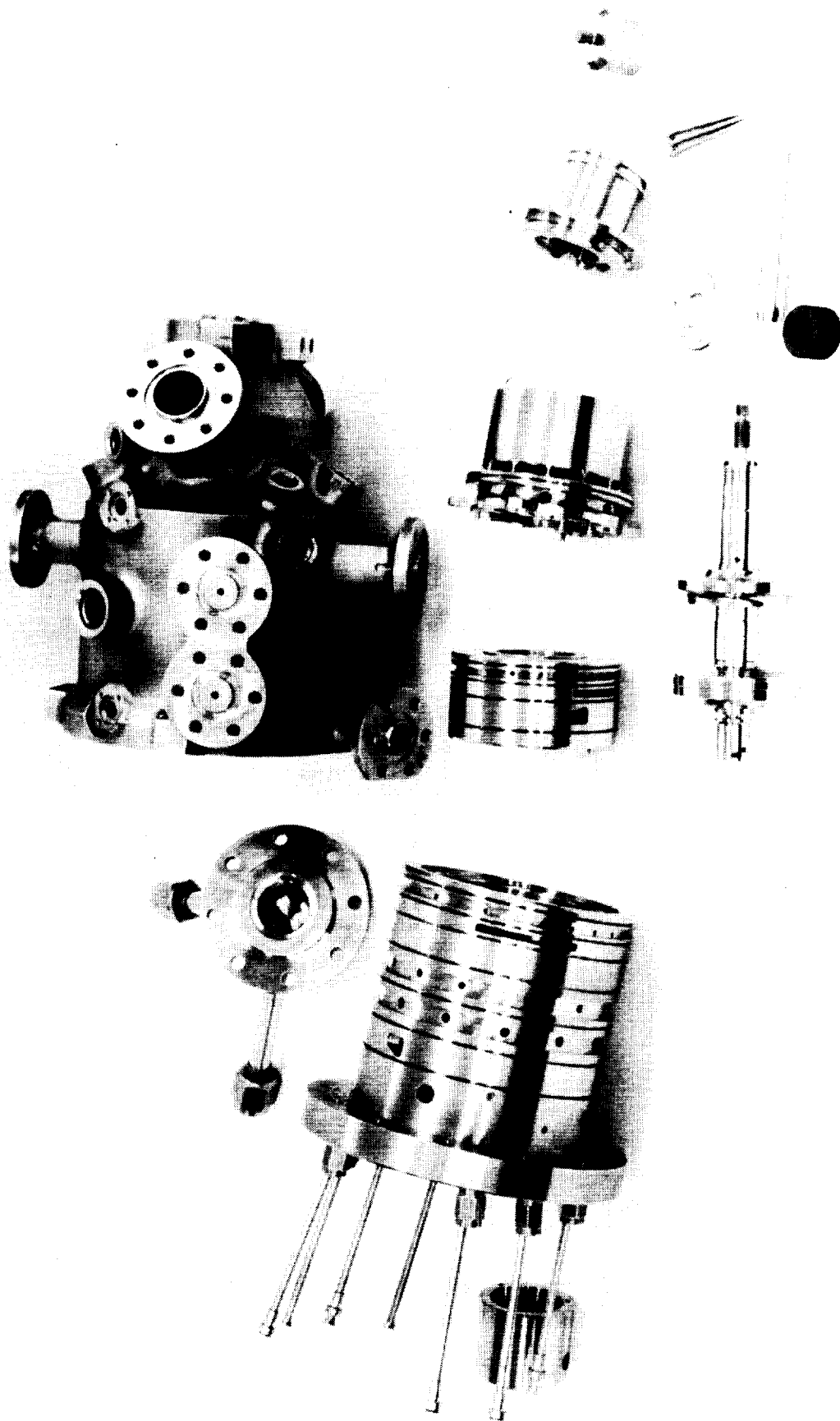
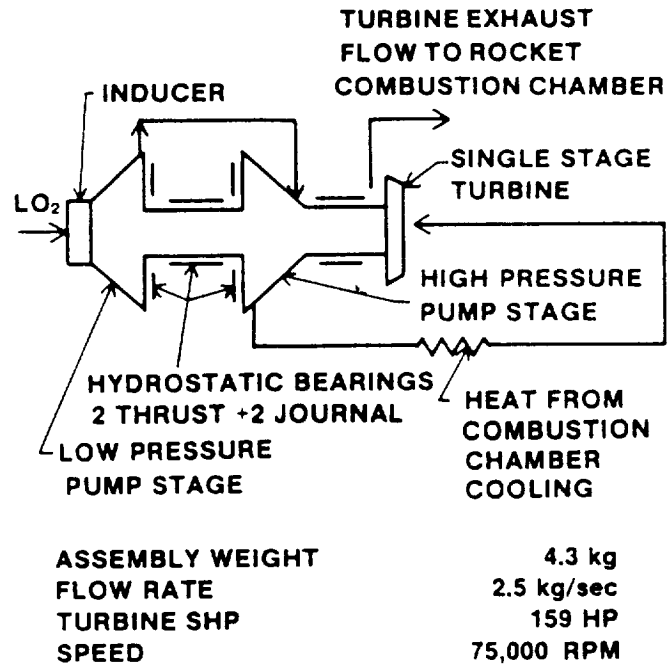


Figure 6. Oxidizer Turbopump Components Fabricated from Monel K-500 and Monel 400



	PUMP	TURBINE
O ₂ INLET TEMPERATURE (K)	89	478
O ₂ INLET PRESSURE (ATM)	2	306
O ₂ DISCHARGE PRESSURE (ATM)	313	163

Figure 7. Advanced Rocket Engine Oxygen Turbopump Design Parameters

I, Introduction (cont.)

The hazards of metal ignition and burning are the subject for this investigation. The materials ignition hazards associated with the use of warm GO_2 in rotating machinery are as follows:

Adiabatic Compression

Mechanical Rub

- Thermal Growth
 - Bearings
 - Turbine Tip
- Bearing Failures
- Startup and Shutdown Transients

Debris

- Impact of Foreign Materials
- Rubbing of Foreign Materials

From well documented oxygen fire experience, it is quite apparent that proper material selection, as well as design, is a key factor in demonstrating the concept feasibility.

II. PROGRAM TASK OBJECTIVES

The experimental program had multiple objectives. The initial objectives were to create a data base for metal ignition thresholds under conditions which simulated the OTV bearing and turbine environment. The experimental parameters included oxygen pressure, and temperature, surface rubbing, and high speed oxygen flow with entrained contamination particles. The use of analytical parameters to pre-define the relative goodness of candidate materials was also a primary objective.

As the experimental project evolved, and data were examined, additional objectives were incorporated. One was to develop a plausible explanation for the observation that certain metals became much more difficult to ignite in friction heating when the oxygen pressure increased while others showed little benefit. Another was to determine if surface modification of the selected turbopump material (Monel K-500) could be used to reduce the friction heating and the wear rates and if the in situ formation of natural oxide lubricants could be used to advantage.

III. DATA BASE

A large number of experimental material ignition studies in oxygen have been conducted. Dean & Thompson⁸ investigated the ignition and subsequent burning of 19 materials in oxygen at pressures between 3.4 and 54 ATM (50 and 800 psia) using electrically heated tubes. In these tests most materials could be heated to temperatures approaching their melting points before ignition took place. The data suggested that many but not all of the materials were more susceptible to ignition as the pressure increased, and once ignited, experienced higher burning rates. These early data identified the more common iron based alloys to be more ignition prone than the nickel base alloys.

Monroe & Bates^{9,10} also conducted electrically heated tests on similar materials in oxygen at pressure between 17 and 68 ATM (250 and 1000 psia). In contrast to the earlier work, these experiments forced a sample rupture which simulated a compressor mechanical failure. The rupture introduced two additional variables: one was the exposure of fresh metal unprotected by an existing oxide film, the second was the external energy applied at the fracture surface. The environmental temperature at which ignition was reported is significantly different for the two test methods as shown in Figure 8 for 304 stainless steel. Bates reported ignition at temperatures as low as 533°K (500°F) when specimens ruptured in 54 ATM (800 psi) O₂ while Dean reported that ignition did not occur until nearly the material melting point $\approx 1533^{\circ}\text{K}$ (2300°F). Neither reference provided data at the higher OTV operating pressures.

Even more recently, Bransford¹¹ heated aluminum in oxygen using a laser heat source with care given not to disturb the oxide film on the molten aluminum surface. Bransford was able to raise the aluminum surface temperature to 1930°K (3500°F) prior to experiencing ignition. This compares with 802°K (1100°F) for Dean and under 449°K (350°F) for Bates using their respective test method. Based on these reported test results, it can be postulated with a reasonable level of confidence that the presence and nature of the surface oxide are factors which must be accounted for in selecting a test method and ignition criteria.

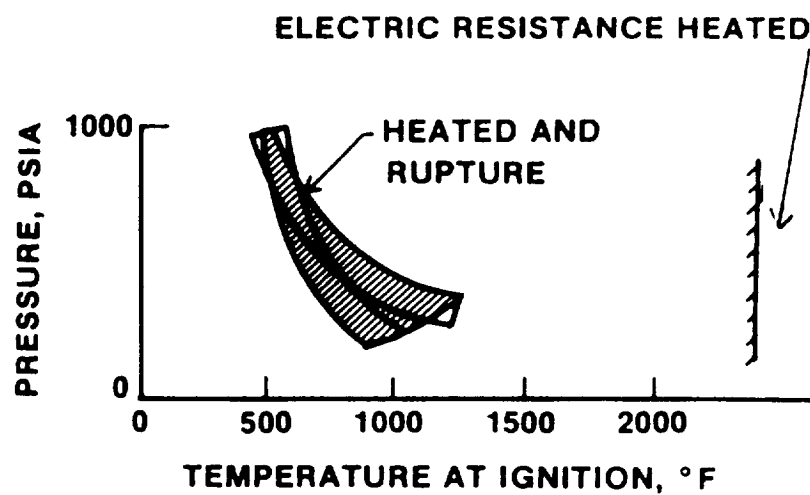


Figure 8. Comparison of Ignition Temperatures of 304 Stainless Steel in Heated Oxygen Gas at High Pressure as Determined by Resistance Heating With and Without Rupture

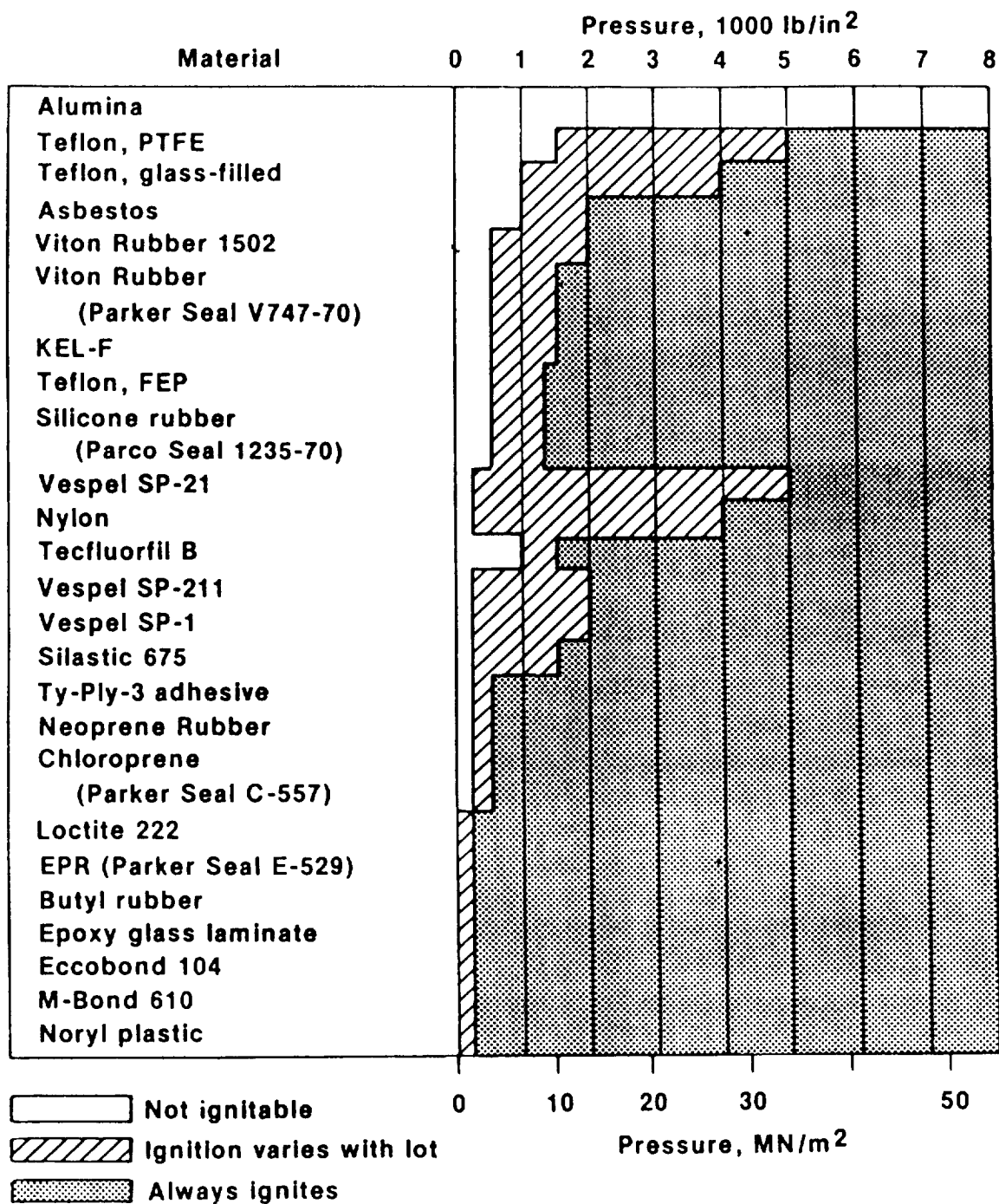
III, Data Base (cont.)

The early work identified the most common iron-based alloys and stainless steels to be much more prone to ignition and rapid burning than the nickel-based alloys. Pure nickel appeared to provide exceptionally good resistance to ignition. These tests, however, did not simulate the dynamic environments of high-speed turbines, pumps, bearings, and seals.

In the subsequent years a large data base has been accumulated by the Compressed Gas Association, the NASA and subcontractors in support of the Apollo Mission and by a recently formed ASTM sponsored G-4 committee for compatibility and sensitivity of materials in oxygen enriched atmospheres.

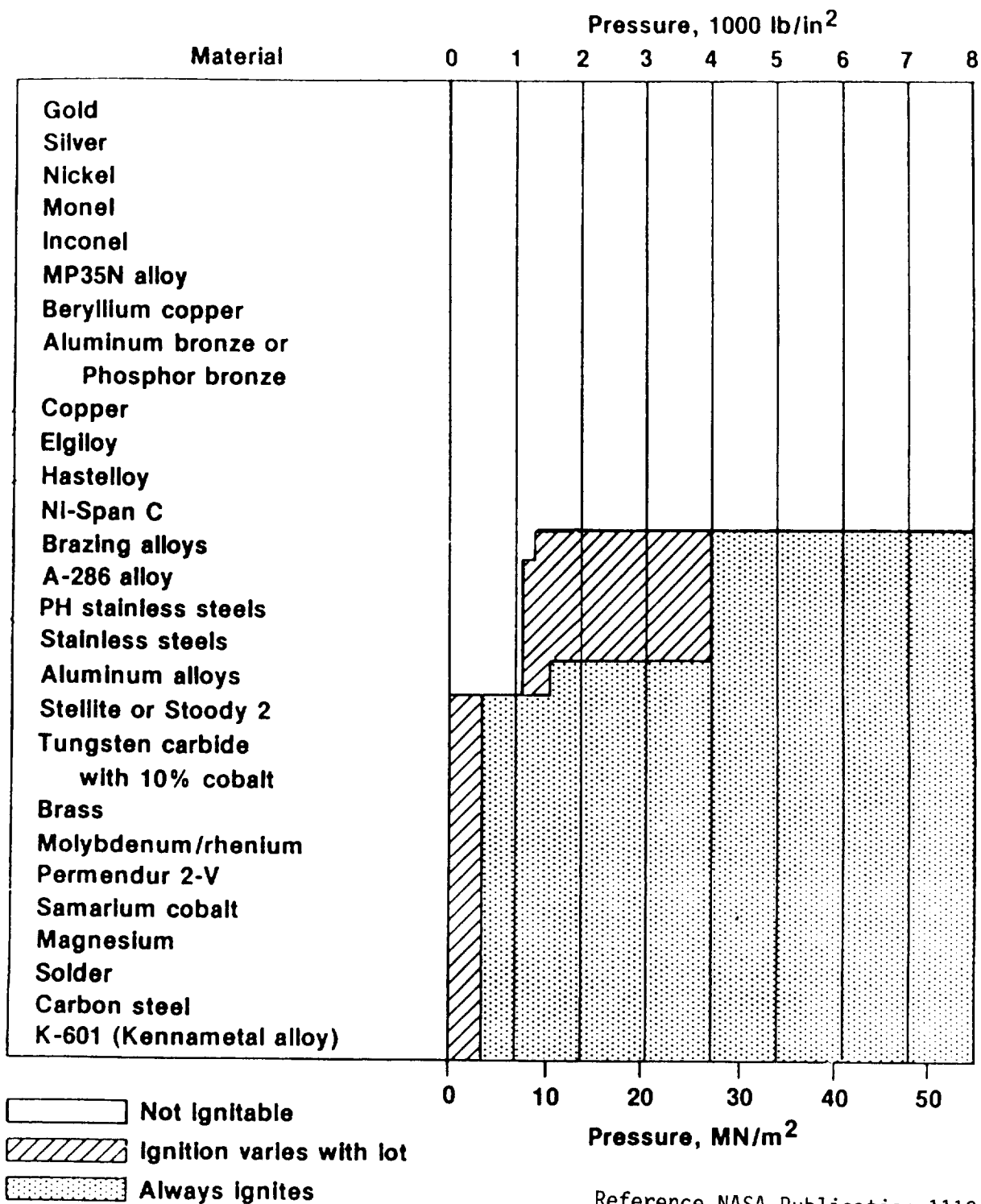
Figures 9 and 10 reproduced from a 1983 NASA Ref. Publication 1113 "Design Guide for High Pressure Oxygen Systems" summarize the material experience base. These two figures indicate range of ignitability for the most common non-metallics and metals respectively. First it should be noted that all non-metallics listed with the exception of the metal oxides such as Alumina, have the potential to ignite in oxygen at pressures which are low compared to the operational requirements of the OTV engine. Since the conditions under which these non-metallics can ignite are configuration sensitive, environment sensitive and application sensitive as well as material batch sensitive; the first OTV engine design ground rule was "No Soft Seal Materials will be Allowed."

Referring to Figure 10, which provides only a brief list of common engineering metals, it can be seen that nearly half are unacceptable at OTV operating pressures 34 MPa (5000 psi). Even metals which were previously considered acceptable such as Aluminum bronze have been downgraded based on data generated after 1983. Unacceptable metals include stainless steel and aluminum alloys that are in common use in oxygen systems. A simple yes/no criteria for metal selection is known to be inadequate as the ignition thresholds have been demonstrated to be application sensitive. It is known that data obtained by static heating of metals in high pressure oxygen will understate the true ignition hazard, and thus additional testing under simulated dynamic environments is required.



Reference NASA Publication 1113

Figure 9. Range of Ignitability for Nonmetallics



Reference NASA Publication 1113

Figure 10. Range of Ignitability for Metals

IV. TURBOPUMP AND TEST MATERIAL SELECTION

The primary criteria for material selection for a rocket engine turbopump are generally structural margin, high cycle fatigue and material density. In the case of a high pressure cryogenic pump requiring close clearance bearings and turbine tips, thermal expansion coefficient and modulus of elasticity become additional factors. In the case of an oxygen pump, the resistance to ignition must also be included. Table I and Figure 11 itemize some candidate materials that were suggested for use in an advanced oxygen pump. Inconel 718 is most commonly selected because of its high strength and good ductility at cryogenic temperatures.

In order for ignition to occur three things are required; a fuel, an oxidizer and an ignition source. The turbopump material is the fuel and the ignition source is the energy contained in the high speed rotational parts and in the high velocity high pressure oxygen. The present approach to the design/material selection is to remove as much of the energy contained in the fuel as possible and to preclude the conversion of kinetic and potential energy to concentrated thermal energy at local spots subject to rubbing or impact. The additional material physical properties of interest in oxygen applications are therefore; heat of combustion, thermal conductivity or diffusivity, melting and ignition temperatures.

Table II from Ref. 12 overviews the heat of combustion of many common engineering materials. The metals that appear on the bottom of the list will be preferred as they represent very poor fuels. From a practical/engineering viewpoint gold, silver, platinum, etc. in addition to being high cost, are structurally inadequate and heavy.

Moving up to the list one finds copper and nickel and their alloys highly attractive. The iron and chrome containing stainless steel alloys in common use in oxygen systems are much less attractive.

Several different approaches have been suggested for combining the heat of combustion, the thermal conductivity and the material melting point into a single parameter which will allow ranking of metals for use in oxygen service.

Table I. Materials Selection Matrix

Alloy	Composition	Burn Factor	Strength, ksi 800°R	Ductile/Brittle Transition Temperature	Oxidation** Resistance	Coefficient Expansion*	Typical Use and Reason
Silver	99 Ag	2	8	None	Fair	10.9	Bearings low friction
Nickel 201	99 Ni	550	11A	None	Good	8.5	Not in common use low strength
Zr-Cu	99.8 Cu .2 Zr	35	45	None	Poor	18.4 (1200°R), TBD (140°R)	Not in common use
Monel 400	BAL Ni 31.5 Cu Mn 2	1390	40 to 100	None	Good	8.9 (1200°R), 6.1 (140°R)	Fire brakes not in common use
Monel K-500	BAL Ni 29.5 Cu 2.7 Al .6 Ti	2090	105	None	Good	8.5 (1200°R), 6.2 (140°R)	Fire brakes when higher strength is required
Duranickel 301	95 Ni 4.4 Al .6 Ti	2900	120	None	Good	N/A	Not in common use
CRES 316	BAL Fe 17 Cr 12 Ni 3 Mo	4515	33	None	Good	9.3 (1200°R), 7.2 (140°R)	Low cost structural material
Invar	64 Fe 36 Ni	5444	N/A	None	Poor	3.5 (1200°R), .9 (140°R)	Low expander coefficient
Hastalloy X	BAL Ni 22 Cr 18 Fe 9 Mo	7160	50	None	Excellent	8.3 (1200°R)	Oxidation resistant
CRES 440	BAL Fe 17 Cr 2 Mn/Si	2783	55	0°F	Good	11 (1200°R)	Bearings, wear resistance
Graphite	Carbon	5156	-	None	Poor	.2 (800°F), .1 (-320°F)	
SiC	-	1145	-	None	Good	.6 (800°F), .5 (-320°F)	Bearings low friction
Inc 600	76 Ni 8 Fe 15 Cr	3226	80	None	Good	8.5	
Inc 718	52 Ni 18 Fe 19 Cr 8 TA MoCb	4600	147	None	Good	7.8	Structural housing high strength

As determined by Gluzek, et al B.F. = $\frac{\Delta H_f}{\text{Therm Diff.}}$ for 100g samples
Typical Fty (ksi)

*10⁻⁶ in./in./°F

**Est. for 4000 psi oxygen at 1200°R

N/A - Not Available

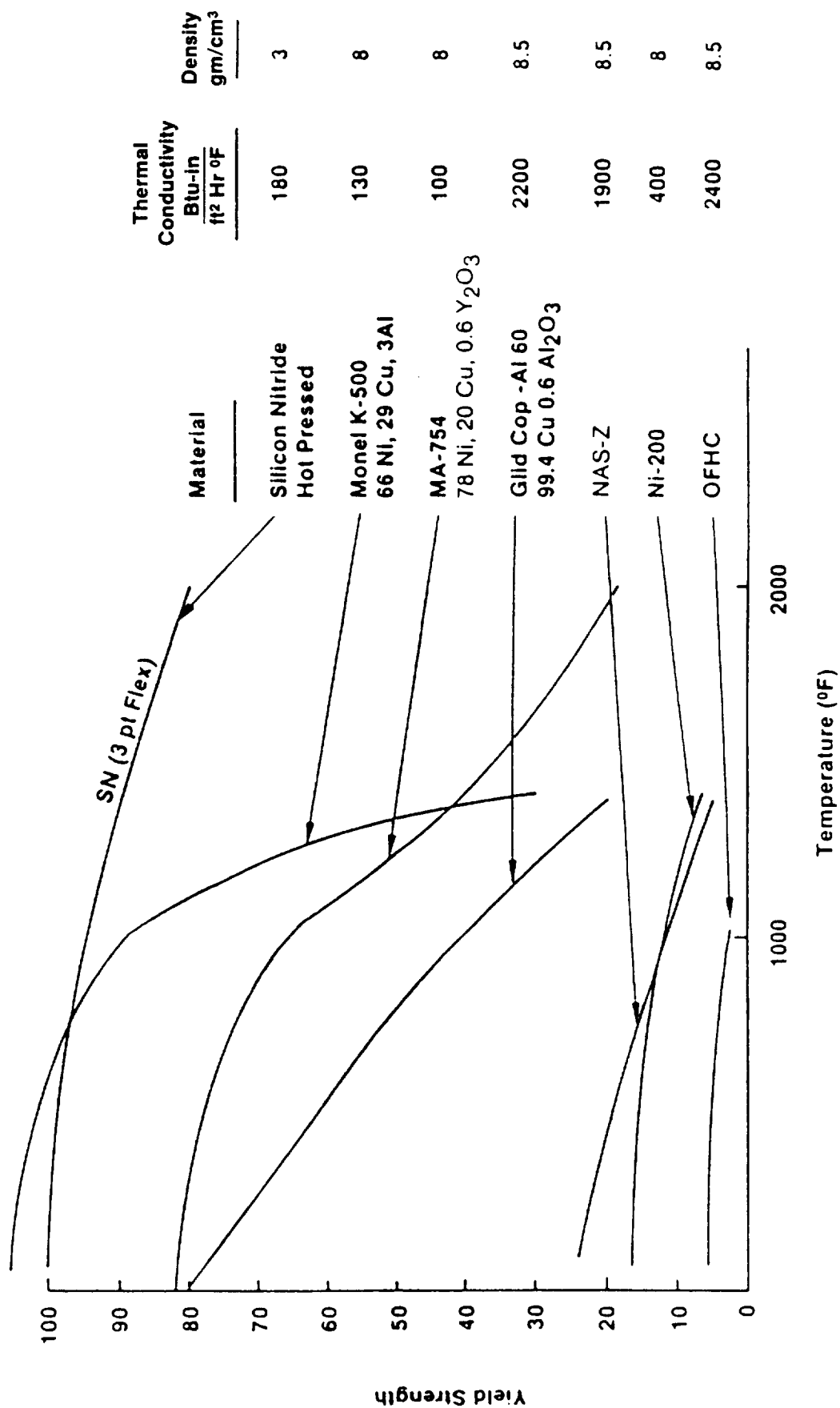


Figure 11. Structural and Thermal Properties of Materials for Use in Oxygen

ORIGINAL PAGE IS
OF POOR QUALITY

Table II. Heat of Combustion of Metals and Alloys

<u>Material (Oxide Formed)</u>	<u>$-\Delta H_c$, cal/g^a</u>	<u>$-\Delta H_c$, cal/cc^b</u>
Beryllium (BeO)	15,865	29,350
Aluminum (Al ₂ O ₃)	7,425	20,062
Magnesium (MgO)	5,900	10,266
Titanium (TiO ₂)	4,710	21,195
Chromium (Cr ₂ O ₃)	2,600	18,720
Ferritic and Martensitic Stainless Steels	1,900-2,000	14,726-15,500
Austenitic Stainless Steels	1,850-1,900	14,850-15,251
Precipitation Hardening Stainless Steels	1,850-1,950	14,390-15,167
Carbon Steels	1,765-1,800	13,872-14,147
Iron (Fe ₂ O ₃)	1,765	13,872
Manganese	1,673 ^d	~12,200
Molybdenum	1,458 ^d	14,900
Inconel 600 ^e	1,300	10,960
Aluminum Bronzes	1,100-1,400	8,250-10,500
Zinc (ZnO)	1,270	9,068
Tin (SnO ₂)	1,170	7,628-8,517
Tungsten (WO ₃ , Assumed)	1,093 ^c	21,094
Cobalt (CoO) ^e	970 ^e	8,633
Nickel (NiO)	980	8,722
Monel 400 ^e	870	7,682
Yellow Brass, 60 Cu/40 Zn	825	6,914
Cartridge Brass, 70 Cu/30 Zn	790	6,615
Red Brass, 85 Cu/15 Zn	690	5,966
Bronze, 10 Sn/2 Zn	655	5,751
Copper (CuO)	585	5,218
Cadmium (CdO)	541 ^c	4,679
Lead (PbO)	250	2,837
Palladium (PdO)	192 ^c	2,308
Platinum (PtO ₂)	164 ^{c,e}	3,520
Silver (Ag ₂ O)	35	368
Gold	1.9 ^d	37

^a 1 cal/g = 4.186 kJ/kg. Except as noted, from Lowrie (9).

^b Calculated from $-\Delta H_c \cdot \text{density}$. 1 cal/cc = 4.186 J/cc

^c Heat of formation from Weast (10) and converted to Cal/g.

^d From Hust and Clark (15).

^e From Grosse and Conway (1).

Source, Reference 12

IV, Turbopump and Test Material Selection (cont.)

Bates¹⁰ proposed a simple analytical parameter, defined as the material burn factor, to identify the ignition potential of a material. Most simply stated, the burn factor is the heat of formation of the most stable oxide of the material, divided by the material's heat absorption capability, expressed as follows:

$$DBF_{mp} = (\Delta H^{\circ}_f \text{ (metal oxide 298}^{\circ}/\Delta H_{298-MP} + \Delta H_{\text{fusion}} \text{ (MP)})$$

where ΔH°_f is the heat of formation of the oxide, ΔH_{298-MP} is the heat capacity of the metal between ambient temperature and the melting point, and ΔH_{fusion} is the heat required to melt the metal.

Subsequent work by Gluzek¹³, defined a modified burn factor expressed as the heat of formation of the most stable oxide of the material, divided by the material's heat dissipation capability, expressed as follows:

$$B_F = \frac{\Delta H^{\circ}_f}{\alpha} = \frac{\text{heat of oxidation}}{\text{thermal diffusivity}}$$

where

$$\Delta H^{\circ}_f = \frac{\text{Kg-Cal}}{100 \text{ gms alloy}}$$

$$\alpha = \text{cm}^2/\text{sec}$$

Comparison of the metals ranking, using the different burn factor calculations, showed reasonable overall agreement, as indicated in Table III. Notable exceptions are the relative position of aluminum and nickel. However it was not obvious that either of these analytical parameters were valid for use in a friction heating or particle impact operating environment.

IV, Turbopump and Test Material Selection (cont.)

Table III. Burn Factor Ranking of Typical Materials

	<u>Dynamic Burn Factor Bates (Ref. 10)</u>	<u>α Burn Factor Gluzek (Ref. 13)</u>
Best	Silver	Silver
	Copper	Copper
	Monel 400	Nickel
	Monel K 500	Aluminum
	Nickel	Monel 400
	Iron	Iron
	410 SS	Monel K 500
	304 SS	410 SS
Poorest	Aluminum	304 SS

The materials for this test program, as shown in Table IV, were selected to provide a wide range of burn factors for candidate turbine and pump materials so that the test results could be correlated with the predictive method. The thermal diffusivity based B_F was selected because it more nearly matched the test results of Ref. 8 in terms of burning rate rank order. However, it is expected that test methods representing different operating hazards could provide a different ranking of materials such that more than one analytical ranking parameter will be required.

Table IV. Candidate Materials Tested

<u>USN Designation</u>	<u>Common Name</u>	<u>Burn* Factor</u>
C 15000	Zirconium Copper	35
N 02200	Nickel 200	550
	Silicon Carbide	1145
N 04400	Monel 400	1390
N 05500	Monel K 500	2090
N 06600	Inconel 600	3226
S 31651	316 Stainless Steel	4515
K 93601	Invar	5444
N 06002	Hastelloy X	7160

* a $\frac{\Delta H_f^0}{\alpha} \frac{\text{Cal-S}}{\text{g-cm}^2}$

V. TEST METHODS

A. SELECTION

Numerous test methods are available for ranking the ignition threshold of materials in oxygen. Figure 12 from Ref. 14 defines the available options. The test method has been shown to play a significant roll in defining the material ignition threshold which is a function of time dependent energy input and physical forces acting on the surface where the energy is being applied.

Since precise analytical models are not available, it is essential that the selected test method reproduce both the heating and dynamic forces expected in actual application. All forms of static testing were therefore considered unacceptable for the present application in which particle impacts and friction induced heating represents the most likely failure mode of the turbopump.

B. TEST SYSTEM DESCRIPTION

Two types of tests were selected to evaluate materials and operating hazards. The first was the high velocity particle impact test to simulate solid particle contamination within the hot high speed O_2 flow portion of the turbine. The second was a friction heating test that simulated a turbine tip rub or a bearing rub during a start or shutdown transient or loss of bearing coolant.

All testing was conducted at the NASA White Sands Test Facility.

1. Particle Impact Test (PIT)

The PIT test system consists of a 2-in.-dia (OD), 3-1/2-in.-long monel chamber connected to a high-flow, high-pressure, high-temperature GO_2 supply. The test chamber assembly shown in Figures 13, 14 and 15, contains an upper cylindrical cavity which is 3/4 in. in diameter and 1 in.

ASTM-G63

- CALORIMETER TEST
- UNPRESSURIZED LIQUID OXYGEN
COMPATABILITY MECHANICAL IMPACT TEST
- LIMITING OXYGEN INDEX TEST
- AUTOGENEOUS IGNITION TEMPERATURE TEST
- GASEOUS FLUID IMPACT TEST
- PRESSURIZED MECHANICAL IMPACT TEST
- FRICTION RUBBING TEST
- PARTICLE IMPACT TEST
- PROMOTED IGNITION TEST
- ELECTRIC ARC TEST

OTHER TEST METHODS

- LASER HEATING
- RESONANCE CAVITY HEATING

Figure 12. Test Methods for Material Ignition in Oxygen

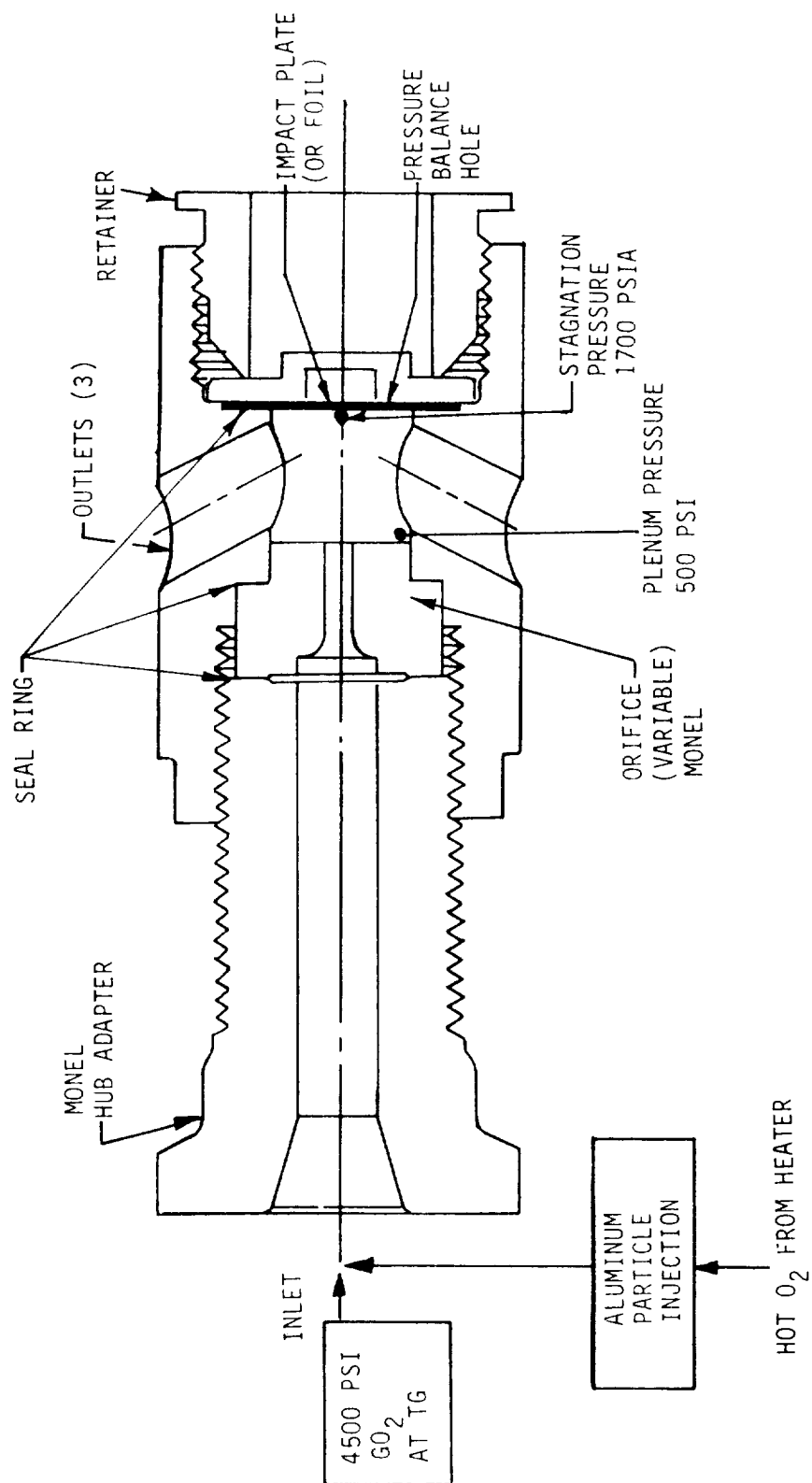


Figure 13. Schematic of Particle Impact Test Apparatus

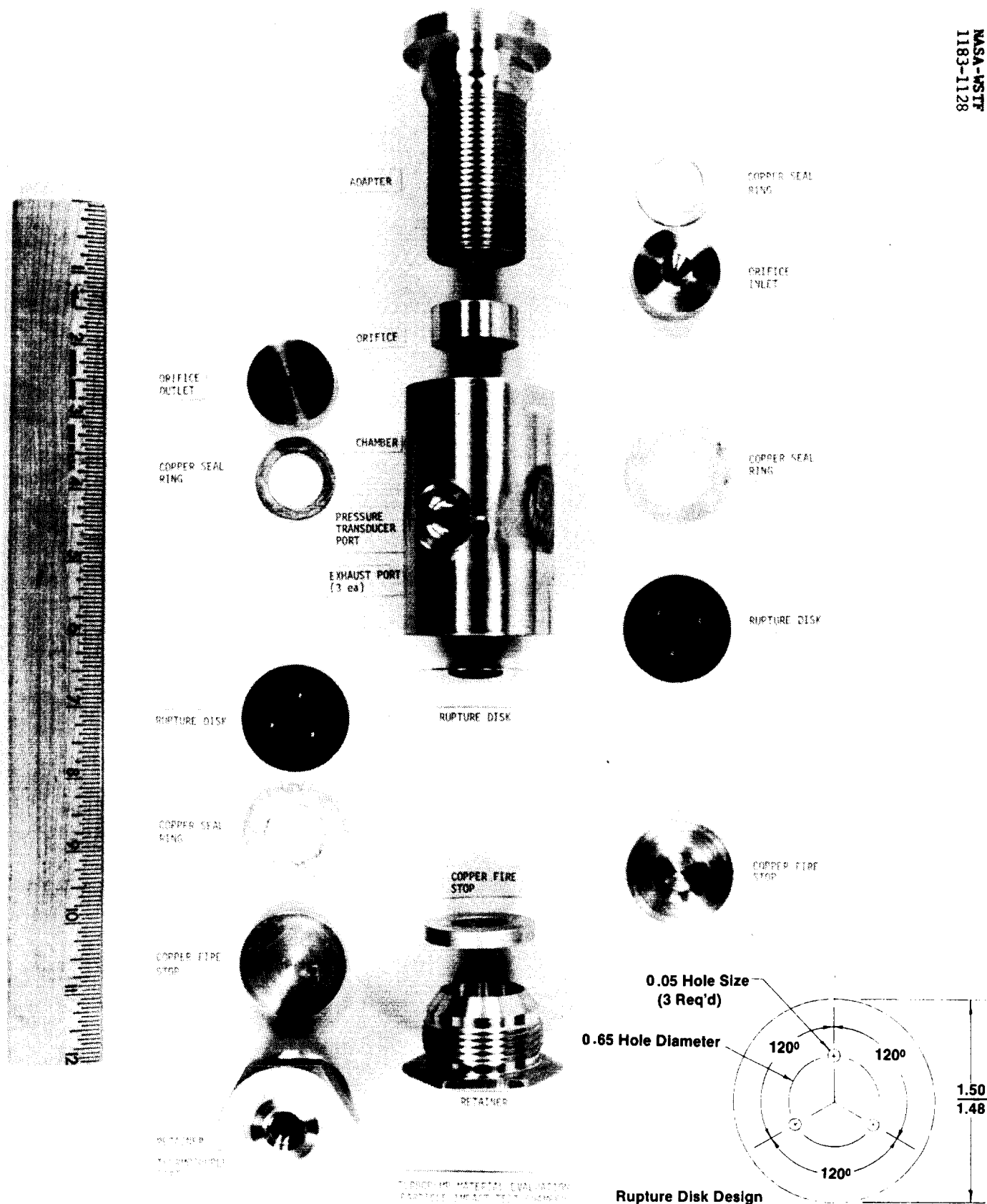


Figure 14. Particle Impact Test Assembly for Rupture Disk Evaluation

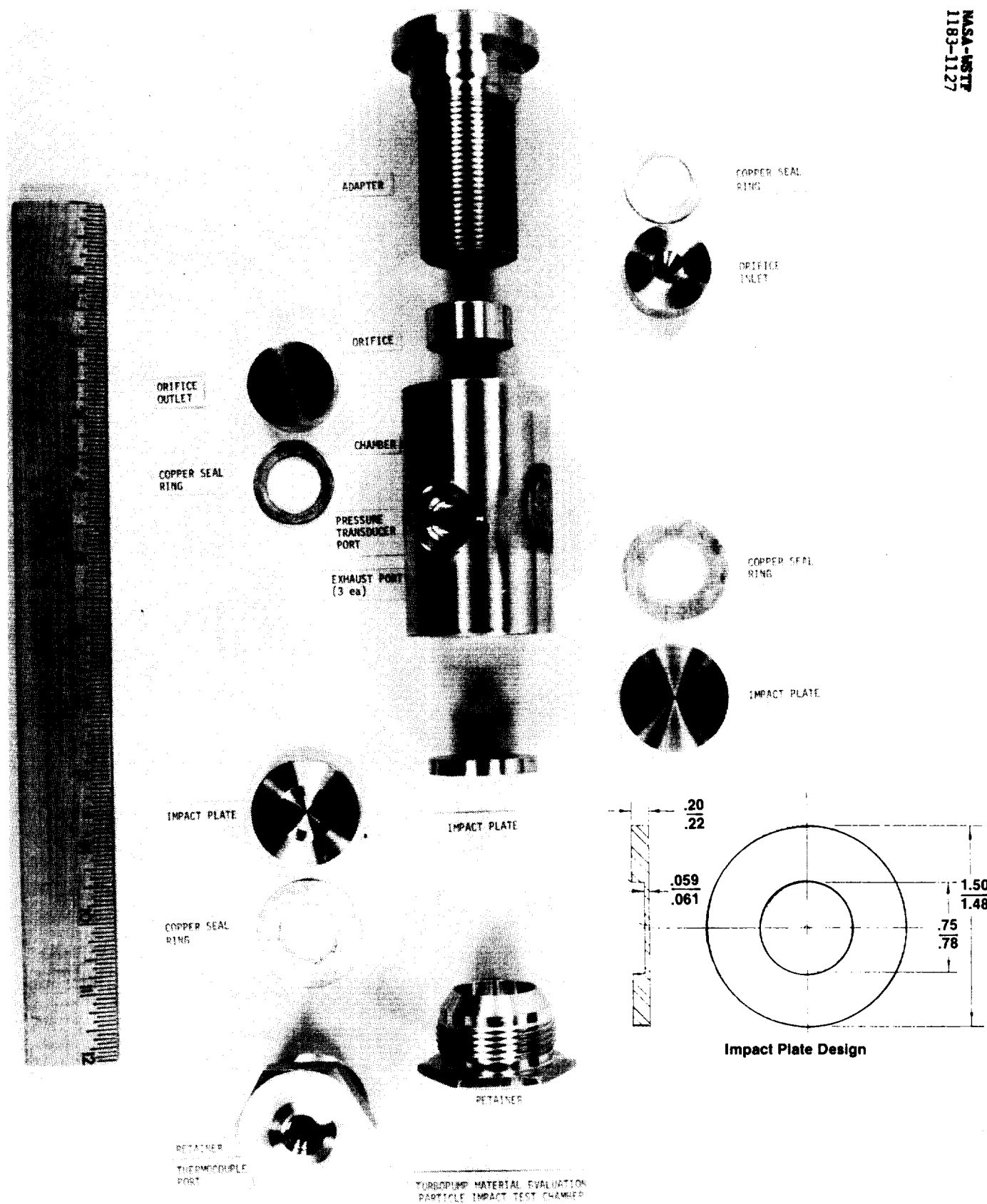


Figure 15. Particle Impact Test Assembly for Plate Impact Studies

ORIGINAL PAGE IS
OF POOR QUALITY

V, B, Test System Description (cont.)

long, an orifice assembly placed at the upstream end of the cylindrical cavity and a target impact plate (test sample) placed at the downstream side. Three gas exit ports are located symmetrically around the cavity. The orifice assembly, along with exit restrictions, are used to set the GO_2 flow rate and/or velocity into the cavity. The target plate and the cup-like backup support fixture are made of the sample material and are positioned perpendicular to the gas flow, as shown in Figure 13. The thickness of the disc depends on whether the disc is to be ruptured or act as a rigid impact plate when struck by the particles.

The gas supply system consists of storage vessels which contain 500 ft^3 of oxygen at 6000 psig. The oxygen supply is controlled by a dome-loaded regulator that maintains essentially constant pressure under the flow conditions. A natural gas-fired heat exchanger is located downstream of the dome-loaded regulator and is capable of heating oxygen up to approximately 800°F for 180-sec flow periods at 3 lbM/sec. The particle injector system is located downstream of the heat exchanger and uses the pressure difference between the flowing oxygen and the injector to insert the test particles into the gas stream.

The test system is instrumented as follows. Inlet chamber and cavity gas pressures are measured using bonded strain gauge pressure transducers. The inlet chamber and cavity oxygen temperatures are measured using various types of thermocouples, selected on the basis of test conditions and the particular test environment. The gas stagnation temperature and pressure at the impact point were measured and related to the supply conditions during calibration tests. Individual target test measurements were not made during subsequent tests.

The data from the instrumentation are recorded and stored using a system similar to that of the friction rubbing test discussed in a later section.

V, B, Test System Description (cont.)

The particle material and size used in the testing were based on the work of Porter¹⁵ who conducted screening tests of candidate particle materials and sizes. In this earlier program, the materials and particle sizes evaluated were selected based on sizes and types anticipated to be found in the Space Shuttle Main Engine propulsion system. This led to the selection of 2024 Aluminum, and Inconel 718 at the 150 and 800 micron level. The screening test data showed that aluminum and larger particle sizes provided the greatest probability of ignition up to the temperature limits of the previous test series of 550°F. The present program utilized 1580-micron aluminum alloy 2017-T4 particles propelled by 4500 psi O₂ at temperatures up to 800°F. The use of large aluminum particles are believed to represent a worst case condition for metallic particle impact. The impact, and burning of a single particle represents an energy release of 0.12 KJ or 5.9 KJ/cm² at the .02 cm² impact areas. In this test method ten such particles randomly strike the 2.85 cm² target surface area during each test. The calculated particle velocity at impact is 260 M/S (853-ft/s).

The test procedure involves the preheating of the test specimen for 30 sec with GO₂, followed by sequential injection of 10 particles of 2017-T4 aluminum of 1580 μm diameter. Temperature data from the calibration run established the preheat time. The calibration measurements revealed a standing shock wave ahead of the impact plate. A stagnation pressure of 1700 psia was measured when the pressure upstream of the nozzle reached 4500 psi. The downstream plenum pressure was 500 psia, as illustrated in Figure 13. Temperatures at the impact plate typically run 40 to 70°F higher than the stream temperatures measured in the upstream flow.

In this test method the temperature of the GO₂ is increased in each sequential test up to the facility limits of 800°F or until a condition of metal ignition on impact is detected.

V, B, Test System Description (cont.)

Particle impact testing was conducted on two types of targets; thick plates which simulate rigid structures such as the turbopump or valve housings and, and thin rupture discs which better simulate the thin leading and trailing edges of turbine blades or vanes. Figures 14 and 15 show the details of the test targets.

2. Friction Heating Test Apparatus (FRT)

The WSTF frictional heating apparatus^{16,17} shown in Figure 16 can simulate failure modes caused by rubbing of hydrostatic bearings and turbine blade tips. The apparatus consists of a high-pressure test chamber, an electric motor and transmission assembly, and a pneumatic actuation cylinder. The high-pressure test chamber (Figure 17) consists of a cylindrical chamber with an outside diameter of 12.7 cm (6 in.) and an inside diameter of 3.8 cm (1.5 in.) and fabricated from Monel 400. The internal cavity of the chamber contains a replaceable copper sleeve and a gas cavity a volume of 49 cm³ (3 in.³). The chamber contains a rotating shaft that extends through the chamber attached at one end to the drive motor-transmission assembly and at the other end to the pneumatic actuation cylinder. The drive motor-transmission assembly is a 15 hp, constant speed electric motor, and a variable speed belt-driven transmission. The assembly provides the capability to rotate the shaft at speeds over a range from 3,000 to 17,000 RPM. The pneumatic actuation cylinder is pressurized with nitrogen and an actuation linkage provides axial movement of the shaft and the capability to apply normal loads of up to 3160 N (710 lbf) on the test samples.

Identical water cooled copper housing assemblies containing bearings and seals are attached to both ends of the chamber. Sealing of the high-pressure oxygen chamber is accomplished by mounting two seals on the rotating shaft in each housing on either side of a copper cooling block. Water under high pressure cools the seals and provides a back-pressure to the chamber pressure seals.

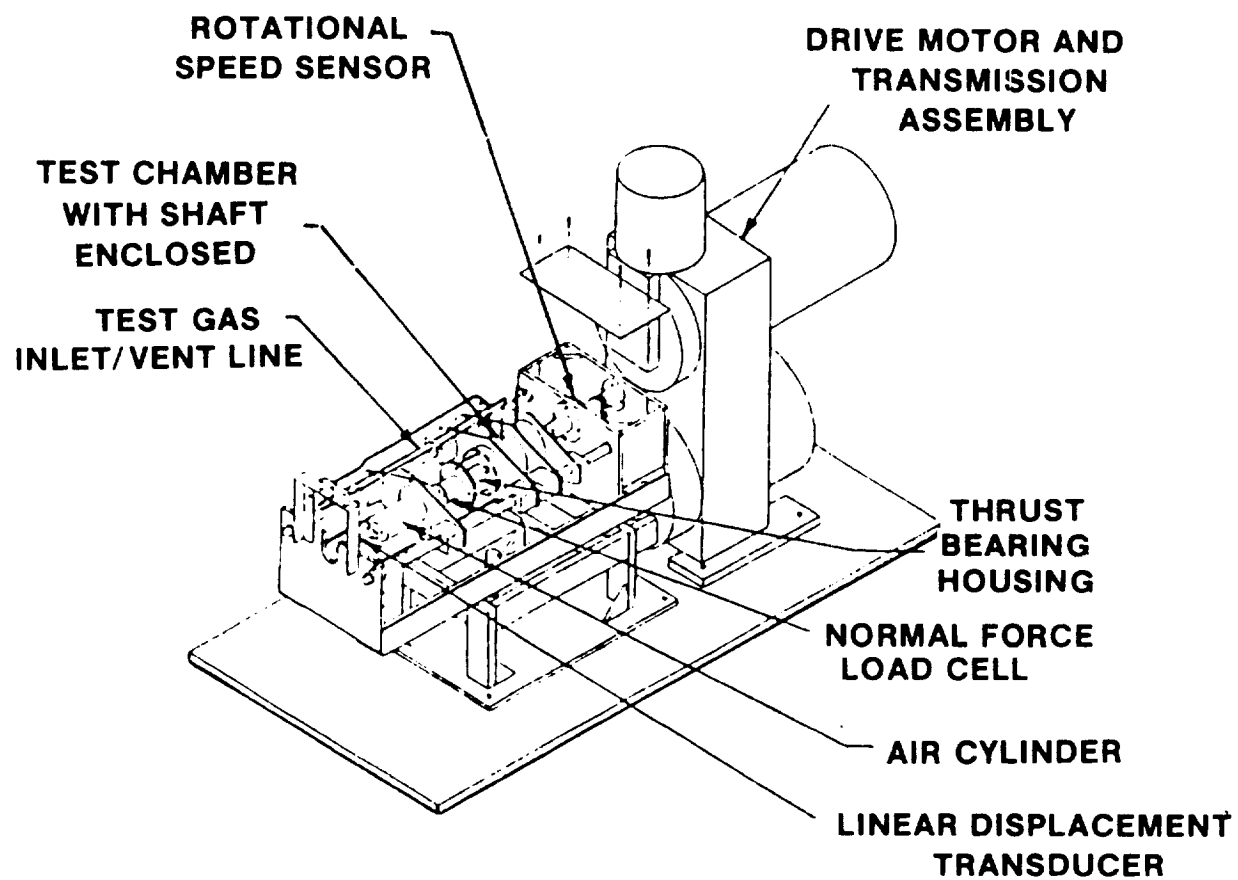


Figure 16. Frictional Heating Test Apparatus

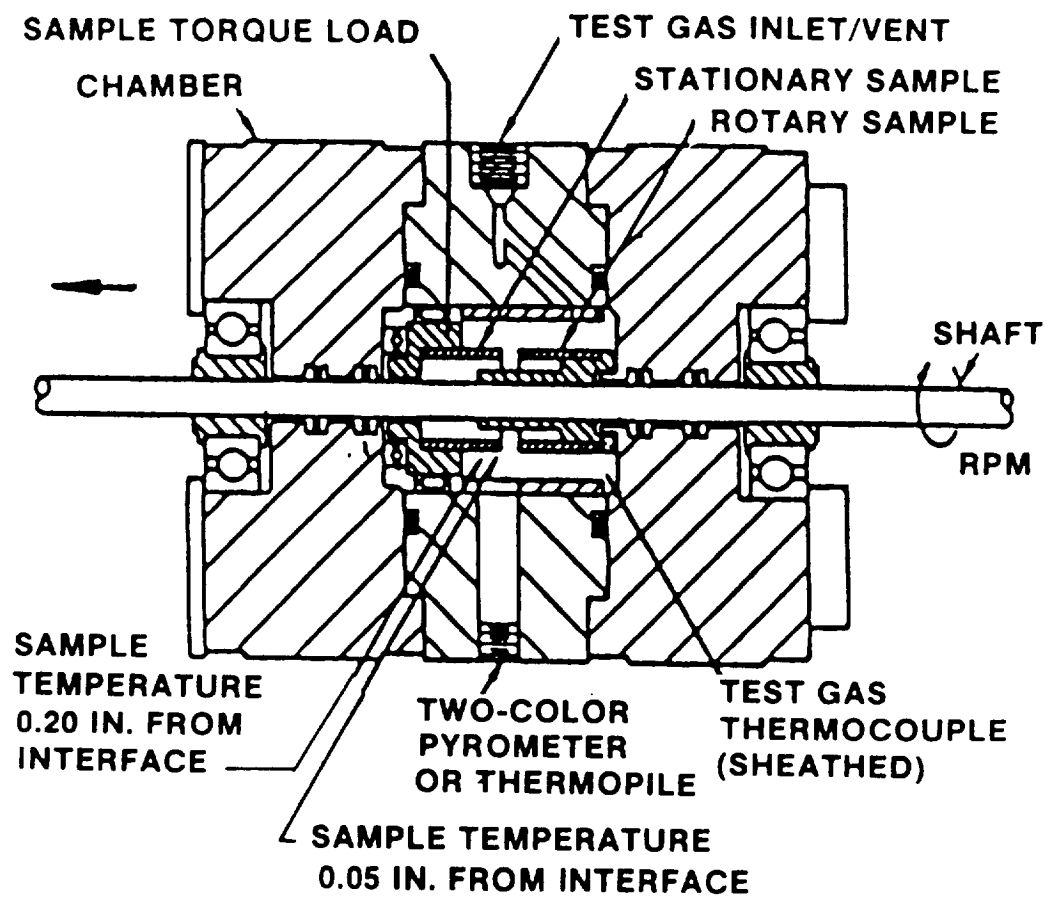


Figure 17. Friction Rubbing Test Chamber

V, B, Test System Description (cont.)

The metallic test samples provide a rubbing surface of 1.8 cm^2 (0.28 in.^2). One sample is mounted to the rotating shaft and the second sample is affixed to the chamber via a sample mounting housing. Contact of the two samples is accomplished by pulling the shaft and rotating sample against the fixed sample using the pneumatic actuation assembly. In the original design, the sample housing was attached directly to the chamber such that, as the samples rubbed, torque was applied to the entire chamber. Movement of the chamber was restrained by an extended arm, attached to the chamber at one end, and positioned against a load cell at the other end (Figure 18a).

During the course of the program, a more accurate torque measurement was required to support testing to determine the effect of varying oxygen pressure on frictional heating of the test samples. The method for measuring torque was changed by mounting the sample housing in a bearing which was attached to the chamber. Movement of the sample housing is now restrained by a pin positioned against a load cell (Figure 18b).

Oxygen or nitrogen are provided to the chamber via a high-pressure gas distribution system which interfaces to the WSTF high-pressure oxygen test facility. The system is capable of providing and regulating oxygen up to 68.9 MPa ($10,000 \text{ psia}$) and nitrogen up to 20.7 MPa (3000 psia).

The measured test parameters, instrumentation and range are defined as follows:

- a. Pressure in the gas chamber, digital Bourdon tube gauge
 $68.9 \pm 0.7 \text{ MPa}$ ($10,000 \text{ psia}$)
- b. Pressure in the pneumatic actuation cylinder, bonded strain gauge transducer $6.9 \pm 0.07 \text{ MPa}$ (1000 psia)

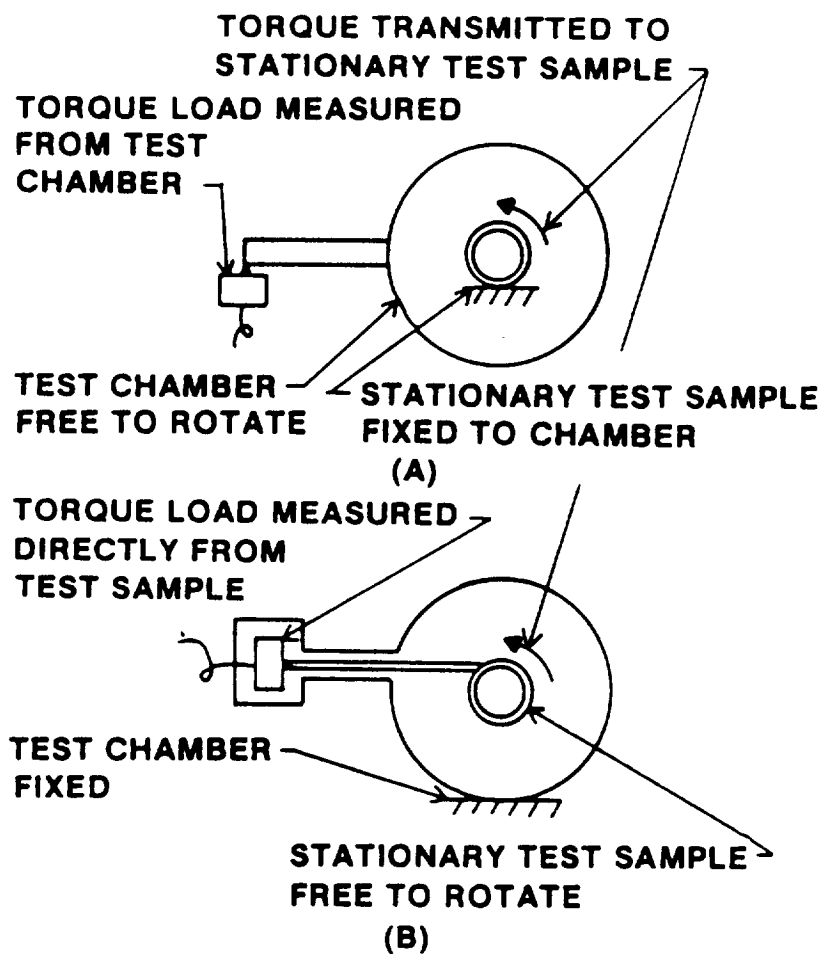


Figure 18. Torque Load Measurement as Made (A) In Original Frictional Heating Apparatus and (B) In Test Apparatus as Modified for the Pressure Study and All Subsequent Tests

V, B, Test System Description (cont.)

- c. Temperature oxygen/nitrogen gas, fixed specimen temperature at 0.13 and 0.51 cm (0.05 and 0.20 in.) from rubbing surface via .12 MM sheathed type K thermocouples ranged 273 to 1477°K (0-2200°F).

A noncalibrated fast response thermopile is employed to sense time phasing and relative intensity of the radiant energy at the rubbing interface. The output data is useful in detecting the time of ignition and thermal instabilities below 1200K. The applied normal load is measured by a 4450 ± 22 N (1000 lbf) load cell, and torque from the rubbing samples by 890 ± 5 N (202 lb) load cell. Axial displacement of the rotating shaft or sample wear is measured using a linear displacement transducer with an accuracy of ± 0.005 cm (0.002 in.). The rotational speed is sensed by a 0 to 20,000 RPM indicator having an accuracy of ± 3 percent of full speed.

The data were digitally processed by a microprocessor and stored on a floppy disk. Data from each instrumentation channel were stored every 100 ms and represented an average value of eight readings taken 8 ms prior to the stored value.

a. Test Sample Design Material and Preparation

The metal test specimens were machined from stock material into hollow cylinders with outside diameters of 2.5 cm (1 in.) and inside diameters of 2.0 cm (0.8 in.) as shown in Figure 19. Two thermocouple wells were drilled on the OD of the cylinder at a specified distance from the rubbing surface as indicated above. The ceramic specimens were prepared using proprietary procedures employed by the suppliers and were supplied in the configuration shown in the figure. The samples were washed with a sodium hydroxide solution, then with a phosphoric acid solution and, finally, with an emulsion agent. The samples were rinsed with isopropyl alcohol and then Freon 113, dried with nitrogen and sealed individually in Teflon bags. Figure 20 summarizes the materials and material combinations employed in the various friction heating tests.

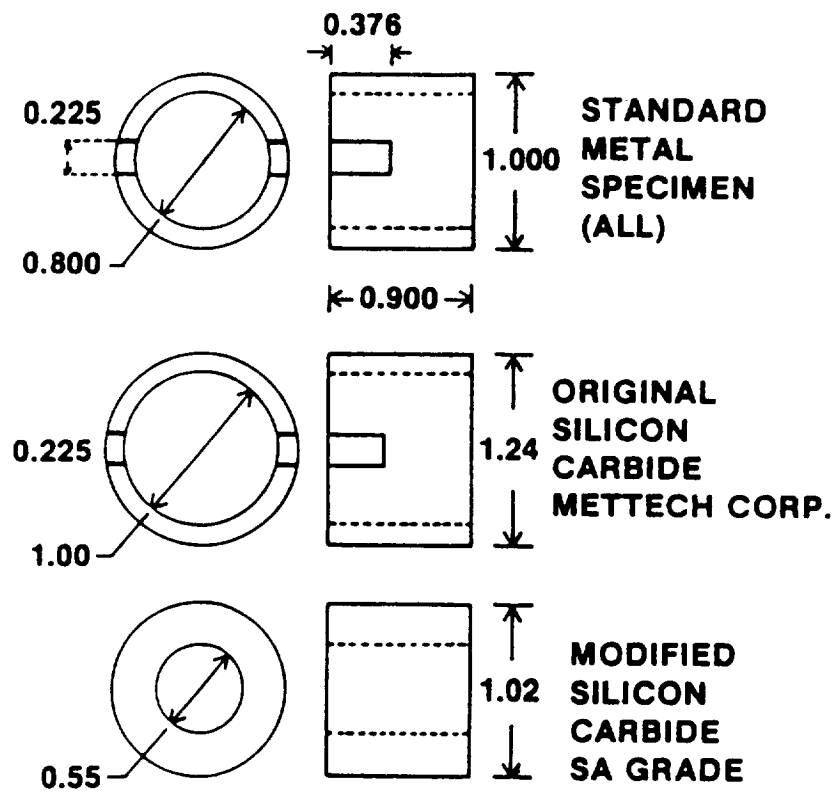


Figure 19. Friction Rubbing Test Specimen Configurations

A LIKE MATERIALS TESTED IN O₂

MATERIALS	BURN * FACTOR
Zr Cu (Cu 150)	35
Nickel 200	550
SILICON CARBIDE	1145
MONEL 400	1390
1015 CARBON STEEL	1400
MONEL K 500	2090
INCONEL 600	3226
316 STAINLESS STEEL	4515
INVAR-36	5444
HASTELLOY X	7160
* $\Delta H_f / \alpha$	α AT 70°F

B UNLIKE MATERIALS TESTED IN O₂

MATERIALS	BURN FACTOR
COPPER 150/316 STAINLESS STEEL	35/4515
NICKEL (ELECTRODEPOSITED)	
MONEL K-500	550/2090
MONEL-K500/316 STAINLESS STEEL	2090/4515
INVAR 36/SILICON CARBIDE	5444/1145
MONEL-K500/SILICON CARBIDE	2090/1145

C LIKE MATERIALS TESTED IN N₂

MATERIALS	BURN FACTOR
1015 CARBON STEEL	1400
MONEL K-500	2090
* Cal-S/g-cm ²	

Figure 20. Selected Material Test Combinations and Their Calculated Burn Factors

V, B, Test System Description (cont.)

The silicon carbide test specimen design was changed after the first test phase to eliminate the stress concentration produced by the drive notches and the wall thickness was increased as shown. Minor modifications to the rotating sample holder were made to allow the testing of the new silicon carbide specimen.

b. Test Procedures and Conditions

Several types of test procedures were employed. One procedure brought the specimens up to the desired rotational speed ± 200 RPM in the ambient temperature gas pressurized chamber without contact load. A ramped compressive stress was then applied at a rate of .14 MPa/sec (20 psi/sec) at the rubbing interface. The load continued to increase until one of the following events occurred.

- (1) The specimen ignited, as determined by a rapid drop in O_2 pressure and increase in specimen temperature.
- (2) The maximum applied load of 3160N (710 lbf) was reached.
- (3) The ram moved its full travel length, 0.51 cm (0.2 in.), because the specimen had failed in compression or melted.

Figure 21 shows a typical set of data from a single test utilizing fixed O_2 pressure and ramped loading.

ORIGINAL PAGE IS
OF POOR QUALITY

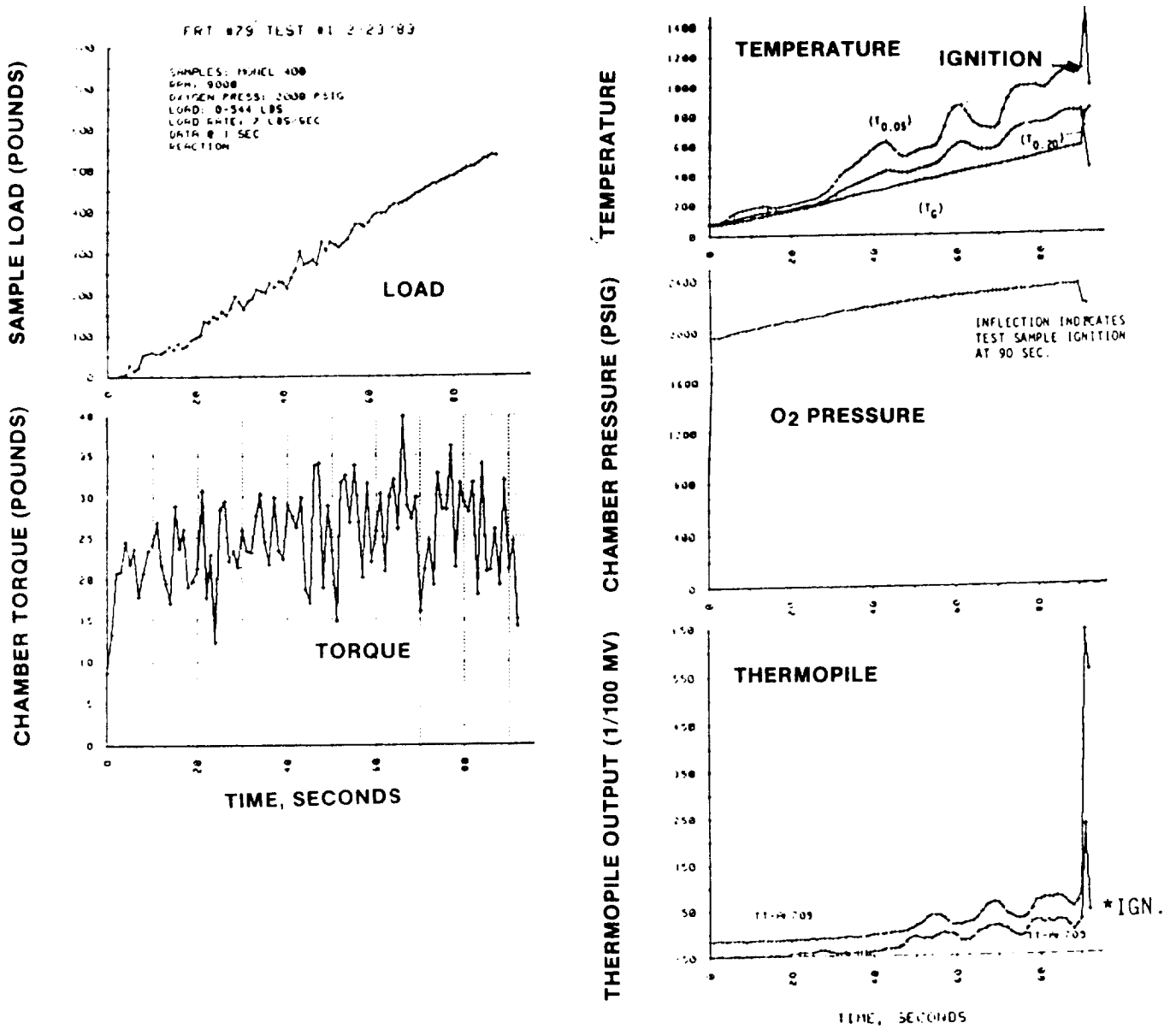


Figure 21. Typical Data from O₂ Ramped Load Friction Rubbing Test

V, B, Test System Description (cont.)

The second test procedure was designed to evaluate the effect of gas composition and gas pressure on friction heating and utilized a fixed speed and contact stress. In these tests, the rpm and contact stress were fixed, and the gas (O_2 or N_2) pressure was increased in steps from 0.69 to 21 MPa (100 to 3000) psi, in order to specifically observe the effect of gas pressure on convective cooling with and without surface oxide reformation during rubbing. Data from one such typical O_2 test are shown in Figure 22. The loads and speeds in these tests were selected to avoid ignition and were thus much lower than the ramped load tests.

A third 5 step loading and unloading test procedure was designed to measure the effect of surface modifications on the wear rate and friction heating of Monel K-500 in oxygen. Monel K-500 was selected for this test phase because it is the OTV turbopump material of construction. The details of this phase of testing are discussed in Section VII.

VI. TEST RESULTS

A. PARTICLE IMPACT RESULTS

1. Test with Impact Plates

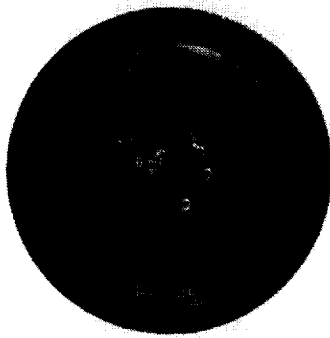
The following sections summarize the results of tests in which impact plates were used as targets. Appendix A contains complete test log and the results for individual tests.

a. Types of Ignition Event Observed

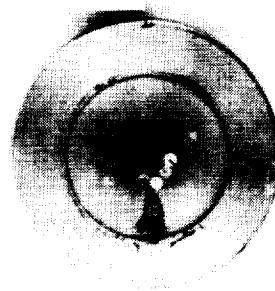
When subjected to particle impact, the impact plates either did not burn, showed slight burning on the target surface, burned partially, or burned completely, as shown in Figure 23. The results of a test in which a zirconium copper sample did not ignite upon particle impact are shown in Figure 23a. The dents made in the sample by the impacting particles can be seen in the photograph. Similar dents typically appeared on impact plates that did not ignite upon impact.

The results of a test in which a Hastelloy X sample exhibited only slight surface burning upon particle impact are shown in Figure 23b. A small triangle-shaped marking extends from the center of a dent made by an impacting particle. Careful observation of the mark reveals that some of the material has been removed from the surface of the impact plate by erosion or burning.

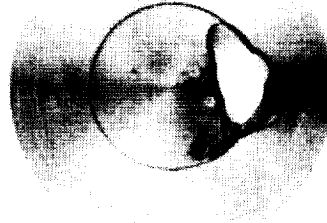
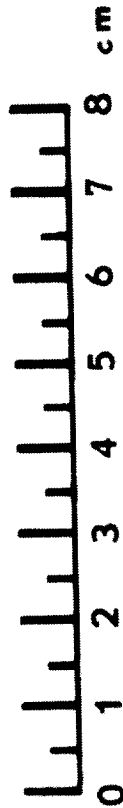
The results of a test in which a type 316 stainless steel sample partially burned are shown in Figure 23c. A hole extending through the target material is visible and indicates that partial combustion of the test material occurred. Burning was quenched before the entire target material was consumed. Each of the impact plates that burned partially exhibited a similar burn pattern.



(a)
ZIRCONIUM COPPER IMPACT PLATE
- NO BURNING -



(b)
HASTELLOY X IMPACT PLATE
- SLIGHT EVIDENCE OF BURNING -



(c)
STAINLESS STEEL 316 IMPACT PLATE
- PARTIAL BURN -

NASA-WSTF
1085-1652

Figure 23. Impact Plates Showing (a) No Burning, (b) Slight Evidence of Burning, (c) Partial Burning

ORIGINAL PAGE IS
OF POOR QUALITY

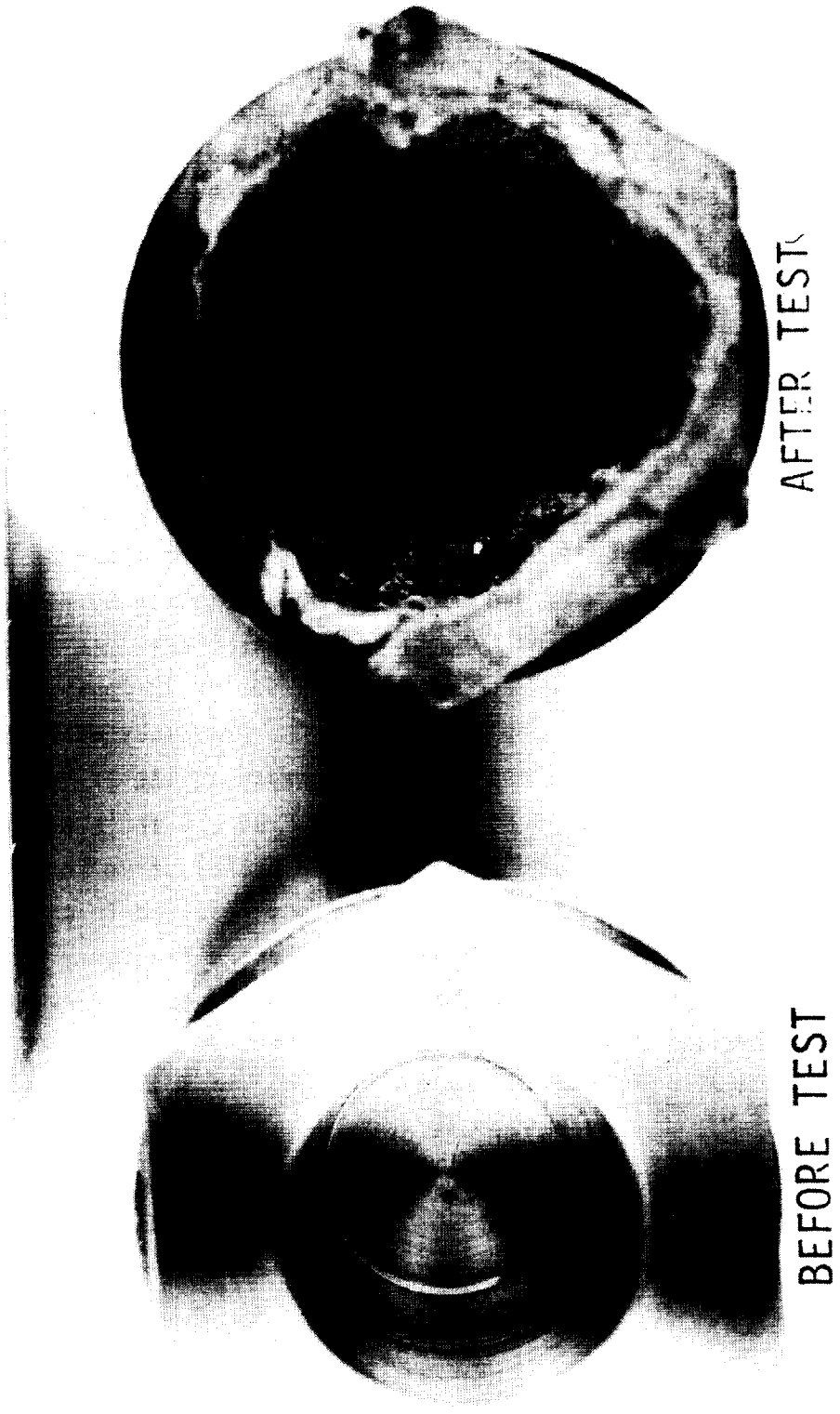
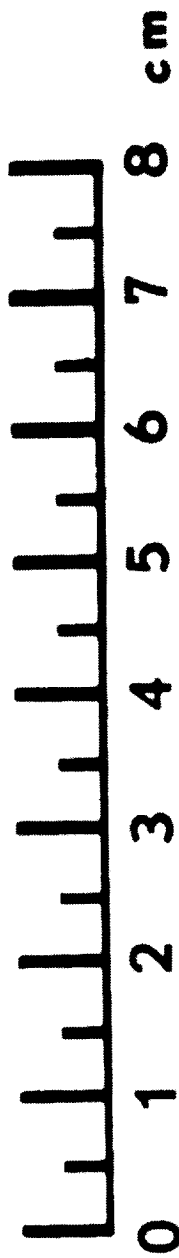
VI, A, Particle Impact Results (cont.)

Chamber photographs taken before and after a test in which a type 316 stainless steel target material burned completely are shown in Figure 24. The target material, the back of which can be seen in the photograph of the pretest assembly, was completely consumed by the reaction. The retainer was almost completely destroyed and the test chamber was irreparably damaged. Such extensive damage to the test chamber was typical of the tests in which target materials were totally consumed.

b. Test Results on Impact Plates

The ignition events resulting from the tests in which target material were configured as impact plates are shown as a function of the initial oxygen temperature in Figure 25. Complete burning occurred only with samples of Invar 36 and type 316 stainless steel. In tests with Invar 36, the sample burned completely in 6 out of 12 tests conducted at oxygen temperatures above 625°K (655°F). The frequency with which the Invar 36 burned completely appeared to increase as the oxygen temperature increased. In the 29 tests conducted with type 316 stainless steel at oxygen temperatures between 450 and 625°K (350 and 665°F), five tests resulted in complete burning of the target, and six tests resulted in only slight surface burning of the target. As shown in Figure 26 the frequency with which burning occurred also appeared to be a function of the oxygen temperature for type 316 stainless steel.

When targets of Hastelloy X were tested, partial burning occurred in 6 of the 19 tests conducted at oxygen temperatures above 625°K (665°F), and slight surface burning was observed in one other test. The frequency of the burning events appeared to increase as the oxygen temperature was increased.



NASA-WSTF
1085-1651

Figure 24. End View of a Test Chamber as it Appeared (a) Before Test and (b) After the Complete Burn of an Impact Plate

ORIGINAL PAGE IS
OF POOR QUALITY

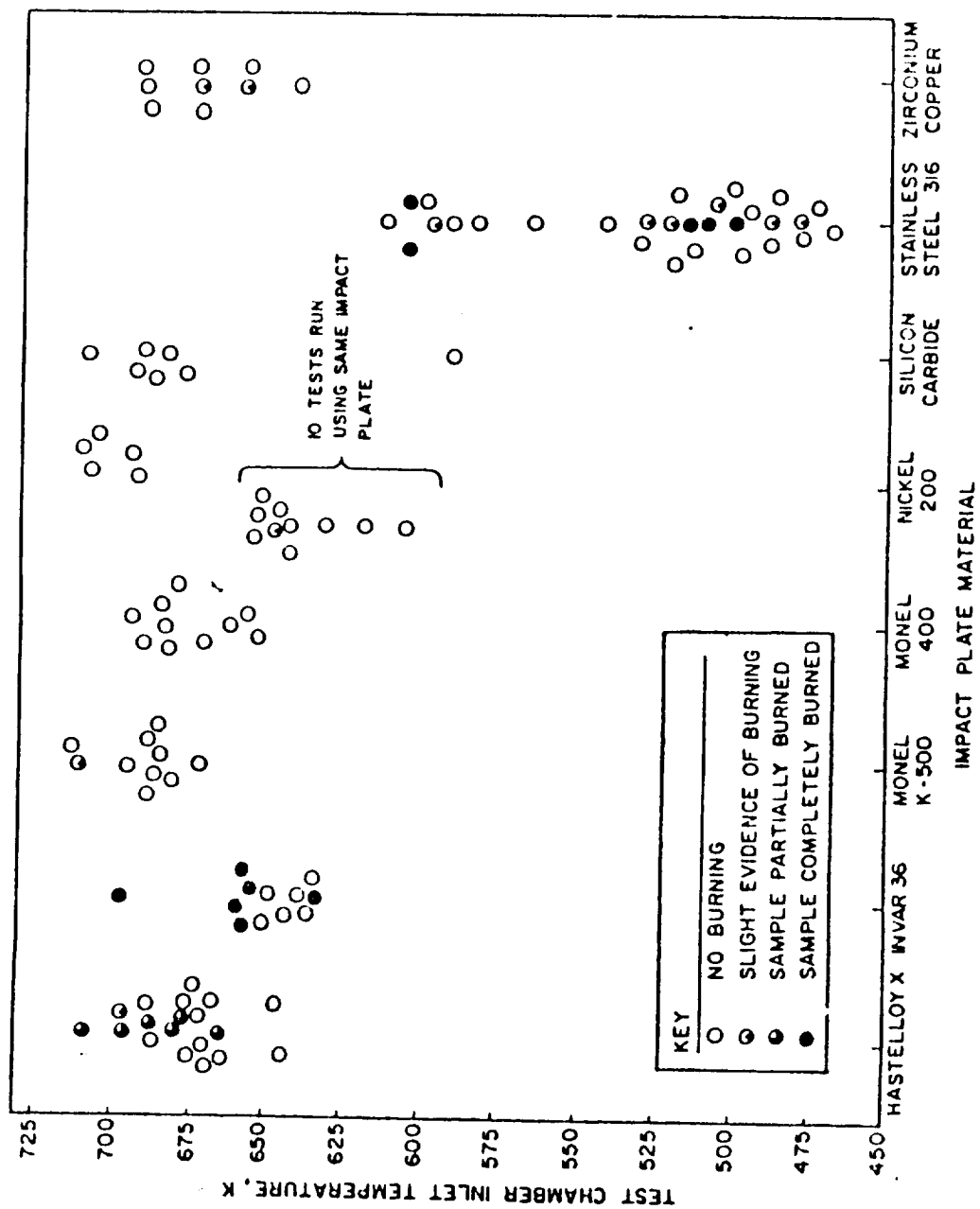


Figure 25. Results of Particle Impact Tests on Impact Plates

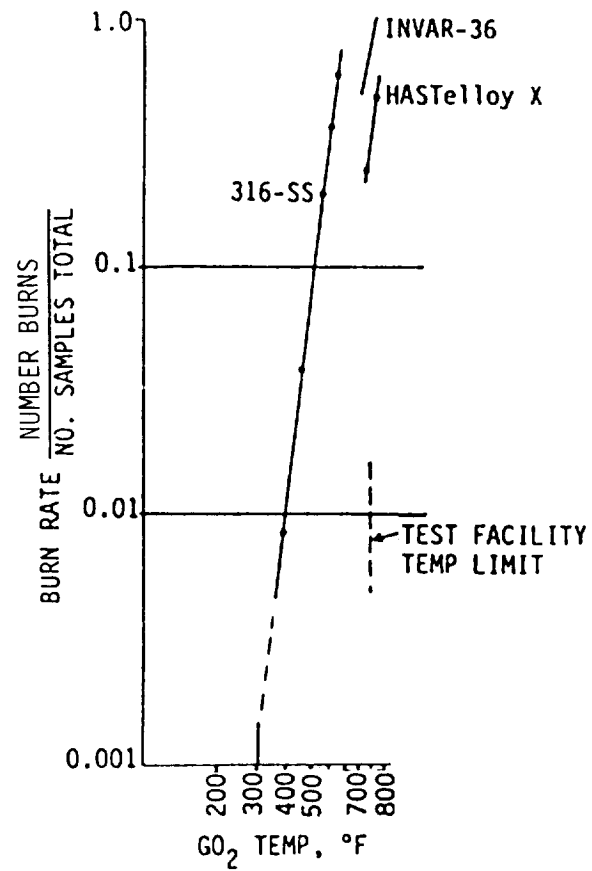


Figure 26. Ignitions Experienced in Particle Impact Testing at 4500 psi

VI, A, Particle Impact Results (cont.)

Samples of the remaining target materials either did not burn or showed slight surface burning at oxygen temperatures above 625°K (665°F). Monel 400 and silicon carbide showed no evidence of burning. Monel K-500 and zirconium copper showed slight surface burning, as did Nickel 200 in one test. However, this one test with Nickel 200 that produced slight surface burning was the ninth test in a series of ten tests using the same Nickel 200 target as the impact plate. The burning event may have been initiated from a particle impacting on aluminum deposited on the surface of the target in the previous eight tests. When Nickel 200 targets were replaced after each test, no evidence of burning was observed out of five tests at oxygen temperatures above 675°K (755°F).

c. Discussion of Test Results

The objective of these tests was to determine the relative resistance of selected materials to ignition by particle impact. In a broad sense, Monel 400, silicon carbide, and Nickel 200, can be ranked as the materials most resistant to ignition, since no samples of these materials were observed to burn in the limited number of tests performed. Similarly, type 316 stainless steel and Invar 36 can be ranked as the materials least resistant to ignition, since samples of these materials were observed to burn completely.

However, an absolute rating for the remaining three materials, which exhibited partial or slight surface burning, is difficult to determine. In general, Hastelloy X, which exhibited partial burning, can be ranked as less resistant to ignition than Monel K-500 and zirconium copper, which exhibited only slight evidence of burning.

A comparison of 316 Stainless Steel with Invar 36 and Hastelloy X at 31 MPa (4500 psi) is shown in Figure 26. The data presented are the ratio of the number of tests resulting in metal burning to the total

VI, A, Particle Impact Results (cont.)

number of tests conducted within each 50°F temperature test band. The probability of igniting the Invar 36 and Hastelloy X by contamination particle impact is only slightly less than the 316 Stainless.

2. Test with Rupture Disks

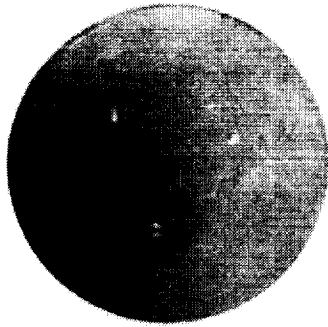
Thin sheets of metal were employed to simulate the edges of turbine blades to determine if impact and rupture is more or less severe than impact only. The following sections summarize the results of tests in which rupture disks of various thicknesses of type 316 stainless steel and Nickel 200 were used as targets. Appendix A contains complete test results for each of the individual tests.

a. Types of Ignition Events Observed

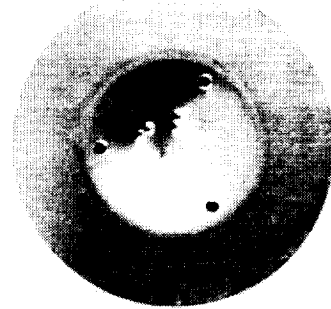
When subjected to particle impact, the target materials configured as rupture disks may neither rupture nor burn, rupture but not burn, or rupture and burn completely, as shown in Figure 27. A rupture disk as it appeared prior to test is shown in Figure 27a. The result from a particle impact test in which a disk neither ruptured nor burned is shown in Figure 27b. Dents caused by the impact of the particles are visible. Similar dents appeared on disks that neither ruptured nor burned upon impact.

The result of a test in which a disk was ruptured by the particles but did not burn is shown in Figure 27c. The dents made in the disk by the particles are visible. In some of the tests at the lower inlet gas temperatures, dents appeared on the rupture disk but not on the back-up plate behind the disk, indicating that the disk was hit and ruptured by the particles. In tests at higher inlet gas temperatures, dents appeared on both the disk and back-up plate, indicating that the first particles to arrive hit and ruptured the disk, and the following particles hit and dented the backup plate.

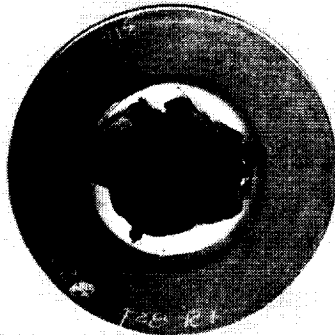
ORIGINAL PAGE IS
OF POOR QUALITY



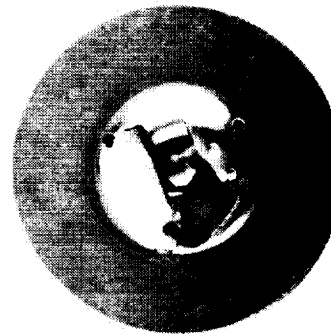
(a)
RUPTURE DISK BEFORE TEST



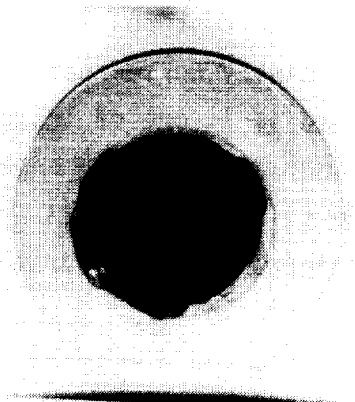
(b)
NO RUPTURE, NO BURNING



(d)
RUPTURE PRIOR TO PARTICLE IMPACT
NO BURNING



(c)
RUPTURE DUE TO PARTICLE IMPACT
NO BURNING



(e)
BURNED RUPTURE DISK

**Figure 27. Examples of the Results of Particle Impact Tests Using
316 Stainless Steel Rupture Disks**

NASA-WSTF
1085-1653

VI, A, Particle Impact Results (cont.)

A disk that was ruptured by gas flow over pressure prior to impact by particles is shown in Figure 27d. No evidence exists that a particle hit the disk and several dents can be seen on the backup plate. A rupture disk that was burned is shown in Figure 27e. The material in the impact area was consumed and the fire was quenched at the inside edge of the copper seal ring.

b. Ignition Resistance of CRES-316 and Nickel 200 Foil and Plate

In five tests of the 0.38 mm (0.015 in.) thick CRES-316 rupture disks, two did not rupture or burn and three ruptured but did not burn. These results are displayed in Figure 28. When the temperature of the inlet gas was increased above 513°K (465°F), the disk was ruptured by gas pressurization prior to the impact of particles. For the rupture disks that were 0.5 mm (0.020 in.) thick, two did not rupture and/or burn, three ruptured but did not burn, and four ruptured and burned completely. Generally, the disks also ruptured and burned more frequently at the higher temperatures. In one case, the disk burned at only 480°K (420°F), which was 28°K (50°F) lower than the temperature at which two disks neither ruptured nor burned. However, it is uncertain if the disk ruptured and then burned, or if the disk did not rupture but ignited and burned by only particle impacts.

The limited test results indicate that the rupturing of thin 316 disks is not significantly worse than the impact on thick plates, and if any trend could be observed it is one of lesser ignitions on thin sheet possibly due to the manner and rate at which energy is transferred from the particle to the target. The thin targets will deform and thus reduce the rate of energy transfer, thus minimizing the temperature at the impact point.

Figure 29 shows the results of similar data for 0.13 and .038 mm (0.005 and 0.015 in.) thick Nickel 200 foil. No ignitions were experienced in any of the testing at temperatures up to 650K (750°F). The rupture of the thin material again produced no adverse effects.

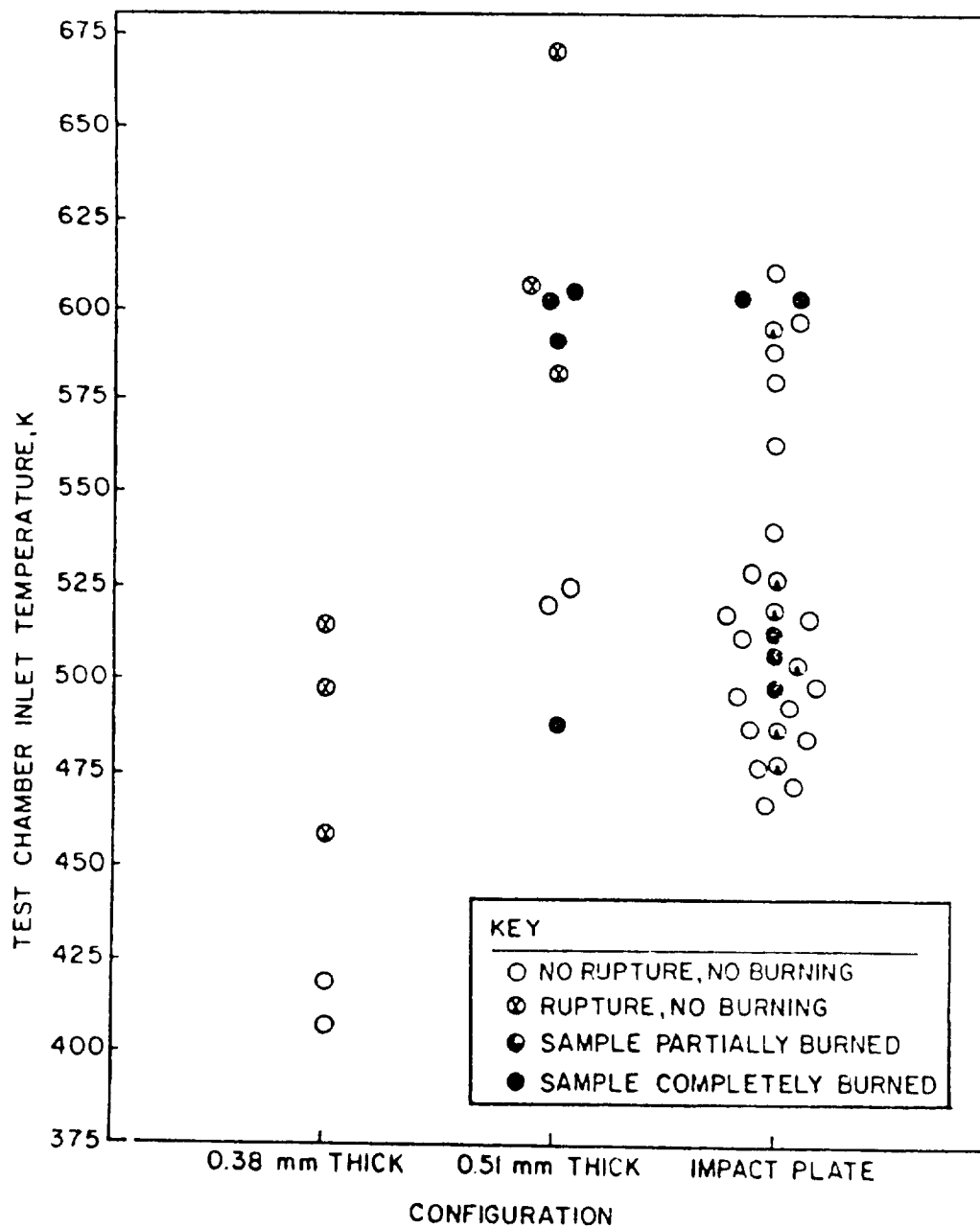


Figure 28. Comparison of Particle Impact Tests on CRES 316 Rupture Disks of Different Thickness and Plate Impact

VI, Test Results (cont.)

B. FRICTION HEATING TEST RESULTS

The results from this test method are presented in four parts. The first covers rubbing of like materials that have burn factors ranging from 35 for copper to over 5000 for two iron based super alloys. The test variables include oxygen pressure and rubbing speed. The linearly increasing load vs time method was used in all tests. The 2nd section covers the results from unlike materials having different burn factors as listed in Figure 20. The same time variable load was applied in each case. A single value for oxygen pressure and surface speed was selected and comparisons of rubbing like and unlike materials were made.

The third section discusses the friction results where the contact load was kept constant and the gas pressure and composition was varied. Comparison of the heating rates using oxygen and nitrogen in the test cell are made.

The fourth section is focused on wear of Monel K-500, the material employed for the OTV turbopump. The test parameters included oxygen pressure, contact load and surface modifications which might be beneficial in reducing friction heating and wear. The contact loads in these tests were much lower than the previous tests in order to avoid burning and thus allow the wear rates and the resulting surface damage following each test be measured and observed. The test durations were extended to allow equilibrium thermal conditions to be achieved and produce more easily measurable wear.

In addition to visual inspection of the failed specimen, several different criteria were employed in ranking materials in there ability to withstand ignition. One was simply the time required to produce ignition under a fixed set of test conditions, i.e., RPM, oxygen pressure and load application rate. A second is the material temperature at which ignition is detected as measured by the thermocouple nearest the rubbing surface. The use

VI, B, Friction Heating Test Results (cont.)

of temperature eliminates differences in time to ignition caused by differences in the material friction coefficient and thermal conductivity. A third often used criteria is energy based i.e., the product of the normal contact pressure P and V , the surface rubbing velocity (PV).

Figure 30 shows the copper alloy 150 (Cu-0.15 Zr) and 316 stainless steel test specimen following a typical 6.9 MPa (1000-psig), 9000-rpm test. This copper alloy consistently failed in compression as the melting temperature was approached and in no case did ignition occur. In contrast the figure also shows one of the more severely burned stainless steel specimen.

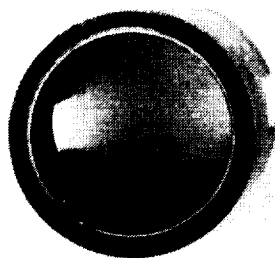
Table V summarizes the ramped load tests conducted on similarly configured specimens for different materials. In most situations, each test condition was repeated three times and unless otherwise noted the most adverse results were used for stating ignition threshold. Table VI summarizes the test results of unlike metals in ramped loading testing. Table VII summarizes the testing using fixed loads in which the gas pressure was varied.

1. Like Materials

The relative ranking of materials was accomplished using data obtained at the maximum speed capability of the machine (17,000 RPM) at 6.9 MPa (1000 psi) oxygen pressure which, at present, appears more adverse than higher pressure for most materials. The effect of O_2 pressure is discussed in greater detail in subsequent sections.

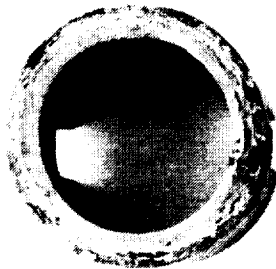
Table VIII documents the ranking of the test materials based on the average PV products obtained from the three test runs conducted on each material. A high average PV product indicates greater resistance to ignition by friction heating. Of the materials tested, nickel 200, Inconel 600, and Cu-150 were the most resistant to ignition. The copper alloy 150 failed mechanically and did not ignite in these tests. The PV products before the samples failed were large enough to indicate that this material is just as

Typical
Pretest

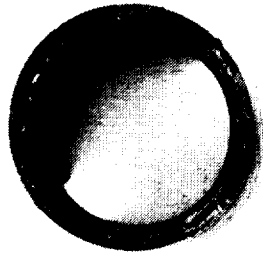


Rotary

Copper 150
Post Test



316 Stainless Steel
Post Test



ORIGINAL PAGE IS
OF POOR QUALITY

Thermocouple
Wells



Stationary

Burned

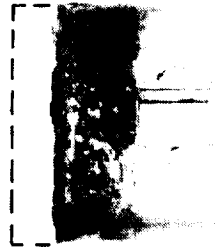


Figure 30. Test Specimen Design and Typical Results 9000 RPM 1000 psi O₂

Table V.
Test Data Compilation for Friction Rubbing (Ramped Load)

FRT no.	Speed		Pressure, psig	Load, ^a psi	Rate, psi/s	Post-test samples ^b		Time of test/s	Temp °F at 0.05 in.
	RPM	ft/s				Rotary	Stationary		
316 Stainless Steel									
22	5000	19	1000	1577	16	R9	R7	100	1500
23	5000	19	1000	1450	20	R9	R7U	70	1400
24	5000	19	1000	1510	21	R9	R7U	69	—
32	9000	35	1000	608	21	R6E	R6E	27	—
34	5000	19	3000	2143	24	R9	R9	86	2000
35	3000	11	1000	2705	17	N2	N2	> 155	—
84	9000	35	1000	597	21.3	R6E	R6E	28	1200
85	9000	35	1000	633	18.6	R6E	R6E	34	1200
101	5000	19	100	1163	18.8	R6E	R6E	62	1600
102	5000	19	0	1984	16.5	N2	N2	> 120	> 2000
103	5000	19	50	877	19	N2	N3	45	—
104	5000	19	100	1365	20.4	R6E	R6E	67	2200
109	5000	19	500	1234		R6E	R6U	56	1800
140	17000	67	1000	406	16	R6E	R6E	24	800
141	17000	67	1000	512	18	N2	N2	28	400
143	17000	67	1000	459	18	R6E	R6E	25	1247
	5000	19	4500	2739	19			138	.450
Zirconium copper (Cu 150)									
111	9000	35	1000	1181	19	—	—		
145	17000	67	1000	1043	19	N5	N2		
146	17000	67	1000	1209	19	N5	N2	63	1650
147	17000	67	1000	1556	19	N2	N3	75	1880
148	17000	67	1000	2288	15	N2	N3	115	1880
Nickel 200									
142	17000	67	1000	1651	21	R7E	R73	80	> 2200 ^c
144	17000	67	1000	2182	19	R8U	R7E	120	> 2200 ^c
156	9000	35	1000	2313	21	N3	N3	105	> 2200 ^c
157	13000	51	1000	2408	21	N3	N3	120	> 2200 ^c
158	15000	59	1000	2355		N3	N3	112	> 2200
161	17000	67	1000	2436	22	N	N	120	> 2200 ^c
	17000	67	4000	2511	535 ^c	N	N	25	> 1940
Inconel 600									
195	17132	67	1072	1400	21.9	R	R	64	1351
194	17104	67	1239	1950	20.1	R	R	97	1486
196	17094	67	1088	2050	21.8	R	R	94	1109
Silicon carbide									
123	9000	44	1000	1167	13	N5	N5		
177	17000	83	1000	106	21	N5		7	
178	9000	44	1000	244	15	N5	N1	17	
Monel K-500									
179	17000	67	1000	1174	25	R6E	R6E	46	1600
180	17000	67	1000	1025	25	R6E	R6E	42	1500
181	17000	67	1000	1025	25	R6E	R6E	41	—
Monel 400									
162	17000	67	1000	1050	23.3	R6E	R6E	45	—
163	17000	67	1000	1114	24.2	R6E	R6E	46	1200
164	17000	67	1000	1138	24.2	R6E	R6E	47	
82	9000	35	3000	2791	21.7	N	N	130	1200
79	9000	35	2000	1922	21.5	R	R	90	1070
75	5000	19	1000	2580	19.2	R	R	134	1500
68	9000	35	1000	1689	22.5	R	R	75	1160
72	7000	28	1000	2664	19.7	R	R	135	1600
Invar-36									
149	17000	67	1000	686	27	R7E	R7E	24	364
150	17000	67	1000	703	27	R7E	R7E	25	339
154	17000	67	1000	714	25	R9U	R7E	26	900
Hastalloy-X									
151	17000	67	1000	661	20	R6E	R6E	33	750
152	17000	67	1000	643	22	R6E	R7E	28	1000
153	17000	67	1000	799	19	R6E	R6E	41	1000

^a The contact load normally is the peak contact load within 0.5 s of the reaction. ^b The post-test sample code is as follows. N1: No-reaction, very little wear; N2: No-reaction, slight wear and deformation; N3: No-reaction, mushroomed; N4: No-reaction, melted and totally deformed; N5: No-reaction, shattered; R6: Reaction, ¼ of sample consumed; R7: Reaction, ½ of sample consumed; R8: Reaction, ¾ of sample consumed; R9: Reaction, total sample consumed; E: Even consumption of the rubbing surface; U: Uneven consumption of the rubbing surface; W: Sample welded but did not react; M: Sample melted but did not react. ^c Rapid ramp rate used to attempt ignition, test, or seal failure caused test termination without ignition.

Table VI. Summary of Data for Dissimilar Materials

Test No.	Material Sta	Rot	RPM	fps	O ₂ psi	Load psi	Load Rate psi/sec	Time of Test sec	Ign. Temp °F .05 in.	Friction Coef	Wear in.	PV $\frac{\text{KW}}{\text{m}^2} \times 10^{-5}$
252	M-K500	M-K500	17,000	67	100	1210	18.5	66	1700	.08		1.72
255	M-K500	M-K500	17,000	67	1200	1307	18.1	72 i*	1800	.06	0.0	1.80
256	M-K500	M-K500	17,000	67	1100	1184	18.5	64 i	1800	.07	0.0	1.68
257	ZrCu	316 SS	17,000	67	1100	600	19.3	31 i	750	0.2	0.0	0.83
258	ZrCu	316 SS	17,000	67	1100	671	19.7	34 i	500	0.1	0.0	0.90
259	ZrCu	316 SS	17,000	67	1100	636	19.3	33 i	500	0.15	0.0	0.87
260	M-K500	316 SS	17,000	67	1100	618	22.1	28 ix2**	200	-	0.0	1.16
261	M-K500	316 SS	17,000	67	1100	583	17.7	33 i	700	0.15	.02	1.33
262	M-K500	316 SS	17,000	67	1000	530	20.4	26 i	580	0.10	0.0	1.49
263	INV-36	SiC	17,000	67	1050	883	18.4	48 i	1600	0.1	0.04	1.16
264	INV-36	SiC	17,000	67	1100	848	18.4	46 f	1650(f)	.07	0.04	1.33
265	INV-36	SiC	17,000	67	1025	1131	19.5	58 i	1400	.07	0.08	1.49
266	M-K500	SiC	17,000	67	1000	530	20.1	26 f	1400(f)	0.15	.02	-
267	M-K500	SiC	17,000	67	1100	707	17.6	40 fi	1600	0.1	.04	1.03
268	M-K500	SiC	17,000	67	1100	477	19.1	25 f	1200(f)	0.12	.02	-
272	EFNi	M-K500	17,000	67	1150	1237	19.0	65 i	1200			1.75
273	EFNi	M-K500	17,000	67	1200	1201	17.2	70 i	1550		0.0	1.63
274	EFNi	M-K500	17,000	67	1200	1237	18.2	68 i	1700	0.1		1.34

* i = ignition

f = fracture no ignition

fi = fracture with ignition

**ignition quench and reignition

Table VII.

Test with Fixed Load Variable O₂ Pressure

FRT No.	RPM	Speed <u>FT/Sec</u>	Gas Pressure psig	Load lb in. ²	Time Sec	Max Temp °F		Friction Coefficient	Condition
						.05	.20		
Mone1 K-500									
236	5000	19	O ₂ 100 1000 3000	285	60 - 80	1000	740	.15	N-1
				285	80 - 185	700	470	.20	N-1
				285	185 - 225	650	340	.25	N-1
237	5000	19	O ₂ 100 1000 3000	320	20 - 60	1000	750	.12	N-1
					60 - 130	625	500	.14	N-1
					130 - 200	550	340	.18	N-1
238	5000	19	N ₂ 100	220	0 - 8	1000	500	1.0 - 3.0	HF
242	5000	19	O ₂ 3000 3000 3000	321	20 - 40	900	500	.30	N-1
				142	80	375	250	.20	N-1
				53	100 - 135	240	180	.20	N-1
244	5000	19	N ₂ 3000	321	4.6	817	262	--	V
245	5000	19	O ₂ 1000	320	0 - 40	1000	620	.20	N-1
	6000	23	O ₂ 1000	320	150 - 200	800	520	.15	N-1
	17000	67	O ₂ 900	320	240 - 300	700	500	.15	N-1
	13000	50	O ₂ 850	320	325 - 350	750	550	.13	N-1
246	9000	34	O ₂ 1100	357	5 - 35	900	550	--	N-1
	9000	34		892	40 - 70	1750	1200	.13	N-1
	9000	34		1285	75 - 105	1900	1300	.10	N-1
	9000	34		1705	116	2069	1400	--	R
247	5000	19	O ₂ 1100	321	0 - 47	400	300	.25	N-1
	17000	67	O ₂ 1040	321	90 - 150	800	550	.12	N-1

Table VIII.

**Average Heat Rate per Unit Area (PV Product) Required for Ignition by
Frictional Heating of Pairs of Like Material**

A) Data from this Contract

USN DESIGNATION	MATERIAL	HEAT RATE PER UNIT AREA (PV PRODUCT)		BURN*** FACTOR
		kW/m2 x 10-5	STANDARD DEVIATION	
C 15000	COPPER-0.15 Zr*	NOT IGNITABLE		35
N 02200	NICKEL 200	2.88	0.56	550
N 06600	INCONEL 600	2.54	0.48	3226
N 04400	MONEL 400	1.47	0.07	1390
N 05500	MONEL K-500	1.46	0.14	2090
N 06002	HASTELLOY X	1.05	0.18	7160
K 93601	INVAR 36	0.78	0.17	5444
S 31651	STAINLESS STEEL 316	0.63	0.09	4515
--	SILICON CARBIDE (SIC)	**	—	1145

* DID NOT IGNITE, FAILED MECHANICALLY

** DID NOT IGNITE, SHATTERED AT
RELATIVELY SMALL CONTACT PRESSURES

*** Cal-sec/gm-cm2

B) Data from Other Programs Using the Same Test Method

C 36000	BRASS 360	.74 to 1.26	223
	ALUMINUM 6061-T6	0.074	1026
	TI-6AL-4V	0.0035	14623

VI, B, Friction Heating Test Results (cont.)

resistant or possibly more resistant to ignition than nickel 200 or Inconel 600. Of the materials tested, Invar 36 and type 316 stainless steel were the easiest to ignite. However, as a comparison, the PV products reported by Benz and Stoltzfus¹⁷ for Aluminum 6061-T6 and Ti-6Al-4V (Table VIIIB) under similar test conditions were one and two orders of magnitude less, respectively, than the PV products observed in these tests for the Invar 36 and type 316 stainless steel.

2. Friction Heating of Unlike Materials

The following test conditions were maintained in this series.

- Initial Pressure: 1000 psig Oxygen
- Initial Temperature: Ambient
- Surface Speed: Approximately 67 ft/sec (17,000 rpm)
- Maximum Contact Pressure Limit: 3275 lbf/in.²
- Contact Pressure Rise Rate: 19 ± 1 lbf/in.²-sec

Figures 31 through 35 provide data from a typical test showing how each significant event was determined. The interface load rise rate was determined from the slope of the total load vs time curve using the area of the metal sample (0.283 in.²) as the bearing surface.

A summary tabulation of results from the baseline Monel K-500 tests and the unlike materials evaluated in the present series are documented in Table VI and shown graphically in Figure 36. A comparison of current Monel-Monel baseline tests (Nos. 255 and 256) with previous data, (Test Nos. 179-181), is given in Table IX.

FRT#259: ZrCu-Stat.; 316 SS-Rot.

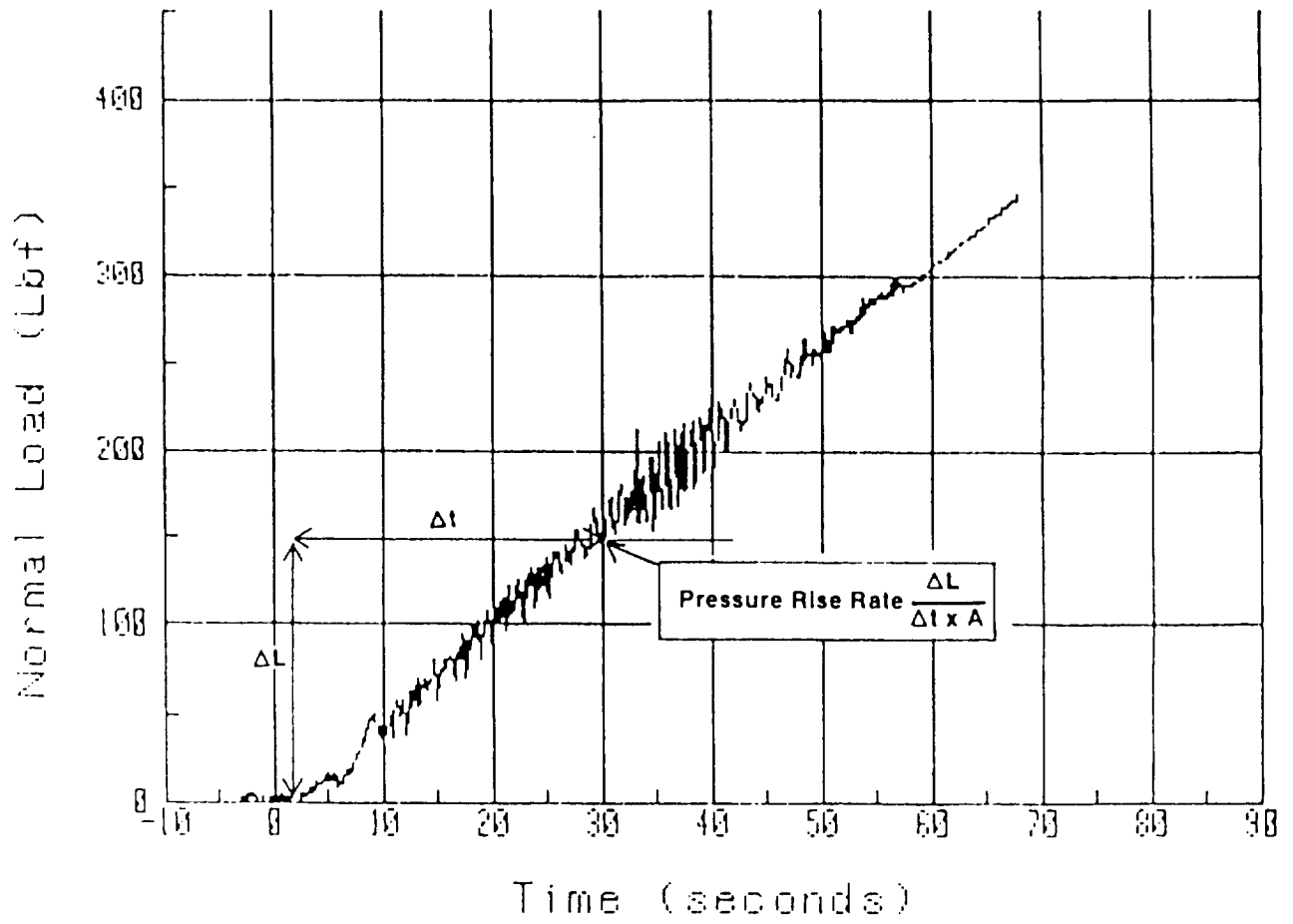


**Figure 31. Total Load vs Time Dissimilar Materials (Cu/Steel)
Friction Heating Ignition Tests**

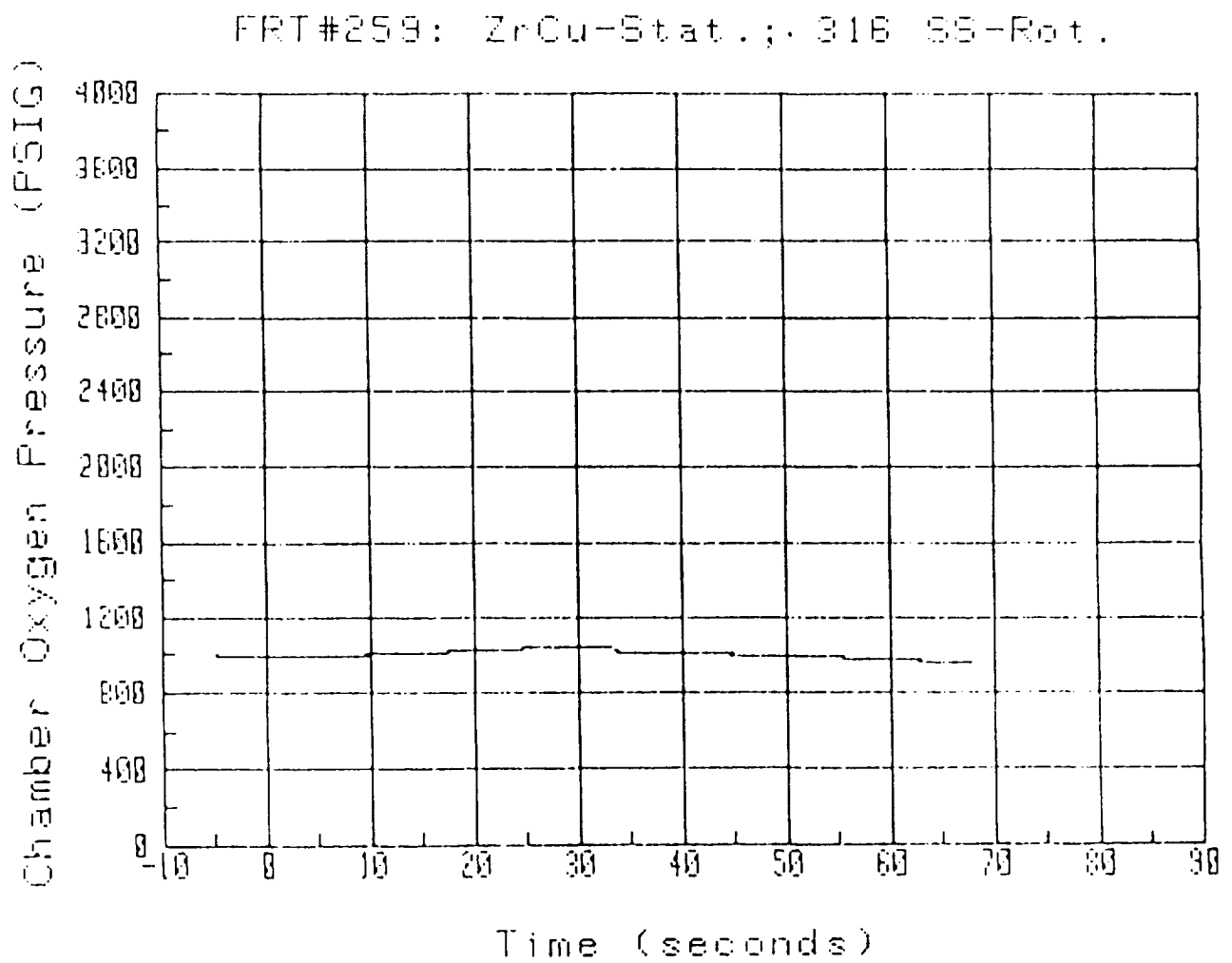


Figure 32. Copper-Stainless Steel Friction Heating Test O₂ Pressure vs. Time

FRT#259: ZrCu-Stat.; 316 SS-Rot.

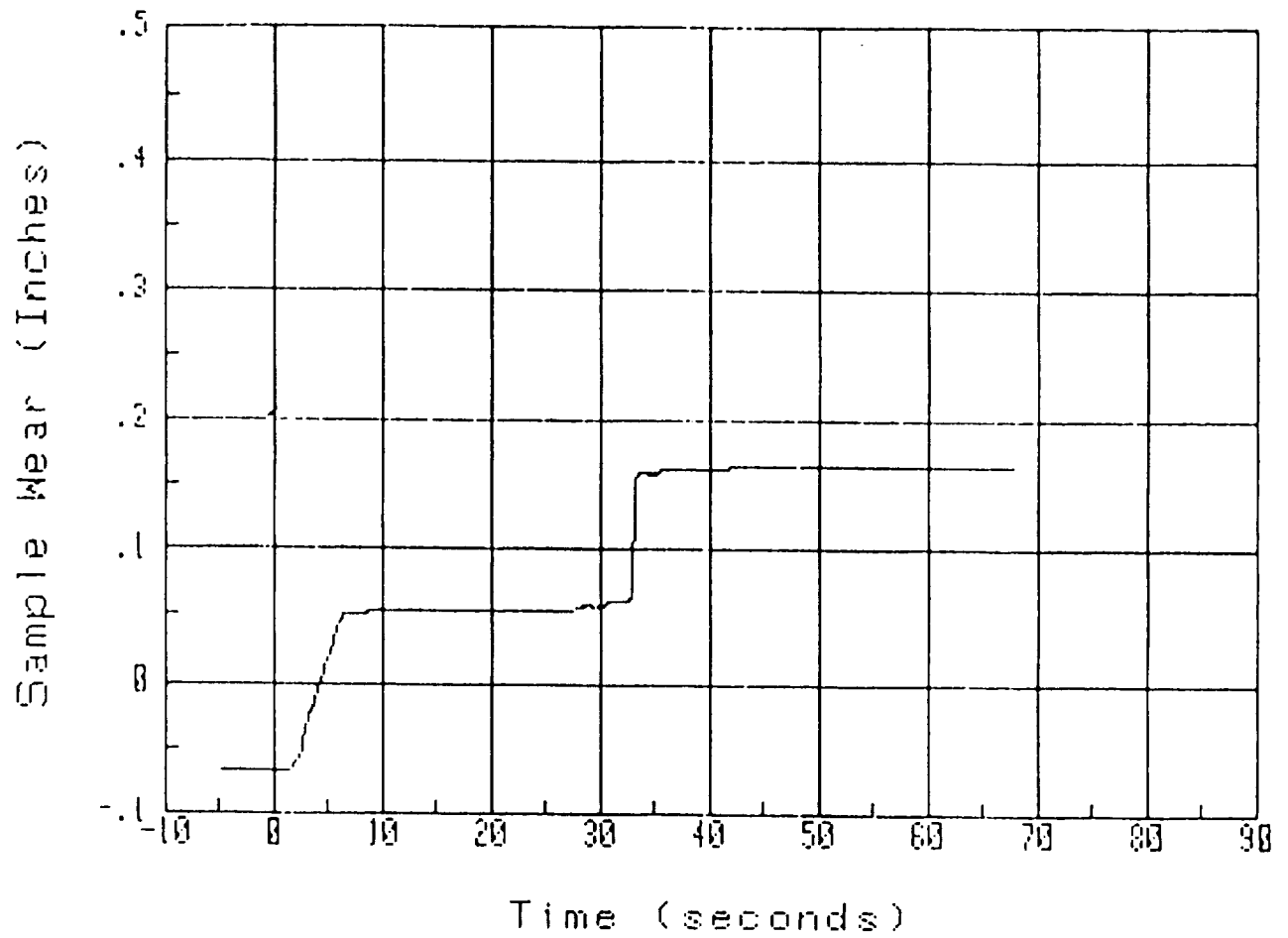


Figure 33. Copper-Stainless Steel Friction Heating Ignition Test Displacement vs. Time

FRT#259: ZrCu-Stat.; 316 SS-Rot.

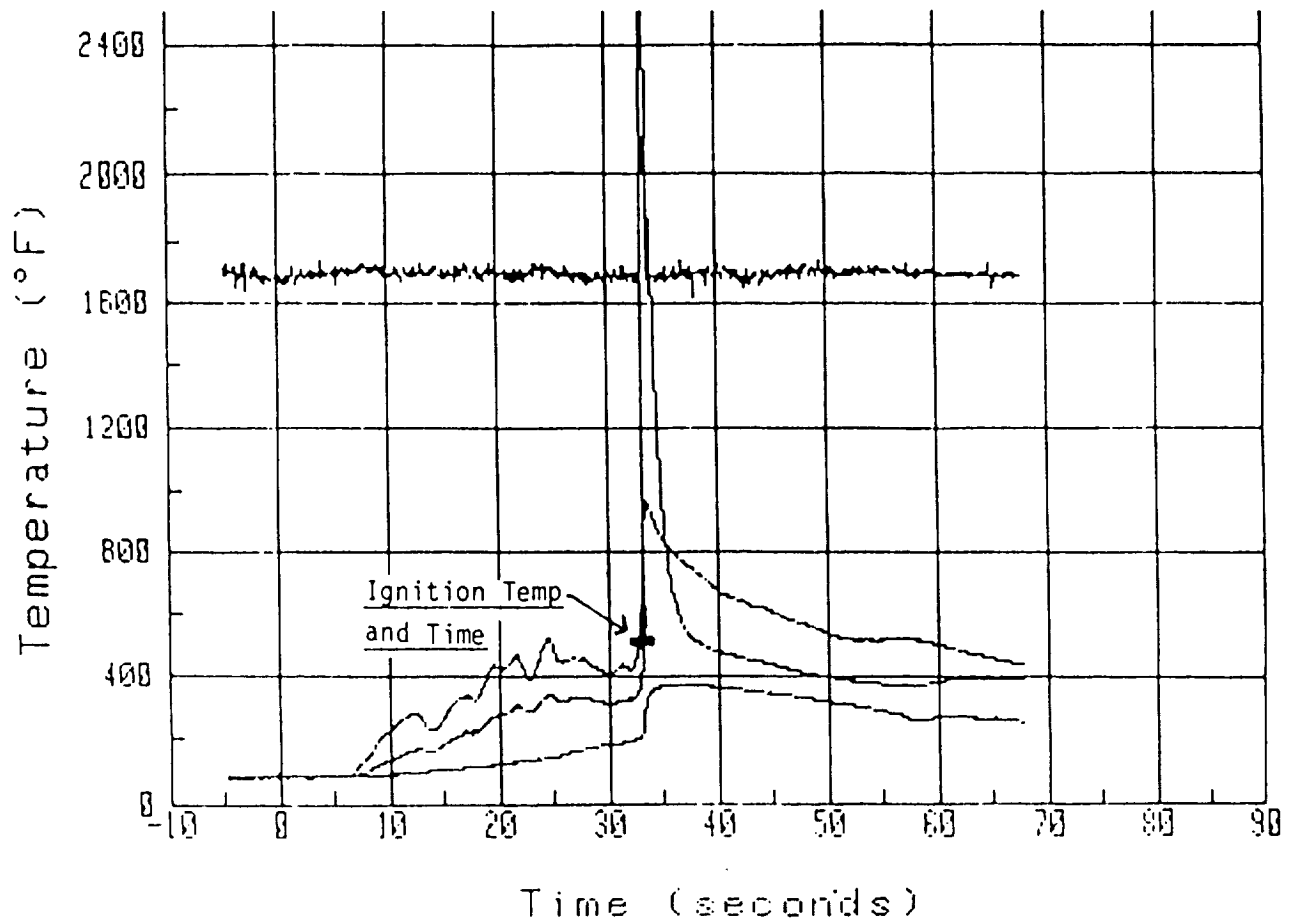


Figure 34. Copper-Stainless Steel Friction Heating Ignition Test Temperature vs. Time

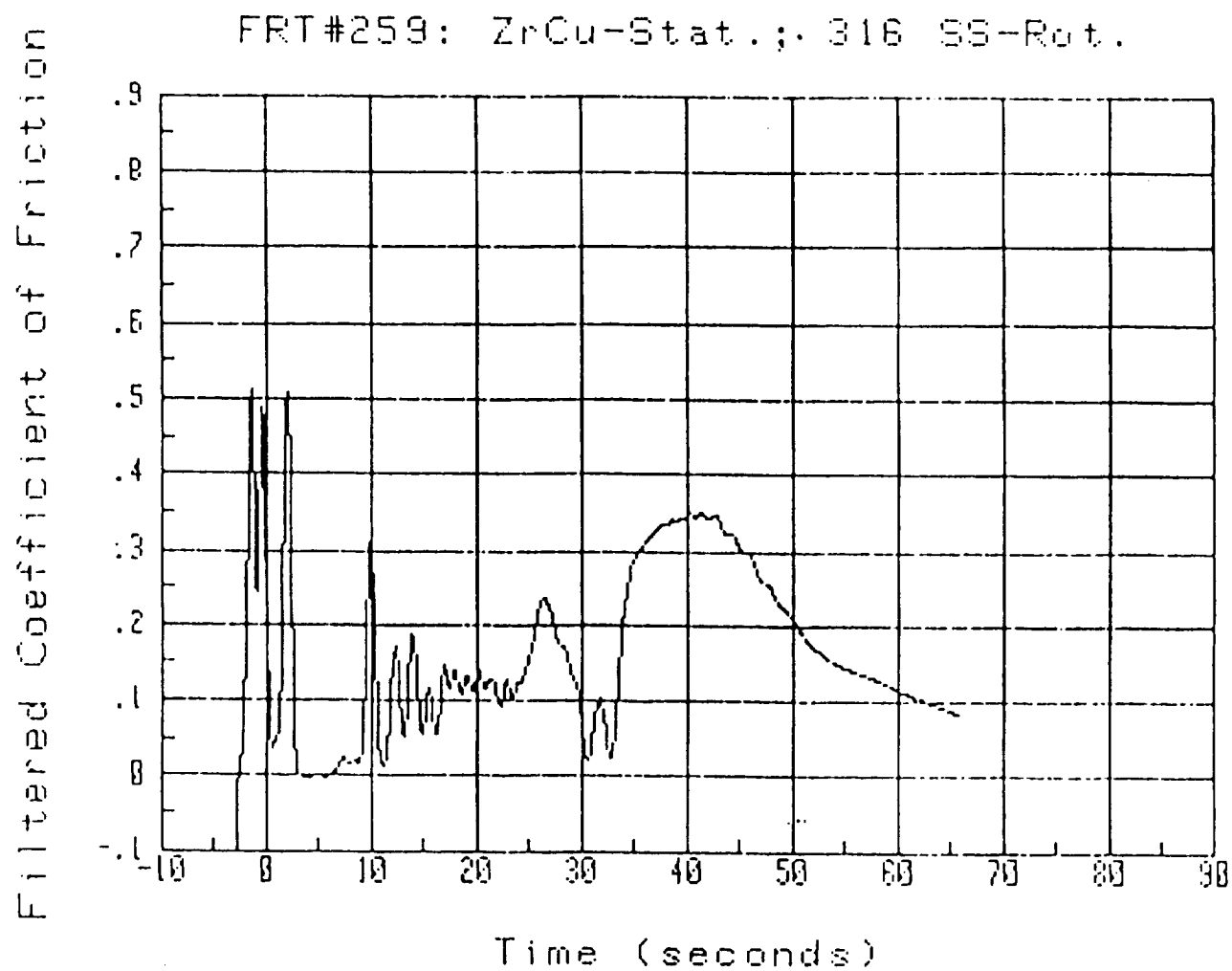


Figure 35. Copper-Stainless Steel Friction Coefficient

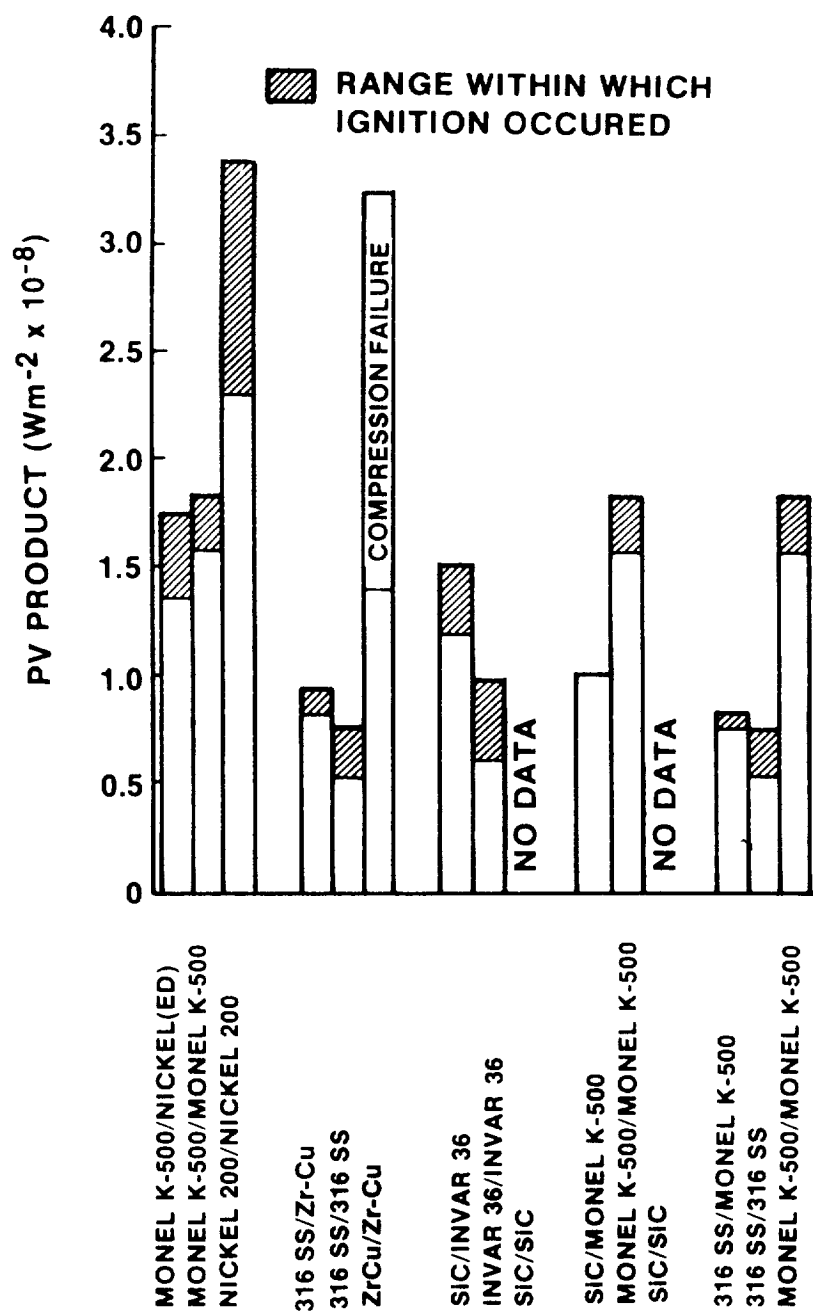


Figure 36. PV Products Required to Ignite Pairs of Different Materials

Table IX. Baseline Data Comparison For Mone1 K-500

<u>Present Test Series</u>									
<u>Test No.</u>	<u>Material Sta & Rot</u>	<u>Speed RPM</u>	<u>FPS</u>	<u>O² psia</u>	<u>Load psi</u>	<u>Load Rate psi/sec</u>	<u>Time of Test (sec)</u>	<u>Ignition Temp °F</u>	<u>Friction Coef</u>
255	M K-500	17,000	67	1200	1307	18.1	72	1800	.06
256	M K-500	17,000	67	1100	1184	18.5	64	1800	.07
				Avg	1246		68	1800	
<u>Previous Tests</u>									
179	M K-500	17,000	67	1000	1174	25	46	1600	-
180	M K-500	17,000	67	1000	1025	25	42	1500	-
181	M K-500	17,000	67	1000	1025	25	41	-	-
				Avg	1075		43	1550	

VI, B, Friction Heating Test Results (cont.)

The load application rate on previous tests was higher than the present series; 25 vs 18 psi/sec. This resulted in the present series of tests requiring a longer duration to reach the limiting load and ignition. The O_2 pressure was also 10 to 20% higher in the new series.

The average load at which Monel K-500 ignition occurred was 15% higher in the present series, while the temperatures were approximately 200°F higher. This trend is expected, as both the reduced load application rates and the higher O_2 pressure have been noted to have second-order effects which tend to extend the time and load required to cause ignition. In viewing the overall test results, differences of 20% in load at ignition and several hundred degrees of temperature should therefore not be considered significant in the subsequent evaluation of unlike materials.

The tabular format used in comparing the ignition potential of unlike materials with the like materials is as follows. The first two columns, in Tables X - XIV document like material rubbing data from previous testing. The unlike material data from the present series is provided in the last column. The average values are presented for each measured parameter where multiple tests at a given condition were conducted.

The results of rubbing a burn resistant material such as copper with an easily ignitable stainless steel is displayed in Table X. The load application rate for the copper, stainless steel and copper-stainless steel is identical (18-19 psi/sec) and, thus, the data are directly comparable.

The three copper vs copper tests were terminated without ignition when the copper failed in compressive yield at temperatures approaching the melting point. The relative ease of igniting 316 stainless steel is noted by the consistent lower load, temperature and time required to cause metal burning as compared to the copper.

Table X. Rubbing of Low and High Burn Factor Metals
Copper and Stainless Steel

Rotating	Cu	316-SS	316-SS
Fixed	Cu	316-SS	Cu
Time To Ignition	63 *	24	31
(sec)	75 *	28 *	34
	<u>115</u> *	<u>25</u>	<u>33</u>
Avg	84	26	33
Load at	1209 *	406	600
Ignition, (psi)	1566 *	512 *	671
	<u>2288</u> *	<u>459</u>	<u>636</u>
Avg	1684	459	636
Temp at	1650 *	800	750
Ignition (°F)	1880 *	400 *	500
	<u>1880</u> *	<u>1247</u>	<u>500</u>
Avg	1803	1024	583
Load Rate psi/sec	19	18	19

*Test limit by deformation No ignition

Table XI. Rubbing of Low and Moderate Burn Factor Metals
Nickel and Mone1 K-500

Rotating	Nickel	M K-500	Nickel (Electroform)
Fixed	Nickel	M K-500	M K-500
Time To Ignition	80	72	65
(sec)	120	64	70
	<u>120</u>	46	<u>68</u>
Avg	107	42	68
		<u>41</u>	
		53	
Load at	1651	1307	1237
Ignition (psi)	2182	1184	1201
	<u>2436*</u>	1174	<u>1237</u>
Avg	2090	1025	1225
		<u>1025</u>	
		1143	
Temp at	> 2200	1800	1200
Ignition (°F)	> 2200	1800	1550
	<u>> 2200*</u>	1600	<u>1700</u>
Avg	> 2200	<u>1500</u>	1483
		1675	
Load Rate psi/sec	21	25 old data	18
		18 new data	

*No ignition

Table XII. Rubbing of Moderate Burn Factor and High Burn Factor Metals
Monel K-500 vs 316 Stainless Steel

Rotating	M K-500	316-SS	M K-500
Fixed	M K-500	316-SS	316-SS
Time To	72	24	28
Ignition (sec)	64	28 *	33
	46	<u>25</u>	<u>26</u>
	42	26	29
	<u>41</u>		
Avg	53		
Load at Ignition	1307	406	618
(psi)	1184	512 *	583
	1174	<u>459</u>	<u>530</u>
	1025	459	577
	<u>1025</u>		
Avg	1143		
Temp at	1800	800	-
Ignition (°F)	1800	400 *	700
	1600	<u>1247</u>	<u>580</u>
	<u>1500</u>	1024	640
Avg	1675		
Load Rate psi/sec	25 old	18	20
	18 new		

*No ignition

Table XIII. Rubbing of Moderate Burn Factor Metal and Ceramic
Monel K-500 and Silicon Carbide

Rotating	Silicon Carbide	M K-500	M K-500
Fixed	Silicon Carbide Mettech-Compound	M K-500	Silicon Carbide SA grade **
Time to	7 *	72	26 f
Ignition sec		64	40 i
		46	<u>25</u> f
		42	30
		<u>41</u>	
	Avg	53	
Load at	106 *	1307	530 f
Ignition sec		1184	707 i
		1174	<u>477</u> f
		1025	571
		<u>1025</u>	
	Avg	1143	
Temp	No data	1800	1400 f
at °F		1800	1600 i
Ignition		1600	<u>1200</u> f
		<u>1500</u>	1400
	Avg	1675	
Load Rate psi/sec	21	25 old	19
		18 new	

f = Mechanical Failure
i = Ignition

*Specimens contained notch; Failed Mechanically

**Unnotched, increased wall thickness specimen of SA material supplied by
Carborundum, Inc.

Table XIV. Rubbing of Moderate Burn Factor Ceramic and High Burn Factor Metal
Silicon Carbide and Invar 36

Rotating Fixed	Silicon Carbinde Silicon Carbide (Mettech Compound)	INVAR-36 INVAR-36	INVAR 36* Silicon Carbide (SA Grade)
Time to Ignition (sec)	7 **	24 25 <u>26</u> Avg 25	48 ignition 46 fracture <u>58</u> ignition 51
Load at Ignition (psi)	106 **	686 703 <u>714</u> Avg 701	883 848 <u>1131</u> 954
Temp at Ignition (°F)	No data	364 339 <u>900</u> Avg 534	1400 1650 <u>1200</u> 1417
Load Rate psi/sec	21	26	19

*composition of failed specimen verified by SEM analysis as Fe, 36% Ni 0.5% Cr
**specimen contained notch; failed mechanically

VI, B, Friction Heating Test Results (cont.)

It was postulated that copper in contact with stainless steel would act as a heat sink and inhibit ignition of this high burn factor material. The experimental results indicated that this was not the case. The copper was successful in lowering the interface temperatures, as measured by the thermocouple located in the copper 0.05 in. from the rubbing surface. However, 316 stainless steel ignition took place only 7 sec later than was observed in the stainless steel vs stainless steel tests. The load at ignition for the Cu-SS was 636 psi vs 459 for the SS-SS and 1684 psi with no ignition for copper-copper.

Similar results were observed for low vs moderate BF metals, i.e., nickel vs Monel K-500, as shown in Table XI. The Ni vs Monel K-500 responded more like the easier to ignite Monel than the difficult to ignite nickel. Note that the load application rate was lower in the present series and, thus, the time to ignition for the unlike metals is expected to decrease further if the 18 psi/sec were increased to the 25 psi/sec.

Data for a moderate BF metal in contact with a high BF metal (Monel K-500 vs 316 stainless steel) Table XII provides similar results, i.e., the system degrades to that of the most ignition-prone material.

Two test series were conducted in which the rotating specimen was an alpha-grade silicon carbide ring, as shown in Figure 19. (Note the heavier wall cross-section incorporated to overcome structural failures encountered with the original design.) The results of these tests are shown in Tables XIII and XIV. Both the Monel and silicon carbide have moderate burn factors, while the Invar 36 has a very high burn factor and was found to ignite quite easily when rubbed against itself.

VI, B, Friction Heating Test Results (cont.)

Previous testing with the notched silicon carbide specimens revealed mechanical failure to be the limiting factor. Even with catastrophic material disintegration, no ignition were reported in these like-on-like tests. Thermal data were absent due to the inability to attach thermocouples to the silicon carbide.

The current testing without the notch allowed longer test durations and higher loads to be attained. Temperature measurements were made by instrumenting the fixed metal specimen.

In the Monel vs SiC testing, only one of the three tests resulted in ignition. The others terminated when the specimen fractured. Since no previous valid data were available in SiC vs SiC, it is difficult to draw any conclusions except to state that the material is more likely to fail mechanically than to burn when in contact with other low or moderate burn factor materials.

The results of the high burn factor Invar 36 and the SiC proved to be an exception to the previous metal on metal test results. A significant improvement in time, temperature and load to cause ignition of the Invar 36 was observed; this cannot be fully explained at this time, and could be due to the thicker wall of the SA silicon carbide test section or the change in the material supplier.

a. Conclusions

The results of a limited test series involving the friction rubbing heating of unlike metals in a gaseous O_2 environment demonstrated that conditions required to initiate metal burning are established by the limits of most burn prone metal. The introduction of a highly burn resistant metal as one of the rubbing surface was found to be of little value in preventing ignition although it is useful in limiting the propagation.

VI, B, Friction Heating Test Results (cont.)

Exceptions to the above results were observed when a non-metallic (SiC) material was employed in contact with an easily ignitable metal. This combination resulted in a significant increase in the load, time and temperature required to ignite the metal. A valid explanation of this effort is not available. Geometric differences in the SiC and Metallic Test Sections may be a factor and additional testing with consistent geometry is recommended.

3. Gas Composition and Pressure Effects in Friction Rubbing

The effect of O_2 pressure under ramped loading was evaluated for four materials: Monel 400, 316 Stainless Steel, 1015 Carbon Steel, and Nickel 200. Various rotational speeds were investigated.

The results of these tests, shown in Figures 37 through 40, were internally consistent and significantly different from what was expected by the extrapolation of earlier data from Figure 8. The test data indicate that, as the oxygen pressure is increased above the old data base of 6.9 MPa (1000 psia) the time, contact loading and speed required to ignite Monel 400, 316 stainless steel and 1015 carbon steel became progressively greater. The Monel 400 and Nickel 200 became unignitable at the highest pressures. However, once ignited, the burning at high pressure was more extensive. This is most probably due to the greater concentration of O_2 present in the test chamber at the higher pressure.

Figure 37 shows the overlay of the measured temperature 0.12 cm (0.05 in.) from the contacting surface for Monel 400 at 6.9, 13.8 and 20.7 MPa (1000, 2000, and 3000 psi). The time, and thus the friction energy, required to heat the specimen to the ignition temperature of 866°K (1100°F) increased with increasing O_2 pressure. It was not possible to ignite the Monel at 20.7 MPa (3000 psi), even though the same apparent ignition threshold temperature was reached. This lower ignition potential can be explained by

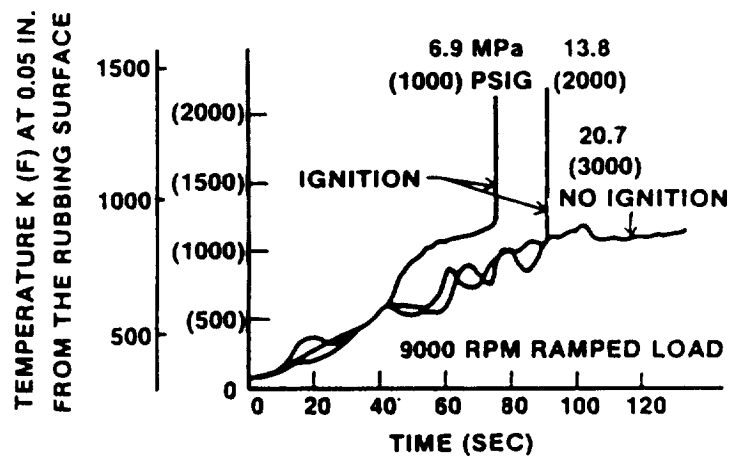


Figure 37. Effect of O₂ Pressure on Heating Rates of Monel 400

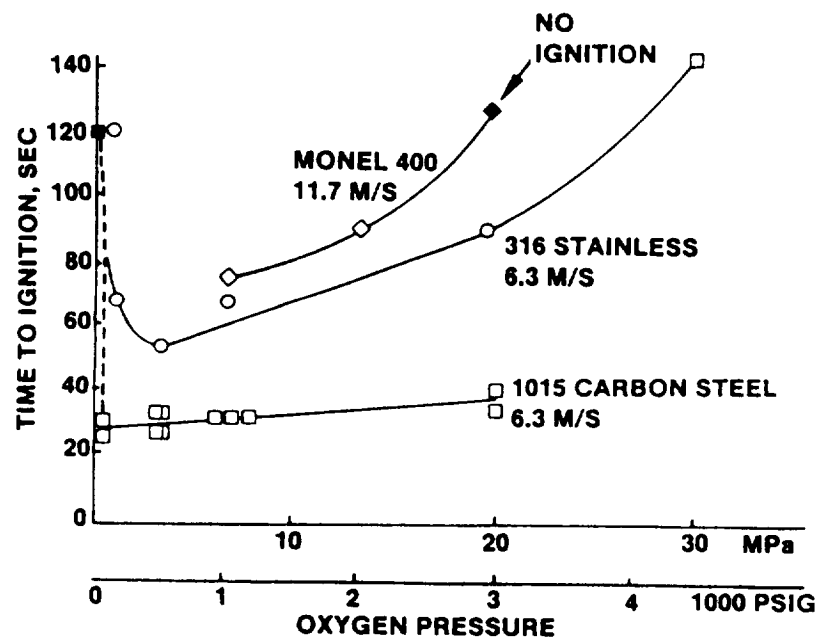


Figure 38. Time to Ignition vs. Oxygen Pressure

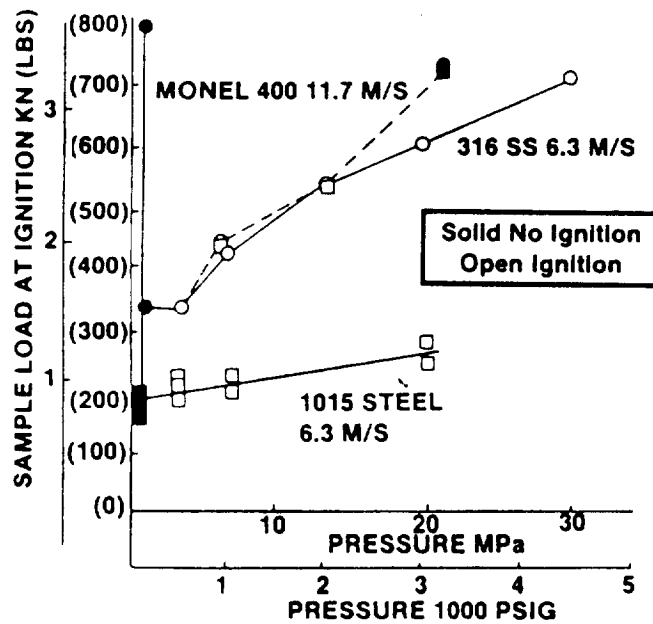


Figure 39. Load at Ignition vs. Oxygen Pressure

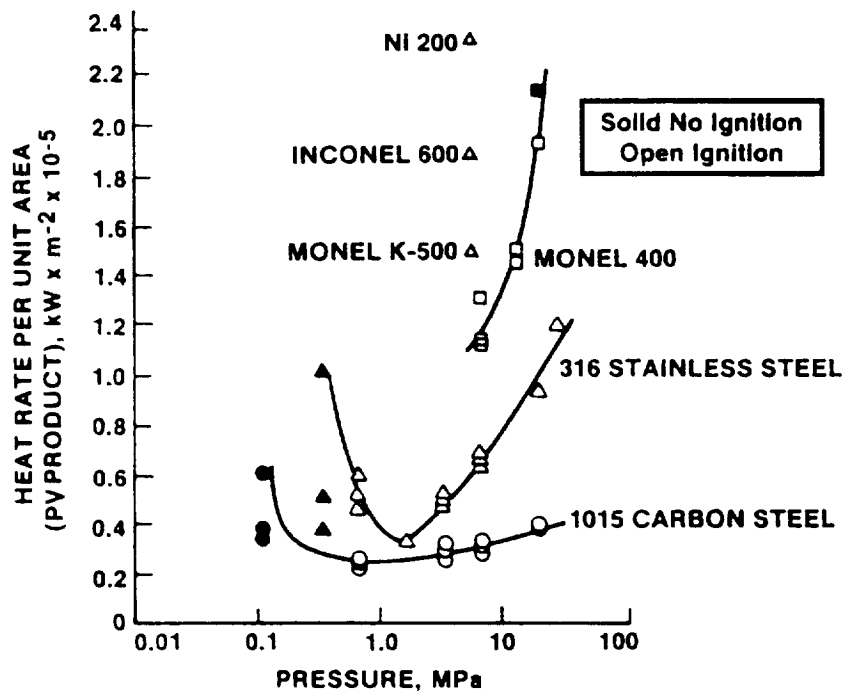


Figure 40. Heat Rate per Unit Area Required for Ignition vs. O₂ Pressure (From Benz & Stoltzfus⁹)

VI, B, Friction Heating Test Results (cont.)

a) better convective cooling at the higher pressure, b) the formation of a thicker protective, insulating oxide film, c) the possibility of lower friction coefficients or d) some combination of these.

The temperature oscillations observed in Figure 37 were common throughout the test program and the frequency always tended to increase with increasing O_2 pressure. These effects are not fully understood and are discussed later in more detail.

Figure 38 compares the time to ignition of 1015 Carbon Steel and 316 Stainless Steel at 6 m/sec (19 fps) surface velocity, and Monel 400 and Ni 200 at 11 m/sec (35 fps), as a function of O_2 pressure. Note that the Monel 400 did not ignite at 20.7 MPa (3000 psi) and it was not possible to ignite the nickel at 27.6 MPa (4000 psi) even when the speed was increased to 22.3 m/sec (67 fps). Figure 39 shows the maximum attainable load on the test specimen in each test. Figure 40 displays the (PV) parameter vs oxygen pressure again indicating greater allowable energy input with increasing oxygen pressure. It is significant to note that the Monel 400 derives much greater benefit from the higher oxygen pressure than either carbon or stainless steel. With the exception of low ignition temperature of the 1015 Carbon Steel shown in Figure 41, the similarity of results in these tests provided encouragement that operation at very high oxygen pressure actually may be less severe than at moderate pressure. The observation that high oxygen pressure can be beneficial when applied to equipment design warrants additional experimental investigation using more metals and a wider range of test environments.

In the fixed load, variable O_2 pressure test for Monel K-500, shown in Figure 22, the highest friction heating temperature is obtained at the lowest O_2 pressure 0.69 MPa (100 psi). Increasing the O_2 pressure to 6.9 and then 21 MPa (1000 and then 3000 psi) results in lower measured temperature and higher measured friction coefficients, Figure 22d.

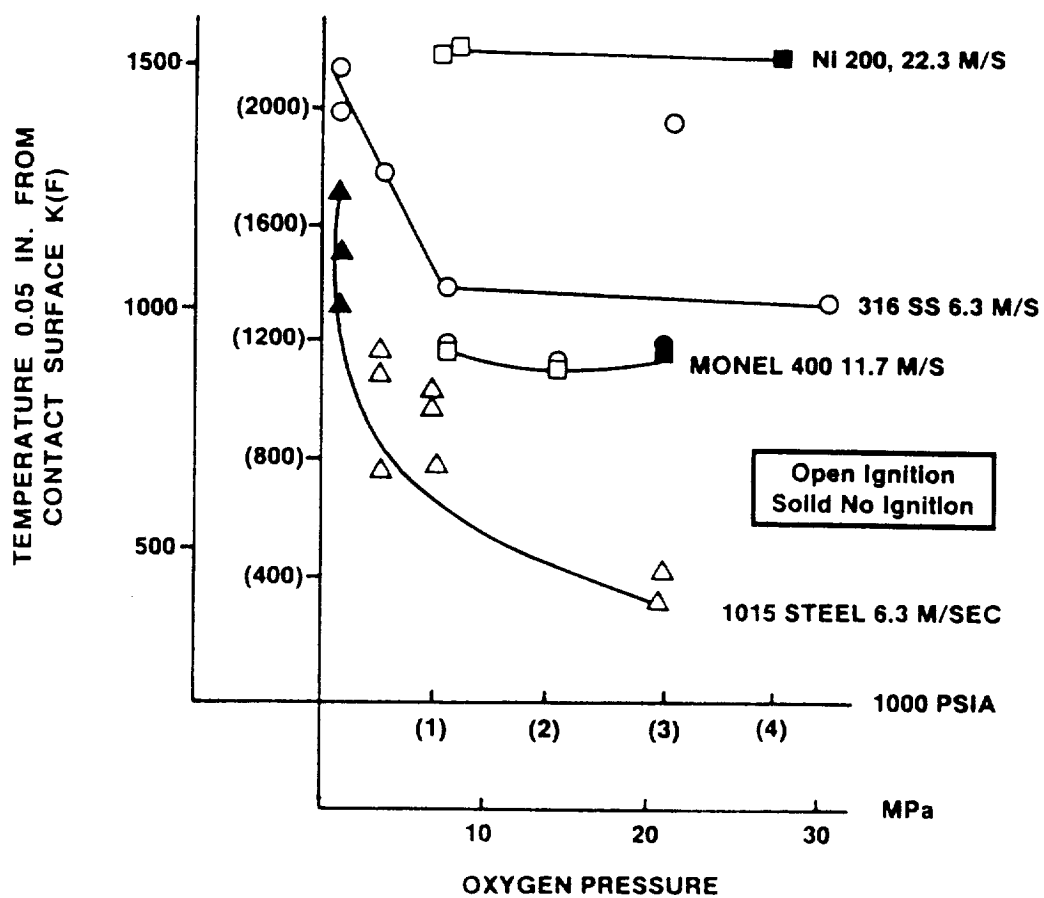


Figure 41. Effect of O₂ Pressure on Ignition Temperature

VI, B, Friction Heating Test Results (cont.)

The reduction in metal temperature which accompanies the increase in O_2 pressure could be attributed to increased convective cooling by the higher density oxygen, while the increase in friction coefficient could be a result of slower rates of oxide formation due to the lower temperature. The average friction coefficient measurements for the Monel K-500 in O_2 at several pressures and rubbing velocities are shown in Figure 42. These data suggest that surface temperature influences the friction coefficient more than either speed or the O_2 pressure.

In order to separate oxidation and cooling effects, additional Monel K-500 tests (Number 238 and 244 Table VII) were conducted in N_2 at 0.69 and 21 MPa (100 psi and 3000 psi). At a given set of pressure and load parameters, the N_2 tests resulted in nearly twice the heating rates and significantly higher (5 to 10 times) friction coefficients. The frictional forces in N_2 became large enough in 5 to 8 sec to fail the drive mechanism shear pin. No cooling benefit of the 21 vs 0.69 MPa (3000 psi vs. the 100 psi) N_2 was observed. These tests clearly indicate that O_2 and the resulting oxide film plays the major role in suppressing the surface heating rates.

Further separation of the effects of gas density induced cooling and friction reduction produced by the oxide film are displayed by the data set in Figure 43. This figure compares the heating of 9 ramped loaded 1015 Carbon Steel specimens in O_2 with 9 identical tests in N_2 at three significantly different pressures. The specimen temperature rise rate on the measurement at 0.127 cm (0.05 in.) from the rubbing surface are plotted in Figure 44 as a function of pressure. The benefits of the O_2 cooling plus oxide film over the N_2 cooling without the film are apparent.

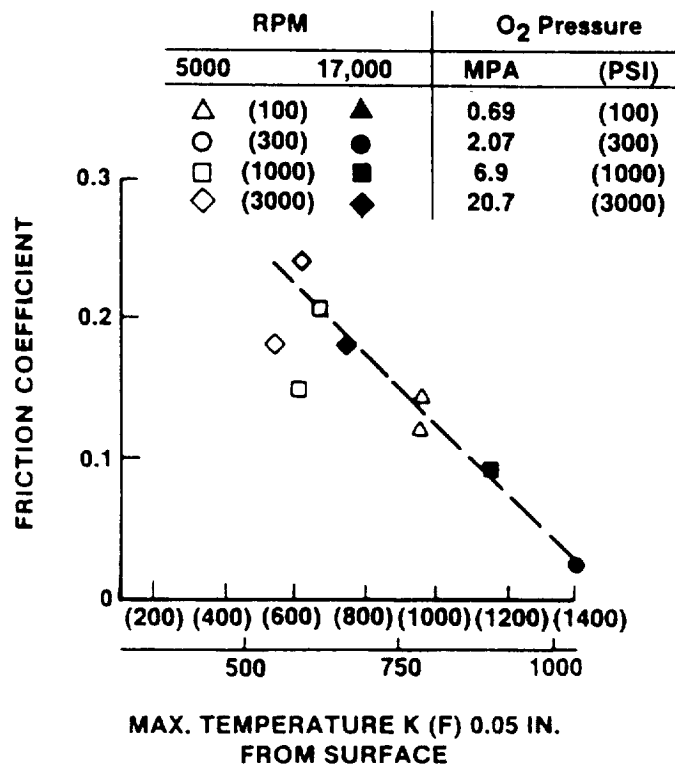


Figure 42. Effect of Surface Temperature and Oxygen Pressure on Friction Coefficient

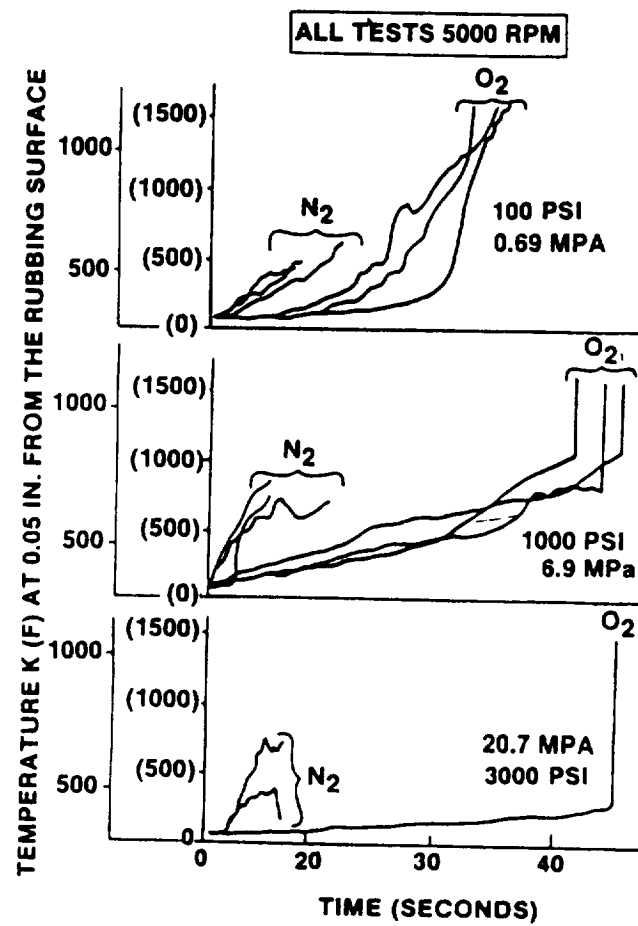


Figure 43. Friction Heating of 1015 Carbon Steel O_2 and N_2

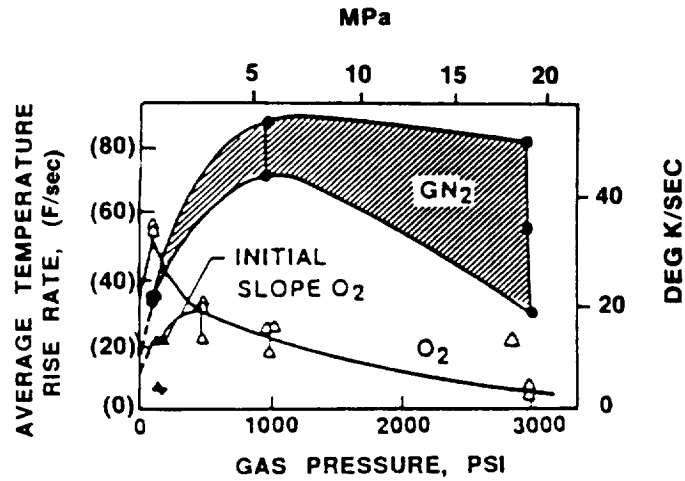


Figure 44. Effect of Gas Pressure on Friction Heating Rates of 1015 Steel Under Ramped Loading at 5000 RPM

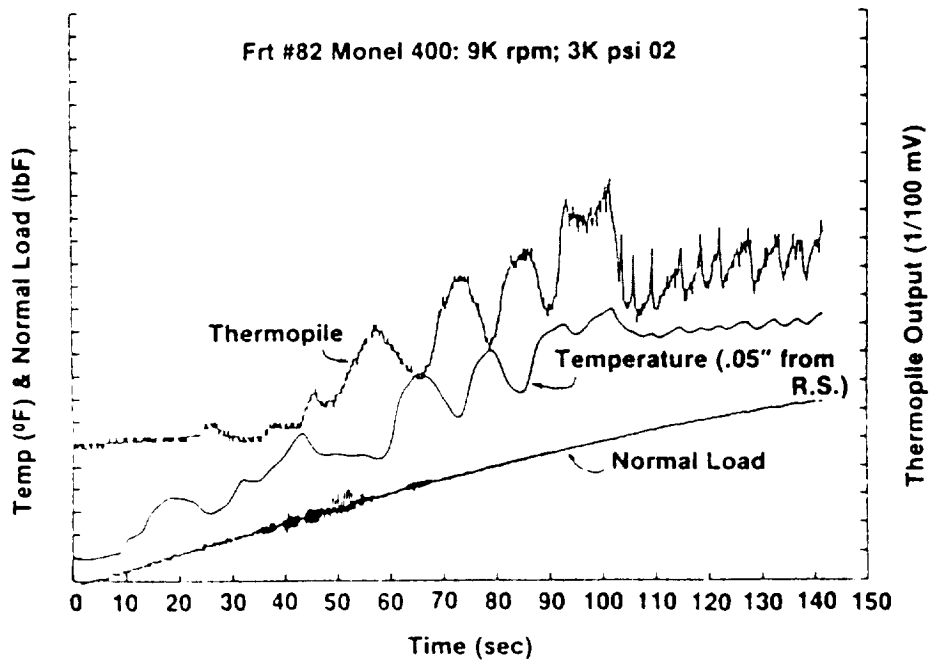


Figure 45. Phase Comparison of Optical and Thermocouple Temperature Measurements

VI, B, Friction Heating Test Results (cont.)

4. Temperature Oscillations

Repeated temperature cycling of the specimen throughout the program was noted. This is evident in Figures 21 and 37 for Monel 400 and this was also observed for 316 Stainless Steel and Monel K-500. The thermal cycling was less apparent in the 1015 Carbon Steel and copper alloy 150. The following observations are noted relative to this effect: 1) the cycling frequency increases at higher O_2 pressure; and 2) the thermopile cycling, which is sensitive to light or spark intensity, is 180 degrees out of phase with the temperature measurement. This can be observed by comparing the position of the peaks of the thermocouple and thermopile in Figure 45. Figure 46 displays the observed mean a time from one temperature peak to the next as a function of the oxygen pressure.

This observed temperature cycling is believed to be a result of oxide scale spalling and reforming. It can be postulated, as illustrated in Figure 47, that oxidation starts at some elevated temperature and the scale or glaze thickness increases to the point where it can no longer support the shear loads and is mechanically removed. The loss of the scale is immediately followed by fresh metal exposure and rapid combined frictional and oxidation heating. The rate of heating diminishes as a new protective film is formed. Since the oxidation rate at high-pressure can occur more rapidly, the cycle can be expected to have a higher frequency.

The thermopile and thermocouple are out of phase because of the low thermal conductivity of the oxide scale. The scale is at a maximum temperature at the surface where the friction energy is being generated. The metal is most insulated by this scale when the scale is at its maximum thickness, thus the metal temperature is at a minimum at this time. Radiation from the hot oxide film reaches a maximum as it approaches its spalling thickness, thus the maximum light intensity corresponds to the minimum sub-surface metal temperature.

ORIGINAL PAGE IS
OF POOR QUALITY

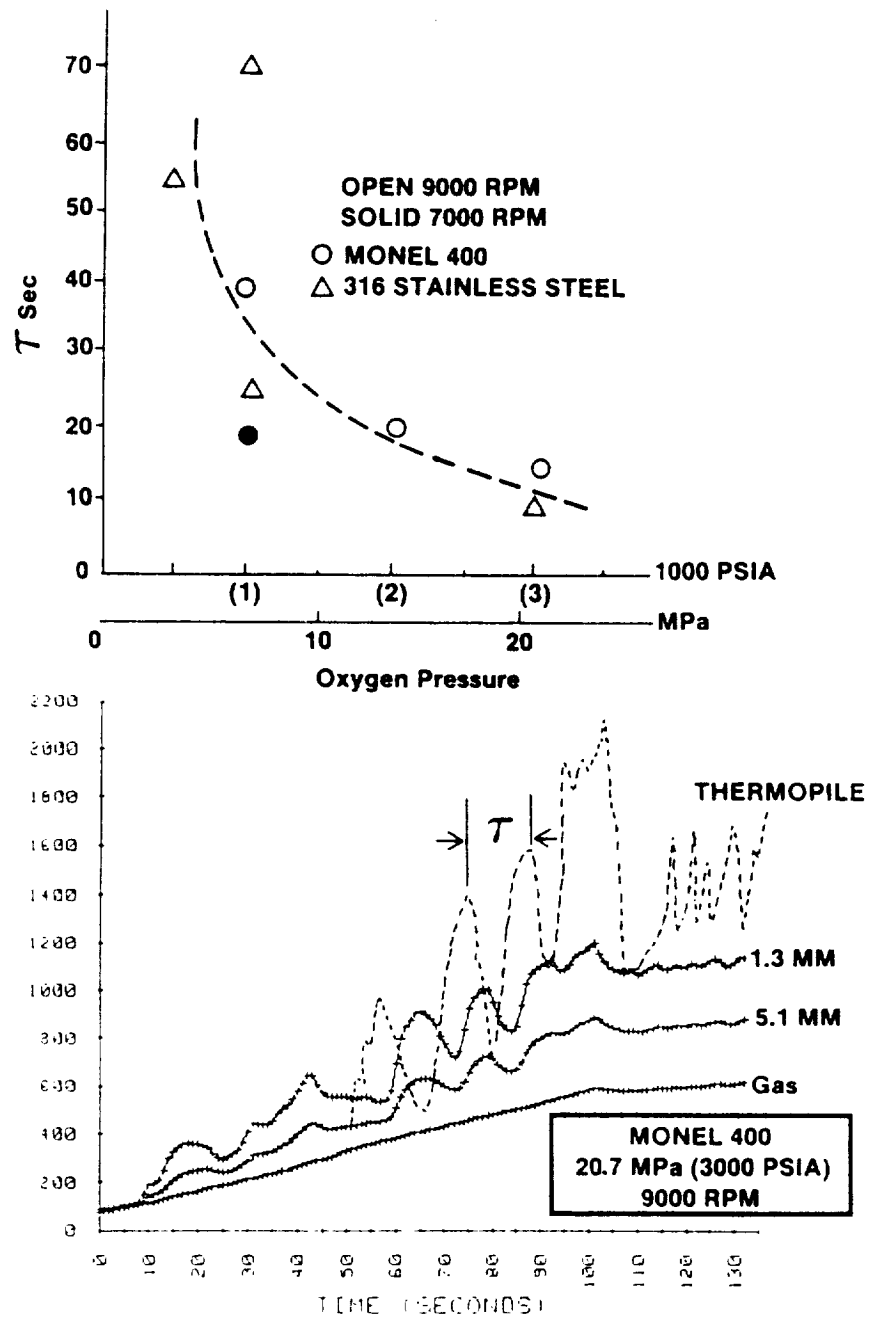


**Figure 46. Effect of Oxygen Pressure on Thermal Cycle Time
in Ramped Loading Tests**

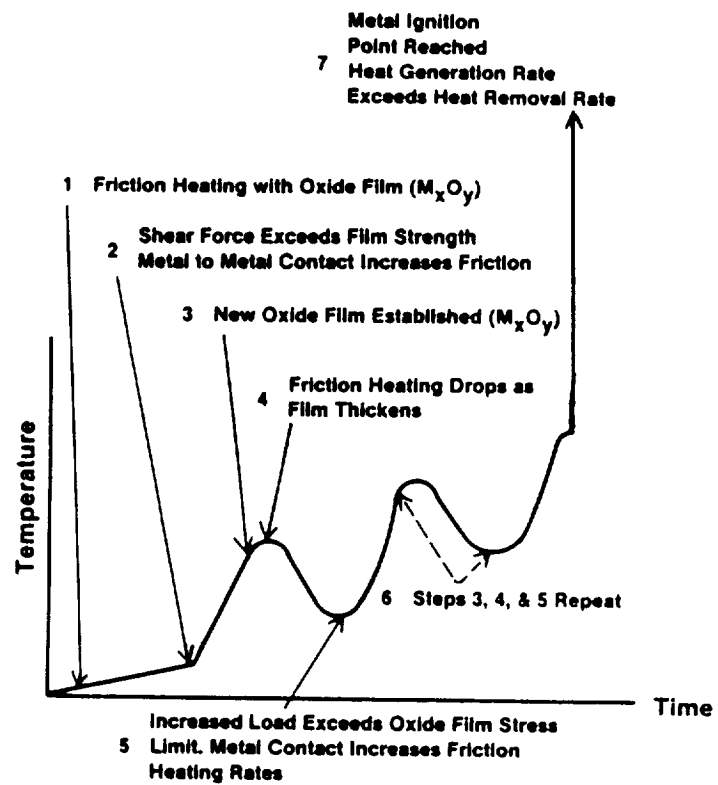


Figure 47. Hypothesis of Events Leading to Ignition in Friction Rubbing Tests

VI, B, Friction Heating Test Results (cont.)

If the above hypothesis is correct, desirable materials for friction rubbing applications should oxidize rapidly to form a high-strength, low-friction film. In order to prevent burning, the material should also have a low burn factor, as indicated in the next section.

5. Burn Factor Correlation

Correlation of the experimental data provided in Table V with the burn factor (BF), based on room temperature thermal diffusivity, is shown in Figures 48, 49 and 50. These data indicate the burn factor can provide a reasonable analytical guideline for ranking the materials employed in the friction rubbing test when temperature and contact loads at ignition are used as correlating parameters. The line drawn below data in the BF vs temperature plot can be assumed to contain design margin, in that the temperature shown is measured 0.0127 cm (0.05) in. from the heated interface. The actual contacting surface could be up to several hundred degrees hotter for the low thermal conductivity materials.

Data for an aluminum alloy and Brass 360, obtained through the same test procedures, Ref. 17, proved to be exceptions. The ignition and burning of brass is indicated by data point "B" in Figures 48, 49 and 50.

The alloy (B360) containing copper plus 3% Pb and 35% Zn behaved significantly different than the Cu (150) containing 0.15 Zr, as shown in Figure 51 and Table XV even though the calculated burn factors are not significantly different. The 360 alloy exhibited thermal instabilities and ignited in less than 30 sec, while the Cu-150 operated more than twice as long without igniting.

Figure 52 was prepared in an attempt to understand why aluminum and the Brass alloy did not fall inline with the other data. Figure 52 displays the metal heat of combustion vs the PV product required for metal

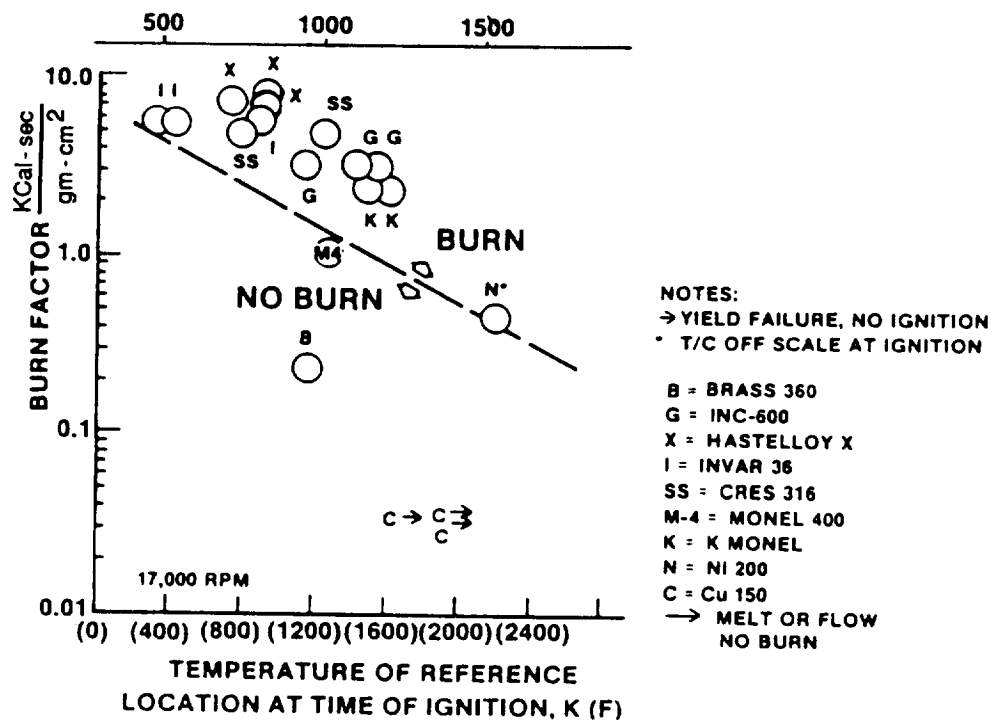


Figure 48. Burn Factor vs. Ignition Temperature in 6.9 MPa (1000 psi) O₂

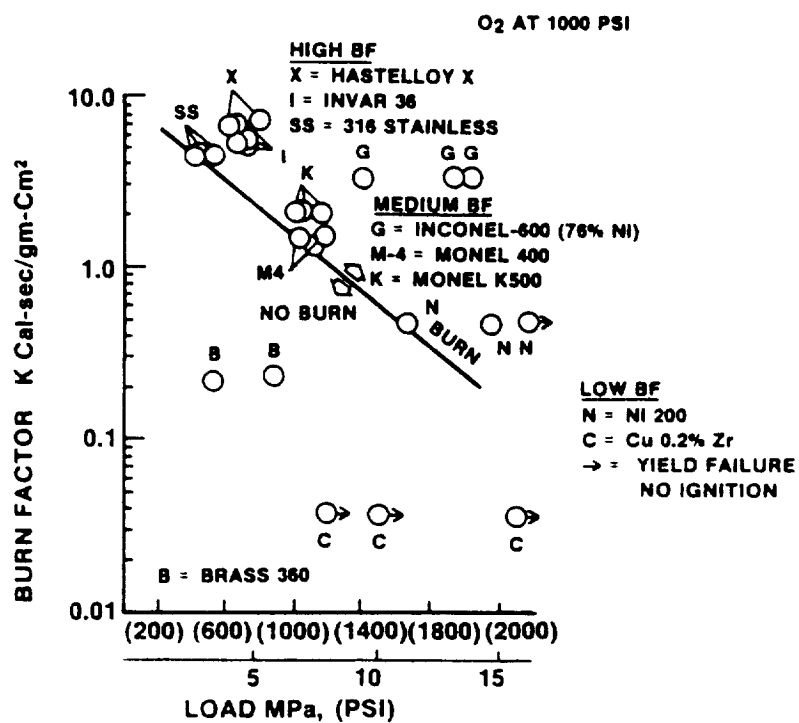


Figure 49. Burn Factor vs. Load at Ignition in 6.9 MPa O₂ at 17,000 RPM

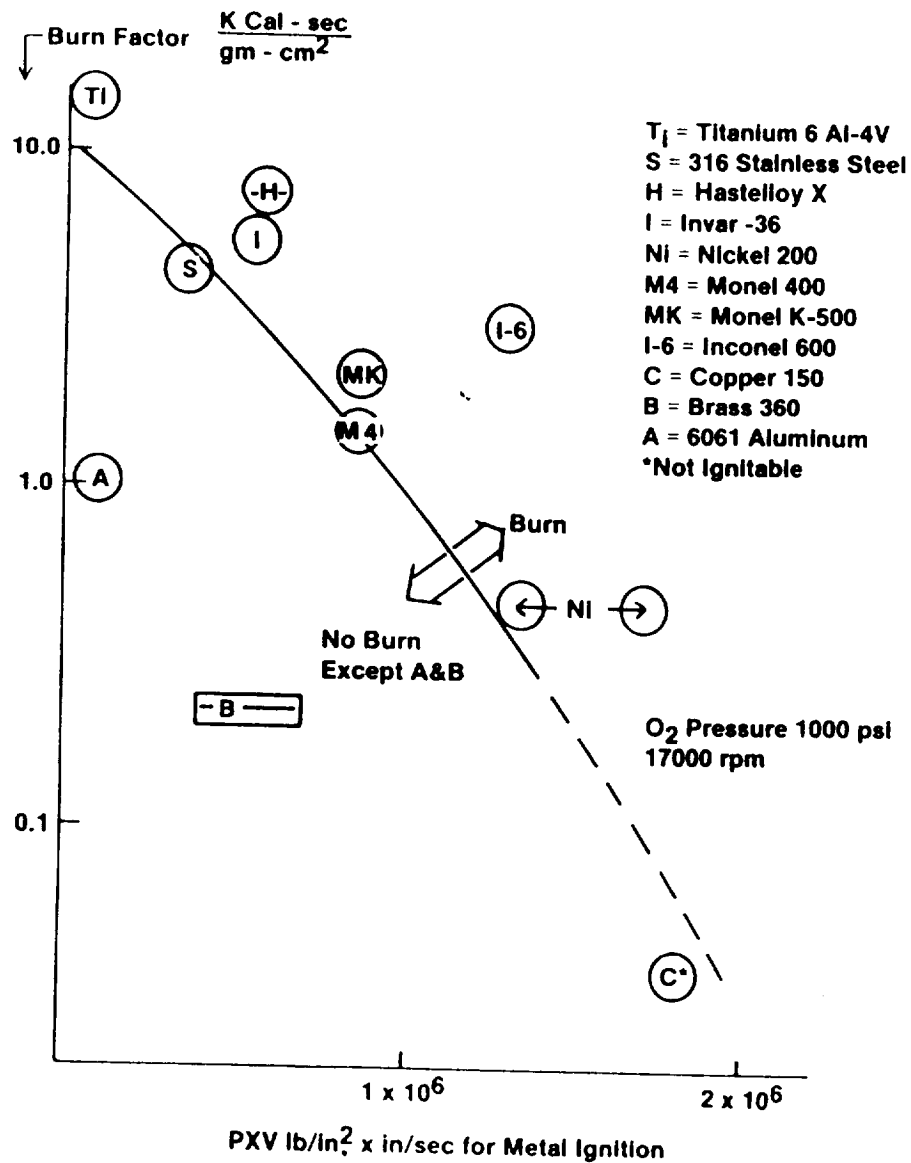


Figure 50. Thermal Diffusivity Based Burn Factor Condition vs. Experimental Ignition PXV Data

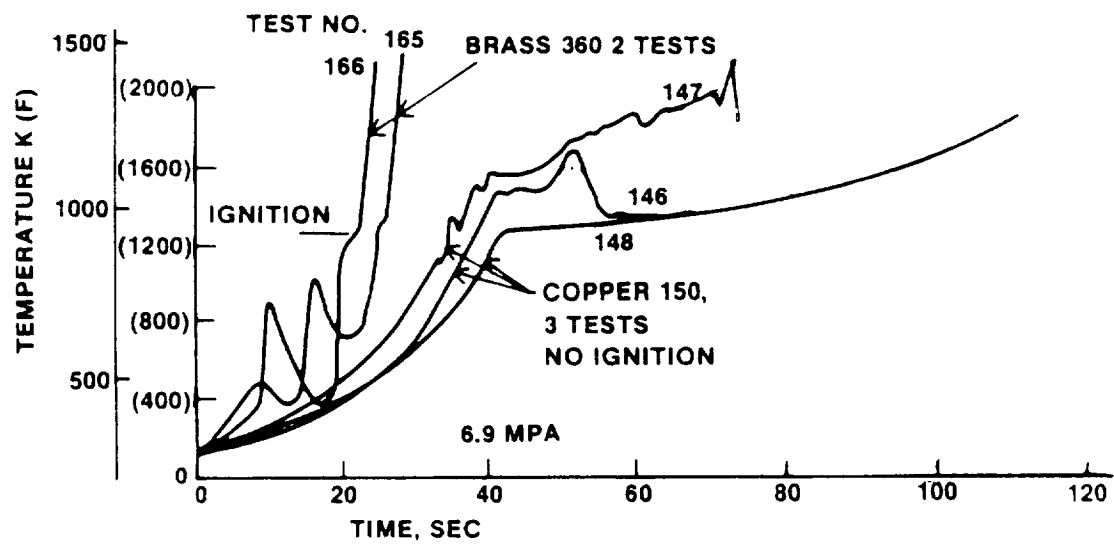


Figure 51. Comparison of Friction Heating Rate Ignition of Brass 360 and Copper 150

Table XV. Comparison of Friction Heating Ignition of Copper 150 and Brass 360 in 6.9 MPa (1000 psia) Oxygen at 17,000 RPM

Alloy	Ignition Temp		Ignition PV kw/M ²	Ignition Load		Burn Factor cal-sec/gm-cm ²
	(°C)	(°F)		N/M ² 10 ⁶	(psi)	
Cu-150	982	(1800)	>2.3 -10 ^{5a} ()	11.2	(1600) ^a	35
Brass 360	649	(1200)	0.74-1.3-10 ⁵	3.6-6.2	(530-930)	223

^aDoes not ignite.

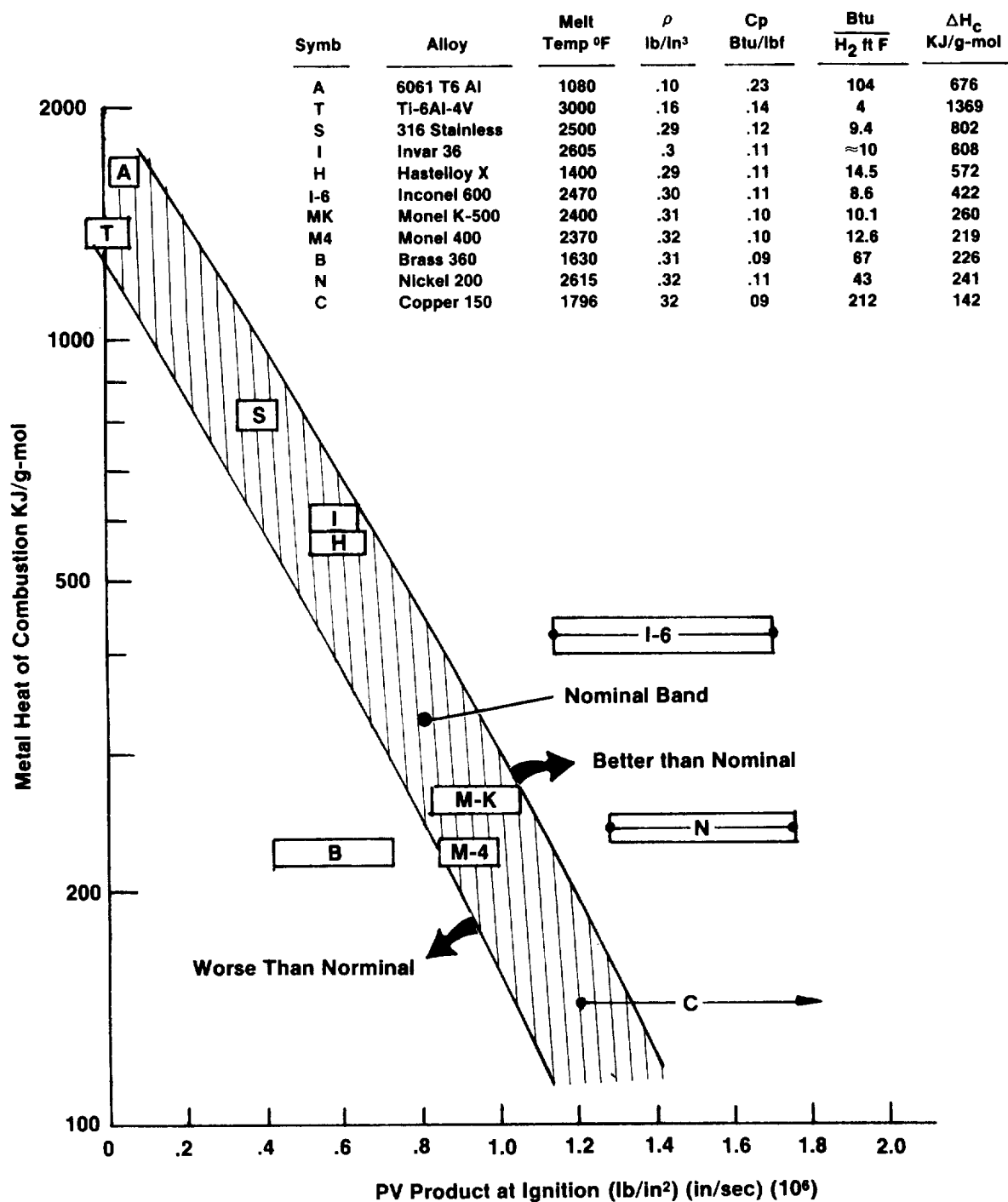


Figure 52. Correlation of Heat of Combustion with PV Product for Metal Ignition

VI, B, Friction Heating Test Results (cont.)

ignition in the 17,000 RPM ramped rubbing tests in 1000 psia oxygen. No attempt was made to account for other physical parameters in the graphical display however the thermal parameters which could influence the results are included in the properties tabulation.

The band drawn through the bulk of the data marked nominal is arbitrary and is provided only to aid in the discussion. In this format the aluminum falls within the nominal band which is in contrast to Figure 50 where aluminum falls below the line. The Brass again falls in a category that indicates worse than nominal operation while the nickel and Inconel 600 are better than nominal. The Brass, Monel and Nickel all have approximately the same heat of combustion. The goodness of the material appears to be in relation to the melting temperature where the brass at 1161K (1630°F) is the lowest and nickel at 1708K (2615°F) is the highest. Melting temperature alone is not the answer as titanium has a melting temperature 3 times that of aluminum but ignites more readily as noted in Table VII. The Inconel 600 has a heat of combustion approximately 2 times that of pure nickel 200 and a much lower thermal conductivity but is equal to nickel in burn resistance. The Inconel 600 contains 15.5% chrome and 8% Iron which appears to be capable of reducing friction heating by nature of the oxidized glaze formed.

One would normally expect the soft lead and zinc oxides formed by the brass to offer a significant reduction in friction coefficient over pure copper. The faster heating rate of this material as compared to Cu 150, in Figure 51, indicates that these soft oxides may do more harm than good.

Further investigation of the nature of the oxides formed in friction heating is the subject of the next phase of the experimental program.

VII. FRICTION HEATING AND WEAR RATES OF MONEL K-500 IN OXYGEN

A. OBJECTIVES AND BACKGROUND DATA

1. Objectives

The bearings, pump impeller turbine and portions of the structural housing of the OTV oxygen turbopump are fabricated from Monel K-500. The balance is Monel 400. The objectives of the phase of the program were to define the friction heating and wear rates of Monel K-500 material as a function of oxygen pressure and applied normal load and also to investigate the use of surface modifications to reduce both wear rate and friction heating.

2. Background

Whenever two surfaces undergo slip or sliding under a load there is wear. Wear could be classified as:

- a. Adhesive wear
- b. Abrasive wear
- c. Erosive wear

Sarkar¹⁸ reports that of the three types of wear mentioned above the adhesive wear is the most destructive.

The tribological behavior of the metals used in turbo-machinery has been investigated by some researchers. Lin et al¹⁹ investigated the friction and wear characteristics of Nickel base (Nimonic 75, C 263, Nimonic 108 and Incoloy 901) alloys in air at room temperature. Lin et al. tested the samples at relatively low speeds (500-600 rpm) and concluded that the mechanism for room temperature wear of these alloys was associated with the strength properties and the changes in the coefficient of friction and the wear rate during sliding related to work hardening and age hardening of the load bearing areas. The work hardening and age hardening are probably due to mechanical and thermal stresses developed.

VII, A, Objective and Background Data (cont.)

Stott²⁰ studied the tribological behavior of Nickel and Nickel Chromium alloys. Friction and wear characteristics were investigated at temperatures ranging from 193 to 1073 K (-113 to 1471 F). They found that the alloys show a transition temperature above which a low coefficient of friction and relatively low wear are observed. Above the transition temperatures the changes in the frictional and wear characteristics were associated with the formation of a thermally softened oxide layer (glaze) on the load bearing areas.

Bisson^{21,22} reported that the presence of any material other than that comprising the sliding surfaces (contaminating film) can have a considerable effect on the friction, wear and surface damage. He studied the formation of solid films on steel, nickel and copper alloys and based on earlier reported data concluded that the films formed of lower shear strength materials give low friction coefficients. Stott et al²³ reports that the shiny, glassy looking film or glaze plays a major role in reducing friction and wear of the alloy surfaces during sliding at elevated temperature. The details of the mechanisms for the formation of glaze are reported by Stott et al²³. None of these previous experiments were conducted using surfaces which were cleaned for oxygen surface, i.e., all surface films removed, and none were conducted in a pure oxygen atmosphere.

B. TEST METHOD

1. Apparatus

The test apparatus employed was identical to that used in the earlier friction heating tests and all tests were conducted at a rotational speed of 17,000 rpm.

VII, B, Test Method (cont.)

The test variables in addition to the surface modifications were the oxygen pressure and the applied loading. The initial tests employed the following normal contact stress vs time profile for a total test duration of 240 S.

<u>Time</u>	<u>Normal Contact Stress</u>
0-40 S	0.34 MPa (50 psi)
40-80 S	1.38 MPa (200 psi)
80-140 S	0.34 MPa (50 psi)
140-180 S	2.7 MPa (400 psi)
180-240 S	0.34 MPa (50 psi)

Figure 53 shows the total normal forced and drive power vs time for an ambient pressure O_2 test on untreated Monel K-500. The repeatability of the measured temperature profiles 1.27 mm (.05 in.) from the rubbing surfaces in Tests 75 and 76 is also shown in this figure.

The applied load was returned to the initial load after each higher load step to allow changes in wear rate and friction heating to be identified. Tests for each type of surface were conducted at 87.5 kPa (12.7 psia) (1 ATM at the White Sands Test Facility) and 6.9 MPa (1000 psi) oxygen pressure using a new pair of wear rings for each test. Comparisons of surface material parts were made with untreated Monel K-500.

The second type of test also conducted, used a constant 0.34 MPa (50 psi) load for a 300 S duration test. The oxygen pressure in the constant load test was 6.9 MPa (1000 psia).

2. Measurements

The following measurements were made:

- a. RPM vs time
- b. Motor drive power vs time (watts)
- c. Normal load vs time (lbF)
- d. Torsional load vs time (lbF)

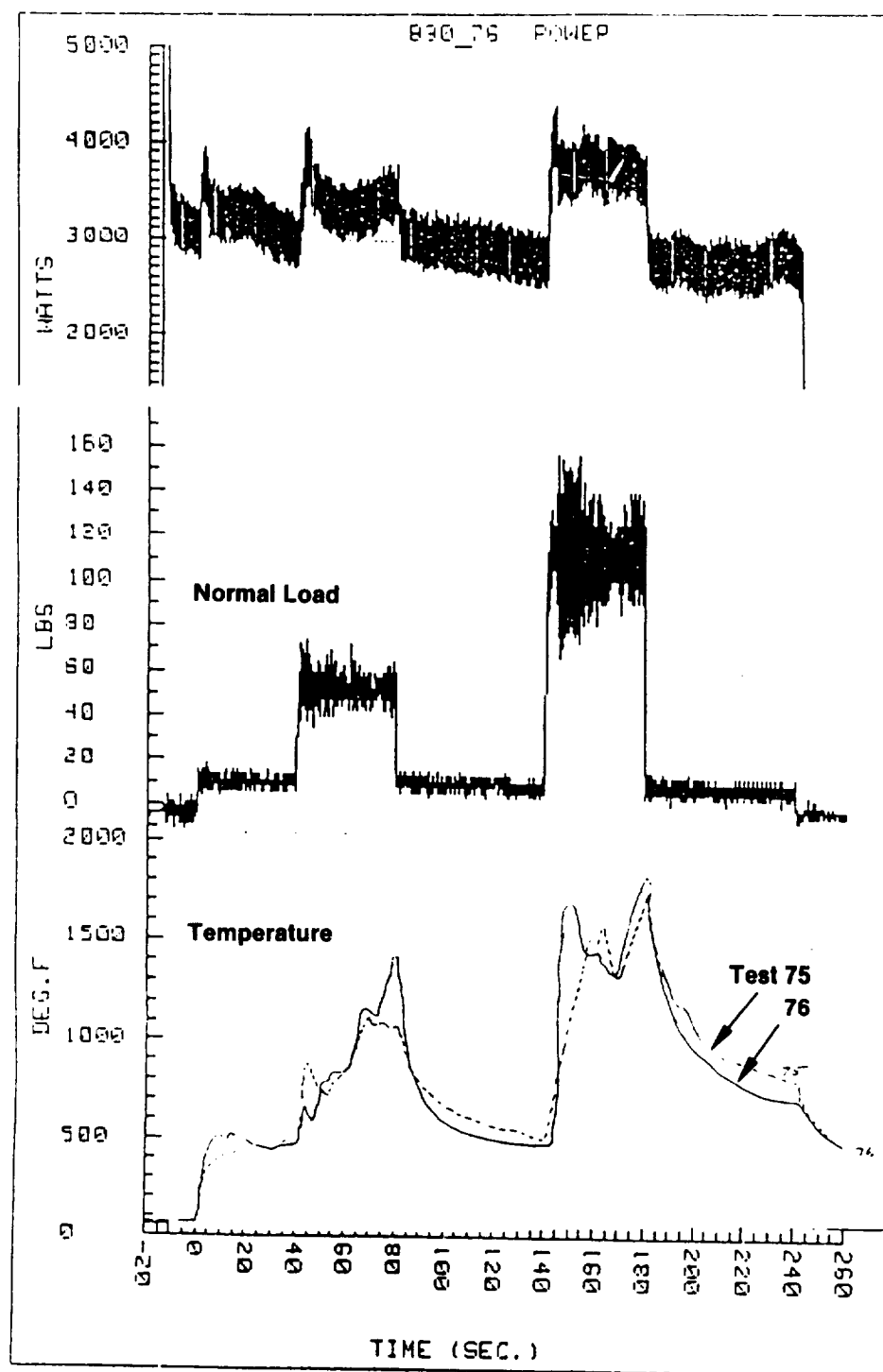


Figure 53. Typical Baseline Monel K-500 Power, Load and Temperature vs. Time Data 14.7 psia O₂ 17,000 RPM

VII, B, Test Method (cont.)

- e. Shaft displacement vs time (in.)
- f. O₂ pressure vs time (psia)
- g. Temperature vs time at 1.27 and 5.08 mm (0.05 and 0.2 in.) from the rubbing surface of the fixed specimen
- h. O₂ temperature in the cell

The temperature at the rubbing interface was also observed by a thermopile. The lack of a valid calibration for the various surface emissions limited this function to defining heating and cooling relative to the data recorded on the thermocouples used for Item g. above. Figure 54 displays these measurements for a typical test. The one large spike in thermopile output at 155 sec is again noted to correspond to a minimum thermocouple reading.

In theory the experimental friction coefficients can be computed from the torque, normal load and speed data, and independently from the sample heating rates and also from the power input after appropriate calibrations. The figure shows the friction coefficient computed from the two force and speed measurements. Figure 55 displays the friction coefficient based on power measurements from Tests 77, 78 and 86, untreated Monel K-500 in 6.9 MPa (1000 psia) oxygen. It can be observed that repeatable data are obtained at the two high load steps only in the 40 to 80 and 140 to 180 time-frame. The power measurement was of little value in computing friction coefficients and is not discussed further.

In addition to the above, each test specimen was weighed and measured before and after testing. This provided 3 methods of computing wear rate data as follows:

- a. Displacement sensor provided on line data
- b. Pre to post test weight reduction
- c. Pre to post test length change

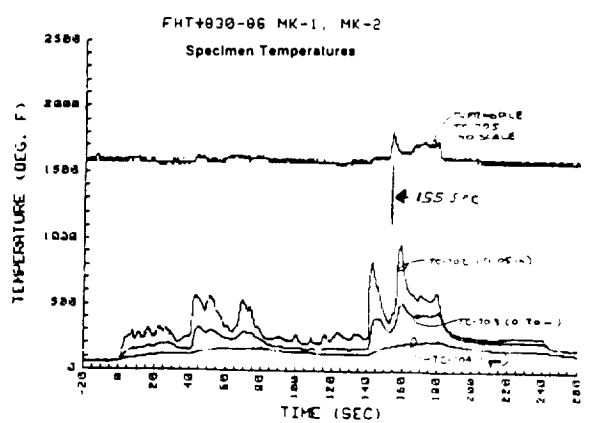
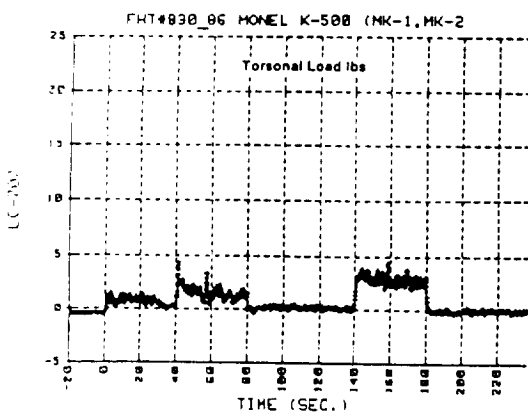
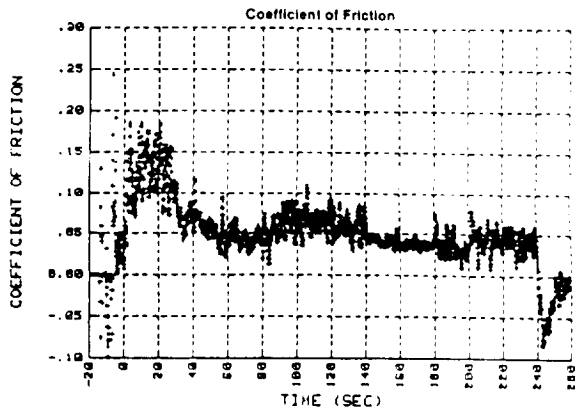
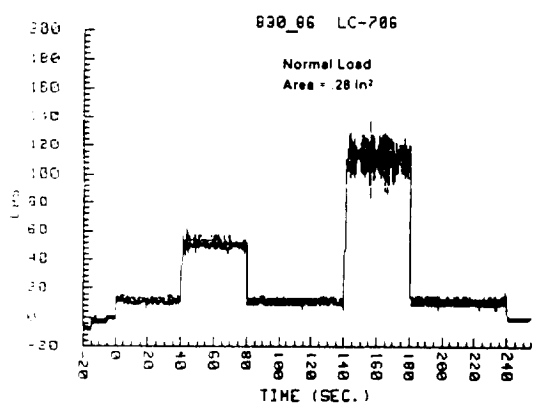
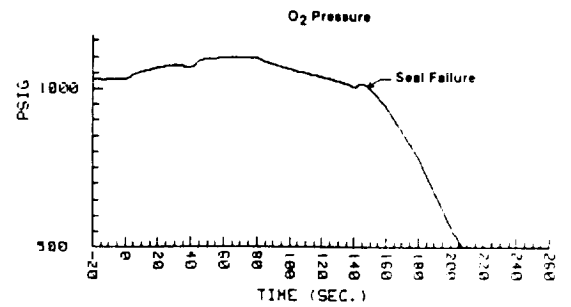
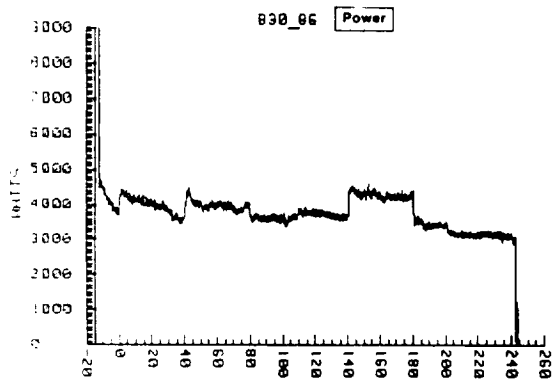
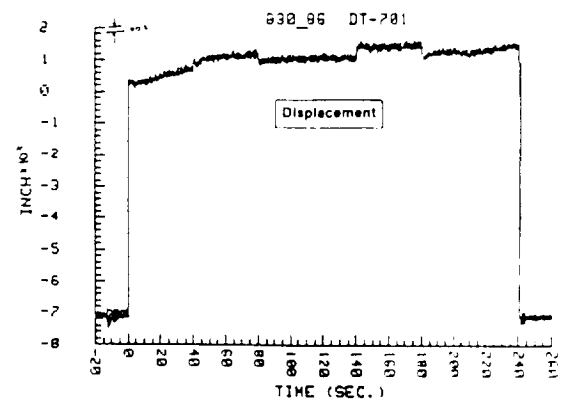
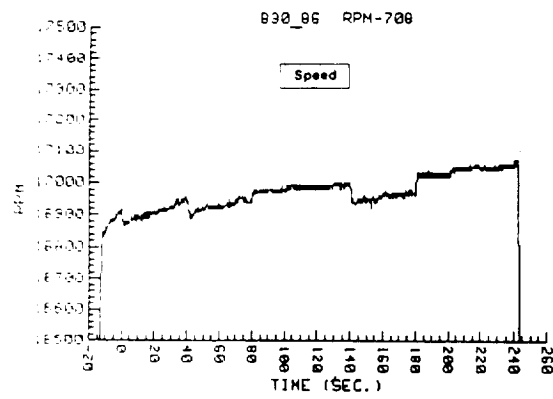
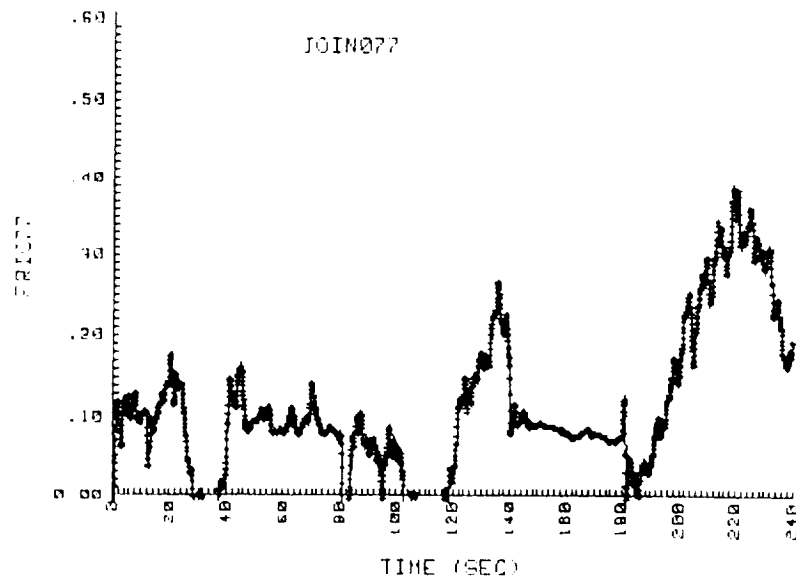
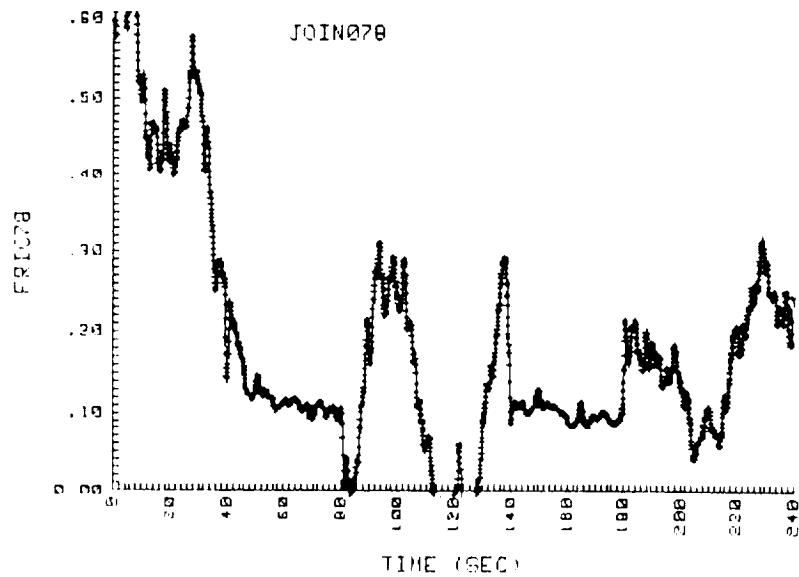


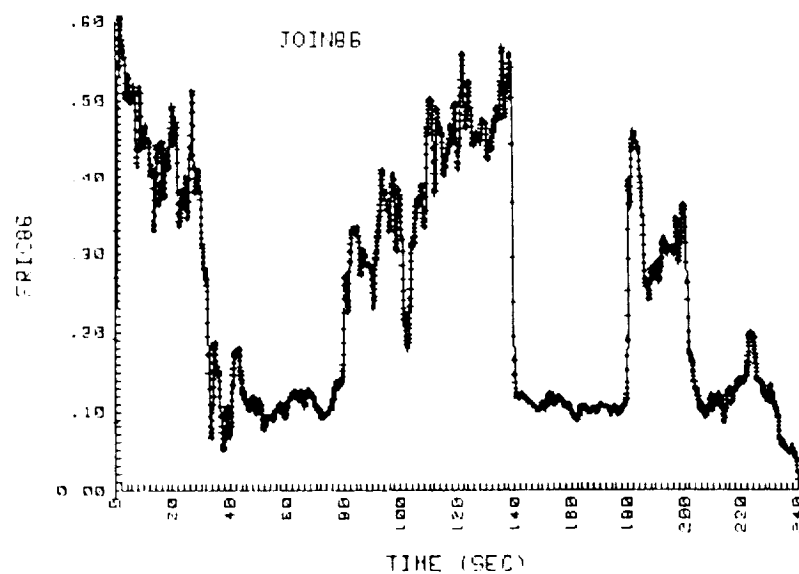
Figure 54. Representative Data Set Unmodified Surface



Test 77



Test 78



Test 86

**Figure 55. Friction Coefficient Computed from Drive Power for 5 Load Steps
(Untreated Monel K-500, 1000 psia O₂, 17,000 RPM)**

VII, B, Test Method (cont.)

The online displacement sensor provided the only method of estimating wear rate vs time during a test.

3. Test Procedures

In the ambient pressure tests the chamber was purged with oxygen to ensure that all air was removed. In tests conducted at 6.9 MPa (1000 psi) the test chamber was pressurized with oxygen after purging. The drive motor was then turned on and the rotational speed of 17,000 rpm was established. The data acquisition system was then activated and the friction test initiated by pressurizing the pneumatic actuation cylinder which applied the desired pre-programmed load to the samples. After the test was completed the data acquisition system was turned off, the test chamber was vented, and the samples were removed and then weighed, measured and visually examined.

C. SURFACE MODIFICATIONS

The test specimen design, shown in Figure 56, consists of the base material Monel K-500 heat treated to provide a hardness of Rockwell C-35 which is the same as specified for the OTV turbopump material. Heat treatment was per QQ-N286E Class A form (1), i.e., age harden 16 hour at 1100°F, cool in 100°F steps to 900°F holding at each step from 4 to 6 hours before cooling from 900 to room temperature. The 8 micron RMS surface finish and flatness was applied after heat treatment.

Table XVI defines the surface modifications applied to the substrate and the source of the surface processing. The Ion implants were accomplished under subcontract to the SPIRE Corp. using their recommended implant dosages.

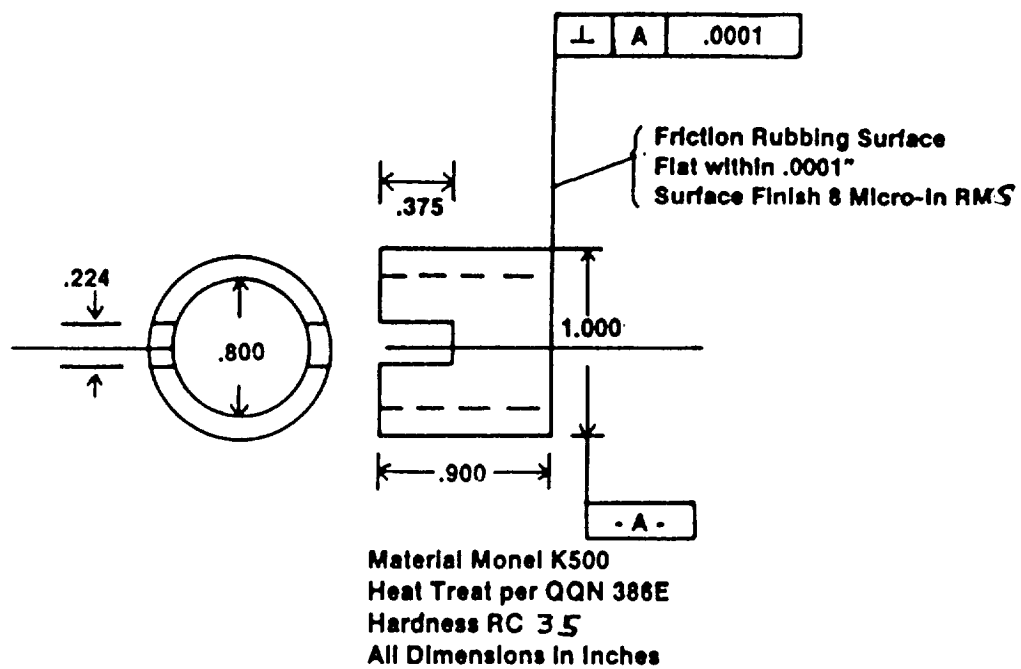


Figure 56. Test Specimen Design

Table XVI. Monel K-500 Surface Modifications

<u>Surface Modification</u>	<u>Designation</u>	<u>Source</u>	<u>Thickness or Density</u>
Ion Implanted Oxygen	I O ₂	Spire Corp.	3×10^{17} Ion/cm ² at 150 Kev
Ion Implanted Chromium	I Cr	Bedford, MA	1×10^{17} Ion/cm ² at 150 Kev
Ion Implanted Lead	I Pb	Bedford, MA	5×10^{16} Ion/cm ² at 150 Kev
Ion Implanted Silver	I Ag	Bedford, MA	1×10^{17} Ion/cm ² at 150 Kev
Electrolized Chrome	E Cr	Electrolizing, Inc. Los Angeles, CA	0.0003 to 0.0005 in. Hard dense chromium
Electroless Ni + Silicon Carbide Composite (NYE-CARB)	E-C	Electro Coatings, Inc. Houston, TX	NYE-CARB $0.003 \pm .001$ in. Ni, 6% P, 30% Silicon Carbide
Electroplated Silver	E Ag	Com-Mil Spec Plating	0.002 - 0.003 in.
Electroplated Gold	E Au	Com-Mil Spec Plating	0.005 - 0.006 in.

VII, C, Surface Modifications (cont.)

1. Test Specimen and Surface Modification Selections

a. Baseline

The baseline material was Monel K-500 having the 8 micron surface finish and the RC 35, (350 Kg/mm² knoop) hardness shown in Figure 56. Post heat treatment hardness testing indicated that the desired hardness was attained.

b. Surface Modification (1) - Oxygen, Ion Implantation

The Monel K-500 was modified by the ion implantation of oxygen. The objectives were to obtain an understanding of the influence of a high concentration of oxygen and surface oxides on the friction coefficient, hardness, and wear resistance of the baseline material.

c. Surface Modification (2) - Lead, Ion Implantation

The presence of soft oxides, as in the 360 brass, appears to have an adverse effect on ignition under heavy loading conditions. The influence of a metal which forms a very soft oxide will be evaluated. Other candidate metals which form soft oxides are boron and rhenium. These could be investigated in future tests.

d. Surface Modification (3) - Chrome, Ion Implantation

Chrome forms a very hard oxide. The favorable results with Inconel-600 (76Ni, 15Cr, 8Fe) suggest a beneficial effect of chrome oxide.

VII, C, Surface Modification (cont.)

e. Surface Modification (4) - Silver, Ion Implantation

Silver has the lowest burn factor of all candidate surface materials. Silver will not form an oxide at elevated temperature but has been reported to provide good lubrication characteristics.

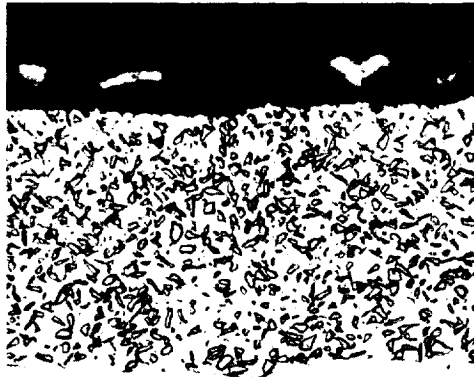
f. Surface Modification (5) - Chrome Plating

Comparison of ion implantation and conventional continuous film plating will be made. The plating provides a 100% surface coating of chrome vs a nominal 10% for ion implantation. The proprietary "Electrolizing" hard chrome plating process was selected and is reported to provide a Rockwell C70, (1070 Knoop) hardness. The harder surface is expected to reduce the wear rate under normal rubbing conditions.

g. Surface Modification (6) - Composite Plating Ni-SiC

Nickel and silicon carbide both have been shown to provide good ignition resistance. Electro Coatings, Inc. provides a proprietary Ni-SiC composite plating which contains 30 volume % 1 to 3 micron particulate silicon carbide in an electroless nickel matrix. The matrix has a hardness of RC68 ($920 \frac{\text{Kg}}{\text{mm}^2}$ Knoop) and the SiC particulate hardness is 1400 on the Knoop scale. The bulk hardness of the coating reported by the manufacturer is 1200 Kg/mm^2 on the Knoop scale. Figure 57 shows a cross section of a typical coating supplied by the manufacturer.

Additional test samples of silver and gold plated onto the Monel were also available as residual cryogenically cycled rings fabricated as part of the OTV turbopump tank.



NYE-CARB[®] COMPOSITE 600X
Cross-Section

Figure 57. Cross-Section of NYE-CARB[®] Composite

ORIGINAL PAGE IS
OF POOR QUALITY

VII, Friction Heating and Wear Rates of Monel K-500 in Oxygen (cont.)

D. TEST SUMMARY

1. Variable Loading Friction Tests

Test Numbers 75 through 109, documented in Table XVII, employed the five step variable loading profile discussed earlier. The tests are listed in the order in which they were conducted. The table shows the specimen material code for the rotating (r) and stationary (s) specimen, the ring serial number, and the weight change for each specimen resulting from the coating processing as well as the subsequent change in friction testing. Some weight loss was reported for the ion implantation as a result of the ion beam surface milling cleaning prior to the ion implant. The material removal apparently exceeded the material addition. The weight change measurements were more sensitive than length change which was also measured.

The after test length of each set of rings was measured by rotating and clamping the wear surfaces face to face until a minimum total length was achieved. The average of multiple measurements taken around the periphery are reported in this table. The change in length reported is the difference between the pre- and post test length.

The change in length, calculated from the change in weight using the 8.46 gm/cc density of Monel K-500 is provided in the table for comparison with the direct measurement of length change.

The test type code shows an A for testing in oxygen at ambient pressure and a B for tests in oxygen at 6.9 MPa (1000 psia).

2. Constant Loading Friction Tests

Table XVIII provides similar data for the constant load tests in the order in which they were conducted.

Table XVII. Summary of Weight and Length Data for the Variable Load Test

Test	Test Type A = Amb O_2 B = 6.9 MPa O_2	Specimen Code	Before/After Coating		Before/After Test		ΔL in. from Δ Weight
			Weight (g)	Length (in.)	Weight (g)	Δ Length (a) (in.)	
75	A	C5 s	N/A	N/A	+.0048	-.0022 ^b	-.0016
75	A	C6 r	N/A	N/A	-.0464		
76	A	C7 s	N/A	N/A	-.0591	-.0026 ^b	-.0039
76	A	C8 r	N/A	N/A	-.0410		
77	B	C9 s	N/A	N/A	-.2023	-.0104 ^b	-.0135
77	B	C10 r	N/A	N/A	-.1414		
78	B	C11 s	N/A	N/A	-.3683	-.0095 ^b	-.0144
78	B	C12 r	N/A	N/A	+.0014		
79	B	I-01 s	-.0013	+.0000	-.1410	-.0085	-.0064
79	B	I-02 r	-.0004	+.0000	-.0213		
80	B	I-Cr1 s	-.0012	+.0000	-.0882	-.0055	-.0046
80	B	I-Cr2 r	-.0009	+.0000	-.0278		
81	B	I-Ag1 s	-.0014	+.0000	-.0852	-.0140	-.0135
81	B	I-Ag2 r	-.0010	+.0000	-.2582		
82	B	I-Pb1 s	-.0010	+.0000	-.0441	-.0045	-.0065
82	B	I-Pb2 r	-.0006	+.0000	-.1224		
83	B	E-Cr1 s	+.0050	+.0004	-.3120	-.0115	-.0192
83	B	E-Cr2 r	-.0013	+.0003	-.1773		
84	B	E-Cr6 r	+.0070	+.0005	-.0222	-.0070	-.0134
84	B	E-Cr7 s	+.0011	+.0003	-.3182		
85	B	E-C6 r	+.7872	+.0034	-.1050	-.0055	-.0069
85	B	E-C7 s	+.7125	+.0029	-.0710		
86	B	Mk-1 s	N/A	N/A	-.2476	-.0090	-.0106
86	B	Mk-2 r	N/A	N/A	-.0226		
87	A	I-Cr3 s	-.0013	+.0000	+.0025	-.0105	-.0018
87	A	I-Cr2 r	-.0006	+.0000	-.0488		
88	A	E-Cr3 s	+.0152	+.0005	+.0033 ^c	-.0255	-.0216
88	A	E-Cr4 r	+.0018	+.0004	-.5498		

Table XVII. Summary of Weight and Length Data for the Variable Load Test (cont.)

Test	Test Type A = Amb O ₂ B = 6.9 MPA O ₂	Specimen Code	Before/After Coating		Before/After Test		ΔL in. from Δ Weight
			Weight (g)	Length (in.)	Weight (g)	Δ Length (a)(in.)	
89	A	I-03 s	-.0008	+.0000	-.0303	-.0015	-.0013
89	A	I-04 r	-.0005	+.0000	-.0028		
90	A	I-Ag3 s	-.0012	+.0000	-.0283 ^C	-.0030	-.0018
91	A	I-Pb5 s	-.0009	+.0000	+.0058 ^C	-.0040	-.0040
91	A	I-Pb6 r	-.0004	-.0001	-.1080		
92	A	Mk-3 s	N/A	N/A	-.6564	-.0540	-.0888
92	A	Mk-4 r	N/A	N/A	-1.6058	Burned?	
93	A	E-C8 r	+.8062	+.0020	-.1676	-.0030	-.0107
93	A	E-C9 s	+.7472	+.0029	-.1057		

94-99 were calibration tests.

100	A	Mk-5 s	N/A	N/A	-.0284	-.0030	.00317
100	A	Mk-6 r	N/A	N/A	-.0523		

101-102 were calibration tests.

103	A	I-cr5 s	-.0012	+.0000	-.1530	-.0080	.00663
103	A	I-Cr6 r	-.0008	+.0000	+.0158		
104	A	E-Cr8 r	-.0054	+.0000	-.0110	-.0080	-.0054
104	A	E-Cr9 s	-.0007	+.0001	-.1265		

105-107 were calibration tests.

			Coating Thickness (in.)				
108	B	Silver5 s	.0027		-.3285	-.0135	-.018
108	B	Silver6 r	.0021		-.1297		
109	B	Gold1 r	.0055		+.3826	+.0020	-0.000
109	B	Gold2 s	.0059		-.4118		

- a This delta-length measurement was made by subtracting the combined length of the test samples after the test from the combined length of the test samples before the test.
- b The combined length of the test samples before the test was not measured for these samples, therefore the delta-length was determined by adding the average lengths of the individual samples measured before the test and subtracting the combined length of the test samples measured after the test.
- c Small piece of thermocouple wire was stuck in one of the thermocouple holes and could not be removed.

Table XVIII. Constant (50 psi) Load Friction Tests in 6.9 MPa (1000 psi) O₂

Test No.	Test Sample	Combined Length		Length Reduction in.	Weight, gms		$\Delta L = \frac{\Delta W}{.0392 \text{ gm/mil}}$
		Pretest	Posttest		Pretest	Posttest	
830-167	MK R MK S	1.7080"	1.7045"	0.0035	30.8093 30.5293	30.7604 30.5220	1.4
830-168	MK-14 R MK-15 S	1.704"	1.702"	0.002	30.7265 30.692	30.6475 30.6928	2
830-169	IPb 4 R IPb-7 S	1.7075"	1.7065"	0.001	30.7594 30.6447	30.7547 30.5759	1.9
830-170	IAg-8 R IAg-9 S	1.7075"	1.7060"	0.0015	30.8297 30.7165	30.8265 30.6633	1.4
830-171	Io-6 R Io-5 S	1.706"	1.7075"	0.0015	30.7854 30.7038	30.7523 30.6252	2.8
830-175	ICR-8 R IgR-7 S	1.707"	1.699"	0.008	30.7253 30.6850	30.7256 30.3173	8.0
830-176	EC-2 R EC-1 S	1.7115"	1.7095"	0.002	31.5340 30.8797	31.5301 30.8745	0.2
830-177	ECR-14 R ECR-13 S	1.704"	1.680"	0.024	30.7393 30.6901	29.8129 30.7058	23.2
830-178	ECR-16 R ECR-15 S	1.705"	1.672"	0.033	30.7215 30.6296	30.7360 28.7671	47.1
830-179	IAg 6 R IAg 5 S	1.705"	1.699"	0.006	30.8203 30.6956	30.8027 30.6874	0.7
830-180	IPb-8 R IPb-9 S	1.707"	1.705"	0.002	30.7495 30.6877	30.7457 30.6747	0.4
830-181	ICr-10 R ICr-9 S	1.705"	1.705"	0.0	30.6342 30.6821	30.6603 30.6230	0.3 (gain)
830-182	IO-8 R IO-7 S	1.705"	1.705"	0.00	30.7581 30.5871	30.8486 30.5720	0.6
830-183	MK-16 R MK-17 S	1.702"	1.703"	-0.001"	30.6712 30.6246	30.6615 30.6070	0.7
830-184	EC-3 R EC-4 S	1.709"	1.7095"	-0.0005"	31.5205 30.6197	31.5207 30.6205	0.3

VII, Friction Heating and Wear Rates of Monel K-500 in Oxygen (cont.)

E. RESULTS AND DISCUSSIONS

The following sections summarize the results for the tests conducted to determine the friction and wear characteristics of heat treated Monel K-500 with surface modifications.

1. Friction Heating

The heat generated due to friction at the areas of contact diffuses to the surroundings to establish an average temperature at the interface once steady state heat transfer is achieved.

Figure 58 provides a comparison of superimposed temperature profiles from four uncoated Monel tests using the time variable loading. All temperatures are measured on the stationary specimen 1.27 mm (0.05 in.) from the rubbing surface. As noted in the figure two tests were in ambient pressure oxygen and two were in oxygen at much higher pressures. The following observations can be made from these data.

- a. No specific temperature can be assigned to set of test conditions but a peak temperature and range can be provided.
- b. Similar time temperature profiles for repeat tests were obtained.
- c. The test specimen operates at a lower temperature in high pressure oxygen.

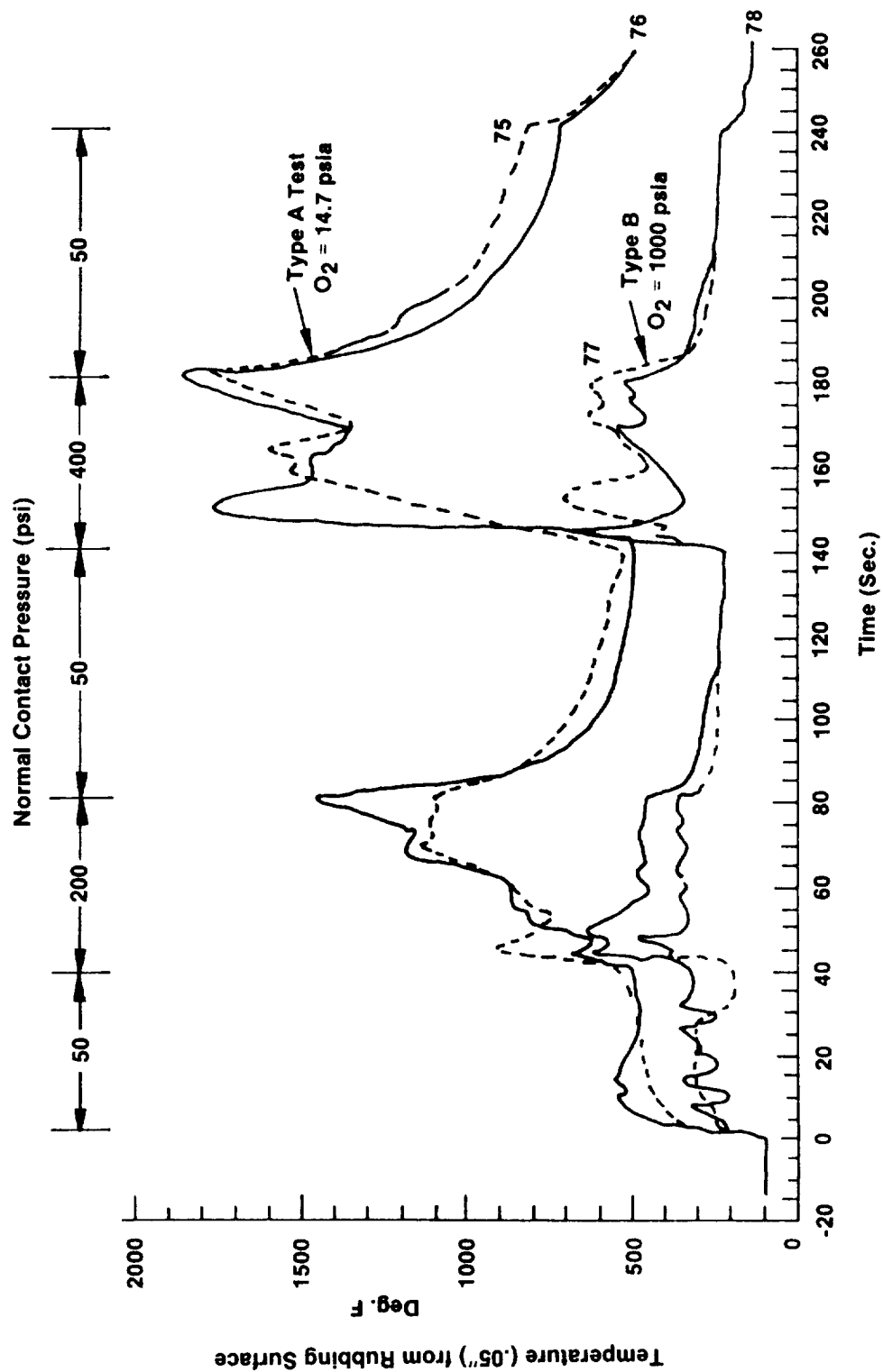


Figure 58. Superposition of Friction Heating Data of Monel K-500, 2 Tests at 1000 psia, 2 Tests at 14.7 psia

VII, E, Results and Discussions (cont.)

- d. Temperature spikes tend to occur at various times during the run but most commonly immediately after a load increase.
- e. The temperatures tend to return to common low value when the contact load is reduced.

Figure 59 compares the temperatures for several surface modifications in the variable load tests conducted in 1000 psia oxygen. At the initial 50 psi load step the silver and Ni-composite surfaces run cooler than the average of 3 untreated Monel specimens. When the load is increased from 50 psi to 200 psi the temperature of the silver plated surface increase rapidly to over 1000°F. This was accompanied by an increase in wear and friction torque measurements. In contrast the Ni-30% SiC composite ran cooler than either untreated monel or the silver plated material. The inability to develop a stable silver oxide film at elevated temperatures is the probable causes of the high friction heating rates.

At the conclusion of each test, when most or all of the modified surface is worn down all the measured temperatures are nearly the same.

A comparison of the measured peak (spike) temperature in the variable load test series at two oxygen environment pressures is shown in Figure 60. In general the data indicates that all tests conducted at a high pressure oxygen environment of 6.9 MPa (1000 psi), showed a lower peak temperature than those for tests conducted at ambient oxygen pressure.

Between 0-40 s, with the load of 0.34 MPa (50 psi), ion implanted lead has the lowest peak temperature for the test conducted at ambient oxygen pressure environment while for the high pressure test silver has the lowest peak temperatures. Elaboration of these early time data in Figure 61 shows that implants of Cr and O₂ eliminated the initial spike as did the electro deposited silver and that all the implants had some benefit.

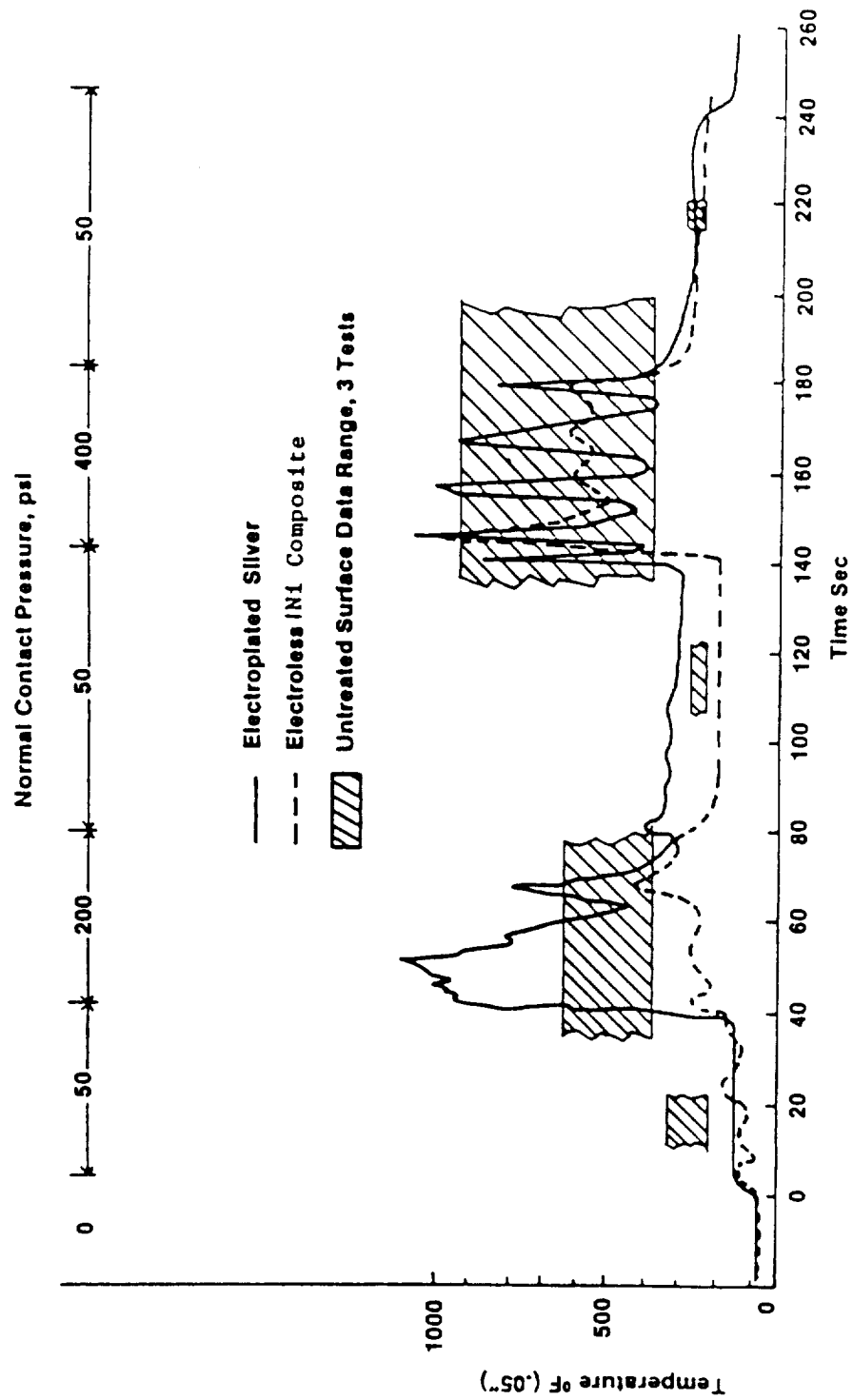


Figure 59. Comparison of Friction Heating of Monel K-500 in 1000 psia O₂ with Selected Surface Treatments

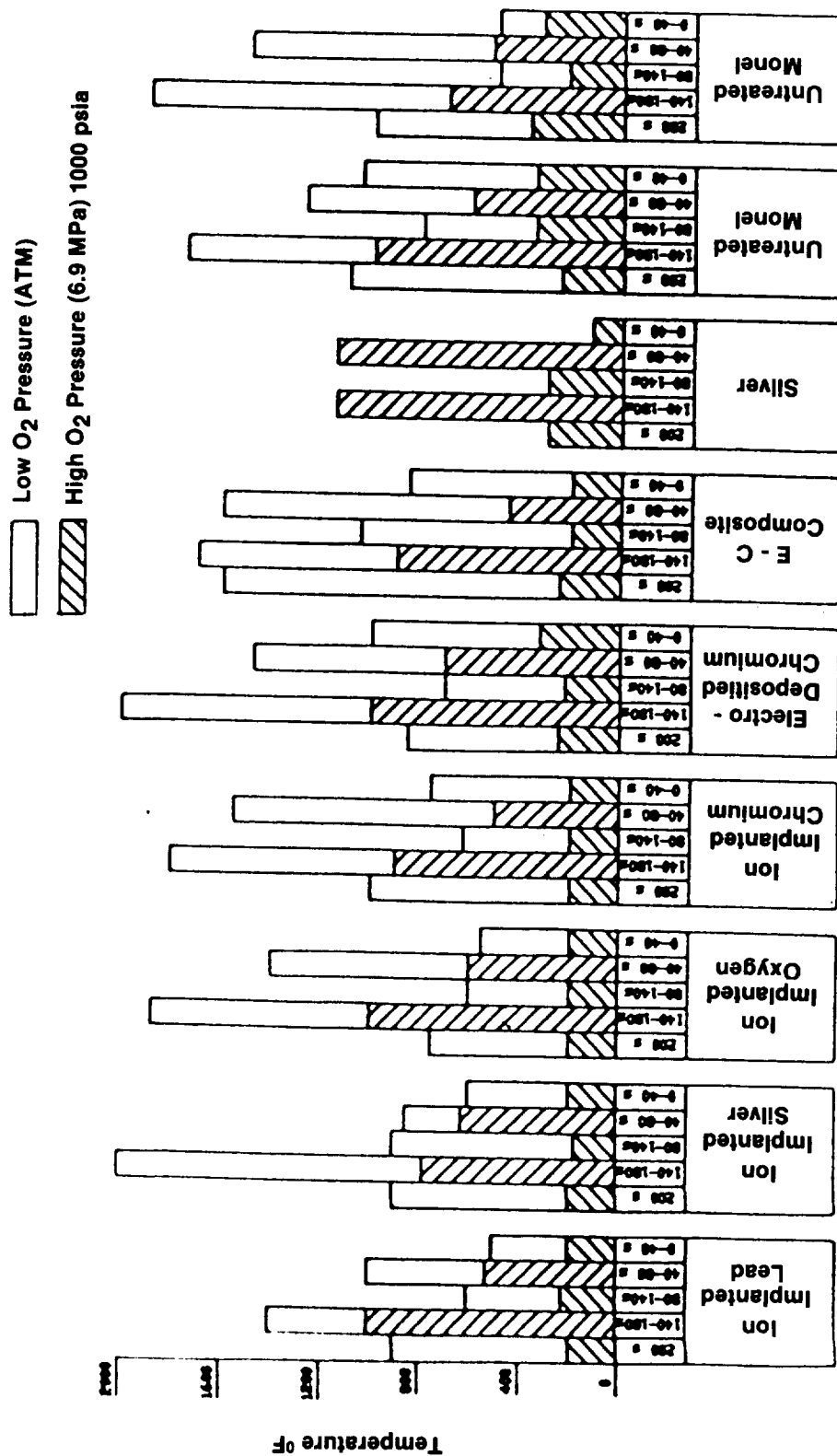


Figure 60. Comparison of Maximum Surface Temperatures for Monel K-500 in Low and High Pressure Oxygen with Surface Modifications and a Step Load

ORIGINAL PAGE IS
OF POOR QUALITY

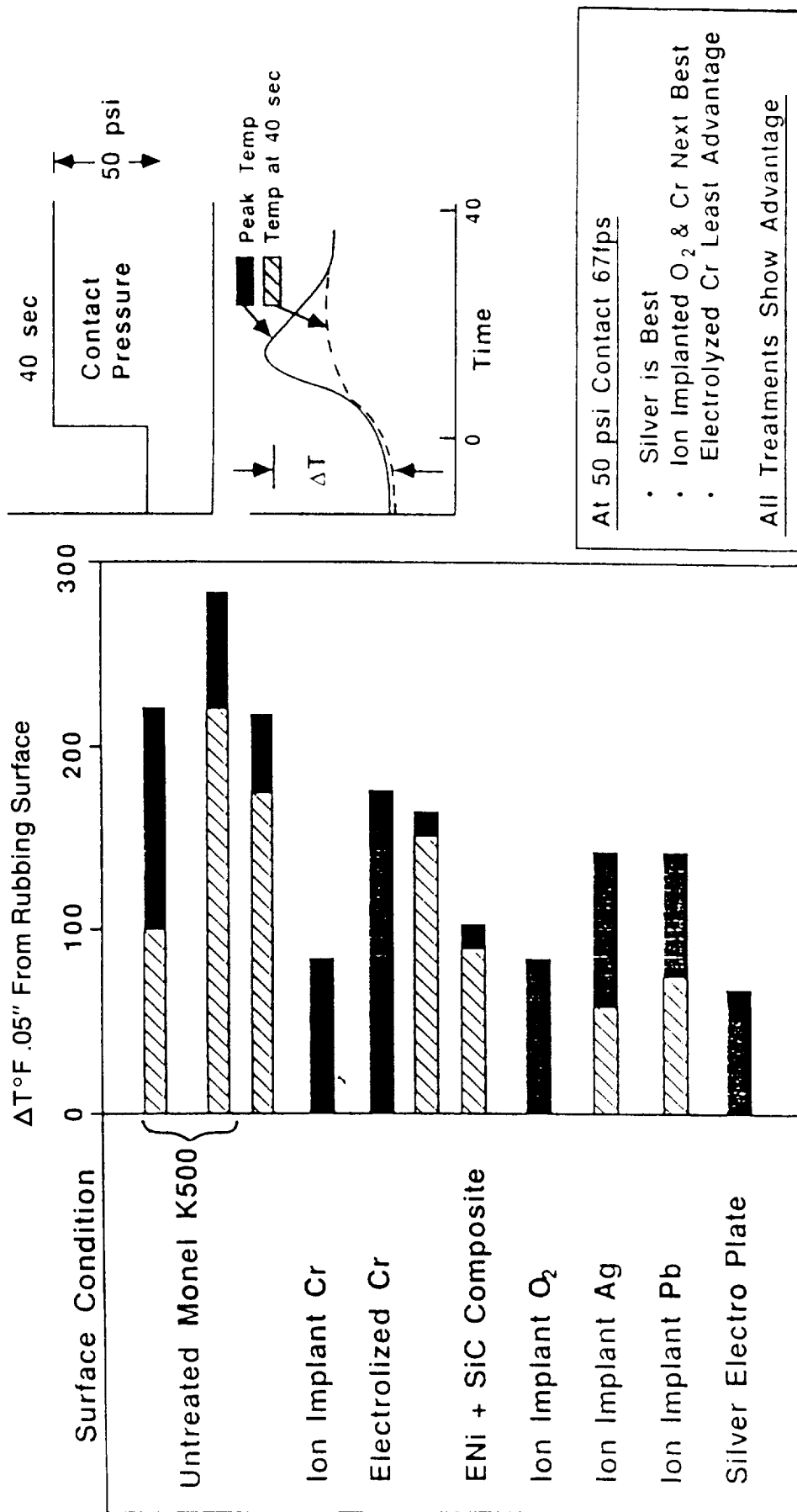


Figure 61. Friction Heating of Monel K-500 in 1000 psia O_2 at 17,000 RPM
Contact Pressure 50 psi for 40 sec

VII, E, Results and Discussions (cont.)

Between 40-80 s when the load was 1.38 MPa (200 psi) ion implanted silver has the lowest peak temperature for the ambient pressure test while for the high pressure test a composite plating of Ni and SiC was the lowest.

Between 80-140 s, when the load was returned to 0.35 MPa (50 psi), the untreated Monel K-500 had the lowest peak temperature for the ambient oxygen pressure test while for the high pressure test all surface modifications had a peak temperature of the order of 366 K (200°F).

Between 140-180 s when the load was at 2.7 MPa (400 psi) the ion implanted lead exhibited the lowest peak temperature for the ambient oxygen pressure test while ion implanted silver exhibited the lowest peak temperature for the high pressure test.

The comparison of the peak temperature at 200 s showed that for the ambient oxygen environment test ion implanted oxygen had the lowest peak temperature while for the high pressure test all surface modifications exhibited a temperature of the order of 366°K (200°F).

Thus, as far as the peak surface temperatures are concerned the data does not indicate that one surface modification is significantly superior to the other, although all the ion implants seem to offer some advantage over untreated Monel.

For tests conducted under a constant load with the oxygen environment pressure as 6.9 MPa (1000 psi) peak surface temperatures during the time intervals are shown in Figure 62 and continued in Figure 63. These figures indicate that under a constant load and high oxygen pressure the temperatures are in the range of 366°K to 477°K (200°F to 400°F) for all the

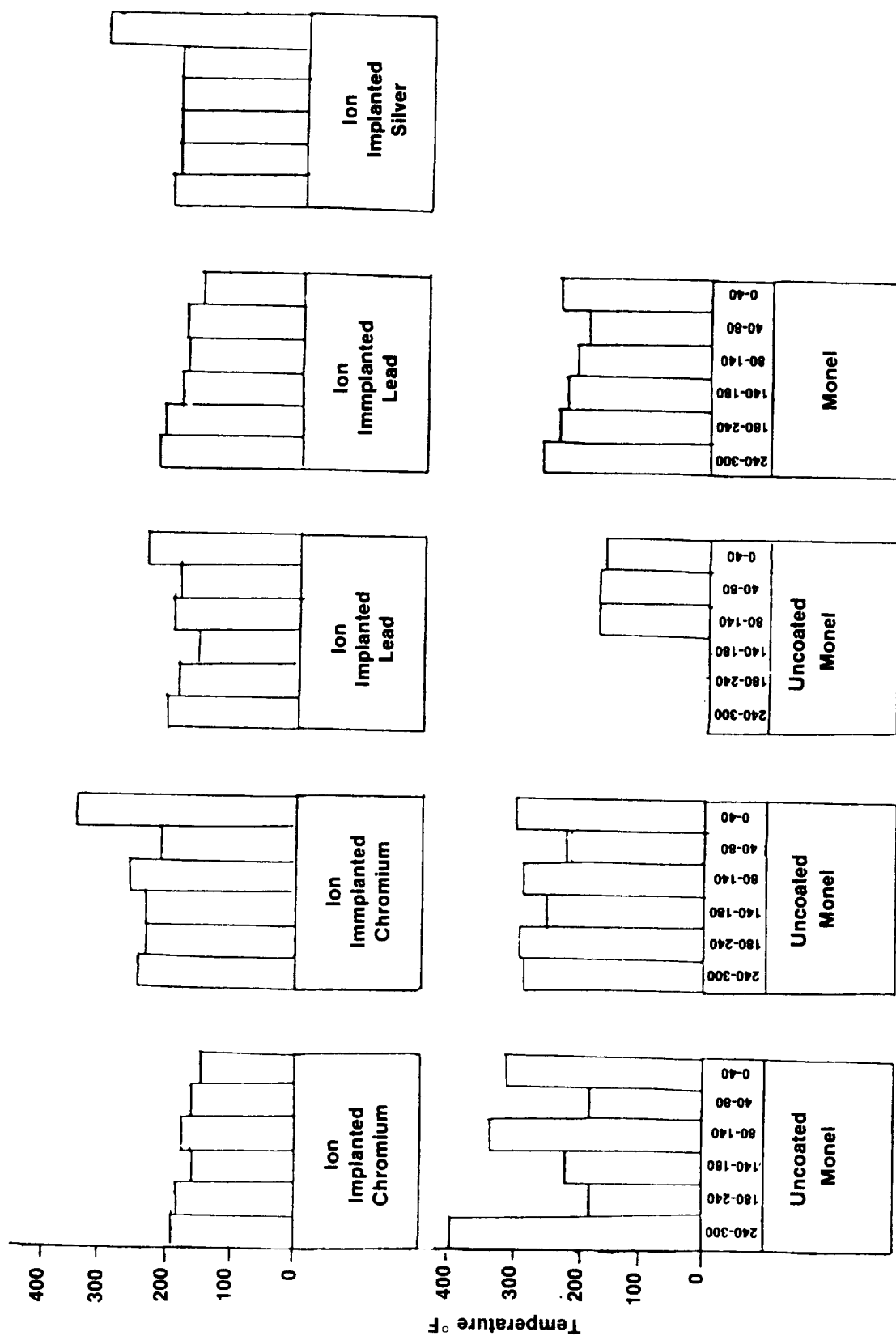


Figure 62. Maximum Temperature Observed in 6.9 MPa O₂, Constant Load Testing

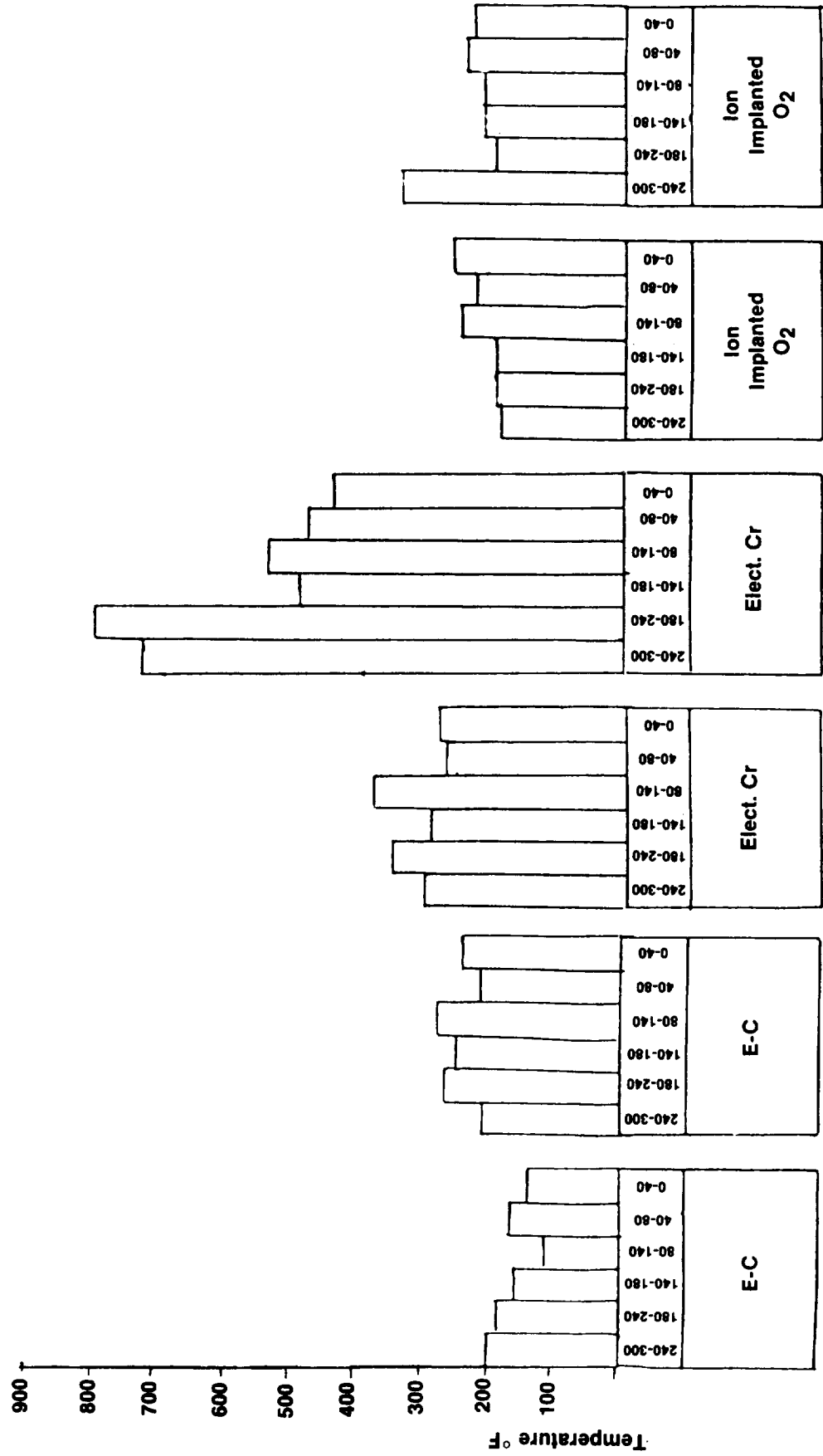


Figure 63. Maximum Temperature Observed in 6.9 MPa O₂, Consant Load Testing

VII, E, Results and Discussions (cont.)

tests except when Monel K-500 was coated with electrodeposited chromium in which case the temperature was in the range of 505°K to 700°K (450°F to 800°F). This discrepancy could not however be reproduced in another test conducted with electrodeposited chromium.

Since the variable and constant load test types are identical for the first 40 s, a direct comparison of the peak surface temperature in the 6.9 MPa (1000 psi) oxygen environment pressure can be made.

Table XIX provides a comparison of the peak temperature during the time interval 0-40 s for the tests conducted with step load and a constant load. The data indicate that during the time interval 0-40 s there is no exact repeatability in the peak temperature for similar coatings, but in general the peak surface temperature for Monel K-500 with surface modifications are lower than untreated Monel K-500. The column on the right of the table provides rank order from best to worse of the peak temperatures for the various surface modifications. The rank order from best down for low contact loads are Electroplated Silver, Ni-SiC composite and ion implanted lead. Only the Electroplated chrome was worse than untreated Monel.

2. Comparison of Overall Wear

The factors that cause wear are mechanical, thermal and chemical (oxidation). These three factors do not operate individually but usually operate in combination and thus increases the complexity of the wear phenomenon. All three independent variables are examined for the various surface conditions.

Wear measurements obtained by three separate methods are listed in Table XX for the variable load testing in, low and high pressure oxygen, and in Table XXI for the constant load testing in high pressure oxygen.

Table XIX. Comparison of Peak Temperatures in the Time
Internal 0-40 s for Step Load and Constant Load

Coating	Peak Surface Temperatures				Avg.	Rank*
	Step = Load K	(°F)	Constant = Load K	(°F)		
Untreated	449	(350)	433	(320)		
Untreated	463	(375)	422	(300)	421K	7
Untreated	449	(350)	344	(160)	(298)F	
Untreated	---	-----	383	(230)		
Ion Implanted Lead	366	(200)	388	(240)	367K	3
Ion Implanted Lead	---	-----	344	(160)	(200)F	
Ion Implanted Silver	366	(200)	433	(320)	400K	6
					(260)F	
Ion Implanted O ₂	366	(200)	383	(230)	383K	4
Ion Implanted O ₂	---	-----	400	(260)	(230)F	
Ion Implanted Cr	366	(200)	499	(350)	385	5
Ion Implanted Cr	---	-----	388	(150)	(233)F	
Electrodeposited Cr	435	(325)	505	(450)	437K	8
Electrodeposited Cr	394	(250)	410	(280)	(326)F	
EC Composite	366	(200)	388	(240)	365K	2
EC Composite			338	9150)	(198)F	
Silver	324	(125)	---	-----	325K	1
					(125)F	

* 1 best

Table XX. Comparison of Wear Data for Test Conducted with Step Load Applied to the Samples at Ambient Oxygen and 6.9 MPa (1000 psi) Oxygen Environment Pressure

		Wear Mil						
		Oxygen Pressure						
		6.9 MPa (1000 psia)			87 KPa MPa (12.7 psi)			
	Test No.	ΔL	ΔW	Disp	Test No.	ΔL	ΔW	Disp
Untreated Monel K-500	77	10.4	13.5	15.8	75	2.2	1.6	37.6
Untreated Monel K-500	78	9.5	14.4	13.3	76	2.6	3.9	14.0
Untreated Monel K-500	86	9.0	9.0	14.8	100	3.0	3.2	7.1
Ion Implanted O ₂	79	8.5	6.4	6.8	89	1.5	1.3	11.0
Ion Implanted Cr	80	5.5	4.6	7.1	87	10.5	1.8	7.6
Ion Implanted Ag	81	14.0	13.5	13.1	90	3.0	1.8	7.3
Ion Implanted Lead	82	4.5	6.5	6.4	91	4.0	4.0	5.2
Electrolized Cr	84	7.0	13.4	10.6	88	25.5	21.6	25.3
Electrolized Cr	83	11.5	19.2	-	104	8.0	5.4	13.3
E-C Composite	85	5.5	6.9	12.8	93	3.0	10.7	10.0

Table XXI. Comparison of Wear Data for Tests Conducted at Constant 50 psi Load in 1000 psi Oxygen

Surface Modification	Test	Nominal Load lbF	Wear Data Mil		
			ΔL from Δ Weight	ΔL	Disp. Sensor
None	168		2.	2.	-
	183	16	0.7	1.	4.5
	167	16	1.4	3.5	4.5
IAg	170	15	1.4	1.5	1.5
	179	16	0.66	6.	0.0
IO ₂	171	18	2.8	1.5	2.5
	182	15	0.6	0.0	0.0
ICr	175	18	8.0	8.0	9.0
	181	15	0.33	0.0	0.0
IPb	180	14	0.4	2.	+6.0
	169	16	1.9	1.	2.5
Ec Composite	176	17	.20	2.	1.
	184	15	0.26	0.5	2.5
Electrolized Cr	177	14	23.	24.	23.
	178	14	47.	33.	46.

VII, E, Results and Discussions (cont.)

Figure 64 compares the measured displacement data from all tests conducted using the variable loading test methods. The left column shows the wear using ambient pressure oxygen while the right column displays the data from the higher O_2 pressure testing. The upper portion of Figure 64 displays the baseline untreated Monel.

Consistent results were obtained in the variable load testing of the untreated monel at the two pressures when repeat tests were conducted. When additional extended duration tests were conducted at constant a 50 psi load it was expected that the early time wear would continue. This however was not the case as shown in Figure 65. Furthermore the wear data for the constant load testing appears random except for the electrolyzed chrome which was very high.

The data provided in these figures were examined by several methods to eliminate possible measurement errors. Figures 66, 67 and 68 compare the pre- to post test specimen measured length change with displacement measurements and also length change computed from weight change. Error free measurements would result in all data falling on a line having a 45 degree slope. It is apparent that some of the measurements are in considerable error and thus engineering judgement must be applied using agreement of 2 out of 3 measurement techniques. The goodness and confidence level for each surface modification can be inferred by the proximity of wear the data to the origin of the plot and the distance from the line.

The most consistent measurements were with constant 50 psi loading in 1000 psi O_2 . In these tests the electrolyzed Cr had the greatest wear with all three measurement methods being in good agreement. The indicated wear was 23-24 mil in Test 177 and 33-47 mil in Test 178. The three ion implanted Cr wear measurements in Test 175 also were in good agreement and showed a consistent and high wear 8-9 mil. All of the other surface including untreated monel indicated much lower material loss.

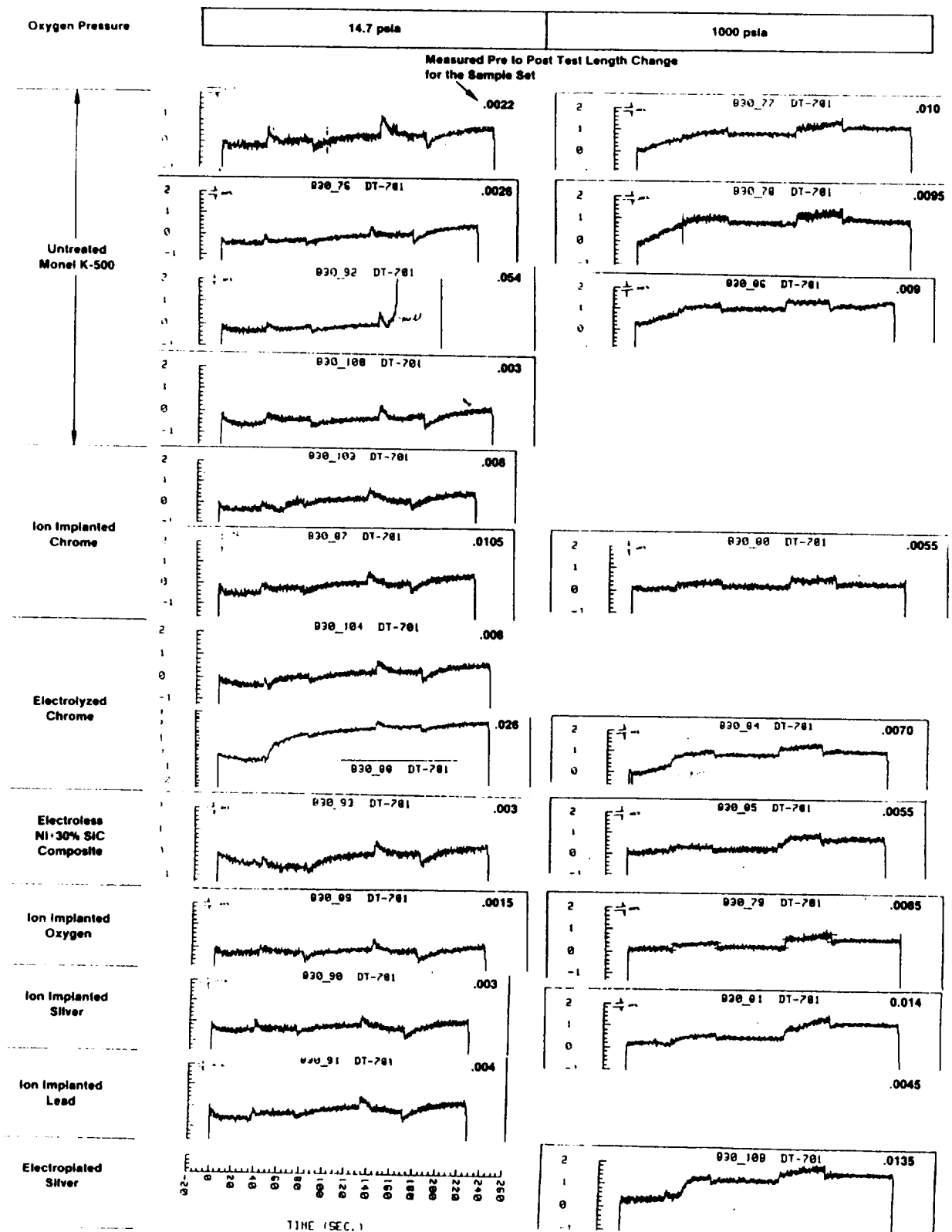


Figure 64. Sample Wear Rates vs. Time, Load, and Oxygen Pressure at 17,000 RPM

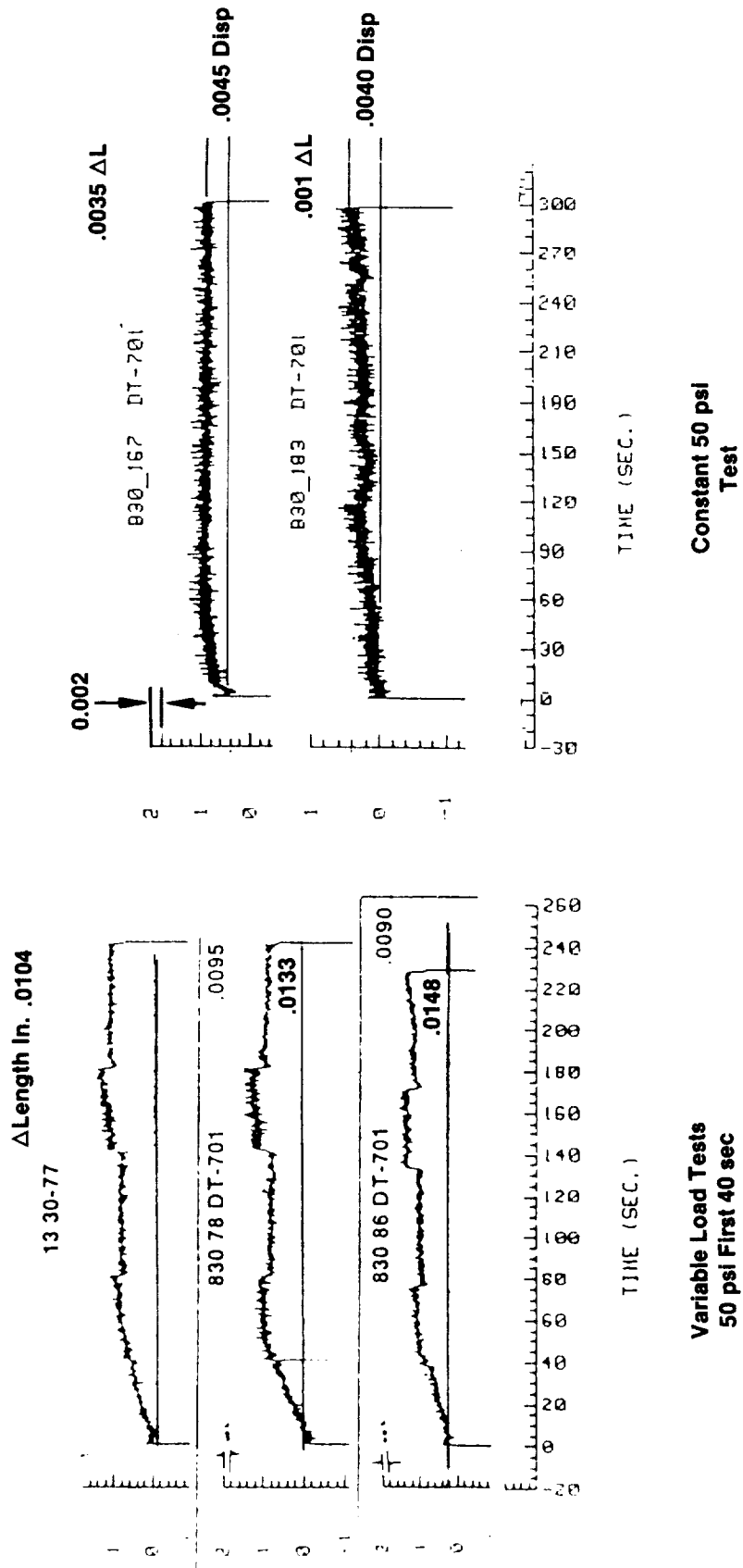


Figure 65. Displacement (Wear) Measurements for Untreated Monel K-500 in 1000 psia Oxygen

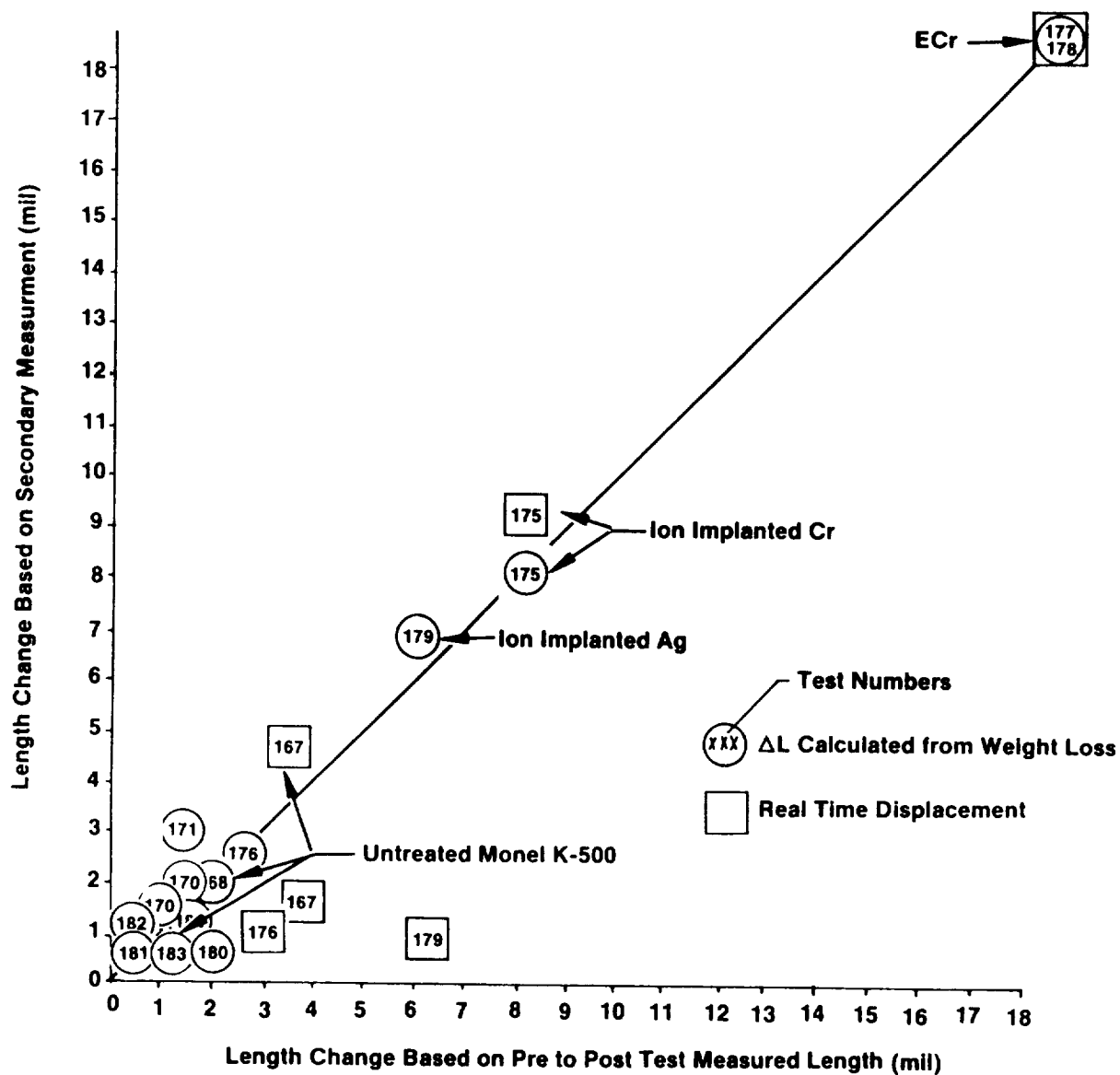


Figure 66. Wear Data at Constant 50 psi Load for 300 sec $O_2 = 1000$ psia

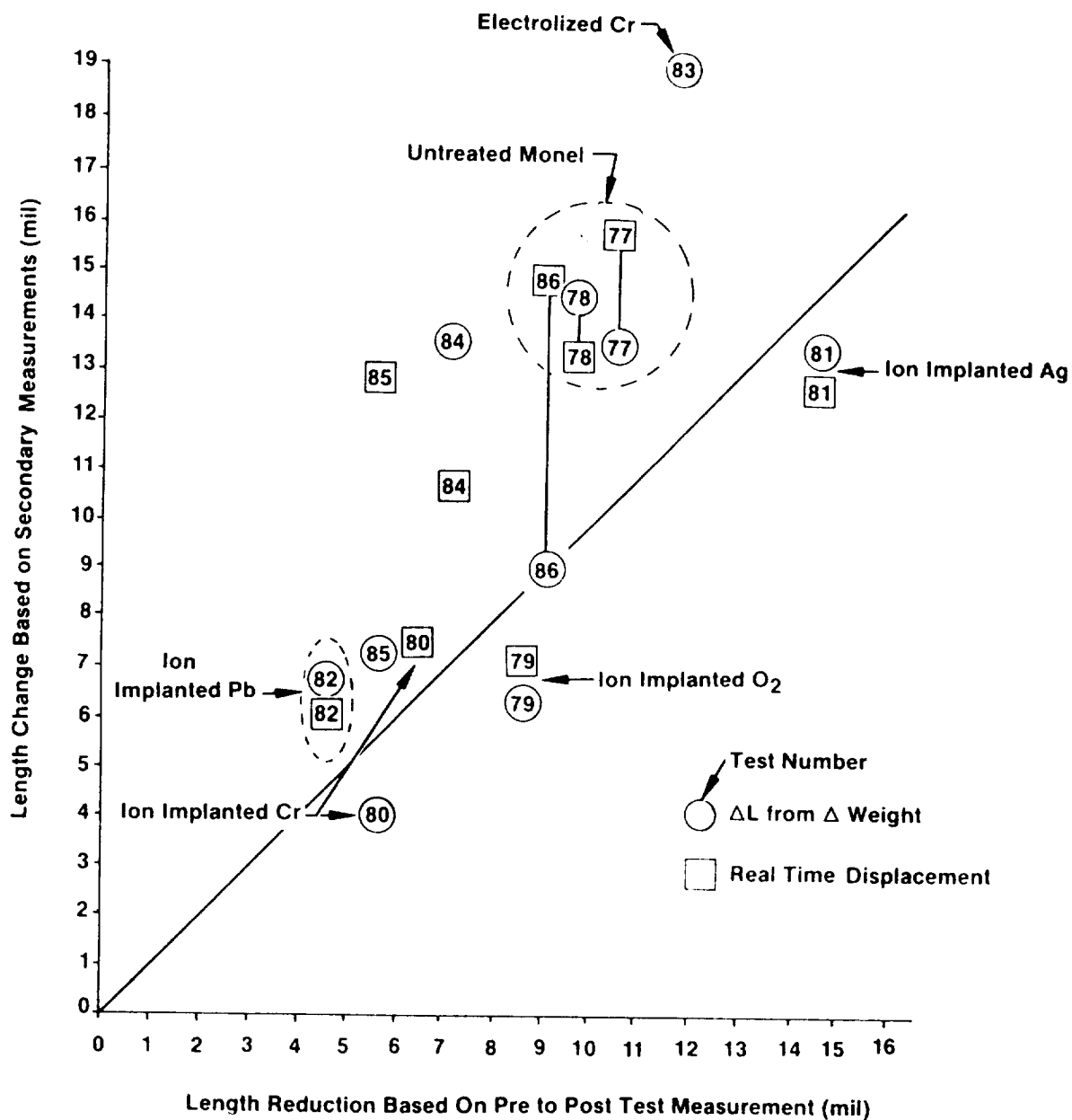


Figure 67. Wear Data for Stepped Loading Cycle ($O_2 = 1000$ psia)

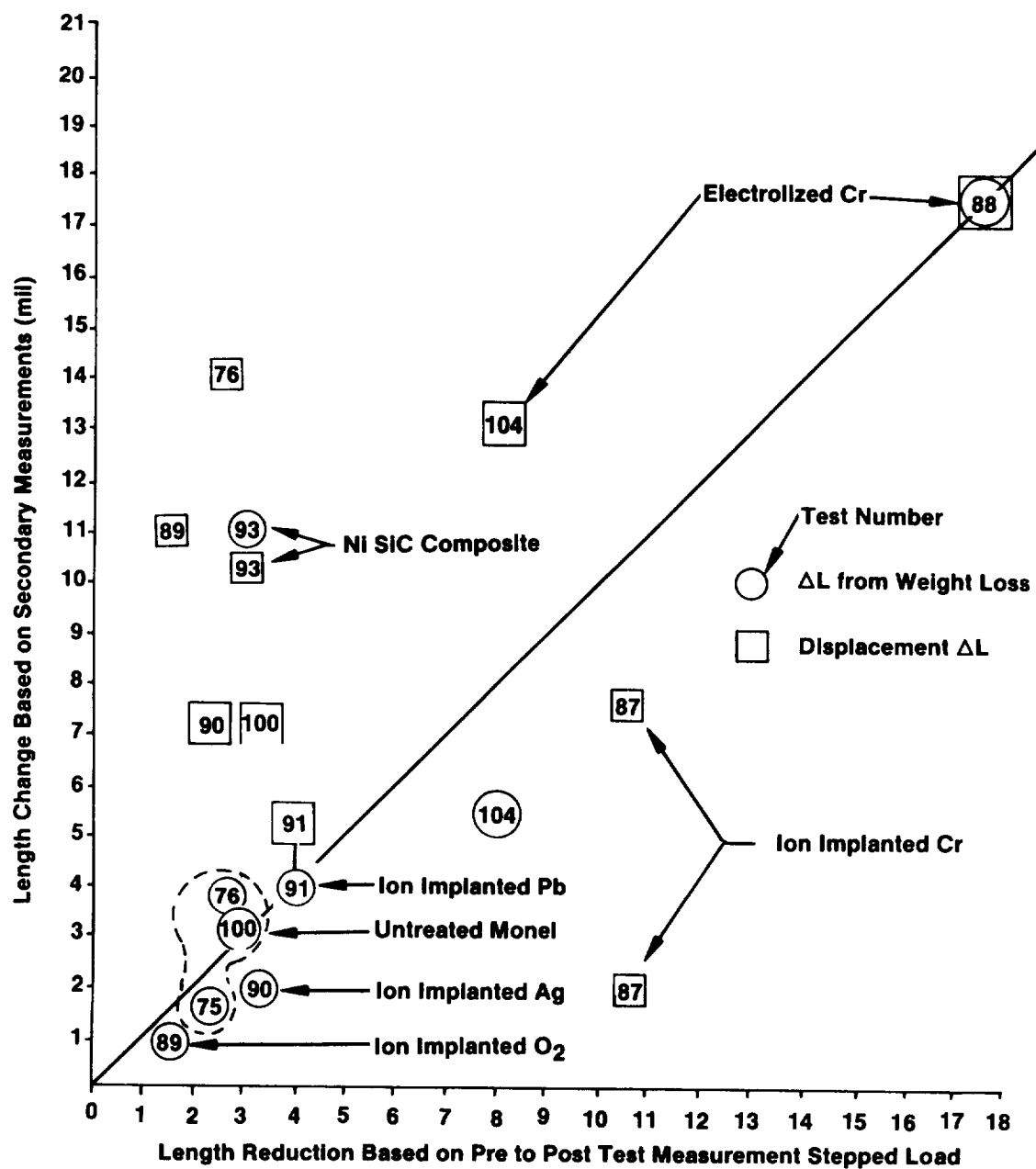


Figure 68. Wear Data for Stepped Loading Cycle ($O_2 = 12.7$ psia)

VII, E, Results and Discussions (cont.)

The material loss for the variable load testing in 1000 psi O_2 was higher. This was expected since the loads were higher. In this series all of the ion implanted specimen seemed to offer some advantage over the three sets of data for the base line untreated monel tests 77, 78 and 86. In these tests the ion implanted Cr and Pb were the most favorable while the electrolyzed Cr Test 83 was the worst. The high wear of the ion implanted Ag on Test 81 was confirmed by 3 independent measurements.

Examination of the data for the variable load tests in ambient pressure oxygen indicates that the displacement measurements are generally much higher than both pre-post length and weight change values except for Test 93 (Ni-SiC composite) where the length change is in disagreement with both the displacement and weight change measurements. In general the displacement measurements could be in error in this entire series since the specimen heating rates were much greater in the low pressure oxygen tests and this could have influenced the online sensor. Two electrolyzed Cr tests resulted in greater material loss, with Test 88 being significantly more (25 mil) than Test 83 (5-10 mil), and both being more than all others under which were 4 mil.

F. EFFECT OF SURFACE MODIFICATIONS AND OXYGEN PRESSURE ON MONEL K-500 WEAR RATES

The online displacement sensor was used to obtain these data. Tables XXII and XXIII provide the material regression rates for each load condition assuming a linear loss over the test duration in which the independent parameters of load and O_2 pressure were held constant.

Table XXII. Comparison of Wear Rates for Monel K-500 with Surface Coating with Step Load

6.9 MPa (1000 psi) Oxygen Environment Pressure

Test No.	Coatings/Load	Wear Rates in./s Times				
		0-40s 50 psi	40-80s 200 psi	80-140s 50 psi	140-180s 400 psi	180-240s 50 psi
77	Untreated Monel K-500	1. 5×10^{-4}	1. 0×10^{-4}	3. 333×10^{-5}	1. 25×10^{-4}	-3. 33×10^{-5}
78	Untreated Monel K-500	2×10^{-4}	5×10^{-5}	1. 667×10^{-5}	7. 5×10^{-5}	-2. 5×10^{-5}
86	Untreated Monel K-500	2. 25×10^{-4}	7. 5×10^{-5}	0	2. 5×10^{-5}	1. 667×10^{-5}
80	Ion Implanted Chromium	2. 5×10^{-5}	5×10^{-5}	3. 33×10^{-5}	1. 25×10^{-5}	0
81	Ion Implanted Silver	5×10^{-5}	1×10^{-4}	1. 6667×10^{-5}	1. 25×10^{-4}	8. 33×10^{-6}
82	Ion Implanted Lead	5×10^{-5}	2×10^{-5}		5×10^{-5}	0
	Electroplated Chromium	1×10^{-4}	7. 5×10^{-5}	1. 667×10^{-5}	2. 5×10^{-5}	1. 667×10^{-5}
85	E-C Composite	5×10^{-5}	5×10^{-5}	0	1. 75×10^{-4}	1. 667×10^{-5}
O ₂ at Ambient Pressure						
75	Untreated Monel K-500	0	-	7.5×10^{-5}		10. 10^{-5}
76	Untreated Monel K-500	0	0	6.6×10^{-5}	0	11. 10^{-5}
92	Untreated Monel K-500	0	0	6.6×10^{-5}		
100	Untreated Monel K-500	0	0	5.0×10^{-5}	Ignited	13. 10^{-5}
87	Ion Implanted Chrome	0	0	6.6×10^{-5}	-	10. 10^{-5}
100	Ion Implanted Chrome	0	0	5.0×10^{-5}	-	13. 10^{-5}
88	Elect. Cr	0	42×10^{-5}	10.0×10^{-5}	0	8. 10^{-5}
104	Elect. Cr	0	10×10^{-5}	6.6×10^{-5}	0	13. 10^{-5}
89	Ion Implanted Oxygen	0	0	8.3×10^{-5}	0	8. 10^{-5}
90	Ion Implanted Silver	0	0	6.6×10^{-5}	-	12. 10^{-5}
91	Ion Implanted Lead	0	0	8.3×10^{-5}	-	13. 10^{-5}
93	EC Composite	-	-	11.7	-	12. 10^{-5}

Table XXIII. Comparison of Wear Rates for Monel K-500 with Surface Coating and Constant Load with 16.9 MPa (1000 psi) Oxygen Environment Pressure

Coatings	Wear Rates in./s Time					
	0-40s	40-80s	80-140s	140-180s	180-240s	240-300s
Untreated Monel K-500	1×10^{-4}	2.5×10^{-5}	8.3×10^{-6}	0	0	1.67×10^{-5}
Untreated Monel K-500	2.5×10^{-5}	1.25×10^{-5}	8.33×10^{-6}	1.25×10^{-5}	8.33×10^{-6}	2.5×10^{-5}
Ion Implanted Chromium	0	0	0	0	1.33×10^{-5}	1.33×10^{-5}
Ion Implanted Chromium	2.3×10^{-4}	0	1.67×10^{-5}	0	8.3×10^{-6}	8.33×10^{-6}
Ion Implanted Silver	0	4.5×10^{-5}	1.33×10^{-5}	4.5×10^{-5}	3×10^{-5}	0
Ion Implanted Silver	7.5×10^{-5}	0	1.67×10^{-5}	0	0	0
Ion Implanted O ₂	6.25×10^{-5}	0	8.3×10^{-6}	1.25×10^{-5}	2.5×10^{-5}	5.0×10^{-5}
Ion Implanted Lead	7.5×10^{-5}	5.36×10^{-2}	7.0×10^{-5}	2×10^{-5}	1.67×10^{-5}	6.6×10^{-5}
Ion Implanted Lead	2×10^{-5}	0	0	2×10^{-5}	6.67×10^{-5}	0
E-C Composite	5×10^{-5}	2.5×10^{-5}	1.67×10^{-5}	1.25×10^{-5}	8.33×10^{-6}	1.67×10^{-5}
Electrodeposited Chromium	2×10^{-4}	1.37×10^{-4}	3.33×10^{-5}	7.5×10^{-5}	3.3×10^{-5}	0
Electrodeposited Chromium	2.25×10^{-4}	1.75×10^{-4}	1.66×10^{-4}	1×10^{-4}	1.83×10^{-4}	6.6×10^{-5}
E-C Composite	3.75×10^{-5}	1.25×10^{-5}	0	1.33×10^{-5}	3.33×10^{-6}	1.66×10^{-5}

VII, F, Effect on Surface Modifications and Oxygen Pressure on Monel K-500
in Oxygen (cont.)

Figure 69 graphically displays the wear rate of untreated Monel at 50 psi contact load in oxygen at 2 pressures. Rate data are presented for the first 40 sec of wear, the 60 sec following the 200 psi load step and the 60 sec following the 400 psi load step. The material loss rate in O_2 at one atmosphere is noted to increase each time the 50 psi load step is applied. Since the test rings were hotter at each subsequent 50 psi load step an Arrhenius type plot ($\text{loss} \propto 1/T$) was prepared to see if the loss rates conformed to normal temperature dependencies. Figure 70 indicates that the regression rate of untreated monel in 12.7 psi O_2 is predictable by the increase in temperature at each 50 psi load step. Post test analysis of the material hardness also showed a loss of the heat treatment near the rubbing surface which can also explain greater wear. The hardness measurements are covered in a later section.

In contrast as noted in Figure 69 the highest wear rates in 1000 psia O_2 were experienced only during the first load 50 psi load step. Much lower wear rates were recorded in subsequent loadings. Since the temperatures were nearly constant this reversal cannot be fully explained except for the possible formation of a low friction surface glaze or a surface work hardening.

Additional analyses of the wear rates of untreated monel were made by comparing the results of the first 40 sec from the variable load test with data from same time period on the constant load tests. Figure 71 shows this comparison and also wear rate vs time for comparable time periods over the remainder of this test.

This figure shows much higher wear rates upon first contact. The inconsistency between the variable load test and the constant load test was to say the least disturbing.

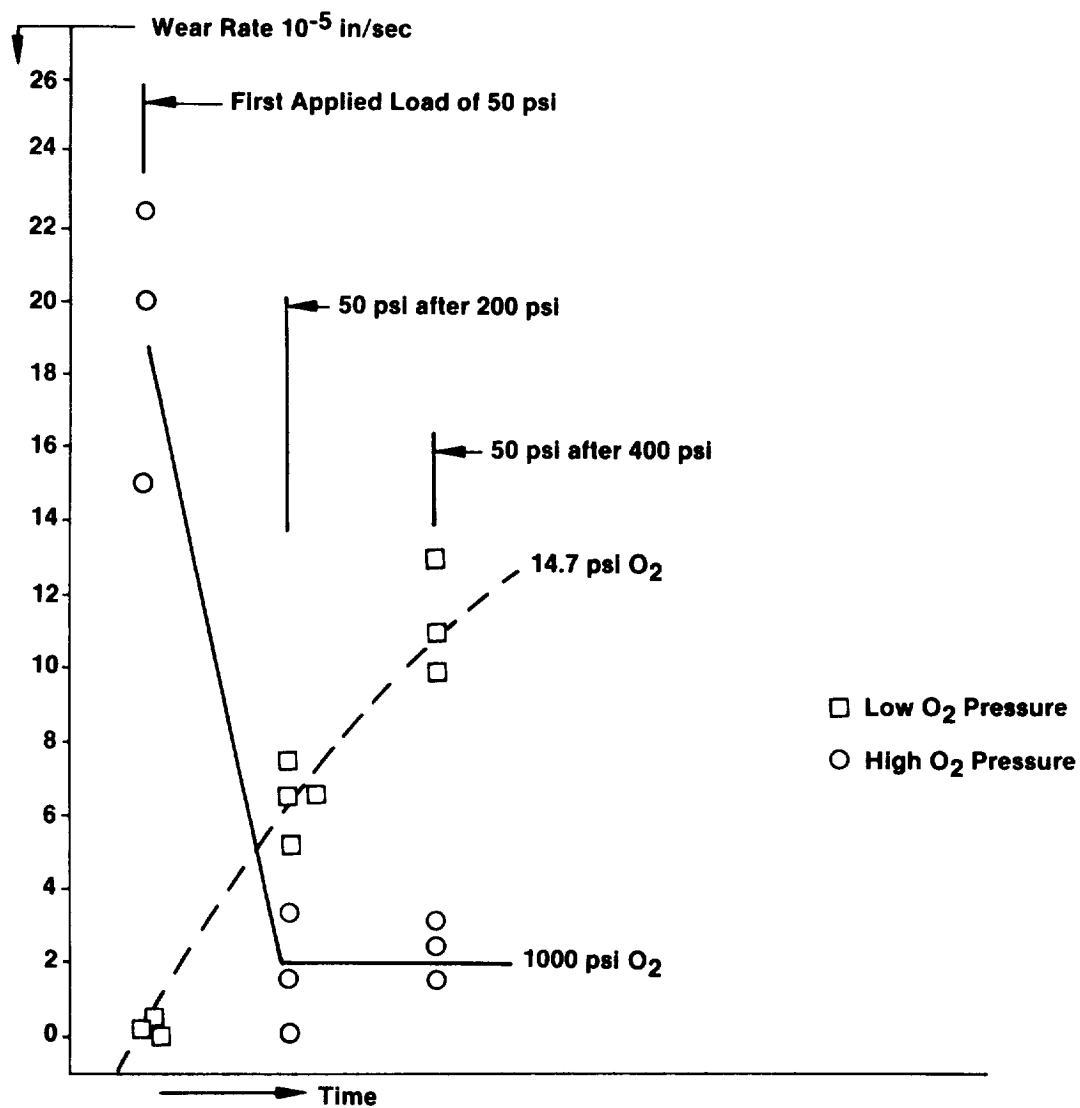


Figure 69. Wear Rate of Untreated Monel K-500 in 14.7 & 1000 psi Oxygen at a Contact Pressure of 50 psi

Test No.	Avg Temp °F					
	Time O ₂ psi	0-40	40-80	80-140	140-180	180-260
77	1000	300	350	200	600	250
78	1000	300	550	250	600	250
86	1000	250	400	250	600	300
75	14.7	400	1000	700	1500	1000
76	14.7	500	1000	600	1500	1000
92	14.7	500	1000	600	Melt	—
100	14.7	900	1100	700	1500	1100

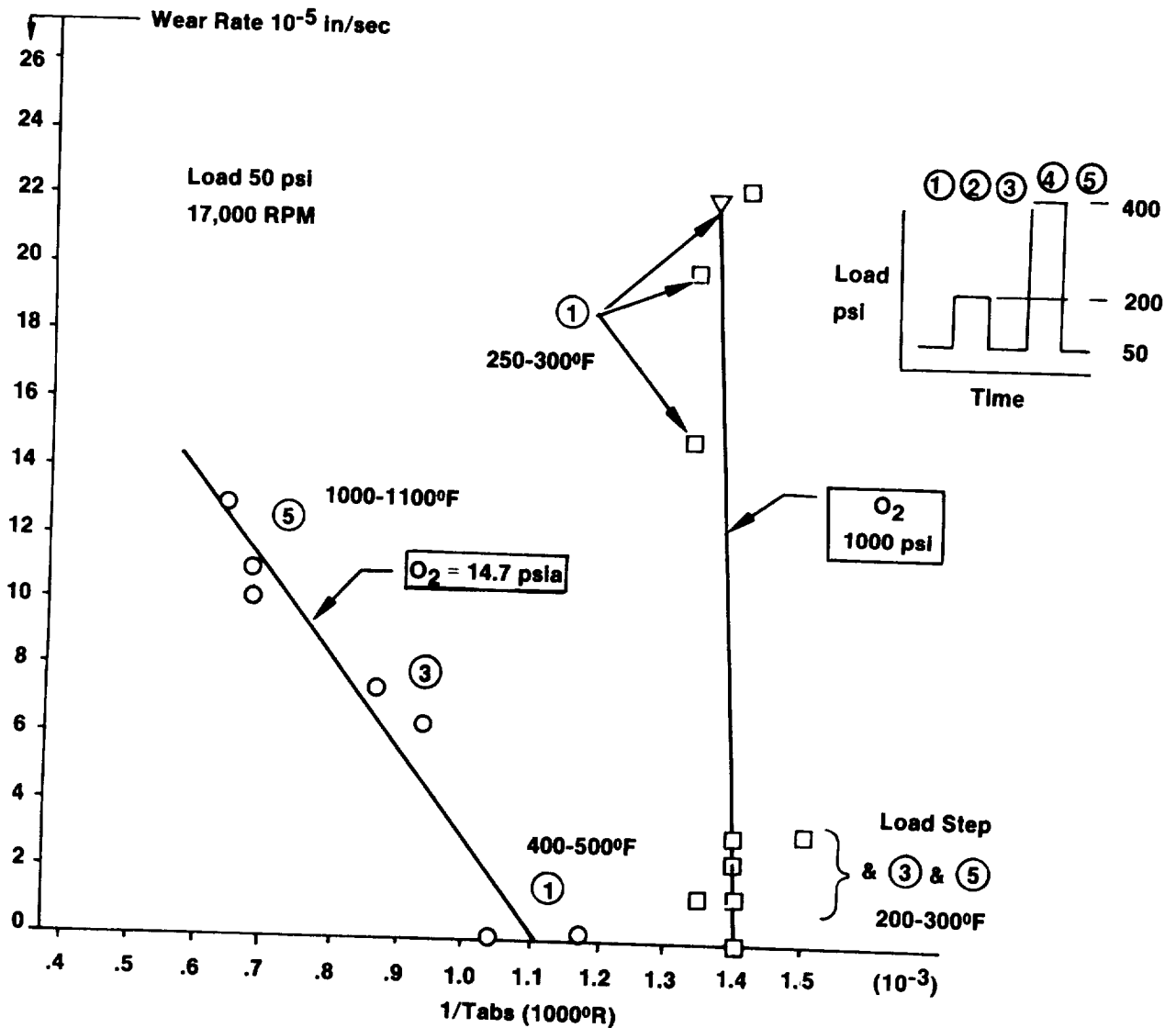


Figure 70. Correlation of Material Loss Rate by the Arrhenius Relation

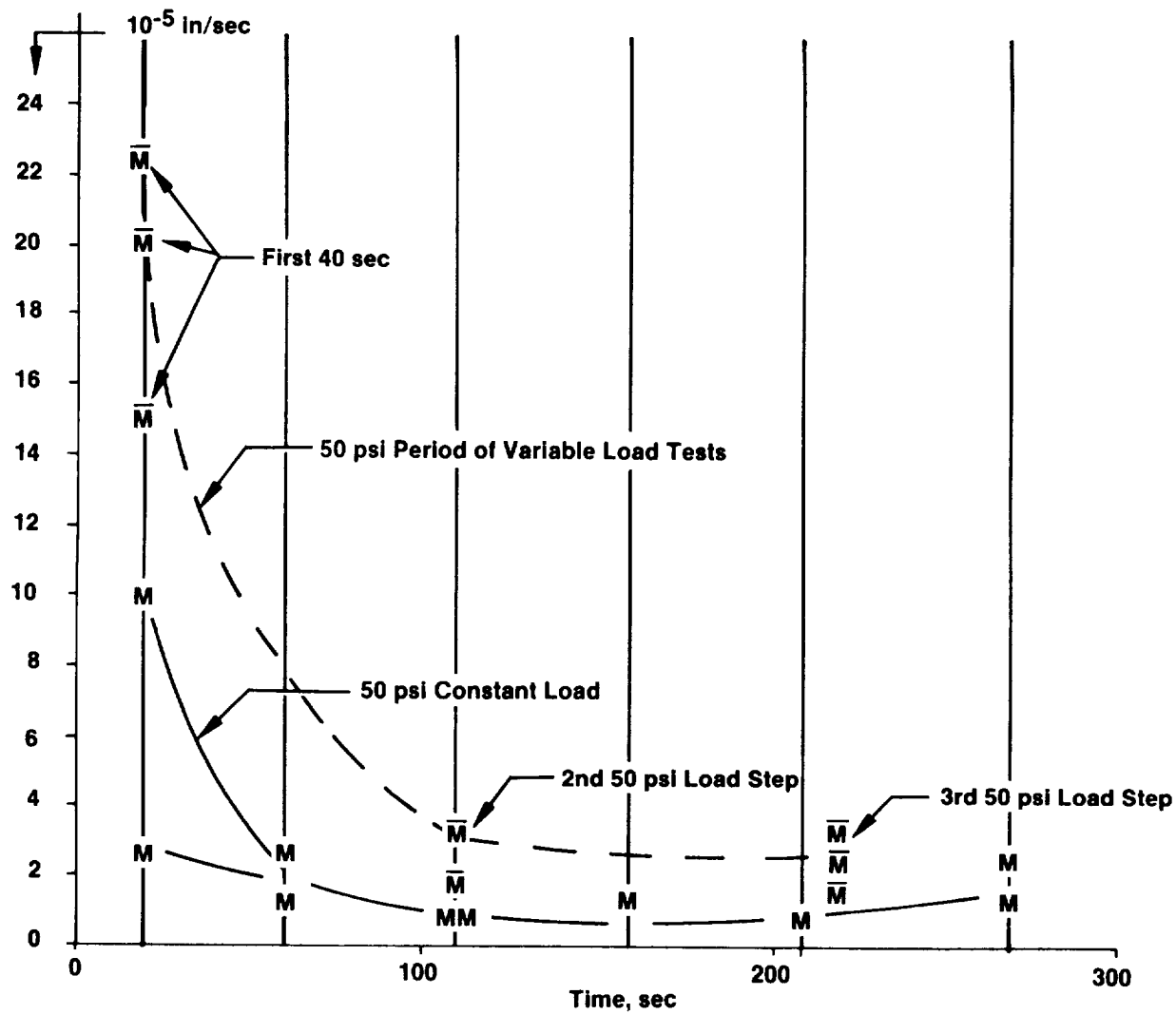


Figure 71. Wear Rates vs. Time Monel K-500 $O_2 = 1000$ psia

VII, F, Effect on Surface Modifications and Oxygen Pressure on Monel K-500
in Oxygen (cont.)

Hardness surveys were conducted to determine if all the specimens had the same initial heat treatment. Measurements were taken in the center and on the cold end furthest away from the heat effected zone. The results were as follows:

<u>Step Load Tests</u>	<u>O₂ Pressure psia</u>	<u>Hardness Away from Rubbing Surface R/45N Rot/Sta</u>
76	12.7	35-36 / 33-37
78	1000	32-33 / 33-36
86	1000	36-37 / 35-37
<hr/>		
<u>Constant Load Tests</u>	<u>O₂ Pressure</u>	
167	1000	35-37 / 35-36
168	1000	35-37 / 34-37
183	1000	33-35 / 35-37

As can be noted all of the test rings had similar hardness values and thus the difference in wear could not be attributed to differences in initial hardness. The expected hardness for the age hardening Monel is RC 35 which translates to 37 on the 45N scale.

Hardness profiles were then taken along the length of the cylinder wall starting at the rubbing end. These are shown in Figures 72 and 73. Figure 72 shows a reduction in hardness near the rubbing surface in 5 of the 6 rings used in the step load test. Test 76 run in 12.7 psia O₂ had the greatest reduction in hardness which can be explained by the higher operating temperatures experienced in the low oxygen pressure tests. Figure 73 shows that 5 of the 6 rings tested at the lower fixed load in high pressure oxygen retained their original hardness to within .03 in. of the rubbing surface. Valid measurements on the contact surface could not be attained because the wear surfaces were too irregular.

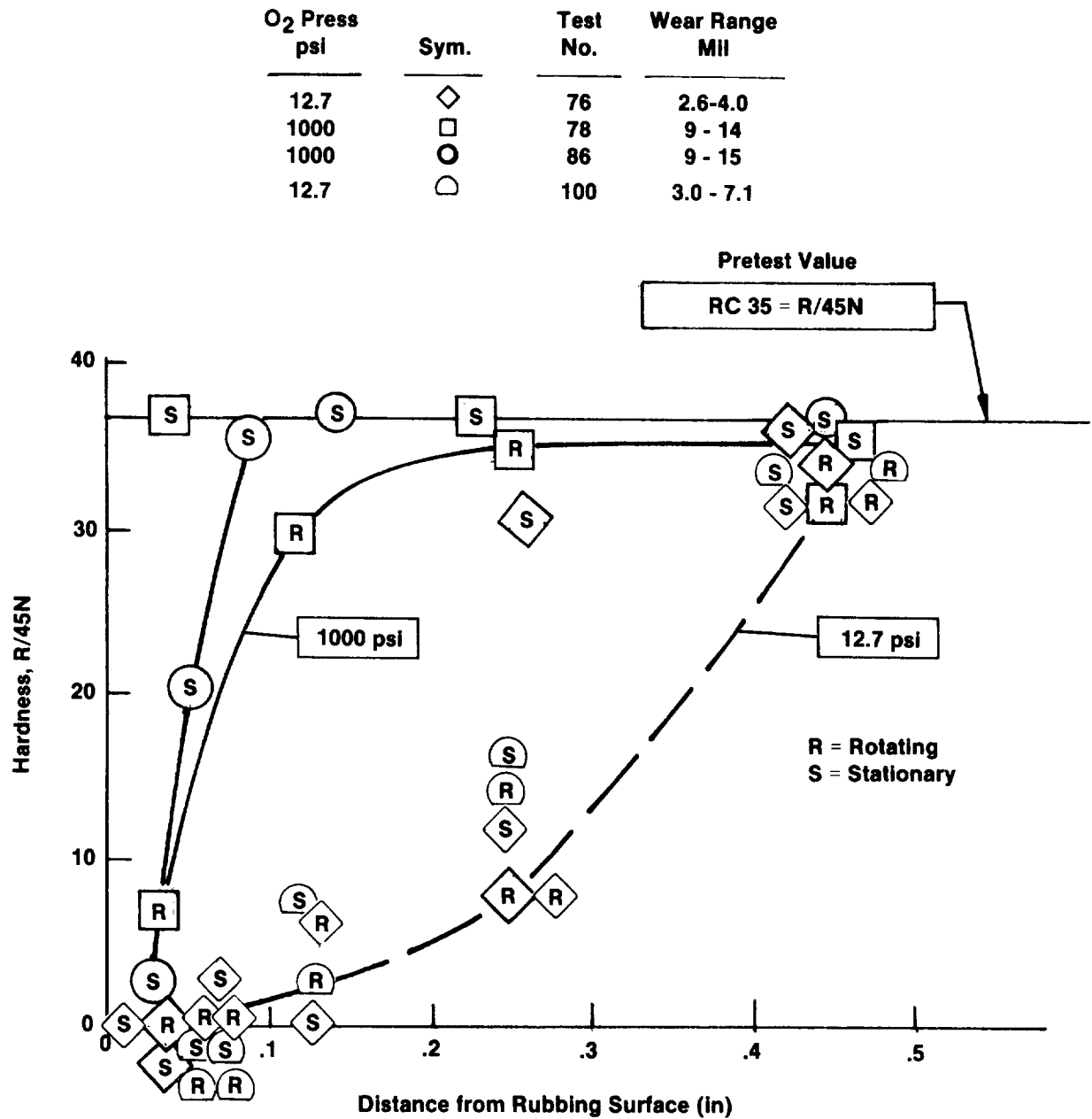


Figure 72. Post Test Hardness Profile Untreated Monel K-500

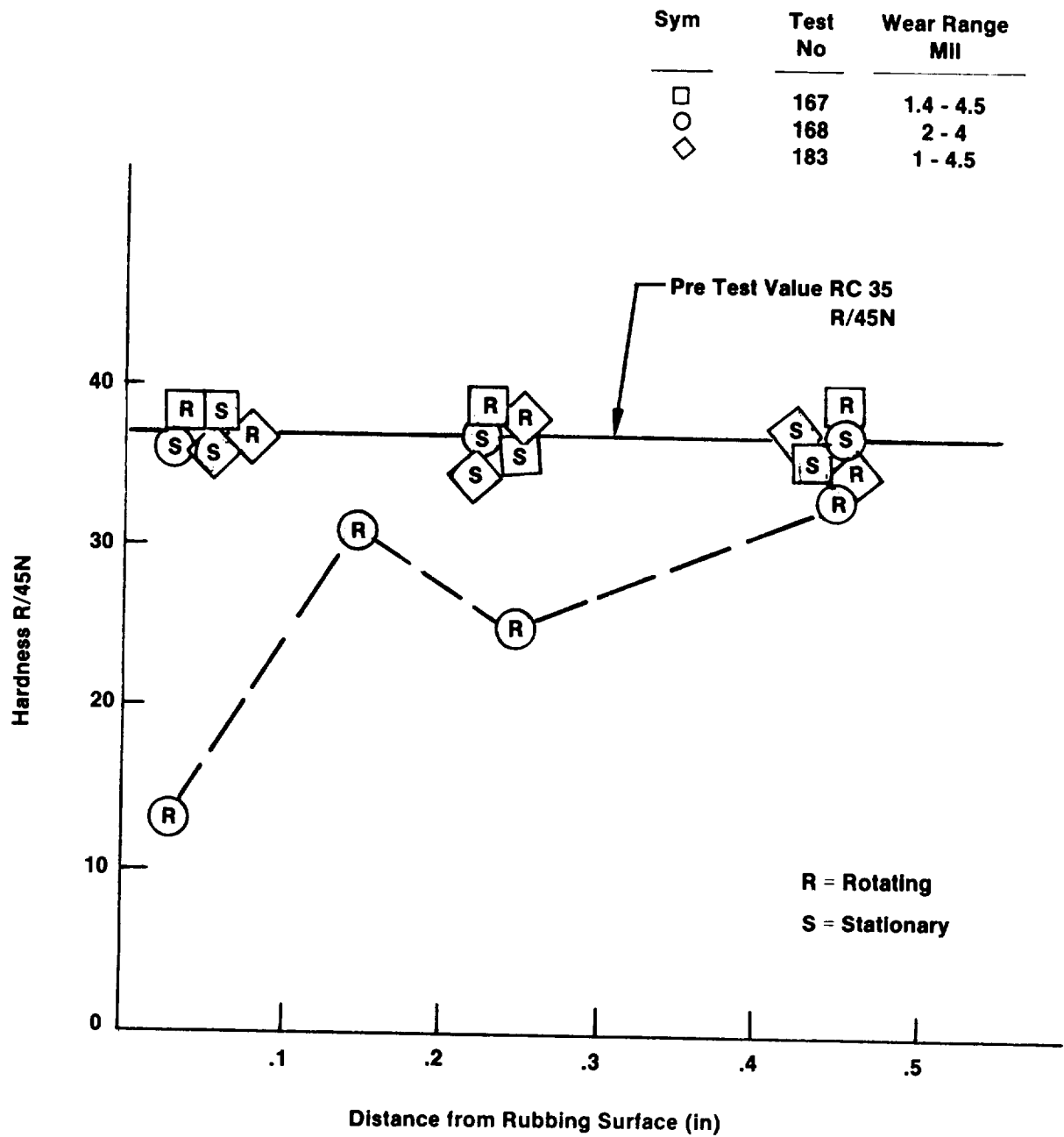


Figure 73. Post Test Hardness Profile Untreated Monel K-500 6.9 MPA (1000 psia) O₂, Constant Loading

VII, F, Effect on Surface Modifications and Oxygen Pressure on Monel K-500
in Oxygen (cont.)

The lower overall wear and the harder post test surface following the constant load tests are expected. The higher wear and softer surface measured following the more heavily loaded step loading tests are also expected due to the higher surface temperatures. The greater depth of softening following the low pressure tests were also expected due to the reduced cooling. The following two factors however are still not explainable:

- 1) The cause of the higher wear rates in Tests 78 and 86 in the first load step and
- 2) The low wear rate in Test 76 where the oxygen pressure was reduced.

The following speculations can be offered. The reduced wear rate after initial contact could be due to work hardening of the surface or development of an oxide glaze which reduces the wear rate.

The advantages of the various surface treatments should also in theory be quantifiable by comparing the material loss rate for the first 40 sec of the variable and constant load tests. Unfortunately no such correlation could be obtained and thus the wear data from this test method which appeared valid at first has become suspect especially at the lower loads. Figure 74 shows the inconsistency between wear of ion implanted Cr in two identical tests, 175 vs 181.

Figure 75 shows the influence of surface modifications on wear rate for the 3, 50 psi load steps in the variable load tests while Figure 76 shows the wear rate as a function of load. Using only the data from the first 50 psi contact period is shown in this figure. All of the ion implants and all the platings show a measurable benefit in the form of reduced wear for the initial contact and little or no advantage for subsequent rubbing.

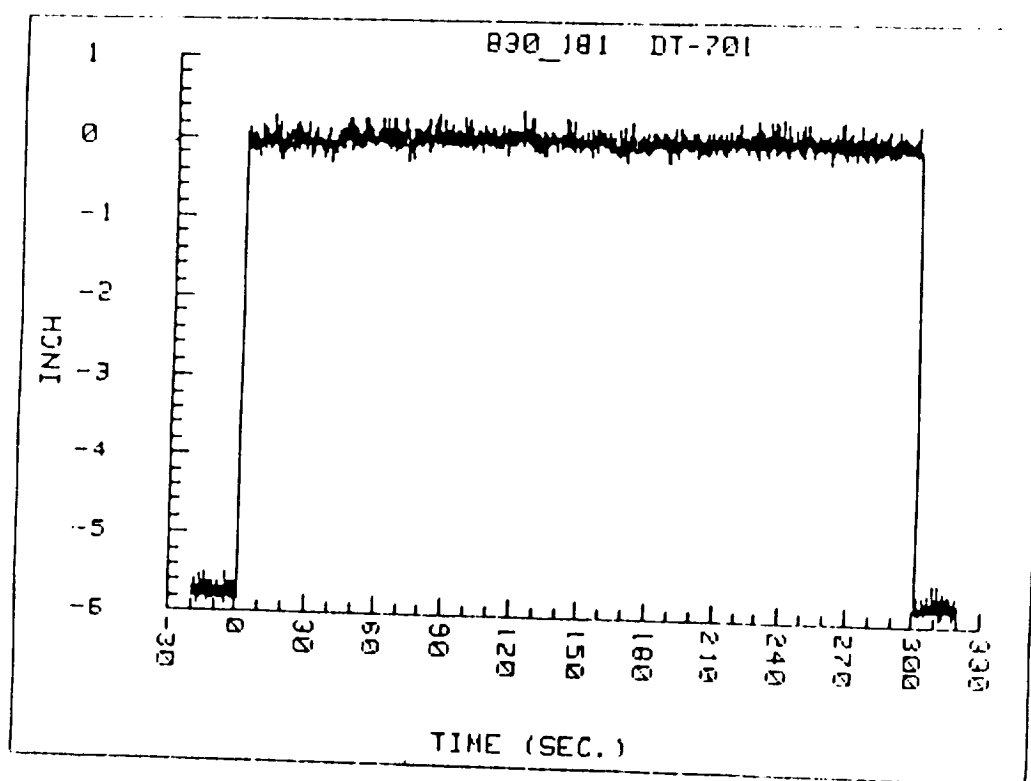
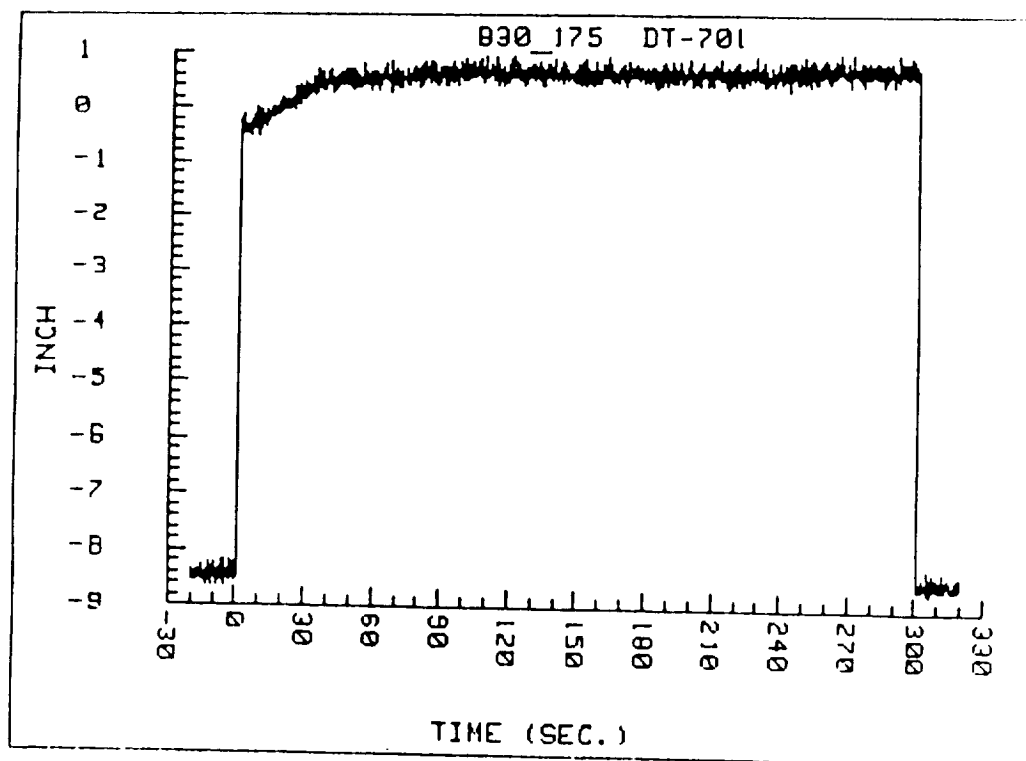


Figure 74. Comparison of Displacement Measurements for Ion Implanted Cr from Tests 175 and 181 1000 psi O₂, 50 psi Contact Load

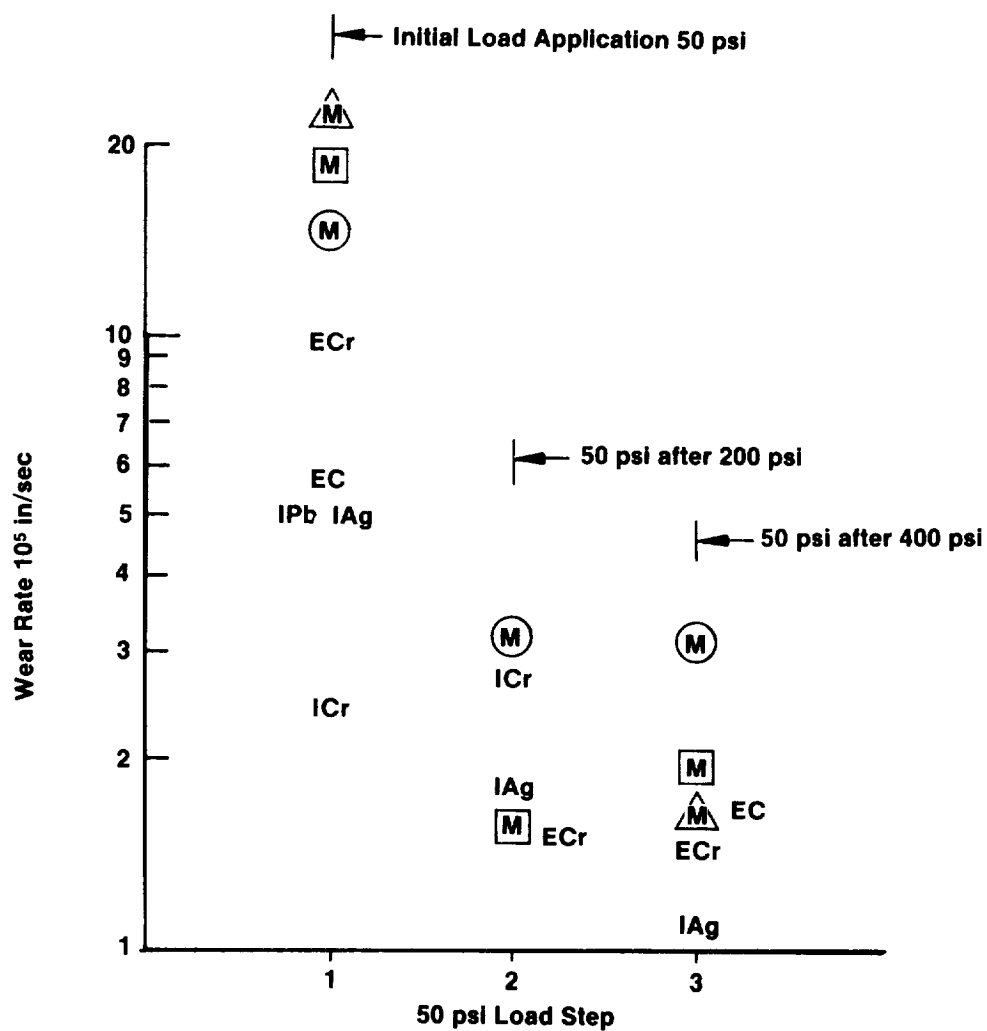


Figure 75. Effect of Surface Modification and Load History on Wear Rate in O_2 at 6.9 MPa (1000 psi)

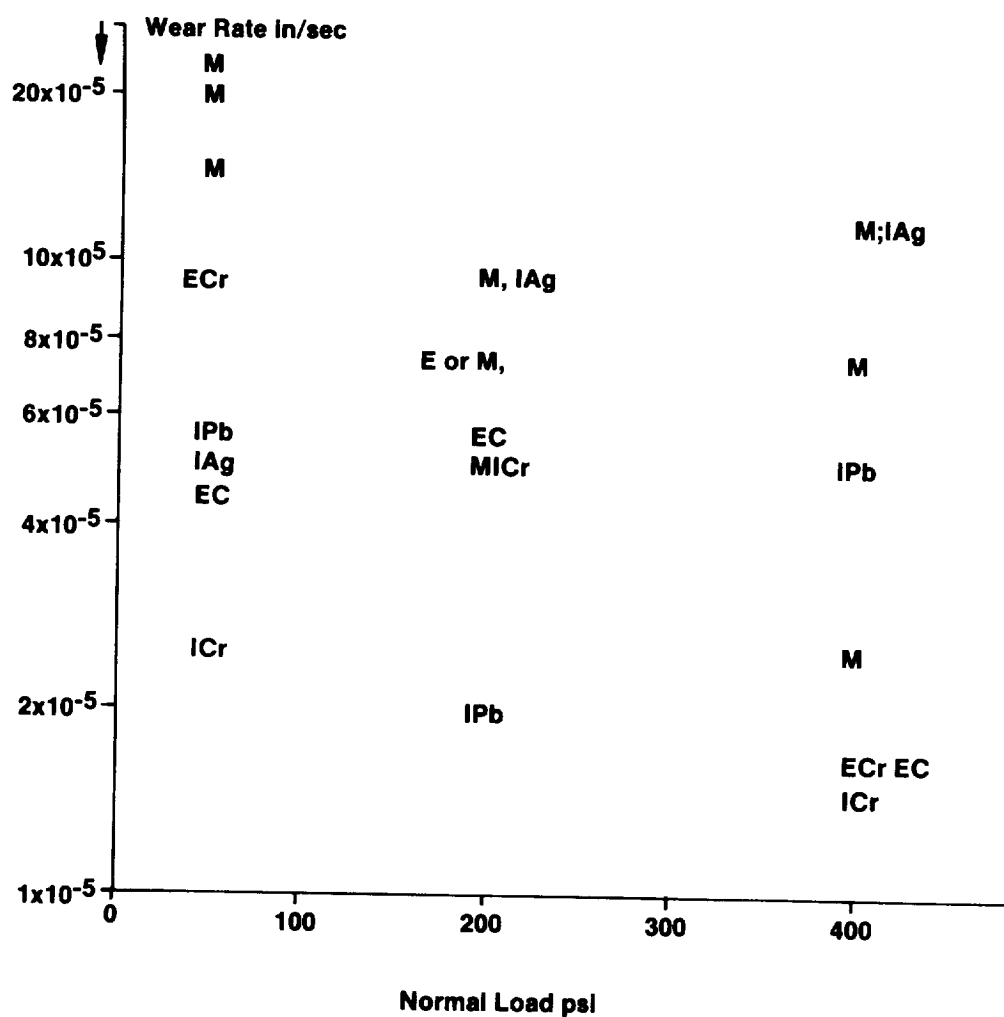


Figure 76. Effect of Surface Modification on Wear Rate as a Function of Contact Pressure in 6.9 MPa (1000 psi) O₂

VII, F, Effect of Surface Modifications and Oxygen Pressure on Monel K-500 Wear Rates (cont.)

Figure 77 summarizes the influence of O_2 pressure and surface treatment on the sample wear. The untreated Monel lost material 3 times faster at 6.9 MPa (1000 psi) than in .088 MPa (12.7 psia) O_2 , even though these operated at much lower temperatures. An oxidation process would appear to be involved. The ion implanted Cr, ion implanted lead, and the electro-plated Ni-SiC composite appeared to be of some advantage in reducing the wear/oxidation rate; however additional tests are required to provide a statistical base for these conclusions.

G. FRICTION COEFFICIENT

1. Friction Coefficients Variable Load Testing

Figure 78 provides a summary of the friction coefficients, computed from normal load and torque measurements for twelve tests at .088 MPa (12.7 psia), and ten tests at 6.9 MPa (1000 psia) O_2 in which valid data were obtained. A portion of the high pressure data have been reproduced in Figure 79 to aid in the discussion of results. The three untreated Monel samples yielded friction coefficients C_f of 0.1 to 0.2 during the first 30 sec in which the 50 psia normal contact load was applied. All of the ion implanted samples indicated friction coefficients reduced by a nominal factor of 2, during this early contact period ($C_f \approx 0.05$). The ion implanted lead provided the greatest friction reduction and in contrast with the brass 360 did not initiate premature metal ignition at the higher loads. Lead forms a soft low melting temperature oxide with good lubricating properties. No significant advantage was observed at the higher contact loads or after 40 sec of rubbing and it could be assumed that the surface modification has been rubbed away. Electro-plated silver also reduces the friction coefficient to a value less than 0.05 at low contact load, however when the stress is increased to 200 psi at 40 sec the samples show a sudden increase in friction of 500% which was

	O ₂ Pressure		
	14.7	1000	
	ΔL In.	ΔL In.	$\frac{\Delta L 1000}{\Delta L 14.7}$
Untreated Monel	.002-.003	.009-.010	3
Ion Implanted Cr	.010	.005	0.5
Electrolyzed Cr	.025	.007-.012	0.5
Ion Implanted O ₂	.0015	.009	6
Ion Implanted Silver	.003	.014	5
Ion Implanted Lead	.004	.005	1
Ni+SIC Composite	.003	.006	2
Electroplated Silver	No Data	—	—
Electroplated Gold	No Data	Friction Weld	—

Increased O₂ Pressure Accelerates Metal Loss Except when Cr is Present

Figure 77. Comparison of Wear Rates in Low (14.7 psia) and High (1000 psia) Oxygen

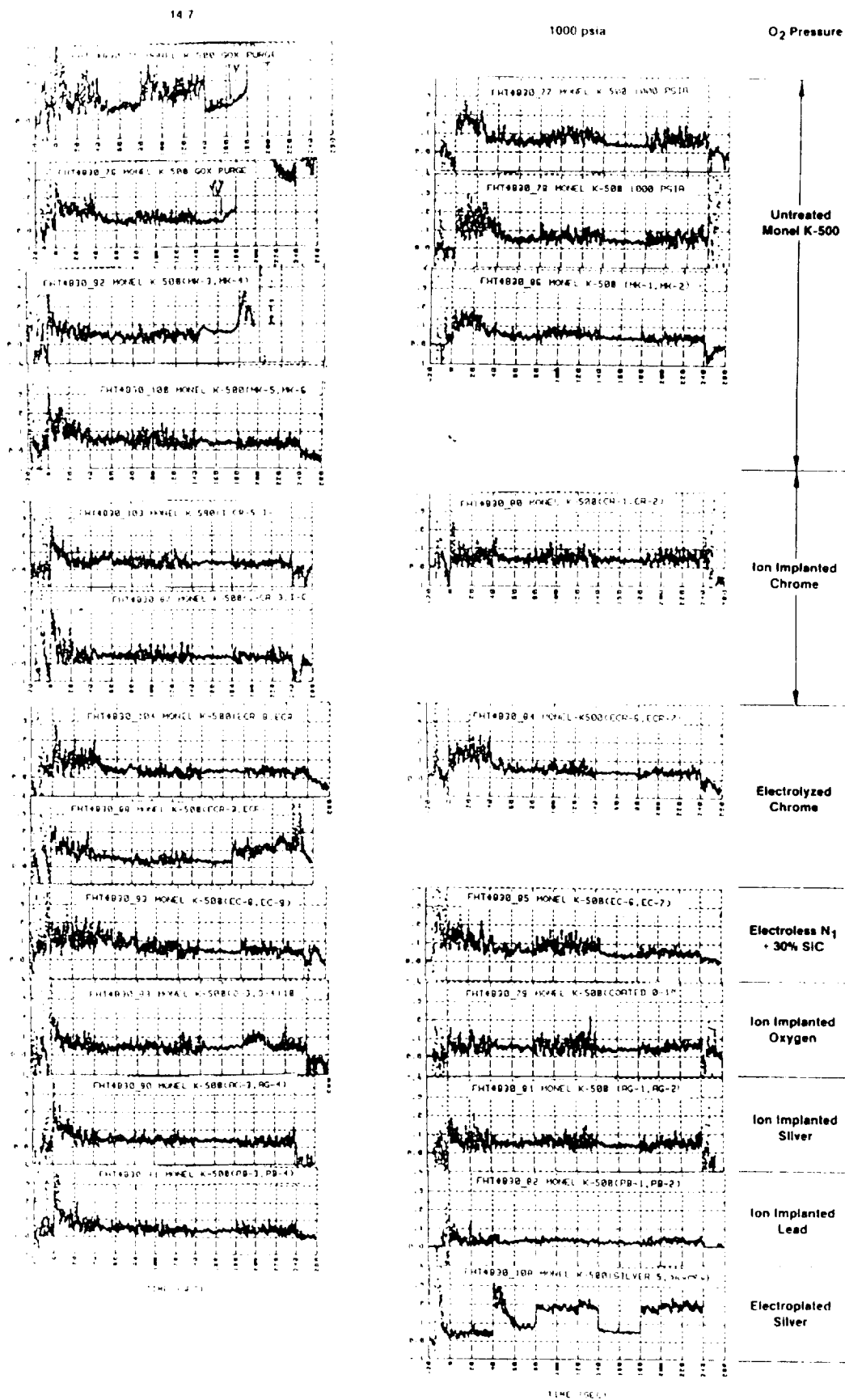
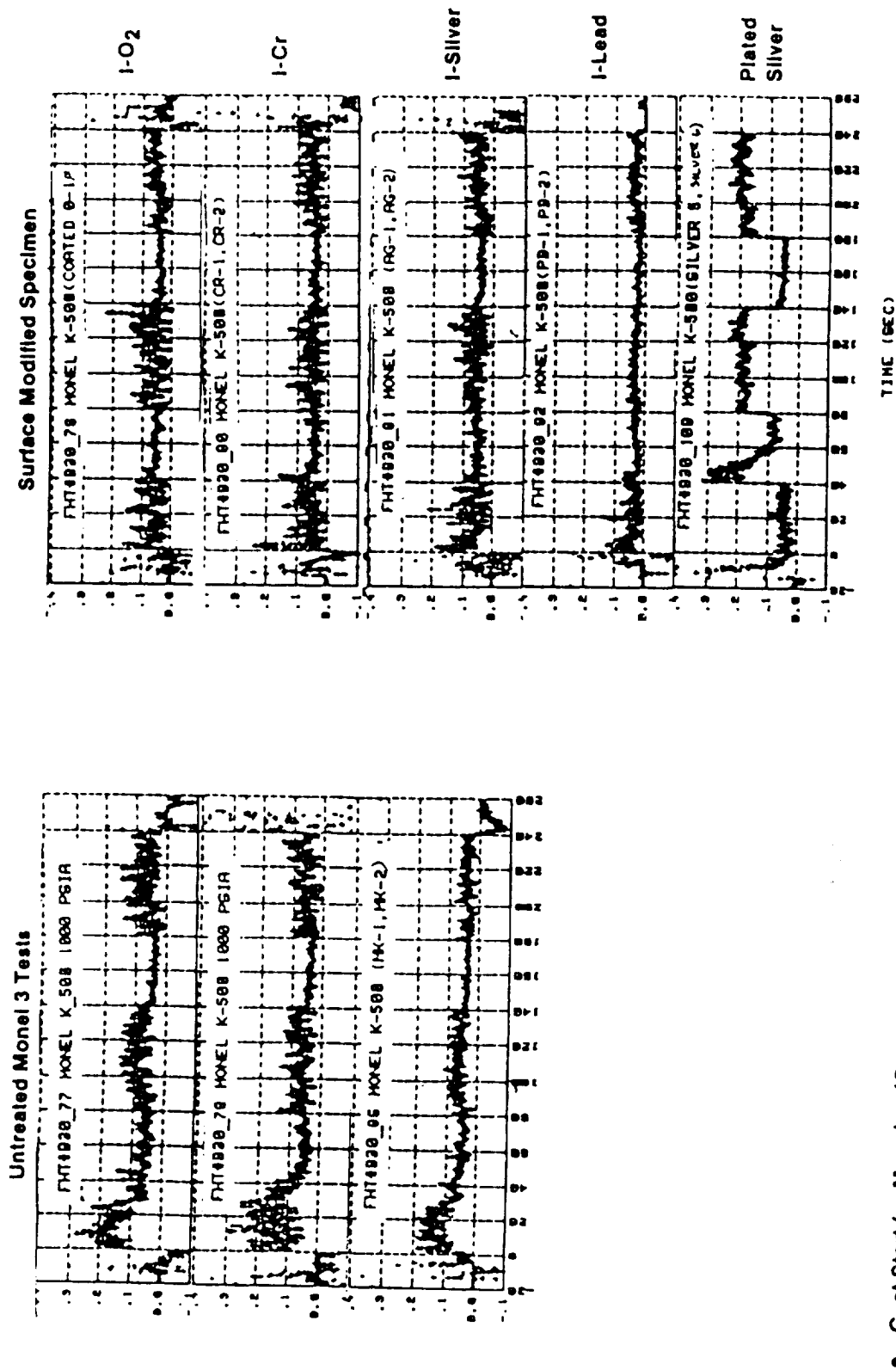


Figure 78. Summary of Friction Coefficients, at 14.7 and 1000 psia, O₂ 17,000 RPM



- C_f at Start for Monel = .15
- C_f of Start for all Ion Implants = 0.05 to 0.1; Lead is Best, Chrome & Oxygen Good
- Silver & Gold Cold Weld at 200 psi Load

Figure 79. Comparison of Friction Coefficients in 1000 psi Oxygen

VII, G, Friction Coefficient (cont.)

shown earlier to be accompanied by rapid heating. The tests conducted in low pressure oxygen showed no significant reduction in friction for any of the surface modifications evaluated.

2. Constant Load Testing

No valid data were obtained from this test series due to problems with the torque measurement system.

H. ANALYSIS OF INDIVIDUAL SURFACE MODIFICATIONS

The following section compares the results for each of the modified surfaces with untreated Monel K-500.

1. Ion Implanted Oxygen

This implant was selected to study the effect of O_2 enrichment at the rubbing surface or as a possible passivation treatment. No particular advantages over other ion implanted materials were observed.

a. Step Load Tests

The data indicated that the peak temperature for the tests conducted with 6.9 MPa (1000 psi) oxygen environment pressure were lower than peak temperatures observed for tests conducted with ambient oxygen environment pressure in all 5 time intervals of the test. The times at which the peak temperatures occurs for the high pressure tests are approximately 20s after the load has been changed from 5000 kN/m² (50 psi) to 20,300 kN/m² (200 psi) or from 5000 kN/m² (50 psi) to 40,500 kN/m² (400 psi) while for the low pressure tests the peak temperatures occur 35s after the load is changed. The values of the peak temperature for the high pressure test during the time

VII, H, Analysis of Individual Surface Modifications (cont.)

intervals 40-80s and 140-180s are 588°K (600°F) and 811°K (1000°F) respectively. The corresponding values for the low pressure tests are 977°K (1300°F) and 1297°K (1875°F) respectively.

The values for the coefficient of friction at the time when peak temperatures occurs is 0.1 in both the high pressure and low pressure tests and there is no appreciable difference in the coefficient of friction after the load is changed from 5000 k/m² (50 psi) to 20,300 k/m² (200 psi). The starting values for the coefficient friction was 0.11 and the value close to the end of the test was 0.05. The decrease in the coefficient of friction is probably due to the formation of the beneficial oxide layer called 'glaze' which may be formed at the contact surface.

b. Constant Load Tests

During the constant load test large fluctuations in the temperature were observed and peak temperatures were 400°K (260°F) and 444°K (340°F) for the two tests conducted.

2. Ion Implanted Chromium

The chromium implant was selected because the presence of Cr₂O₃ near the surface was thought to be beneficial. Measurable benefits over untreated Monel K-500 were observed.

a. Step Load Tests

The peak temperatures with ion implanted chromium in the time intervals 40-80s and 140-180s are 533°K (500°F) and 755°K (900°F) for the high pressure tests and 1116°K (1550°F) and 1255°K (1800°F) for the ambient pressure tests.

VII, H, Analysis of Individual Surface Modifications (cont.)

The coefficient of friction does not change appreciably during the test when the step load is applied. The starting and end value for the coefficient of friction is approximately 0.5.

b. Constant Load Tests

For the two tests conducted the data were not repeatable and peak temperatures were 449°K (350°F) and 363°K (195°F). The interval during which these peak temperatures occurred was different, with the former occurring in the 0-40s of the test period while the latter in 240-300s of the test interval.

3. Ion Implanted Silver

Silver does not form a stable oxide at elevated temperatures. The possibility of blocking the surface oxide was a concern. This material exhibited greater wear than other implants in high pressure oxygen.

a. Step Load Tests

The peak temperatures in the reference time intervals in this case were 602°K (625°F) and 658°K (725°F) for the high pressure tests and 691°K (850°F) and 1366°K (2000°F) for the low pressure tests.

The starting and end values for the coefficient of friction were 0.14 and 0.06 respectively.

b. Constant Load Tests

The peak temperatures in this case was 433°K (320°F) which occurred during 0-40s of the test period.

VII, H, Analysis of Individual Surface Modifications (cont.)

4. Ion Implanted Lead

Lead was selected because of the unfavorable results of the 360 Brass which contained lead copper and zinc. Lead proved to be one of the better implant materials.

a. Step Load Tests

In this case the peak temperatures in the time intervals when the load was 20,300 k/m² (200 psi) and 40,500 k/m² (400 psi) was 547°K (525°F) and 811°K (1000°F) for the high pressure test and 811°K (1000°F) and 1033°K (1400°F) for the ambient oxygen pressure tests.

The start and finish value for the coefficient of friction were 0.06 and 0.03 respectively at high O₂ pressure. The lead also showed an advantage over untreated Monel at low oxygen pressure.

b. Constant Load Tests

There was good repeatability of the peak temperatures in this case, 389°K (240°F) and 383°K (230°F) but the time interval in which they occurred differed during the two tests. The former occurred in 0-40s while the latter in 240-300s intervals.

5. Electrodeposited Chromium

This surface treatment proved to be the worst from all respects, when rubbed against itself.

a. Step Load Tests

Two tests were conducted at high and ambient oxygen environment pressure. In one test at ambient oxygen environment the peak temperatures in the 40-80s interval and 140-180s interval were 1144°K (1600°F)

VII, H, Analysis of Individual Surface Modifications (cont.)

and 1366°K (2000°F) while in the other test the corresponding values for the temperatures were 772°K (930°F) and 1228°K (1750°F). In the high pressure tests the corresponding values for the temperatures in one test were 644°K (700°F) and 558°K (600°F) and for the other test 616°K (650°F) and 755°K (900°F). These values indicate that the repeatability of the test data was not very good.

The start and finish values for the coefficient of friction in this case were 0.22 and 0.08.

b. Constant Load Tests

In this case the peak temperatures differed considerably for the two tests conducted. The peak temperatures were 455°K (360°F) and 710°K (820°F).

Future tests should include a chrome-silver combination (hard on soft) for several reasons. 1) other data suggest this to be a good combination, 2) portions of the turbopump incorporate this combination and 3) it will add to the data base of unlike materials.

6. Composite Plating of Ni-SiC

The composite provided the highest surface hardness combined with a substantial thickness to resist wear for extended periods. An advantage over untreated monel was observed and further testing is suggested.

a. Step Load Tests

The peak temperature values for ambient pressure tests were 1144°K (1600°F) and 1200°K (1700°F) while for the high pressure tests the values were 505°K (450°F) and 755°K (900°F) respectively.

VII, H, Analysis of Individual Surface Modifications (cont.)

The start and finish values for the coefficient of friction were in the range 0.15 and 0.07 for the tests conducted.

b. Constant Load Tests

The peak temperatures in this case were 411°K (280°F) and 366°K (200°F) for the two tests conducted.

7. Electrodeposited Silver

This material functioned well at low contact pressure but tended to heat rapidly when a high contact load was applied. The sudden increase in temperature and friction coefficient indicated the inability to form a protective oxide film on a hot surface was causing local surface welding.

8. Electroplated Gold

This material failed by shearing at the gold-monel interface. The failure is attributed to surface welding due to the absence of a protective oxide film. The next section provides additional documentation of this failure.

I. PHOTOGRAPHIC AND METALLURGICAL ANALYSES

Photographic documentation of the various test specimen and surface modifications were taken before and after testing. Detailed surface analyses were also conducted using optical, Scanning Electron Microscopy (SEM) and Auger Electron Spectroscopy (AES). Appendix B documents the analyses conducted at the WSTF. The following section contains the materials evaluation.

VII, I, Photographic and Metallurgical Analyses (cont.)

1. Pretest Condition

Figure 80 shows an overview of the test rings with the various surface modifications. The composite and the silver plated surfaces are substantially thicker than the others.

Figure 81 shows a 14X enlargement of surfaces before testing. The ion implanted surfaces (upper right) did not change in appearance from the pre-treated surfaces and all of the implanted elements provided identical visual surface finished as shown in Figure 81a. The electrolyzed chrome surface (upper left) was shiny and considerably smoother. All specimens had the same appearance. The edges were more rounded than the original surface and the ion implanted specimen either due to the preparation and masking or plating process. As noted earlier the composite plating (bottom) was much thicker and tended to mask the machining marks on the untreated surfaces. Some of the plated specimens contained small surface imperfections as may be noted on EC-2 while most appeared smooth as shown by specimen EC-5 in Figure 81.

In order to understand the role of oxygen on the surface composition of the Monel K-500 one of the ion implanted oxygen surfaces was examined by AES techniques. Figure 82 documents the atomic composition of the surface treated specimen indicating the percentage of Ni, Cu, Al expected in the monel plus oxygen which was implanted. The other materials, i.e., Zn and C represent surface contamination.

The indepth concentration profile was then determined by ion beam milling (sputtering) the surface away at a rate of approximately 300A/min to obtain the results shown in Figure 83. The carbon was observed to be present only on the surface. The oxygen showed an atomic concentration of 10% for a depth of "1200A" and then reduced to "0" at a depth of 2100A. In the zone where oxygen was present in measurable quantities the following alterations were observed in the monel substate.

ORIGINAL PAGE IS
OF POOR QUALITY

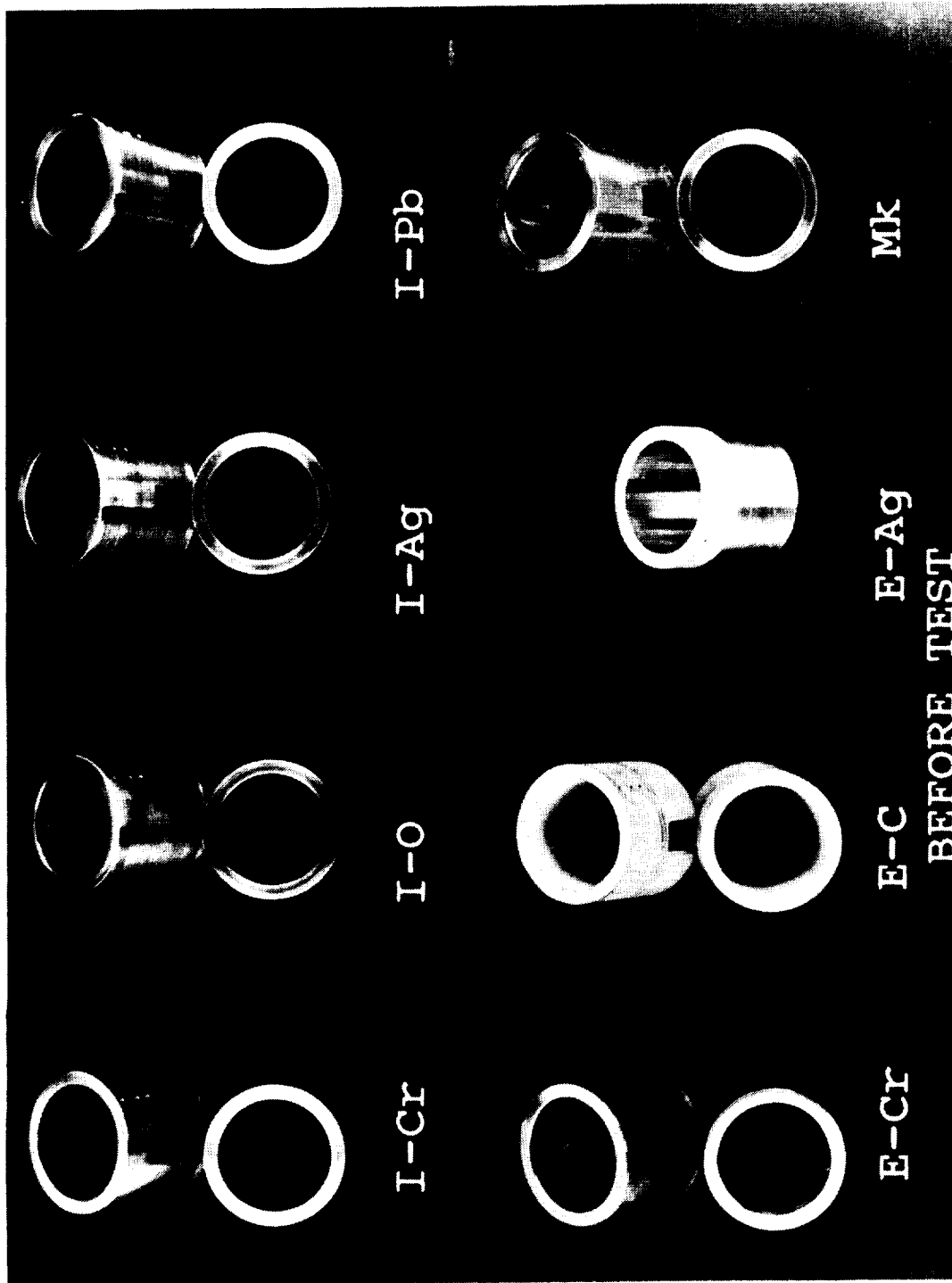
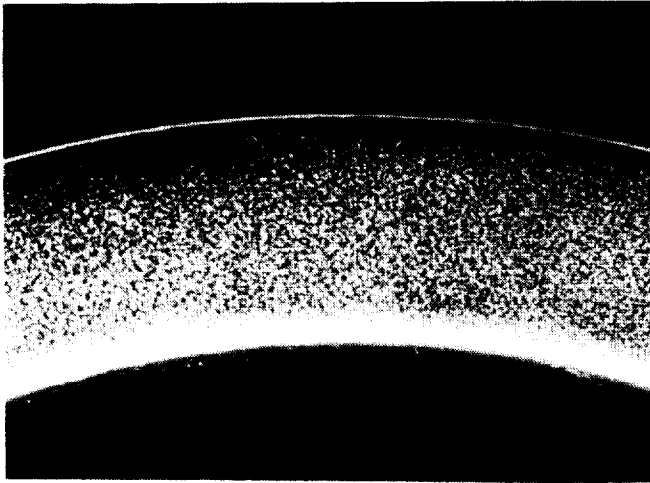
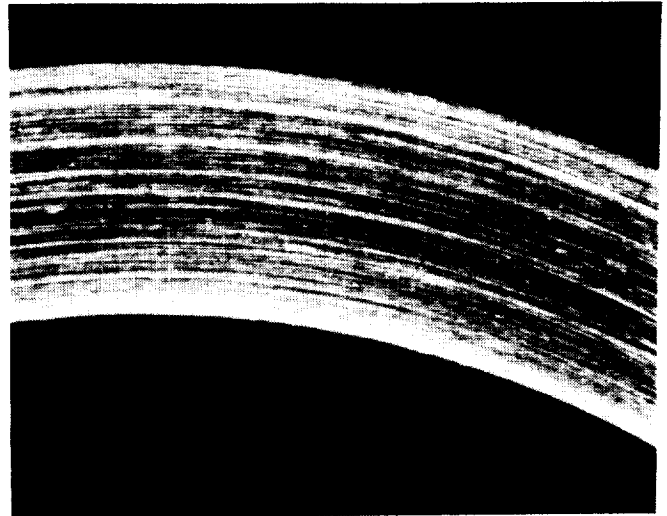


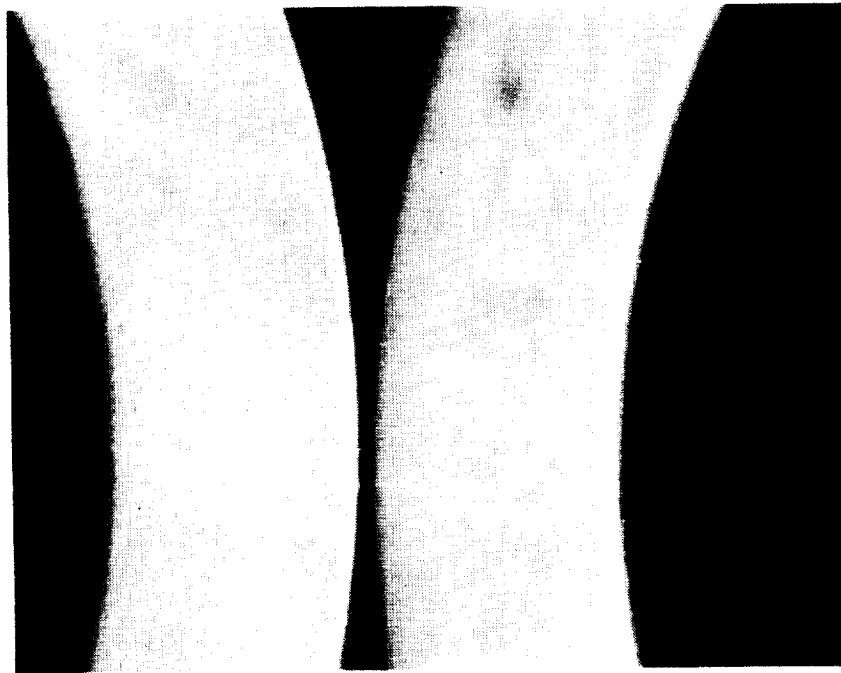
Figure 80. Pre Test Photo of Surface Modified Test Specimen



Specimen ECR-1
Electrolized Cr 14X



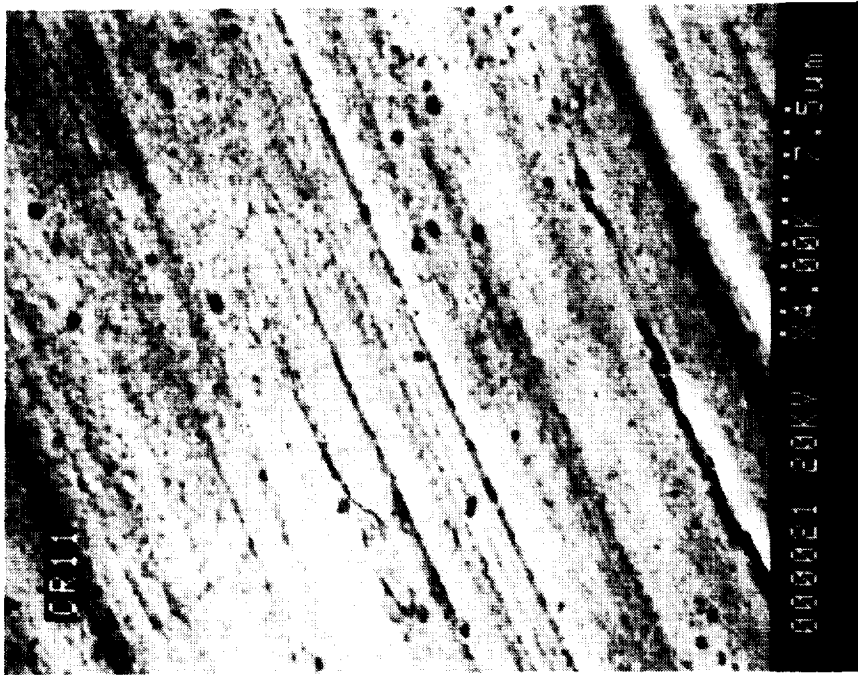
Specimen I-O-10
Ion Implant O₂ 14X



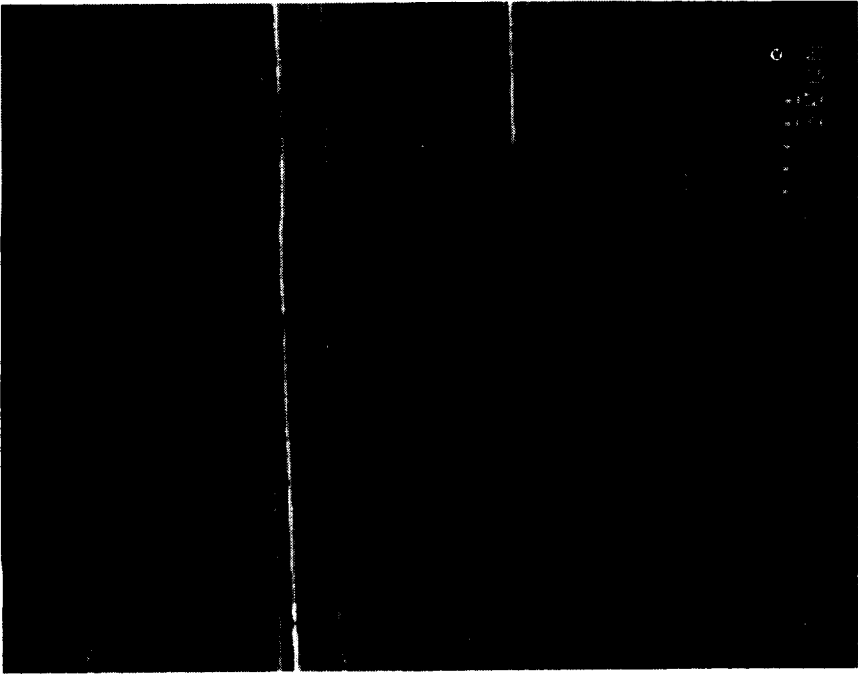
NYE Carb Ni+SiC 14X
Specimen EC-2

Specimen EC-5

Figure 81. Pre Test Surface Comparisons of Electrolized Cr, Ion Implanted Surface and NYE Carb (Ni+SiC)



Ion Implanted Cr Pre Test 4000 X



Ion Implanted Pb Pre Test 1000X

Figure 81a. Pre Test Surface Comparisons (Continued)

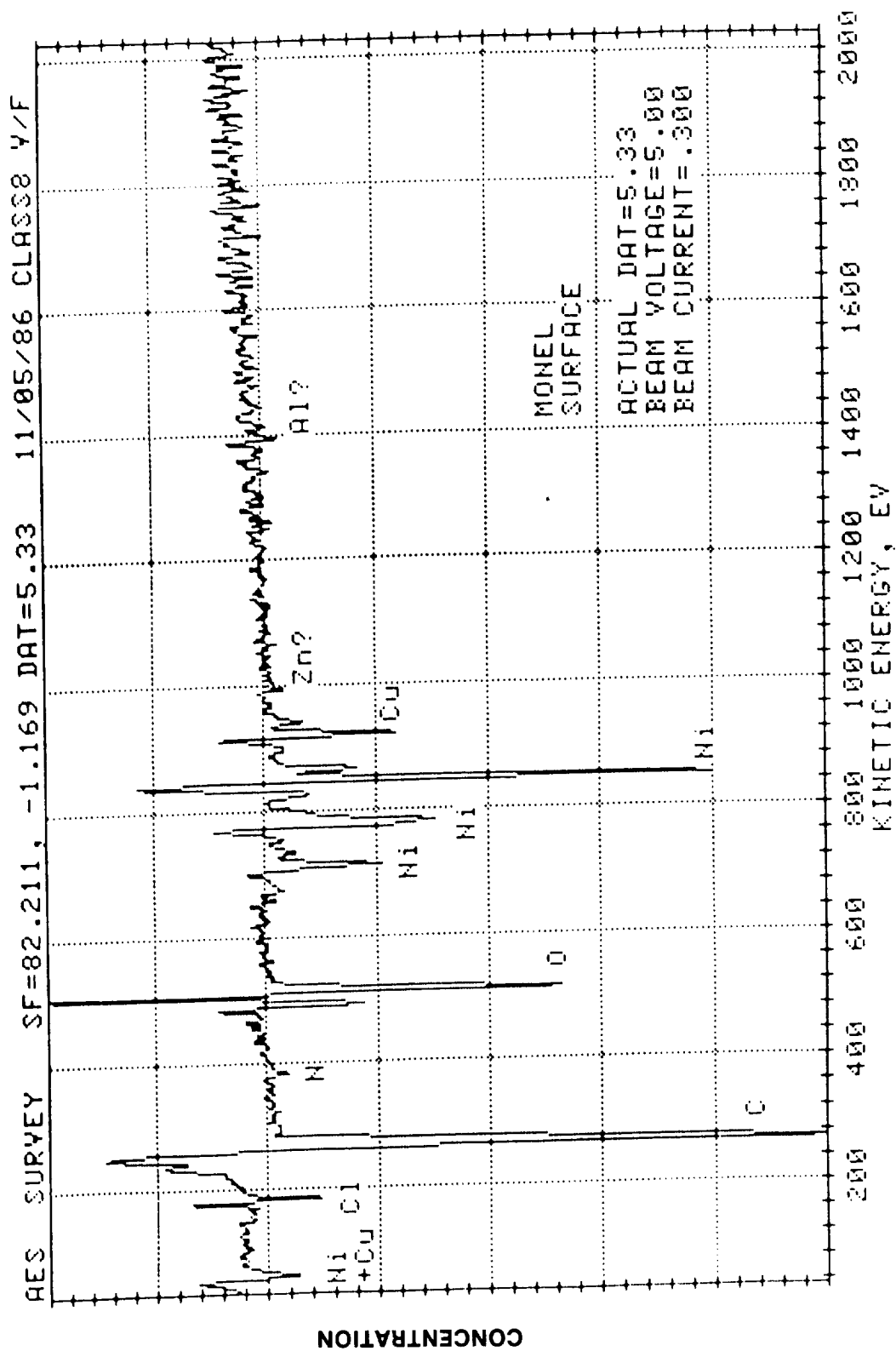


Figure 82. Surface Composition O₂ Ion Implanted Monel K-500

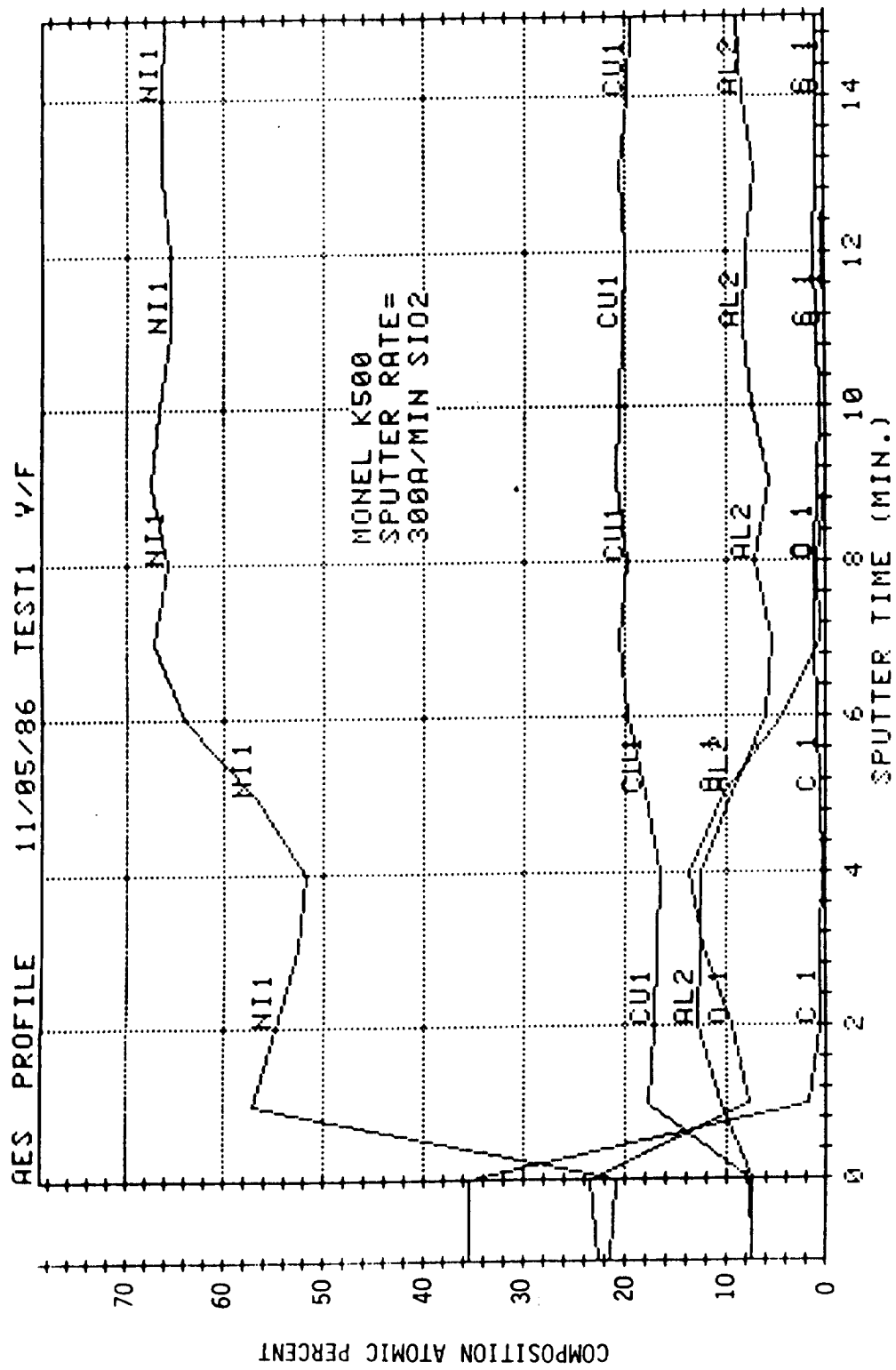


Figure 83. Composition Profile O₂ Ion Implanted Monel K-500

VII, I, Photographic and Metallurgical Analyses (cont.)

- a. The nickel dropped from a nominal 66 A/O* to \approx 55 A/O.
- b. The aluminum concentration increased from an internal concentration of 6 to 8 A/O to a near surface concentration of 10 to 14 A/O.

These measurements indicate that the presence of oxygen at the surface will tend to enrich the surface in aluminum probably to produce Al_2O_3 . Additional discussion of the pre to post test change in near surface composition if ion implanted Cr and Pb is provided in the next section.

2. Post Test Condition

Visual inspections and pre to post test changes in the near surface and chemical composition were investigated using SEM and EDS methods.

Figure 84 shows the post test condition of the rings after testing in O_2 at 1 atmosphere pressure. A glaze can be observed on all of the surfaces except for the composite which spalled in places. Similar results can be observed in Figure 85 where the oxygen pressure was 6.9 MPa (1000 psi). It should be noted that no burning was observed on any of the rings shown. The thick electroplated silver specimen was also completely stripped of the plating as shown in Figure 86. The results were similar to those experienced with gold plating (Test 109) as can be observed in Figure 87. The gold appears to have welded to itself and sheared clearly at the interface of the stationary monel specimen.

A detailed investigation and comparison of the rubbing surfaces exposed to low and high oxygen pressure was conducted. Figures 88 through 99 show the surface condition at 50 and 500X magnification. The pretest photos shown in Figure 88 were typical of the untreated and all ion implanted materials.

*A/O = Atomic Percentage

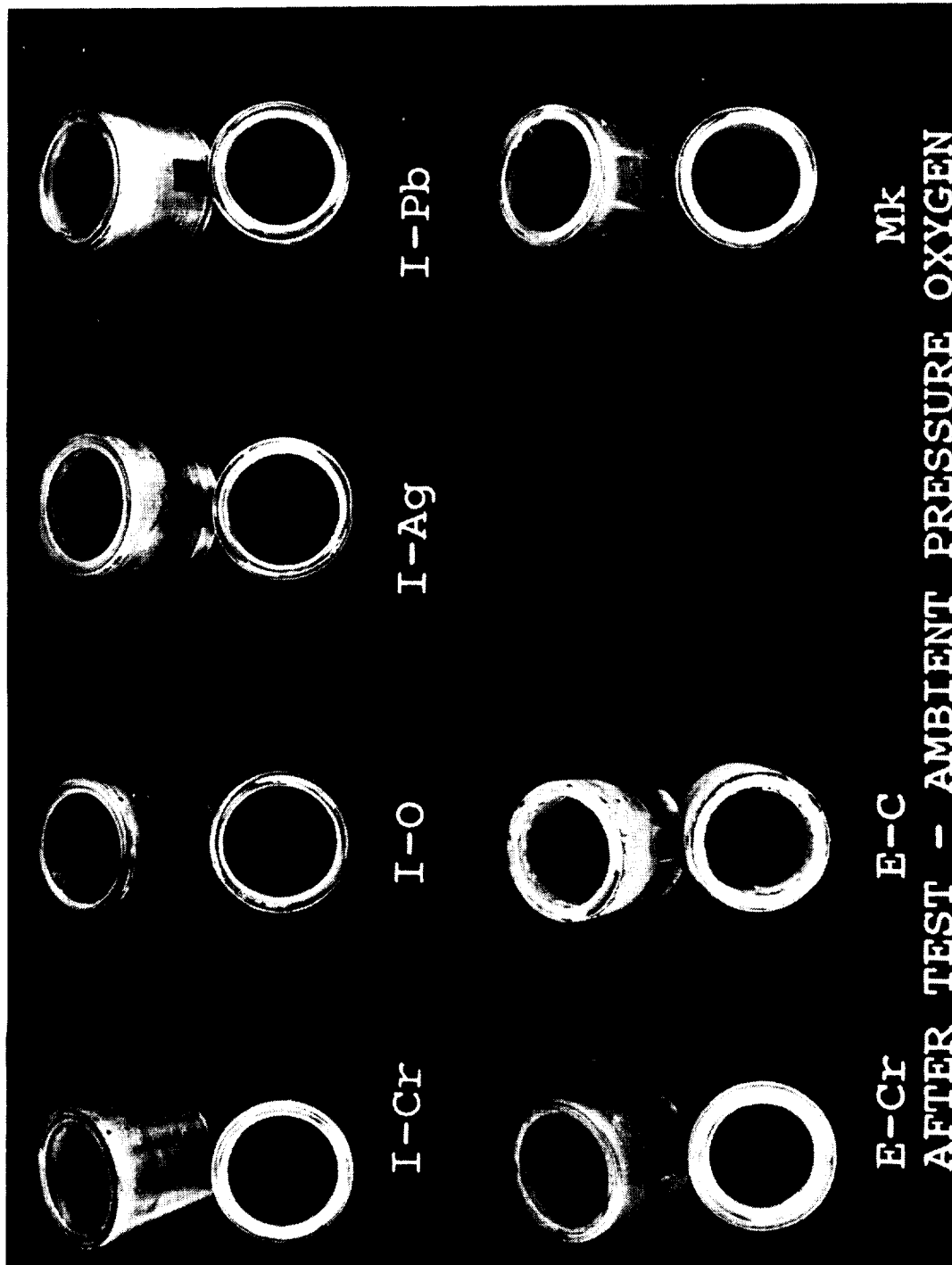


Figure 84. Surface Modified Monel K-500 after Step Load Testing in Oxygen at Ambient Pressure

ORIGINAL PAGE IS
OF POOR QUALITY

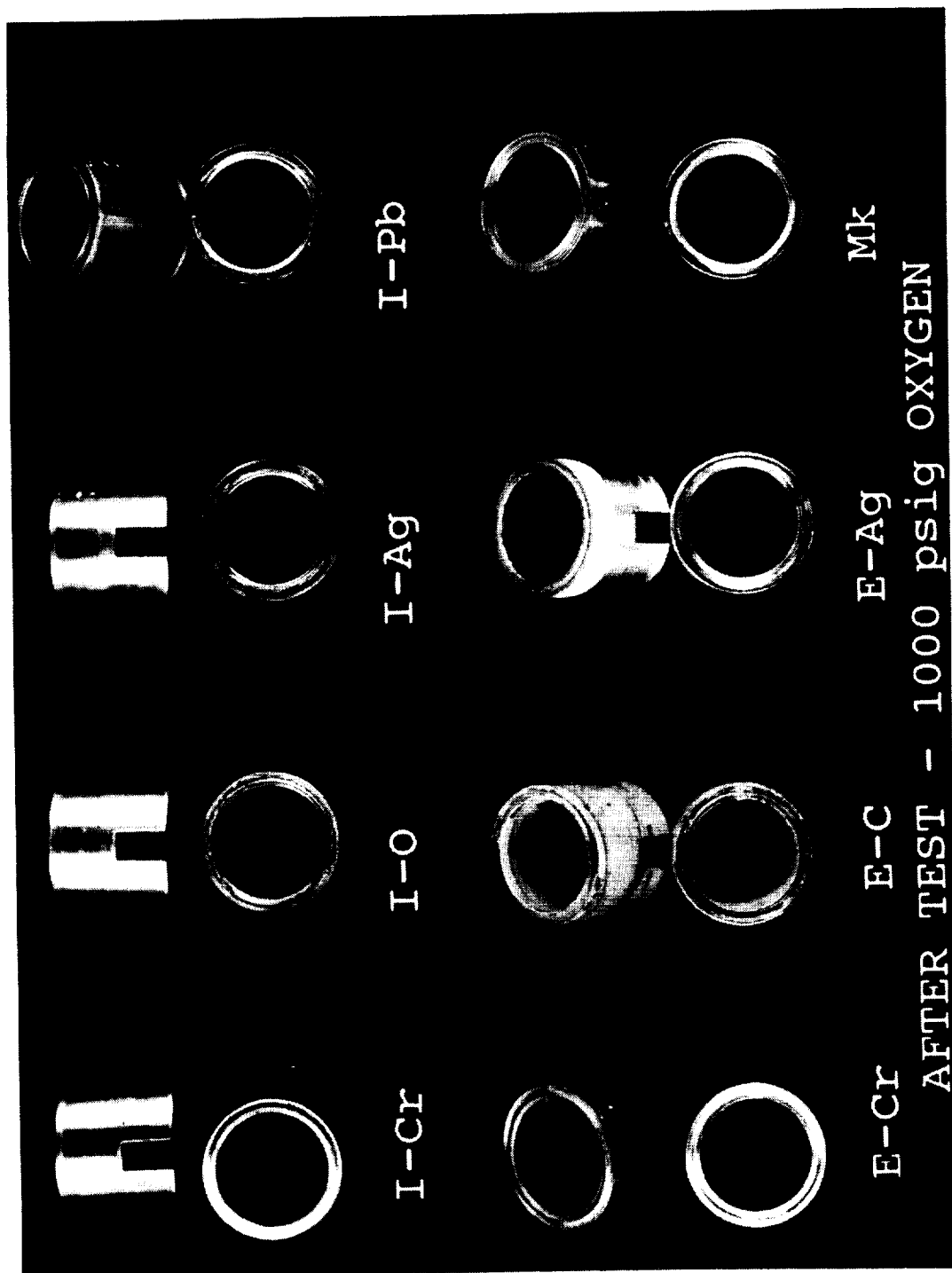


Figure 85. Surface Modified Monel K-500 after Testing in 6.9 MPa (1000 psia) Oxygen

ORIGINAL PAGE IS
OF POOR QUALITY



Figure 86. Electroplated Silver Post Test 108, $O_2 = 6.9$ MPa (1000 psi)

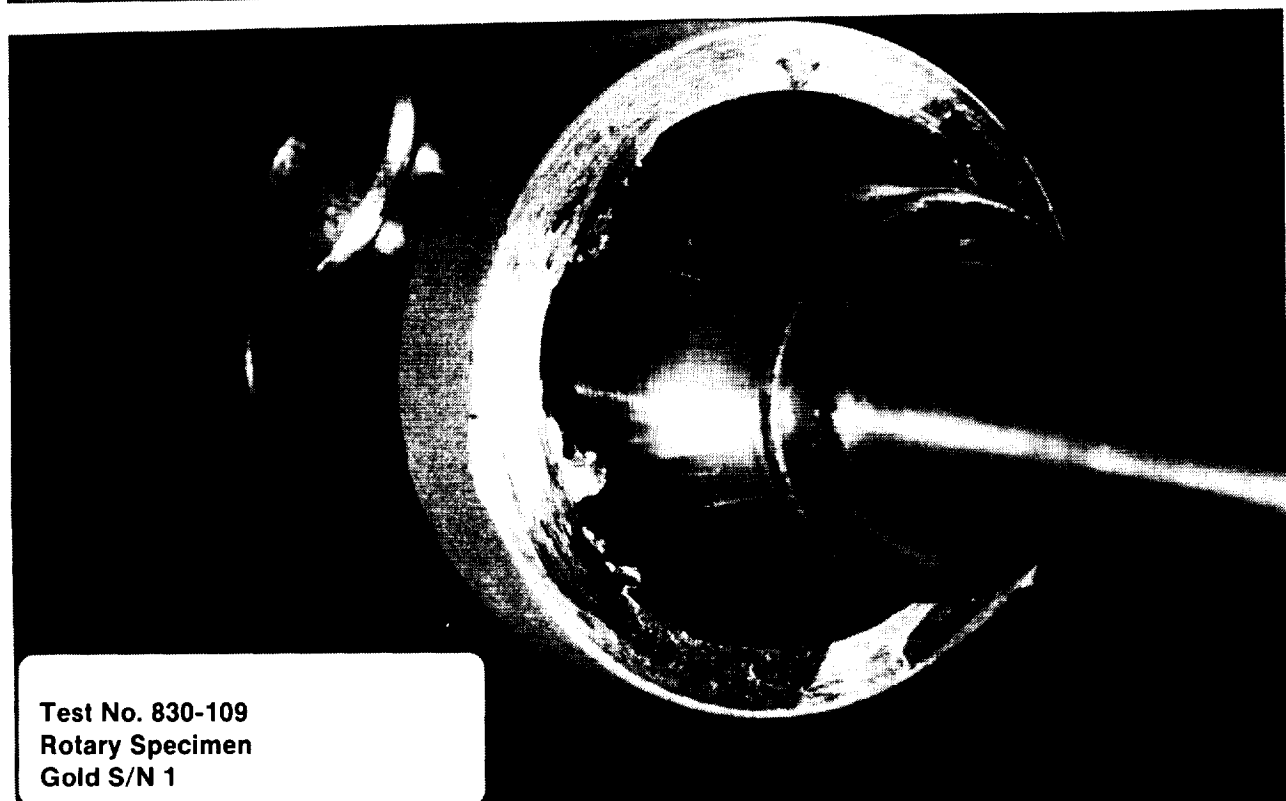
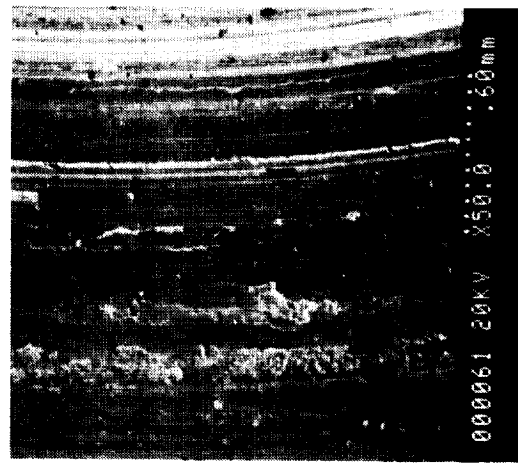
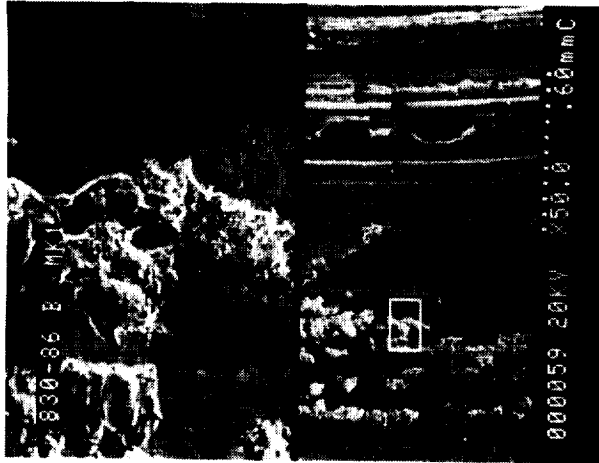
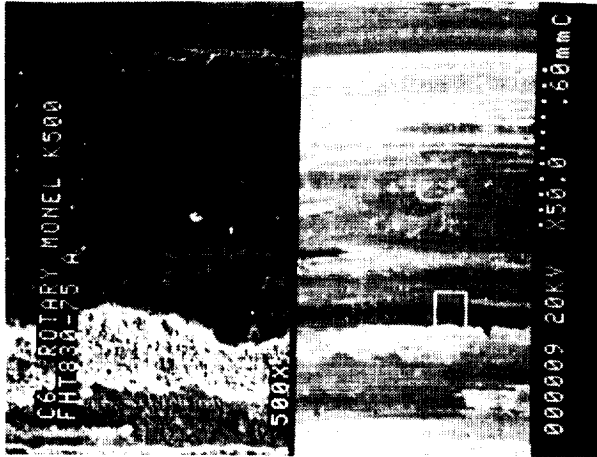


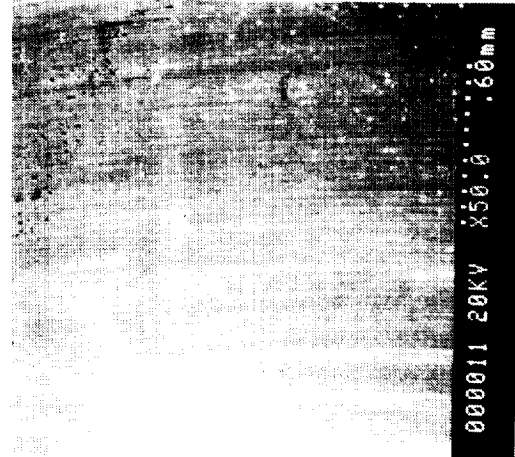
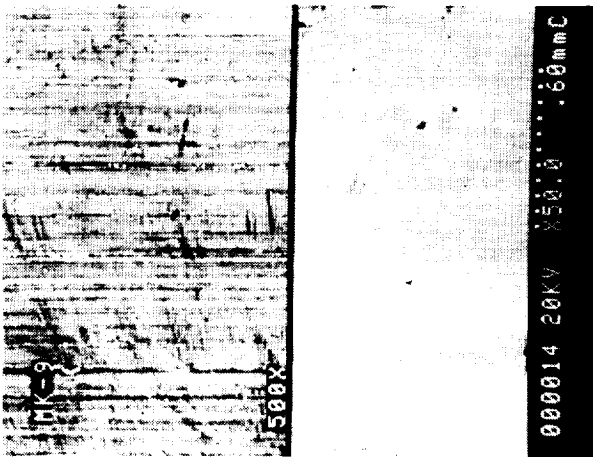
Figure 87. Friction Rubbing of Electroplated Gold in Oxygen Test 109



Test 86

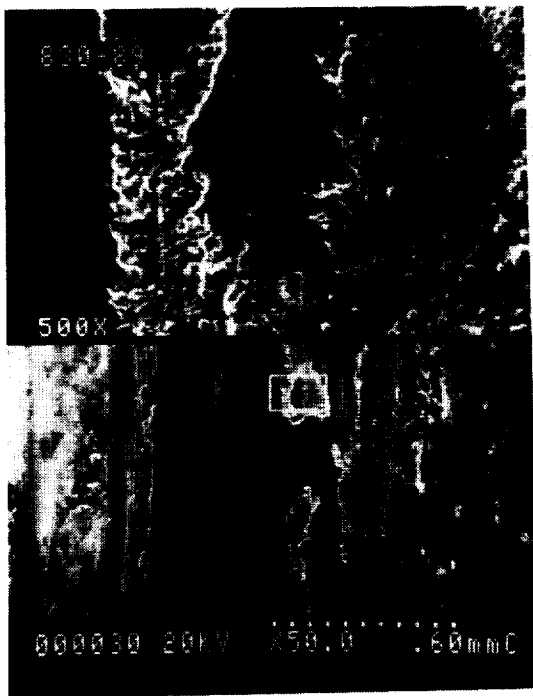


Test 75



Pre Test

Figure 88. Mon K-500 without Surface Modifications, Following Test 75 in O₂ at 1 ATM and Test 86 at 6.9 MPa (1000 psi)



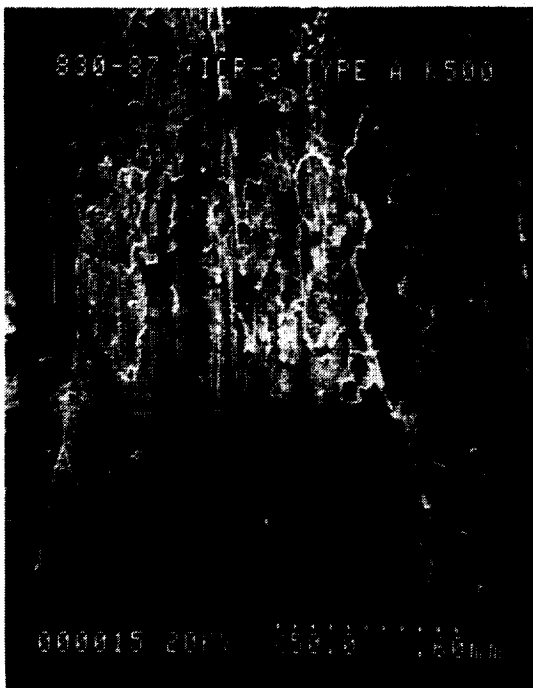
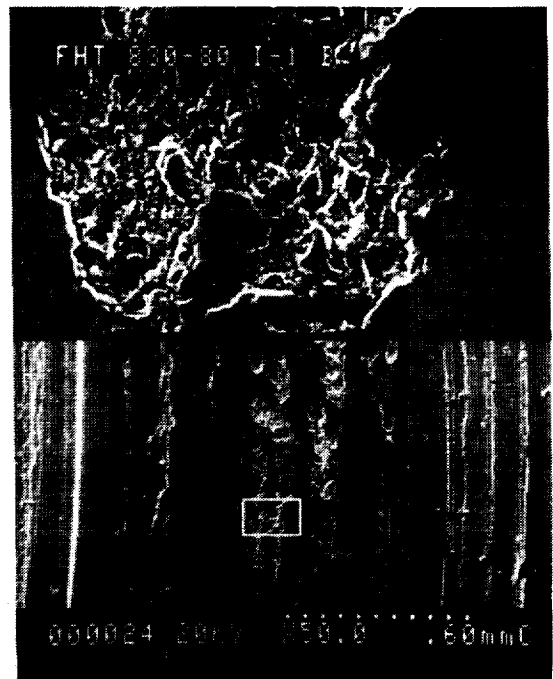
$O_2 = 1 \text{ ATM}$



$O_2 = 6.9 \text{ MPa (100 psi)}$

Figure 89. Ion Implanted Oxygen Post Test 81 and 79 Low and High Oxygen Pressure

ORIGINAL PAGE IS
OF POOR QUALITY



$O_2 = 1 \text{ ATM}$



$O_2 = 6.9 \text{ MPa (1000 psi)}$

Figure 90. Ion Implanted Chromium Post Test 87 and 80 Low and High Oxygen Pressure

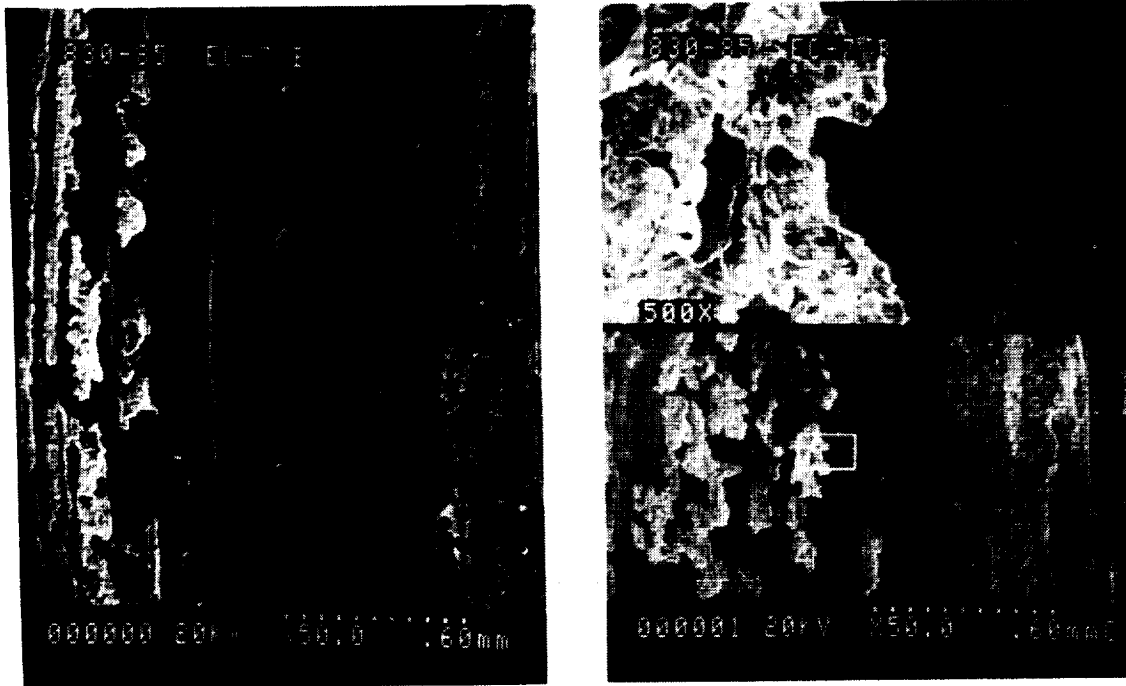
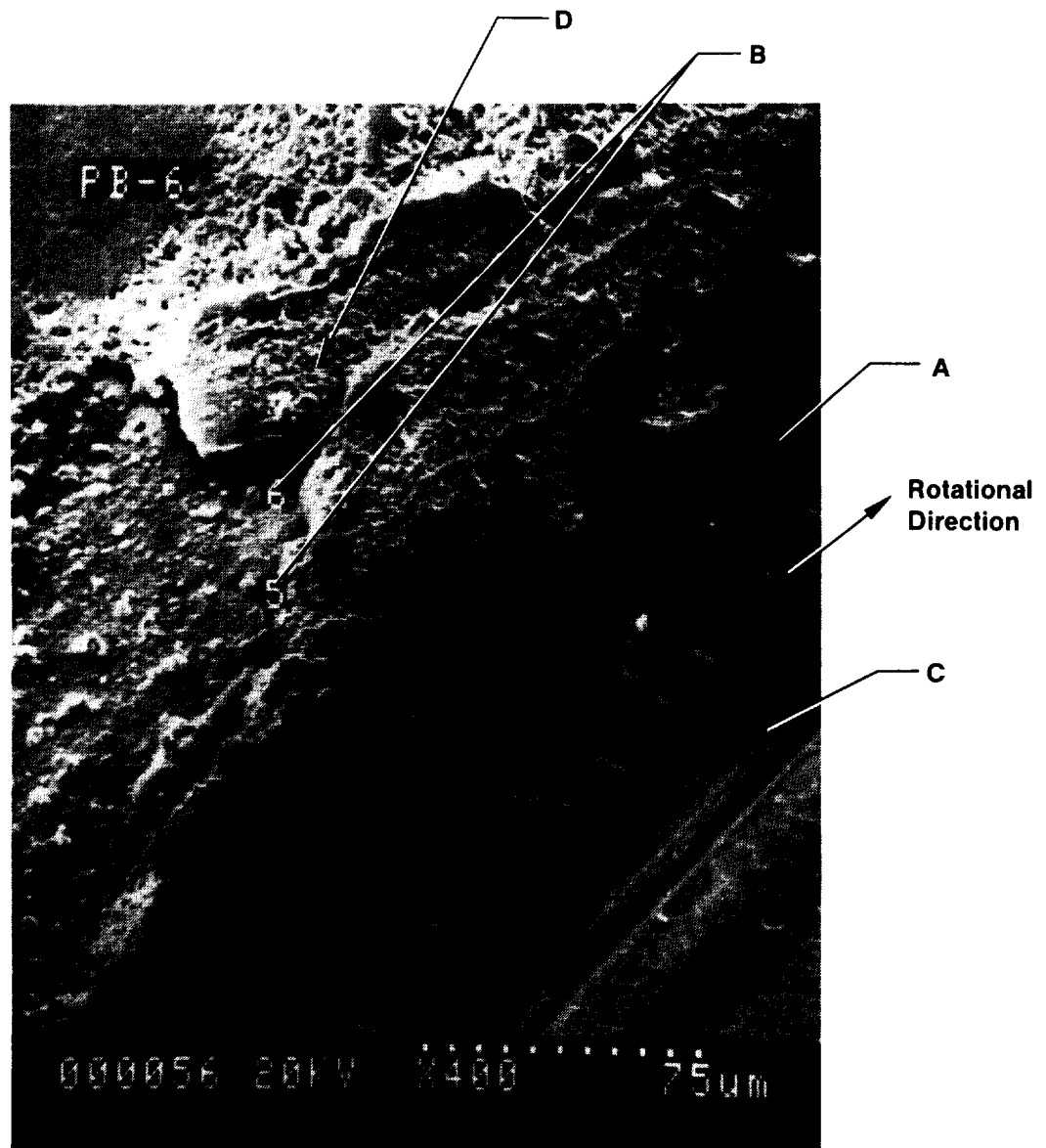


**Figure 91. Monel D-500 with Composite Ni + 30% SiC
Post Test No. 85 6.9 MPa, 1000 psi**

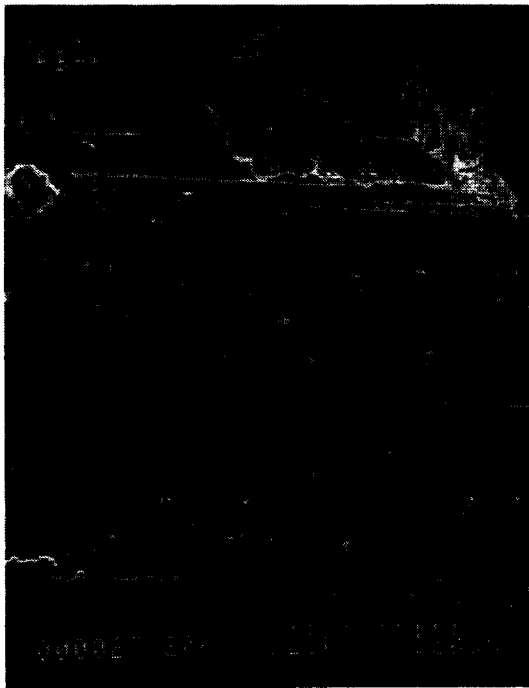
**ORIGINAL PAGE IS
OF POOR QUALITY**

ORIGINAL PAGE IS
OF POOR QUALITY



- A. Smooth Mirror Like Surface, Circumferential with Radial Cracks
- B. Subsurface in Spalled Zone
- C. Deep Glossy Circumferential Grooved, No Cracks
- D. Pitted

Figure 92. Photomicrograph FRT Specimen No. IPb 6, 14.7 psi O₂ 400x



Zone 1 & 2 Smooth Glazed Surface
 3 & 4 Original Surface
 5 & 6 Zone under Spall

Figure 93. Ion Implanted Lead Specimen Post Test No. 91, O₂ = 1 ATM

ORIGINAL PAGE IS
 OF POOR QUALITY

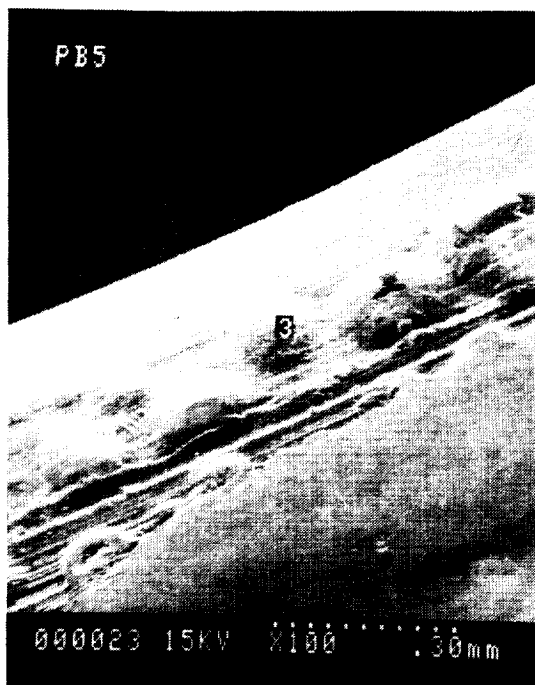
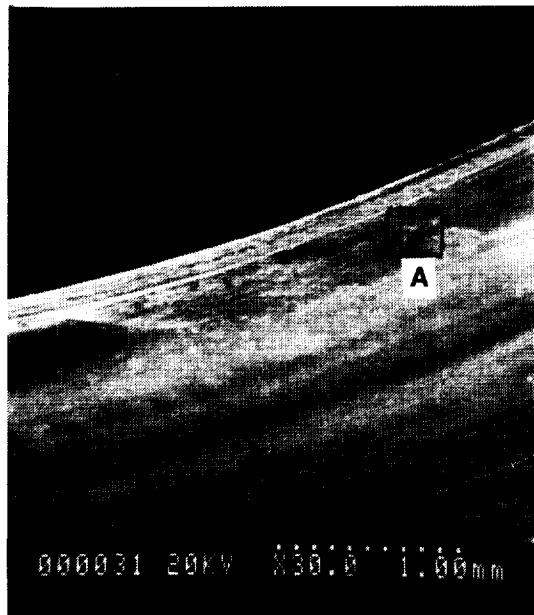
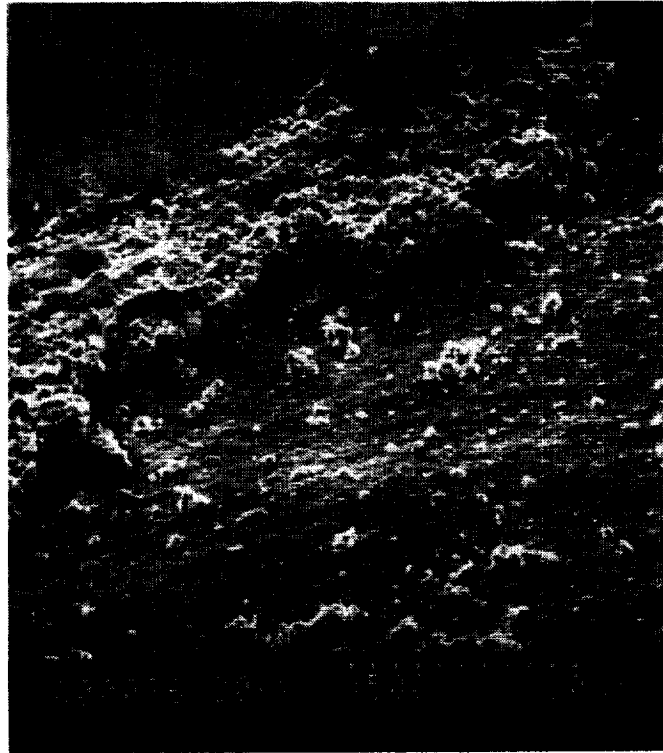


Figure 94. Blistered Zone Ion Implanted Lead Post Test No. 91, $O_2 = 1$ ATM



PB-6



30° Tilt

PB-6

1-21

Figure 95. Spalled Zone Ion Implanted Lead Post Test No. 91

ORIGINAL PAGE IS
OF POOR QUALITY

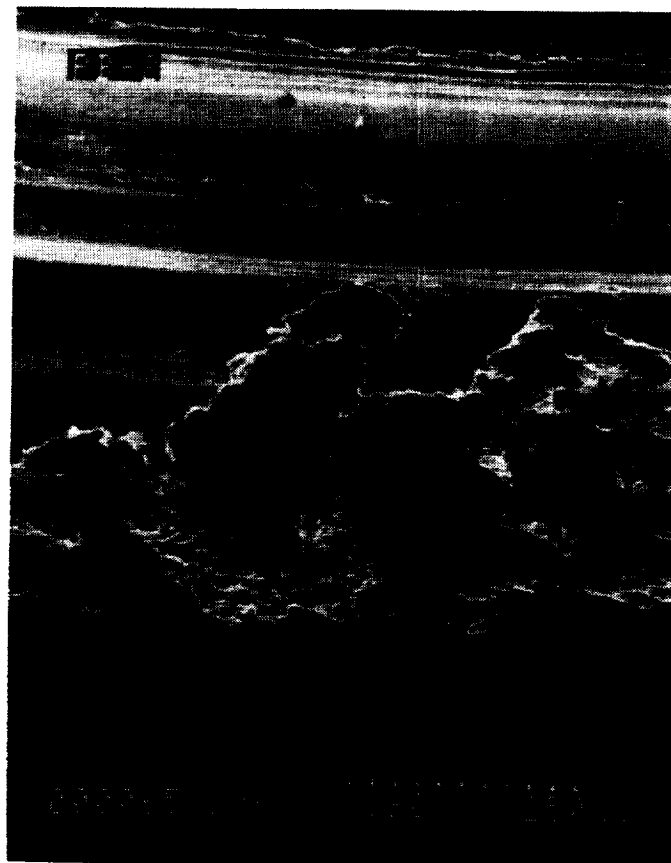
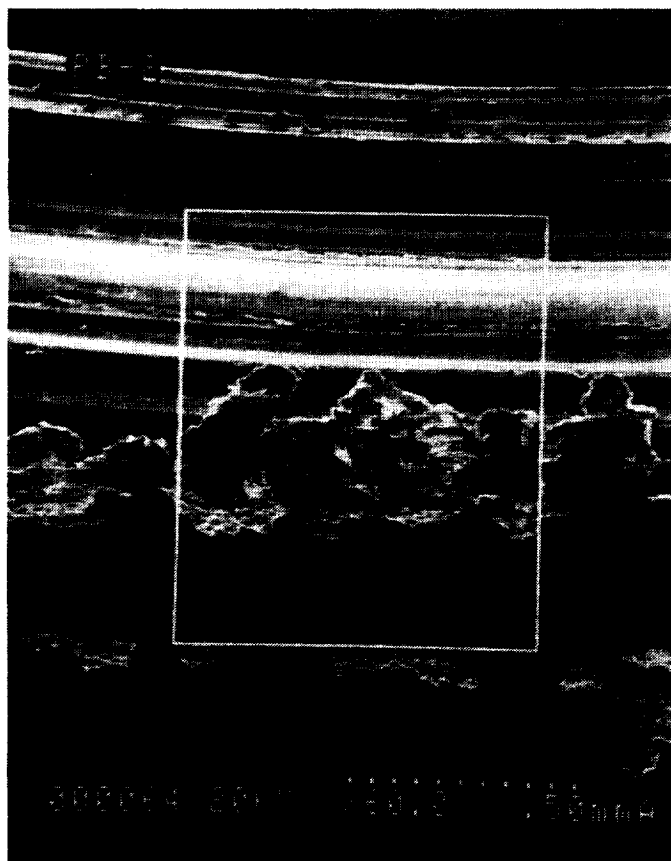


Figure 96. Ion Implanted Lead Post Test No. 82 O₂, 6.9 MPa (1000 psi)

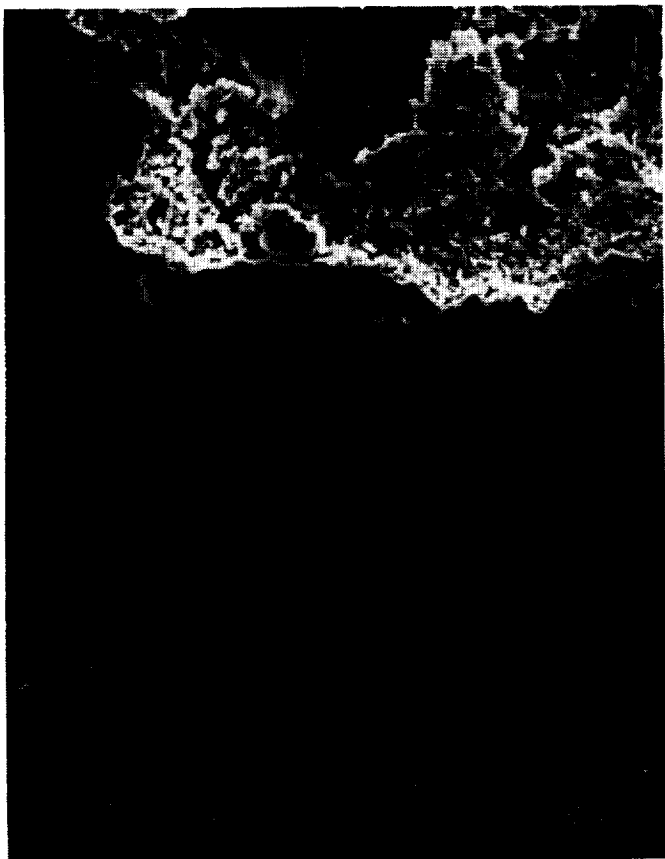


Figure 97. Spalled and Cracked Region for Implanted Lead Post Test No. 82 O₂, 6.9 MPa (1000 psi)

ORIGINAL PAGE IS
OF POOR QUALITY

ORIGINAL PAGE IS
OF POOR QUALITY

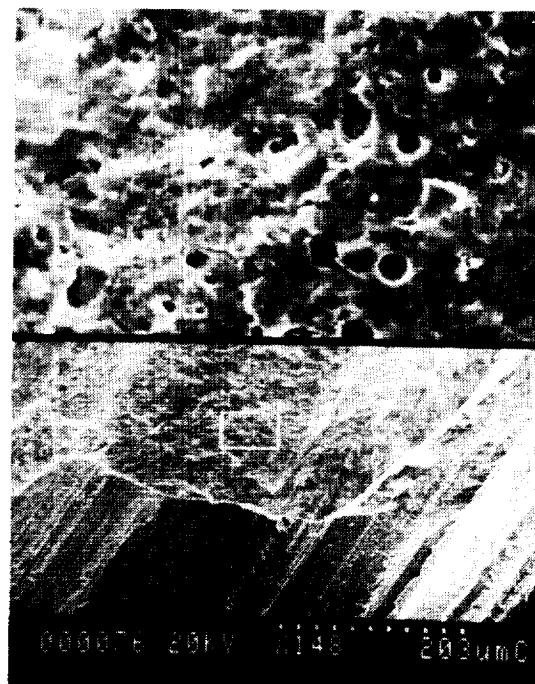
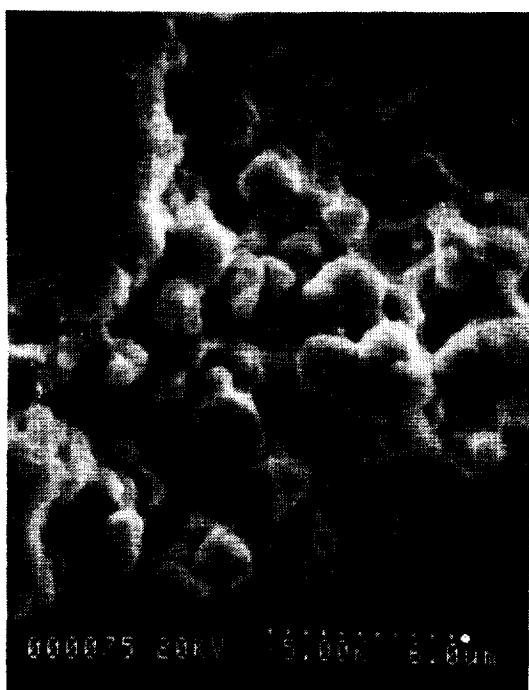
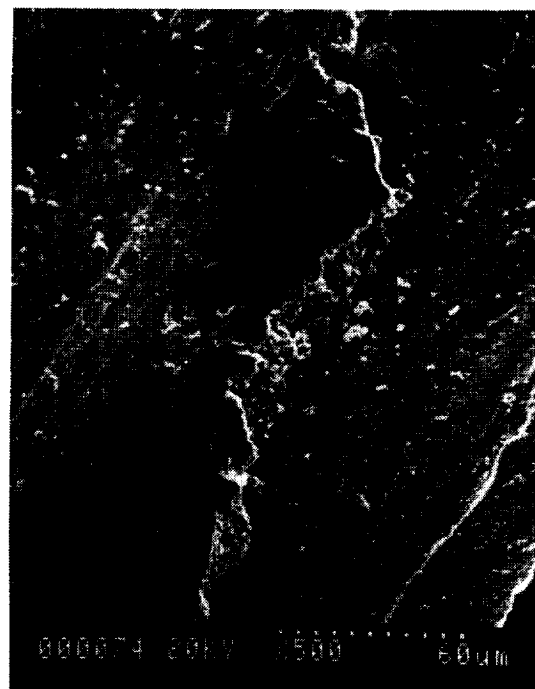


Figure 98. Ion Implanted Silver Post Test 90, Specimen IAg-4, O₂ = 1 ATM

ORIGINAL PAGE IS
OF POOR QUALITY

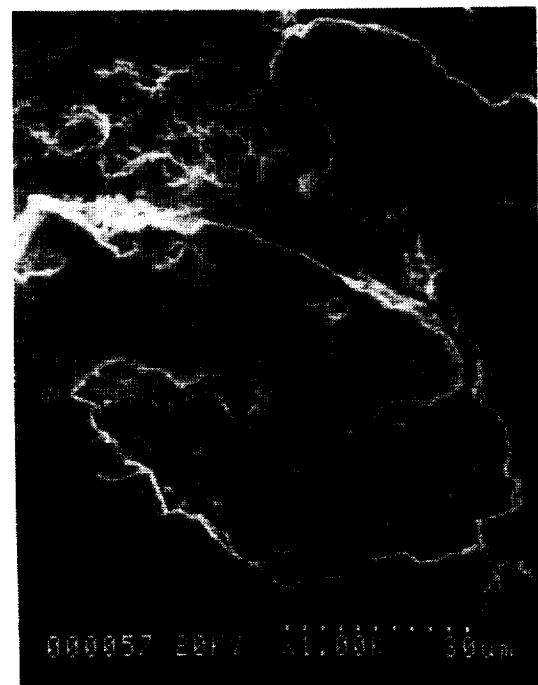
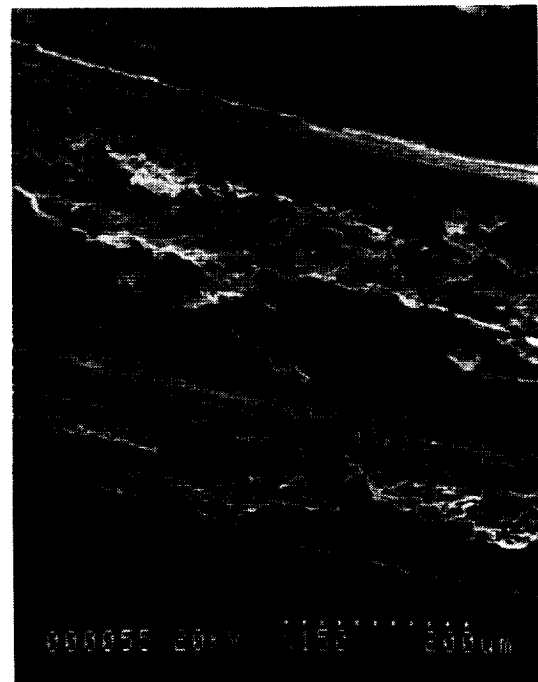
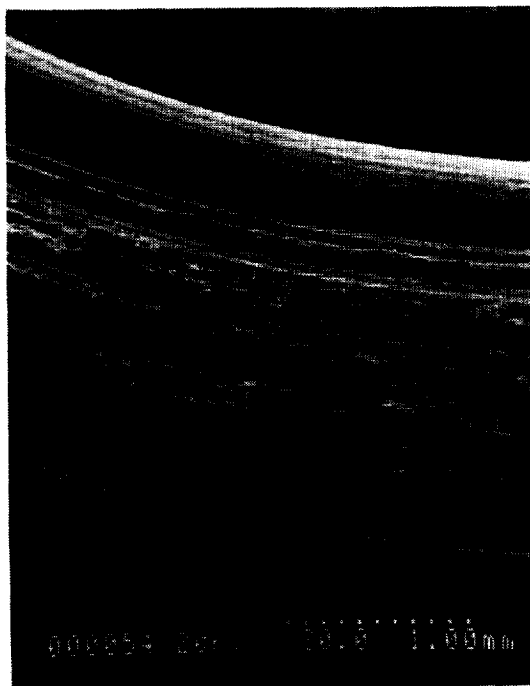


Figure 99. Ion Implanted Silver Post Test No. 81, Specimen I Ag-2, O₂ = 6.9 MPa

VII, I, Photographic and Metallurgical Analyses (cont.)

An overview of all the photos indicates no significant differences in appearance in comparison to untreated Monel or differences between testing at low and high oxygen pressures.

In general the following types of surfaces can be observed.

- a. Very smooth circumferential glazed or mirror like regions with surface cracking transverse to the direction of motion.
- b. Subsurface areas where the top layer appears to have spalled. The top layer could have been molten during the test.
- c. Deep glossy circumferential grooves free of surface cracks. This region could also be a glaze.
- d. Pitted zones of undefined nature.

These are illustrated in Figure 92 which provides a 400X magnification of ion implanted sample PB #6 which was the rotating half of the set used in the 14.7 psia O₂ functional heating Test No 91. The subsurface (.05 in.) temperature measurement indicated that 1033K (1400°F) was attained in the 140 to 180 sec time frame when the contact pressure was 1.7 MPa (400 psi) at 17,000 rpm. Visual evidence of local surface melting suggests that temperatures as high as 1589K (2400°F) were experienced.

Analyses of the elemental composition in Zones A through D indicated that the pretest lead content of 15% by weight had been reduced to less than 0.5% in all areas indicating the original surface was worn away.

VII, I, Photographic and Metallurgical Analyses (cont.)

EDS analyses were conducted to establish the influence of O₂ pressure on wear. These investigations revealed the following compositional changes in the various zones.

Zone Specimen/Maximum Temperature °F	Low O ₂ Pressure		High O ₂ Pressure
	IPb-6/1400	IPb-5	Ipb-2/1000
A Smooth Mirror Like with Radial Cracks	Ni 73 Cu 23 Other Bal		73 24 Bal
B Sub Surface Spall	Ni 58 Cu 39 Other Bal	54 41	
C Deep Glossy Groove	Ni 53 Cu 43		73 21
D Spherical Deposits on Surface	Ni 62 Cu 33	73 21	
Test No./Position	91/R	91/S	82/R

The nominal composition for Monel K-500 is 66.5 Ni and 29.5 Cu. The pretest surface analysis indicated 61 Ni, 22 Cu and 15 ion implanted lead. Monel also contains 2.7% Al, 0.06%/Ti and 0.75% Mn. The latter concentration are too low to detect changes by the test method employed.

It is obvious from the composition analysis that the concentration of Ni has increased from nominal by about 10% in Zone A and decreased by about the same amount in Zone B. Zones C and D do not suggest any specific trends. One would assume from first principles that if melting took place, a zone refining could cause copper, (the lower melting element) to move to the surface. Without melting, nickel would provide a more stable oxide than copper and thus would move to the surface at a rate that has some direct relation to the oxygen pressure.

VII, I, Photographic and Metallurgical Analyses (cont.)

As evidenced by examining the great variety of the surfaces produced following a rubbing test in oxygen it is likely that melting zone refining, diffusion, oxidation, etc. are occurring simultaneously, thus making an indepth analysis of events impractical.

VIII. CONCLUSIONS AND RECOMMENDATIONS

- 1) The burn factor or material heat of combustion can be employed as a guideline for screening metals for oxygen service.
- 2) Materials having a low heat of combustion and burn factor should be selected for oxygen applications when surface rubbing and/or high flow velocities can exist. Alloys of copper, nickel, silver are the most resistant to metal ignition. In fraction rubbing applications the addition of small amounts of chromium to nickel may be beneficial. Monel 400 and K-500 are reasonable selections for the OTV oxygen turbopump; however better materials may exist and further investigations of mechanically alloyed copper and nickel are recommended.
- 3) Aluminum and titanium alloy should be avoided except where these are well isolated from energy sources such as high flow velocity, rubbing, sparks, high strain energy, etc. Stainless steel and related alloys having high iron and chrome contents should also be avoided.
- 4) When dissimilar metals are subject to friction heating in oxygen the ignition threshold is controlled by the material having the highest burn factor. The fact that the mating material is difficult to ignite by itself does little to enhance the system ignition threshold.
- 5) Some materials were found to benefit much more than others from increased oxygen pressure in the friction heating tests. The improvement could not be solely attributed to improved cooling thus suggesting additional benefits due to surface oxidation. Tests where nitrogen at the same pressure replaced the oxygen confirmed the chemical dependency. Additional investigations are recommended to develop an understanding of the mechanisms that suppress ignition at high oxygen pressure.

VIII, Conclusions and Recommendations (cont.)

- 6) Some materials experienced thermal instabilities (cyclic heating and cooling) under a linearly increasing rubbing load. A mechanism involving the formation and spalling of an oxide surface layer has been offered to explain these events.
- 7) The test method employed to evaluate the effect of surface modification on friction coefficient and wear of Monel K-500 did not provide sufficient sensitivity to detect modest improvements. None of the surface treatments yielded a quantum jump in wear resistance. The process of ion implantation appeared to be mildly beneficial at low contact loads and nearly independent of the implanted material.
- 8) Electroplated chrome was found to be undesirable as surface treatment for Monel K-500.

Based on the data obtained and the discussion it can be concluded that:

- 1) The peak temperatures for tests conducted in high oxygen environment pressure were lower than peak temperatures observed with ambient oxygen environment pressure. Monel K-500 with surface modifications has lower peak temperatures than untreated Monel K-500. Overall Ion implanted lead is best while the worst is electrodeposited chromium.
- 2) In high pressure oxygen environment, surface modifications do help in reducing wear. For the step load tests, the worst case was untreated Monel K-500 while the surface modification which performed best were those implemented not with lead and oxygen. For the constant load tests the worst case was electrodeposited chromium and the coatings that performed well were ion implanted lead and ion implanted silver.

VIII, Conclusions and Recommendations (cont.)

- 3) The starting values for the coefficient of friction was between 0.15 to 0.22 for both Monel K-500 with and without surface modifications. During the tests the coefficients of friction changed considerably and the end values for Monel K-500 with surface modification were lower than those for untreated Monel K-500. The data indicate that ion implanted lead had the lowest coefficient of friction in both high and ambient oxygen pressure environment.
- 4) The repeatability of the friction and wear tester was poor and for more detailed analysis it is recommended that another friction and wear tester be designed which would give repeatable data in good precision.

REFERENCES

1. Schoenman, L., "Selection of Burn-Resistant Materials for Oxygen-Driven Turbopumps," AIAA/ASME/SAE 20th Joint Propulsion Conference Paper No. AIAA-84-1287.
2. Schoenman, L., "Advanced Cryogenic OTV Engine Technology," AIAA/ASME/ASEE 21st Joint Propulsion Conference Paper No. AIAA-85-1341, 8-10 July 1985.
3. Schoenman, L., J.M. Stoltzfus, "An Experimental Data Base for Material Selection and Design of High-Speed, High Pressure Oxygen Turbomachinery", CPIA-JANNAF Propulsion Conference, San Diego, 1985.
4. Schoenman, L., "Friction Rubbing Test Results of Dissimilar Materials in High-Pressure Oxygen," Aerojet TechSystems Company Report 23772-M-32, Appendix A, January 1986.
5. Schoenman, L., "Oxygen TPA Material Ignition Study," Aerojet TechSystems Company Report 23772-M-42, pp 23-33, November 1986.
6. Schoenman, L., Stoltzfus, J. and Kazaroff, V., "Friction Induced Ignition of Metals in High Pressure Oxygen," Appendix B, Orbit Transfer Rocket Engine Technology Program, Monthly Report 23772-M-48, May 1987. Also, STM-STP 986, 1988.
7. Copper, L.P., "Advanced Propulsion Concepts for Orbital Transfer Vehicle," NASA TM-83-419, June 1983.
8. Dean, L.E. and W.R. Thompson, "Ignition Characteristics of Metals and Alloys," ARS Journal, July 1961.
9. Monroe, R.W. and C.E. Bates, "Metal Combustion in High Pressure Flowing Oxygen," ASTM STP 812.
10. Bates, C.E., et al, "Ignition and Combustion of Ferrous Metals in High-Pressure, High-Velocity Gaseous Oxygen," J. Material for Energy Systems, American Society for Metals, June 1979.
11. Bransford, J.W., "Ignition and Combustion Temperature Determined by Laser Heating," ASTM STP 910.
12. ASTM Std G94 Standard Guide for Evaluating Metals for Oxygen Service.
13. Gluzek, F., et al., "Liquid Oxygen/Liquid Hydrogen Boost Vane Pump for Advanced Orbit Vehicle Auxiliary Propulsion System," NASA CR-158648, September 1979.
14. Standard Guide for Evaluating Nonmetallic Materials for Oxygen Service, ASTM G 63-83a.

REFERENCES (cont.)

15. Porter, W.S., "Test Report, Metals Ignition Study in Gaseous Oxygen," NASA/White Sands Test Facility TR 277-001, October 1981.
16. Stoltzfus, J.M. and F.J. Benz, "Test Plan Ignition of Metals in Oxygen by Friction Heating," NASA JSC, TP WSTF 412, 27 March 1985.
17. Stoltzfus, J.M. and F.J. Benz, "Determination of the Relative Resistance to Ignition of Selected Turbopump Materials in High Pressure Oxygen," NASA JSC WSTF TR324001.
18. Sarkar, A.D. Friction and Wear. Academic Press, Inc. New York 1980.
19. Lin, D.S., F.H. Stott, Wood, G.C., Wright, K.W. and Allen, J.H. "The friction and wear behavior of Nickel-Base Alloys in air at room temperatures" Wear Volume 27 pp 261-278. Elsevier Sequoia S.A., Netherlands, 1973.
20. Stott, F.H., D.S. Lin, G.C. Wood and C.W. Stevenson "The Tribiological Behavior of Nickel and Nickel Chromium Alloys at Temperatures from 20°C to 800°C - Wear Volume 36 pp 147-174 (1976) Elsevier Sequoia, S.A. Netherlands.
21. Bisson, E.E. in Handbook of Mechanical Wear, edited by Lipson, C., and L.V. Colwell University of Michigan Press, 1961.
22. Bisson, E.E. "Friction, Wear and Surface Damage of Metals as affected by solid surface films" in Handbook of Mechanical Wear edited by Lipson, C. and Colwell, L.V., Ann Arbor. The University of Michigan Press, 1961.
23. Stott, F.H., Lin, D.S. and Wood, G.C. "Glazes" produced on nickel-base alloys during high temperatures Vol. 242, No 11 8 pp. 75-77. Nature Physical Sciences Great Britain (1973).

APPENDIX A
PARTICLE IMPACT DATA SUMMARY

Particle Impact Tests

The results are summarized as follows:

<u>Material</u>	<u>Burn Factor</u>	<u>Number Tests</u>	<u>Number of Burns</u>	<u>Number with Sparks</u> *	<u>Max Test Temp or Min Temp at Ignition °F</u>	
					<u>T₁</u>	<u>T₂</u>
Zr Cu	35	10	0	3	790	850
Nickel 200	550	15	0	1	825	880
Silicon Carbide	1145	7	0	4	-	880
Monel 400	1390	10	0	4	800	850
K Monel 500	2090	10	0	2	750	880
316 Stainless Steel	4515	31	11	1	<450	<450**
Invar 36	5444	11	5	0	675	780
Hastelloy X	7160	20	6	5	725	800

*Sparks are Aluminum burning

**Testing at lower GH₂ temperature is required to obtain the minimum ignition point.

T₁ = Stream Temp Upstream of Orifice

T₂ = Sample Temperature

TABLE I-A. PARTICLE IMPACT TEST RESULTS

TEST #	TEST MATERIAL	INLET PRESSURE (psi)	CALCULATED SAMPLE TEMP (°F)	BURN (yes/no)	FLOW (sec)	NUMBER OF PARTICLES	COMMENTS/REMARKS
25.01	316 (015) *	4539	257		10	0	Disk did not rupture.
25.02	316 (015)	4497	334	No	10	10	Disk did not rupture.
26.01	316 (015)	4511	345	No	10	10	Disk did not rupture.
27.01	316 (015)	4460	420	No	20	10	Impact, rupture.
28.01	316 (015)	4463	521		30	10	Disk ruptured before impact.
29.01	316 (015)	4574	490	No	17	10	Impact, rupture.
31.01	316 (020)	4428	700		30	0	Did not rupture.
32.01	316 (020)	4449	675	Yes	30	10	Sample improperly loaded.
34.01	316 (020)	4463	693	No	30	10	Impact, rupture.
36.01	316 (020)	4532	626	No	30	10	Impact, rupture.
37.01	316 (020)	4560	647	No	30	10	Impact, rupture.
39.01	316 (020)	4449	688	Yes	30	10	VCM 1166
40.01	316 (020)	4435	663	Yes	30	10	(VCR 1181)
41.01	316 (020)	4421	683	Yes	30	1	(VCR 1196)
43.01	316	4553	686	Yes	30	10	(VCR 1262)
44.01	316	4532	647	No	30	1	
44.02	316	4511	670	Yes	30	5	
45.01	316	4511	669	No	30	1	
47.01	316	4574	522	Yes	23	10	(VCR 1337)
48.01	316	4463	509	No	23	5	
49.01	316	4504	495	No	15	10	

* () Thickness of rupture Disk

TABLE I-A (cont.)

TEST #	TEST MATERIAL	INLET PRESSURE (psi)	CALCULATED SAMPLE TEMP (°F)	BURN (yes/no)	FLOW (sec)	NUMBER OF PARTICLES	COMMENTS/REMARKS
50.01	316	4483	497	Yes	15	10	(VCR 1372)
51.01	316 (020)	4490	474	Yes	14	10	(VCR 1382)
53.01	316	4449	534	Yes	30	10	(VCR 1398)
54.01	316	4581	530	No	20	10	
55.01	316	4456	489	No	20	10	
56.01	316 (020)	4483	539	No	20	10	Impact, no rupture.
57.01	316 (020)	4490	533	No	18	10	Impact, no rupture.
58.01	316	4560	552	No	17	10	
62.01	316	4574	666	No	30	10	
63.01	316	4525	677	Yes	30	10	(VCR 295)
64.01	316	4546	653	No	30	10	
65.01	316	4407	705	No	30	10	
66.01	316	4483	692	Yes	30	10	(VCR 333)
67.01	316	4574	684	No	30	10	Plate backwards
141.01	316	4490	622	No	30	10	
142.01	316	4532	580	No	15	10	
143.01	316	4532	540	No	10	10	
144.01	316	4511	529	No	10	10	
145.01	316	4248	500	No	5	10	
172.01	316	4532	547	Yes	10	10	(VCR 731)
173.01	316	4574	505	Yes	10	10	(VCR 736)
174.01	316	4483	490	No	10	10	
175.01	316	4581	508	Yes	14	10	(VCR 748)
176.01	316	4497	473	No	20	10	
177.01	316	4532	469	No	14	10	
178.01	316	4643	484	No	14	10	

TABLE 1-A (CONT.)

TEST #	TEST MATERIAL	INLET PRESSURE (psi)	CALCULATED SAMPLE TEMP (°F)	BURN (yes/no)	FLOW (sec)	NUMBER OF PARTICLES	COMMENTS/REMARKS
179.01	316	4629	471	Yes	12	10	(VCR 771)
180.01	316	4490	451	No	10	10	
181.01	316	4483	448	Yes	10	10	
182.01	316	4477	450	No	10	10	Flash (VCR 788)
183.01	316	4525	431	No	8	10	
69.01	IN36	4500	772	No	30	10	4002
70.01	IN36	4511	788	Yes	35	10	4003
71.01	IN36	4477	861	Yes	90	10	4001 (VCR 441)
72.01	IN36	4400	761	No	30	10	4004
73.01	IN36	4504	775	No	30	10	4017
74.01	IN36	4497	783	Yes	30	10	4005
75.01	IN36	4539	749	No	30	10	4006
76.01	IN36	4490	755	No	40	10	4020
77.01	IN36	4497	745	No	30	10	4019
78.01	IN36	4518	787	Yes	33	10	4007 (VCR 525)
168.01	IN36	4560	791	Yes	45	10	4013 (VCR 632)

TABLE I-A (cont.)

-4-

TEST #	TEST MATERIAL	INLET PRESSURE (psi)	CALCULATED SAMPLE TEMP (°F)	BURN (yes/no)	FLOW (sec)	NUMBER OF PARTICLES	COMMENTS/REMARKS
80.01	Z1Cu	4608	757	No	30	10	2001
81.01	Z1Cu	4379	849	No	90	10	2002
82.01	Z1Cu	4477	788	No	35	10	2003
83.01	Z1Cu	4449	816	No	40	10	2004, Flash (VCR 619)
84.01	Z1Cu	4615	816	No	40	10	2005
117.01	Z1Cu	4546	788	No	45	10	2006
118.01	Z1Cu	4546	843	No	60	10	2007, Flash (VCR 1209)
119.01	Z1Cu	4560	850	No	60	10	2008
120.01	Z1Cu	4497	835	No	90	10	2009, Flash (VCR 1234)
121.01	Z1Cu	4463	819	No	45	10	2010
93.01	M400	4483	779	No	45	10	7001
94.01	M400	4518	833	No	60	10	7002
95.01	M400	4483	776	No	60	10	7003
96.01	M400	4477	835	No	60	10	7004
97.01	M400	4497	855	No	60	10	7005, Flash (VCR 864.5)
98.01	M400	4483	798	No	45	10	7006, Flash (VCR 874.5)
99.01	M400	4393	787	No	45	10	7007
100.01	M400	4372	848	No	80	10	7008, Flash (VCR 901)
127.01	M400	4532	837	No	45	10	7009
128.01	M400	4546	829	No	45	10	7010, Flash (VCR 1339)

TABLE I-A (cont.)

TEST #	TEST MATERIAL	INLET PRESSURE (psi)	CALCULATED SAMPLE TEMP (°F)	BURN (yes/no)	FLOW (sec)	NUMBER OF PARTICLES	COMMENTS/REMARKS
102.01	MK500	4525	814	No	60	10	6001
103.01	MK500	4539	836	No	60	10	6002
104.01	MK500	4532	843	No	60	10	6003
105.01	MK500	4490	843	No	60	10	6004
106.01	MK500	4601	839	No	120	10	6005
107.01	MK500	4567	883	No	120	10	6006, Flash
108.01	MK500	4456	886	No	90	10	6007
124.01	MK500	4511	841	No	60	10	6009
125.01	MK500	4435	868	No	120	10	6010
126.01	MK500	4608	831	No	45	10	6011, Flash (VCR 1322)
129.01	HASTX	4525	824	Yes	45	10	3001, Burned surface only (VCR 1348)
130.01	HASTX	4511	877	Yes	70	10	3002 (VCR 1428)
131.01	HASTX					10	3003, Injected particle at start of test; aborted test.
132.01	HASTX	4477	841	No	70	10	3004
133.01	HASTX	4588	813	No	40	10	3005
134.01	HASTX	4553	820	No	40	10	3006, Flash (VCR 58)
135.01	HASTX	4574	810	No	35	10	3007, Flash (VCR 74)
136.01	HASTX	4553	856	Yes	50	10	3008 (VCR 93)
138.01	HASTX	4523	843	No	60	10	3009
139.01	HASTX	4539	839	Yes	45	10	3010 (VCR 183)
140.01	HASTX	4504	821	No	45	10	3011

TABLE I-A (cont.)

-6-

TEST #	TEST MATERIAL	INLET PRESSURE (psi)	CALCULATED SAMPLE TEMP (°F)	BURN (yes/no)	FLOW (sec)	NUMBER OF PARTICLES	COMMENTS/REMARKS
156.01	HASTX	4518	857	No	60	10	3012
157.01	HASTX	4775	771	No	30	10	3013
158.01	HASTX	4532	816	No	40	10	3014
159.01	HASTX	4539	826	No	40	10	3015
160.01	HASTX	4525	805	No	35	10	3016, Flash (VCR 512)
161.01	HASTX	4490	822	Yes	60	10	3017 (VCR 527)
162.01	HASTX	4539	763	No	30	10	3018, Flash (VCR 536)
163.01	HASTX	4581	792	No	35	10	3019, Flash (VCR 549.5)
164.01	HASTX	4532	800	Yes	35	10	3020 (VCR 562)
167.01	HASTX	4650	766	No	45	10	Reused 3003
146.01	SiCa (THIN)	4511	867		120	10	Destroyed sample @ flow start
147.01	SiCa (THK)	4553	862		60	10	Destroyed sample @ flow start
148.01	SiCa (THK)	4581	880	No	60	10	Flash (VCR 310), Copper backup
149.01	SiCa (THK)	4560	666	No	10	10	Flash (VCR 320), No Acc Vent
150.01	SiCa (THK)	4553	849	No	60	10	
152.01	SiCa (THK)	4553	834	No	60	10	Flash (VCR 400)
153.01	SiCa (THIN)	4525	853	No	60	10	Cloud (VCR 418)
154.01	SiCa (THIN)	4643	823	No	75	10	
155.01	SiCa (THIN)	4525	842	No	60	10	Flash (VCR 451)

TABLE I-A (cont.)

-7-

TEST #	TEST MATERIAL	INLET PRESSURE (psi)	CALCULATED SAMPLE TEMP (°F)	BURN (yes/no)	FLOW (sec)	NUMBER OF PARTICLES	COMMENTS/REMARKS
15.01	N200	4546	586	No	30	10	
15.02	N200	4594	693	No	30	10	SAME SAMPLE
15.03	N200	4747	741	No	30	10	SAME SAMPLE
15.04	N200	4553	770	No	30	10	SAME SAMPLE
15.05	N200	4581	719	No	30	10	SAME SAMPLE
15.06	N200	4511	764	No	30	10	SAME SAMPLE
15.07	N200	4629	784	No	30	10	SAME SAMPLE
15.08	N200	4567	778	No	27	10	SAME SAMPLE
15.09	N200	4567	772	No	25	10	SAME SAMPLE, FLASH (VCR 699)
15.10	N200	4594	764	No	25	10	SAME SAMPLE
110.01	N200	4560	850	No	60	10	5001
111.01	N200	4574	877	No	70	10	5002
112.01	N200	4560	875	No	60	10	5003, FLASH
113.01	N200	4532	882	No	60	10	5004
114.01	N200	4407	855	No	120	10	5005
115.01	N200	4500	911		180	0	5006, OXIDE BUILDUP CHK
170.01	N200	4500	911		180	0	5008, OXIDE BUILDUP TEST



DRAWING
PREPARATION SHEET

Page 1 of 8

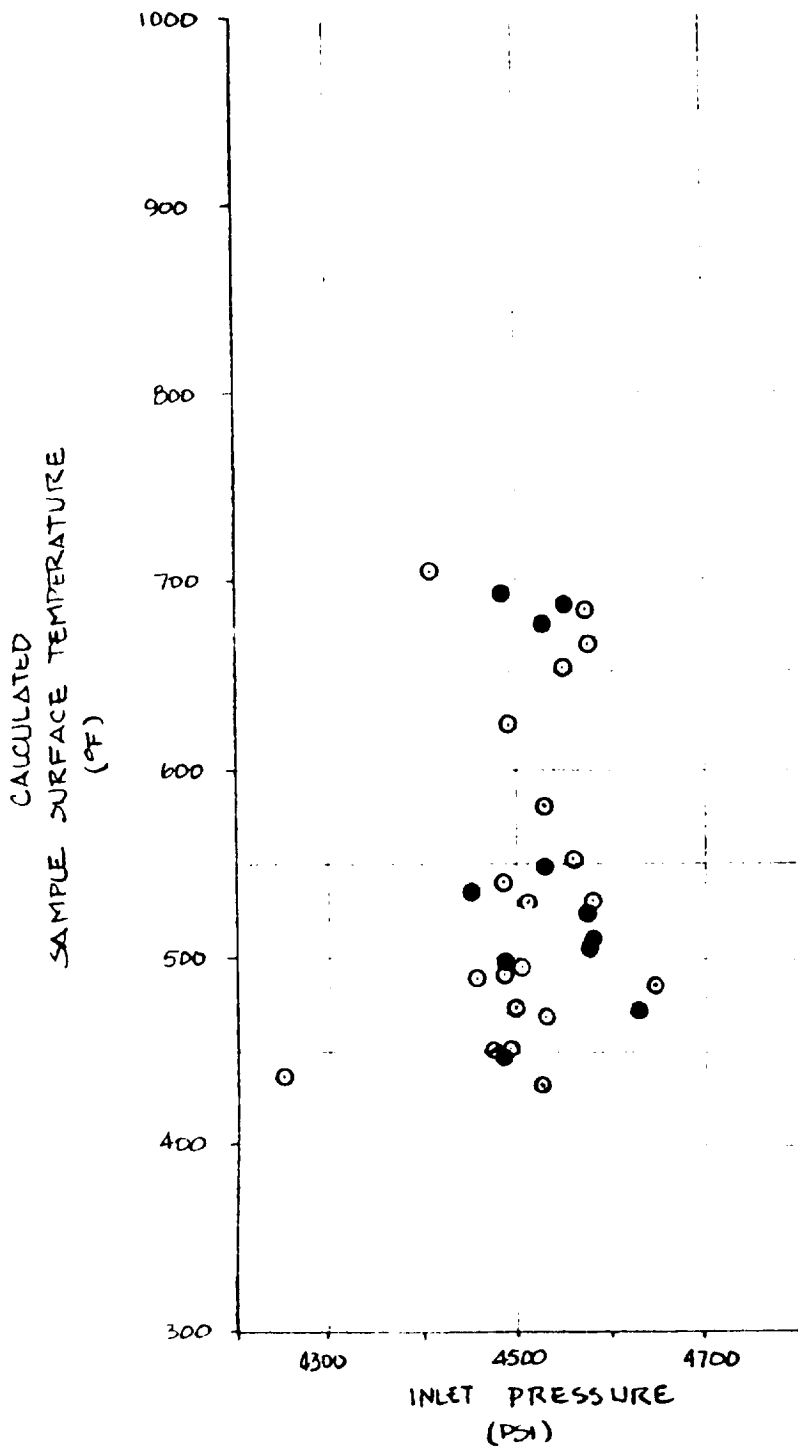
TPS No.

MOD No.

TITLE: TME-PIT

316 SS TEST DATA

ORIGINAL PAGE IS
OF POOR QUALITY



NOTE: 1) IMPACTED W/10 EA. 15BT_μ DIAMETER, 2017-T4 ALUMINUM PARTICLES.

2) COMPOSITION OF 316 SS:

Fe	Ni	Cr	Mo	C	Si	Mn	W	B	P	S
61.8	10	16	2	.08	1	2	-	-	.045	.03
68.8	14	18	3							

Figure 1-A

Contractor Authorized Signatures

NASA Authorized Signatures

A-10

25002



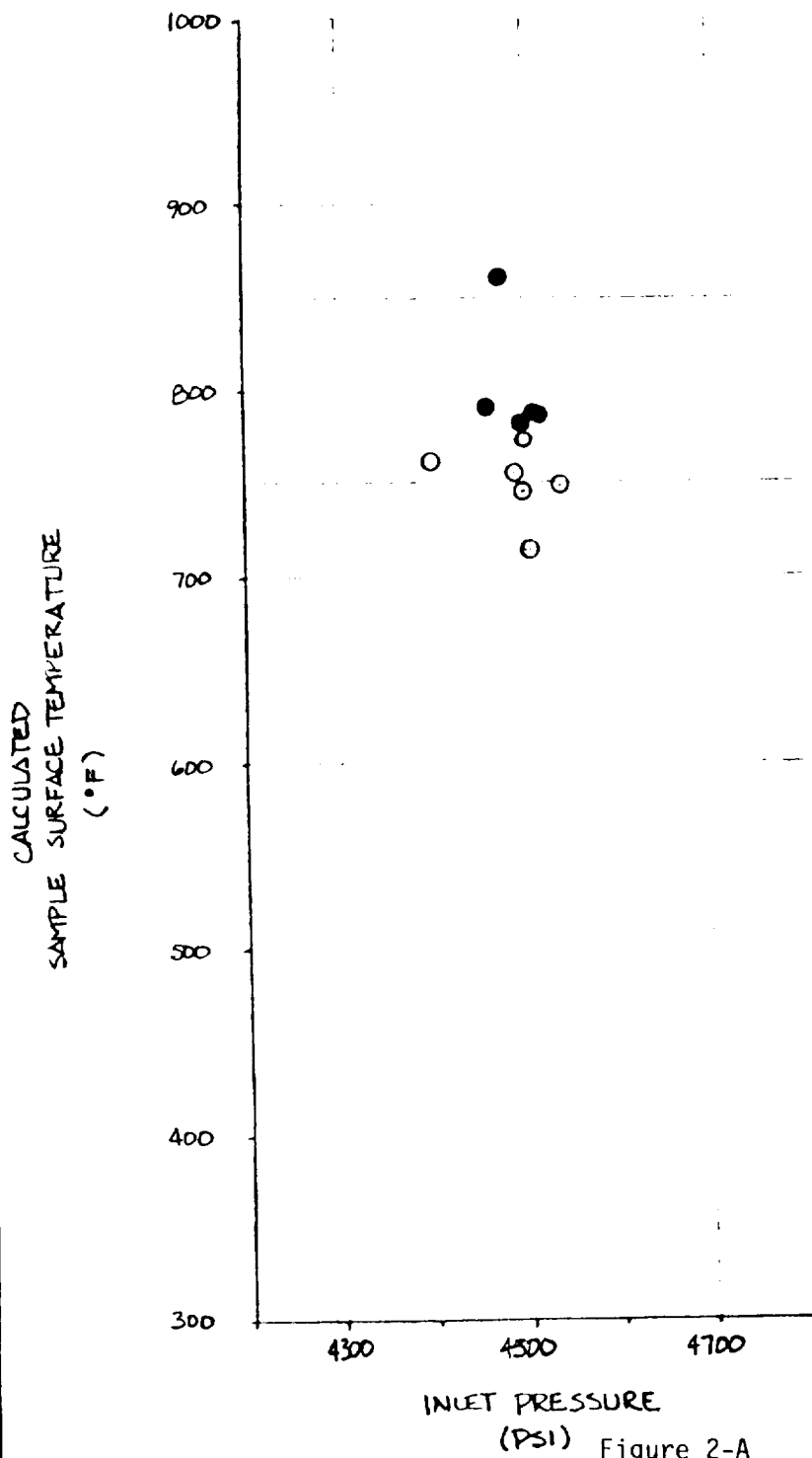
DRAWING
PREPARATION SHEET

Page 2 of 01

TPS No.

MOD No.

TITLE: TME-PIT INVAR 36 TEST DATA



ORIGINAL PAGE IS
OF POOR QUALITY

2003

Contractor Authorized Signatures

NASA Authorized Signatures

A-11



DRAWING
PREPARATION SHEET

Page 3 of 8

TPS No.

MOD No.

TITLE: TME-PIT

ZIRCONIUM COPPER TEST DATA

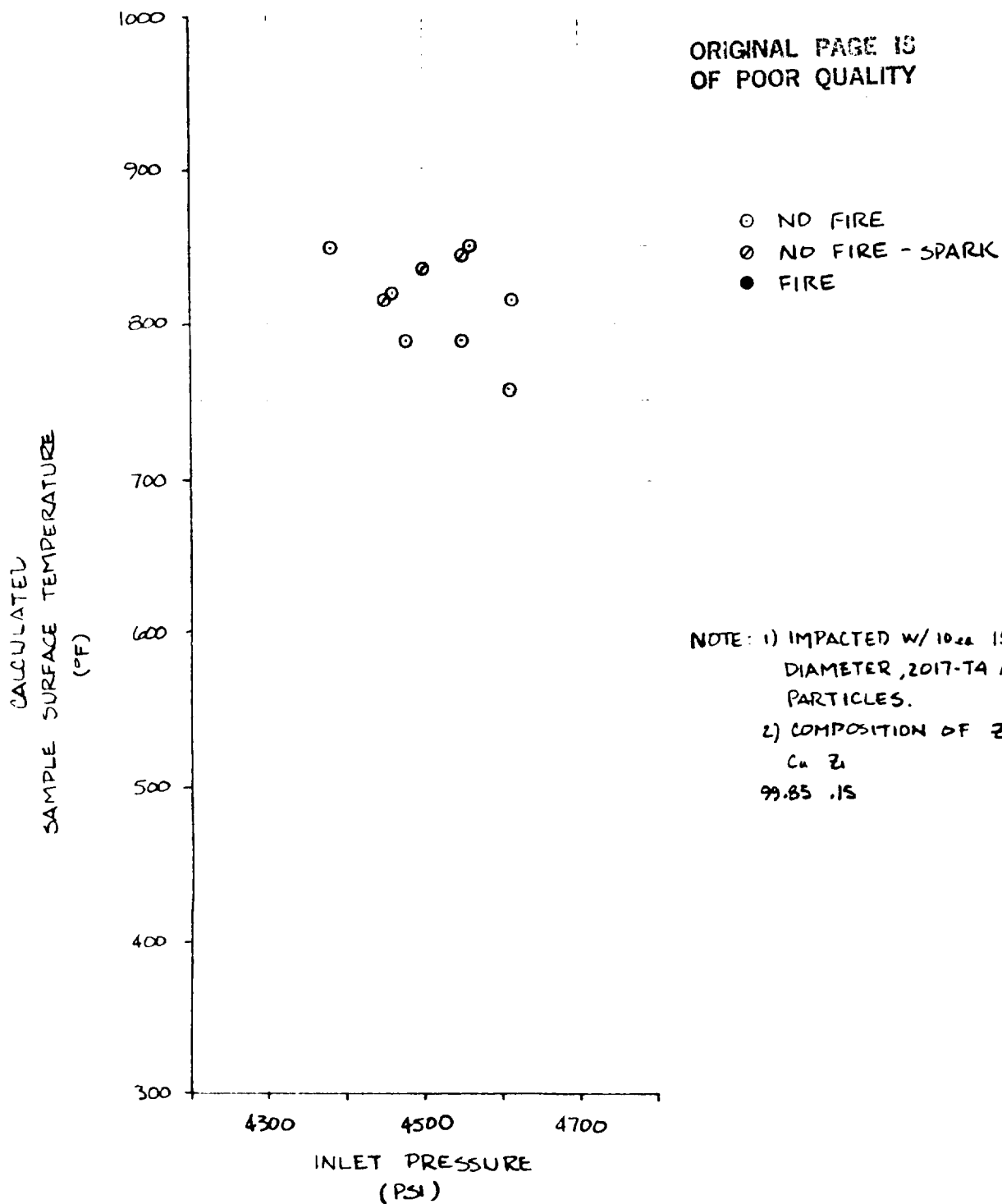


Figure 3-A

Contractor Authorized Signatures

NASA Authorized Signatures

A-12



DRAWING
PREPARATION SHEET

Page 7 of 8

TPS No.

MOD No.

TITLE: TME-PIT MONEL 400 TEST DATA

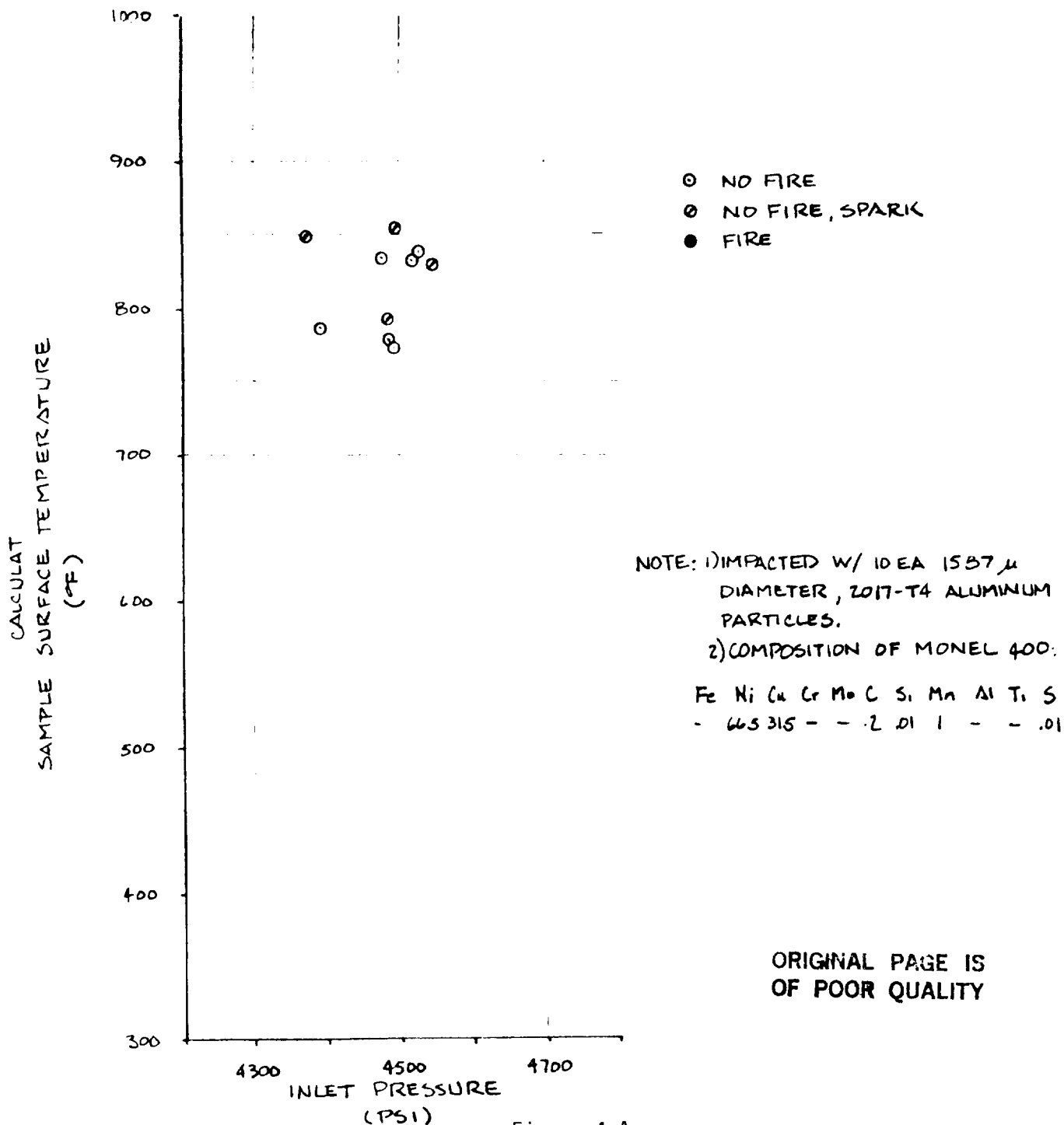


Figure 4-A

Contractor Authorized Signatures

NASA Authorized Signatures

A-13

20035



DRAWING
PREPARATION SHEET

Page 5 of 8

TPS No.

MOD No.

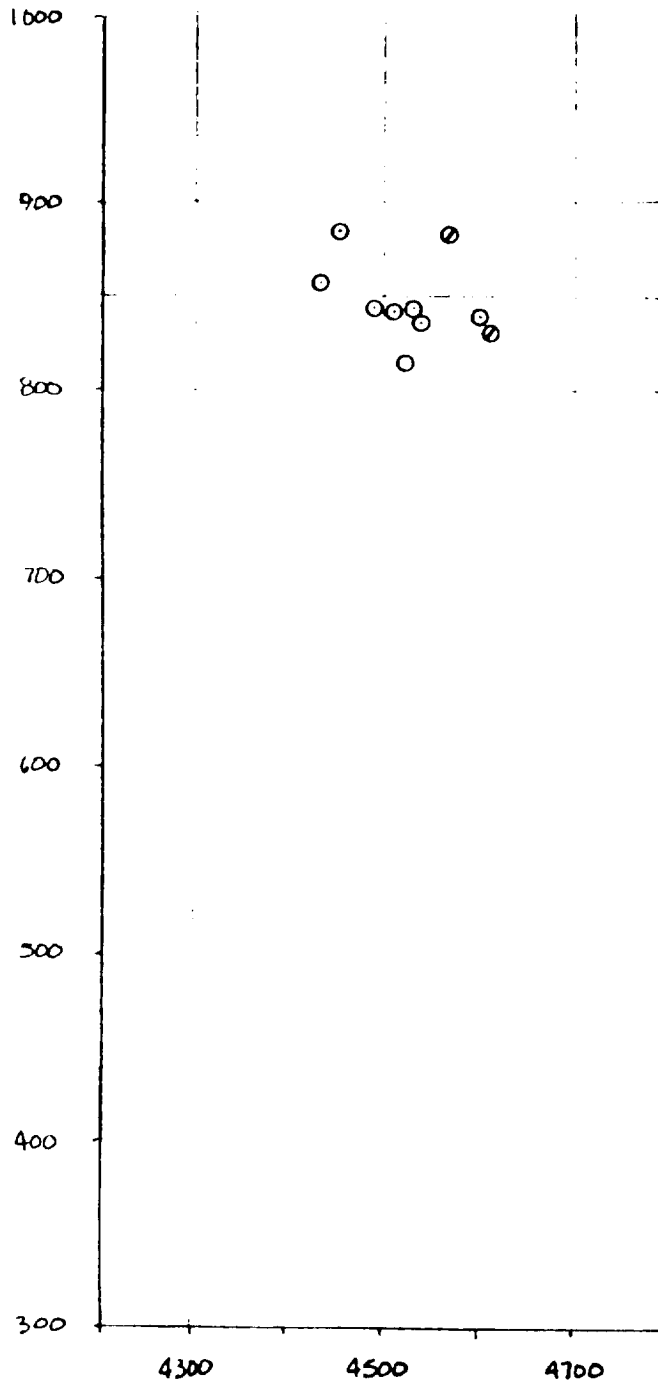
TITLE: TME-PIT

MUNEL K-500 TEST DATA

ORIGINAL TIME IS
OF POOR QUALITY

- NO FIRE
- ◊ NO FIRE, SPARK
- FIRE

CALCULATED
SAMPLE SURFACE TEMPERATURE
(°F)



NOTE: 1) IMPACTED W/ 10 EA. 1587 μ
DIAMETER, 2017-T4 ALUMINUM
PARTICLES.
2) COMPOSITION OF MUNEL K-500
Fe Ni Cu Cr Mo C Si Mn Al Ti S
- 66.5 29.5 - - .1 .2 .8 2.7 .6 .005

Figure 5-A

Contractor Authorized Signatures

NASA Authorized Signatures

A-14

20036



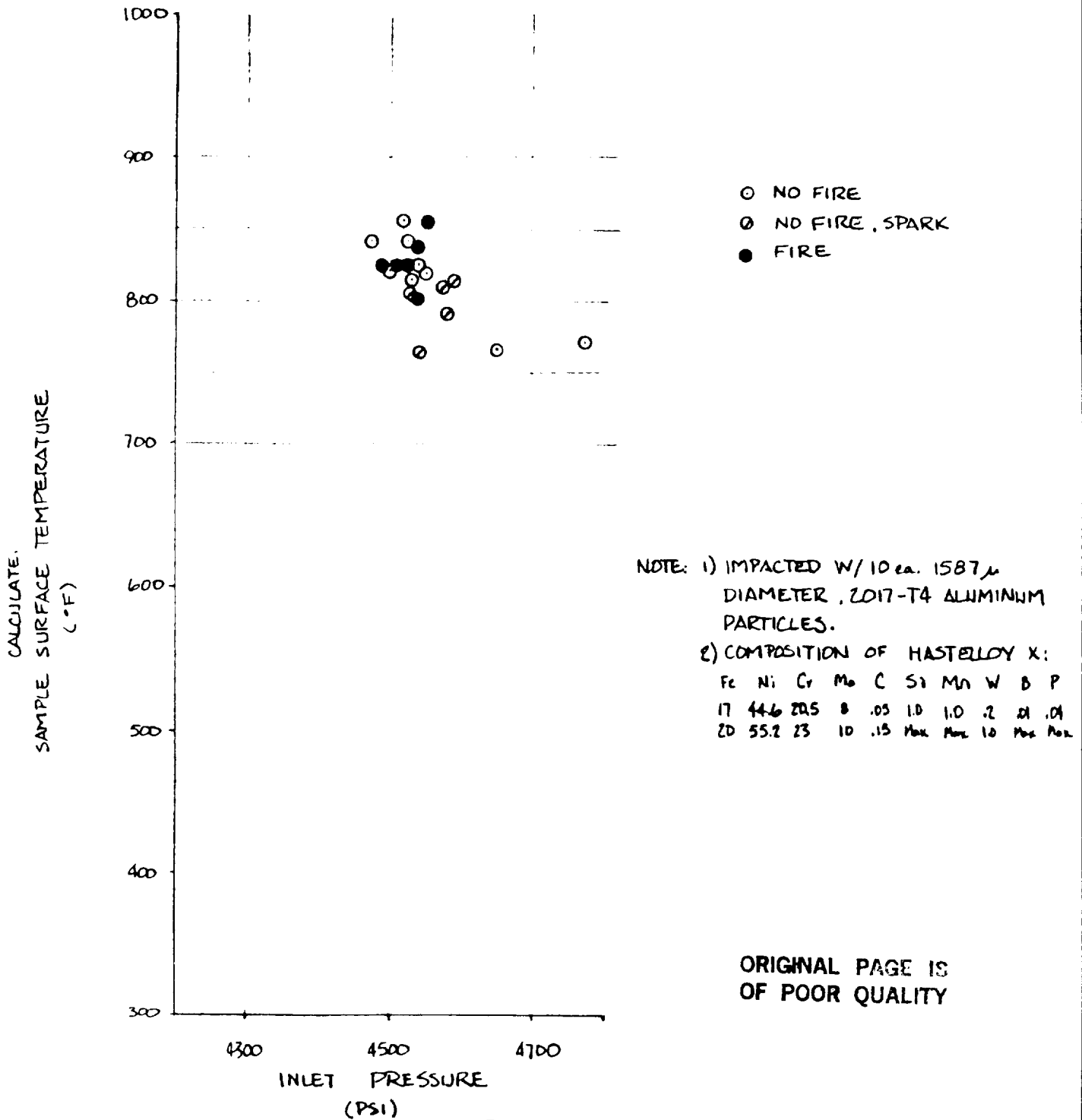
DRAWING
PREPARATION SHEET

TPS No.

MOD No.

TITLE: TME-PIT

HASTELLOY X TEST DATA



Contractor Authorized Signatures

NASA Authorized Signatures

A-15



DRAWING
PREPARATION SHEET

Page 7 of 8

TPS No.

MOD No.

TITLE: TME-PIT

SILICONE CARBIDE TEST DATA

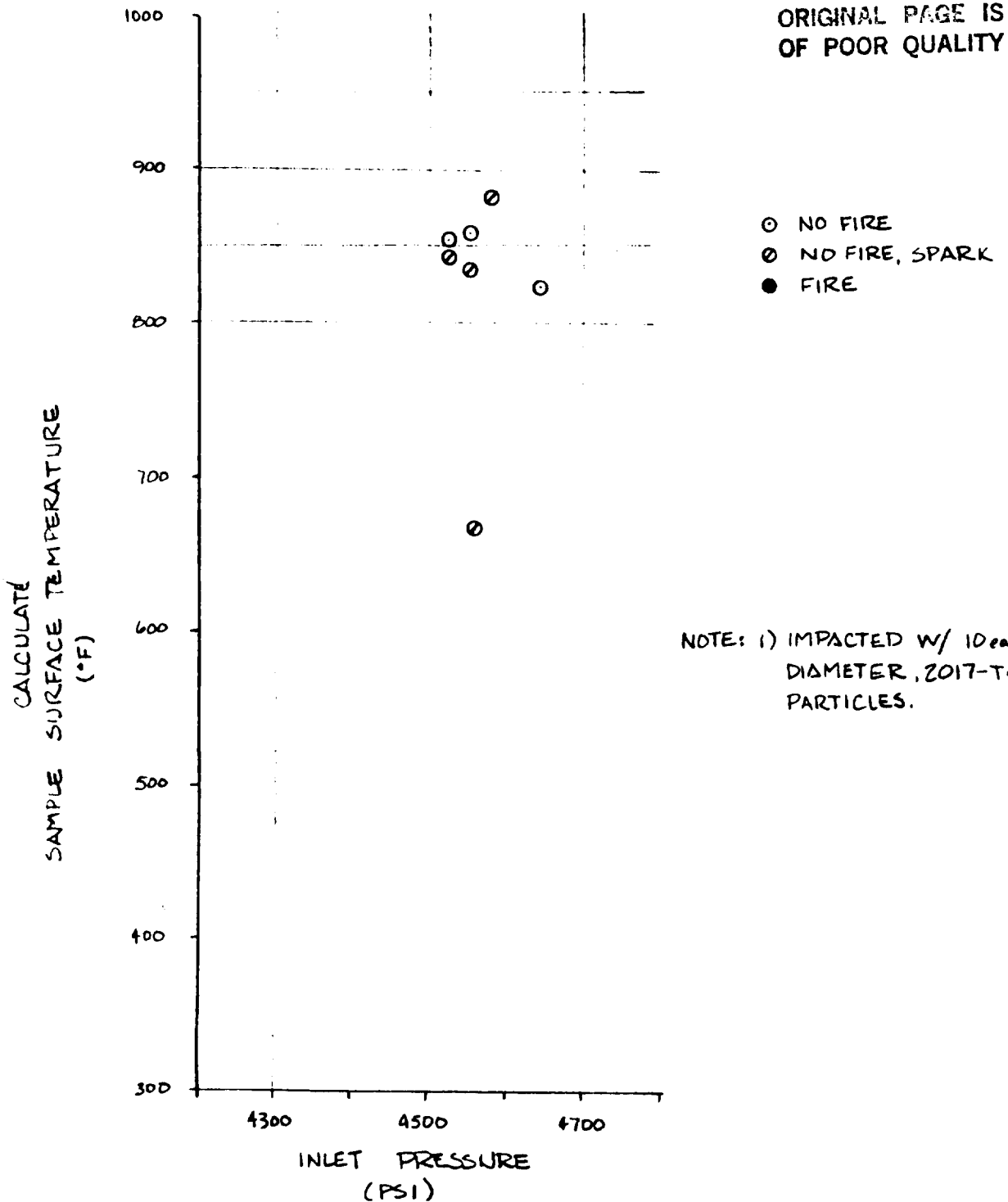


Figure 7-A

Contractor Authorized Signatures

NASA Authorized Signatures

A-16



DRAWING
PREPARATION SHEET

Page 8 of 8

TPS No.

MOD No.

TITLE: TME-PIT

NICKEL ZDD TEST DATA

ORIGINAL PAGE IS
OF POOR QUALITY

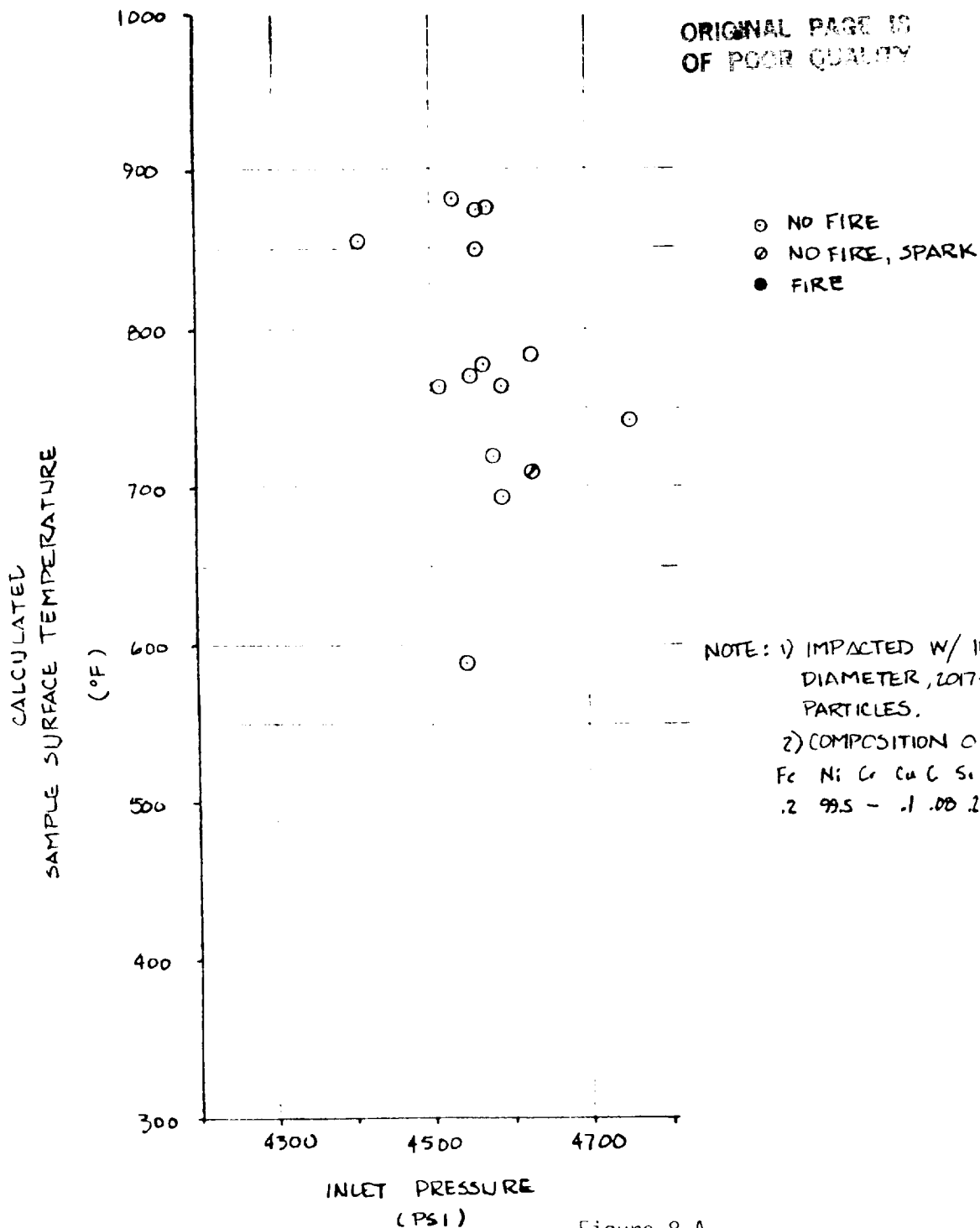


Figure 8-A

Contractor Authorized Signatures

NASA Authorized Signatures

A-17

20039
65002

APPENDIX B

WHITE SANDS REPORT ON COMPOSITION
OF SURFACE MODIFICATIONS

BACKGROUND

Six pretest and six posttest friction heating samples that had been either implanted or electroplated with one foreign material were received for analysis. The requestor wanted to know if any of the foreign material was present in the posttest sample. The samples received were all Monel K 500, the ion implanted materials were silver, chromium, lead, oxygen, and the electroplated materials were chromium, and silicon carbide. The sample ID contains the letter I for implanted or E for electroplated respectively. Samples identification numbers containing the number ten were the pretest and those with the number two were the posttest. Three areas of the posttest samples were analyzed; a flat surface, a gouged area and an area containing both.

DISCUSSION

Implanted materials are present on the surface of a substance to a depth of approximately 0.01 microns. Electroplated materials are usually much thicker, 10 to 50 microns or greater. The composition of all samples was determined using an energy dispersive X-ray analyzer. This technique analyzes the sample to a depth of several to tens or hundreds of microns depending on the sample. Considering the lack of relative surface sensitivity the analytical technique has, it is not surprising that concentrations of only two percent of implanted material were detected in the pretest samples. At these levels the possible error in the analysis could be as high as + or - 100%. At lower levels (tenths of a percent) 300% to 500% errors can be expected. What one should look at when reviewing the results is simply the fact that the implanted or electroplated material was detected and the concentration used to judge relative not absolute abundance.

RESULTS

PRETEST SAMPLES

Silver, chromium, and lead were detected in both the implanted and electroplated pretest samples. Silicon carbide was also present in the pretest electroplated sample, and to a much greater degree than any of the other materials, possibly with the exception of the electroplated chromium. The presence of oxygen in the pretest samples could not be ascertained with any certainty. If it was present, it was there in an exceedingly small concentration.

POSTTEST SAMPLES

The posttest samples showed that the foreign materials were present in some areas and not in others. In some cases more was present on the flat surface and in others, more was present in the gouged area.

Sample ID - I Ag 2

Silver was detected at very low concentrations (0.1%) on a portion of the sample containing both flat surfaces and gouged areas. It was present on the flat surface, at about the same concentration, but was absent in a gouged area of another portion of the same sample.

Sample ID - I Cr 2

A small amount of chromium (0.1%) was detected on the flat surface of this sample. A larger amount (0.3%) was found in the gouged area. The portion containing both types of surfaces contained 0.5%.

Sample ID - E Cr 2

Chromium (0.2%) was detected on the flat surface, 0.1% was detected in the gouged area. The location containing both flat and gouged areas had 1.5% chromium.

Sample ID - I Pb 2

Lead was absent in the area that contained both flat surfaces and gouged areas. It was present (0.7%) in a second flat surface and 1.2% in another gouged area.

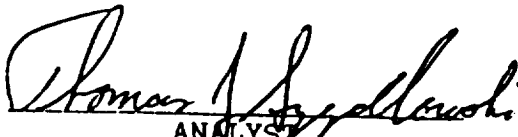
Sample ID - EC 2

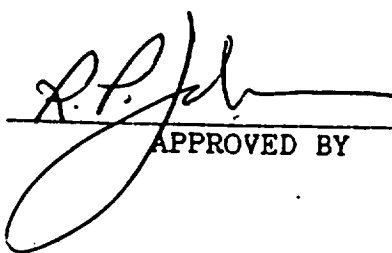
Silicon was more abundant in the gouged area examined than on the flat surface, 1.5% as opposed to 0.3%. The area containing both flat surfaces and gouged areas had 0.6%.

Sample ID - IO+ 2 (*)

Oxygen was detected on all posttest sample surfaces examined. It was present to a much larger degree on the posttest sample than on the pretest sample, and it was more abundant on the flat surface than on the gouged area.

- (*) The software available on the X-ray analyzer is not capable of providing semi-quantitative results when oxygen is to be included. It is for this reason that the raw data (cps) was used to indicate the presence of this element in the pre and posttest samples. No concentrations can be provided for oxygen.


ANALYST


APPROVED BY

